ABSTRACT

WU, ZHENHUA. Behavior of High-Strength Concrete Members under Pure Flexure and Axial-Flexural Loading. (Under the direction of Dr. Amir Mirmiran.)

The AASHTO LRFD Bridge Design Specifications limits its applicability to a maximum concrete compressive strength of 10 ksi (69 MPa). These limitations reflect the lack of research data at the time, rather than the inability of the material to perform its intended function. The present study addresses the need for better understanding of the behavior of high-strength concrete under pure flexure and axial- flexural loading.

The research program, as part of NCHRP Project 12-64, was comprised of both experimental and analytical work. The experimental work included pure flexure tests, axial-flexural tests and ancillary material property tests for high-strength concrete specimens made with three target strengths of 10, 14, and 18 ksi. A total of eighteen specimens were cast and tested in the Constructed Facilities Lab at the North Carolina State University. Thirteen (13) specimens were tested in pure flexure, and five (5) were tested under axial-flexural loading. The variables considered were mainly concrete strength, reinforcement ratio and level of axial load for the axial-flexural tests. The specimens were instrumented so that the strain profile, mid-span deflections and crack widths could be recorded during the tests. Level of the axial load was recorded and maintained while testing the beam-columns. As part of the analytical work, various aspects of the behavior of high-strength concrete members were examined and compared with the measured test data as well as data from the literature. A finite element model was also developed using the general-purpose program, ANSYS.

BEHAVIOR OF HIGH-STRENGTH CONCRETE MEMBERS UNDER PURE FLEXURE AND AXIAL-FLEXURAL LOADINGS

by

ZHENHUA WU

A dissertation submitted to the Graduate Faculty of
North Carolina State University
in partial fulfillment of the
requirements for the Degree of
Doctor of Philosophy

Civil Engineering
North Carolina State University

Raleigh, North Carolina

2006

APPROVED BY:

_____	_____
Dr. Amir Mirmiran	Dr. Sami Rizkalla
Chair of Advisory Committee	Co-chair of Advisory Committee
Civil Engineering	Civil Engineering
_____	_____
Dr. Paul Zia	Dr. Eric Klang
Advisory Committee	Advisory Committee

BIOGRAPHY

Wu Zhenhua, was born in Beijing, capital of P.R.China in August 1978. After graduating from high school, he started his undergraduate study in the Civil Engineering Department of the Tsinghua University in Beijing, China from September 1996. He received his Bachelor of Engineering degree in June 2000.

Mr. Wu worked in a structural design company for one year. Subsequently, he came to the USA to further his education. As a graduate student, he first enrolled in the Department of Civil and Environmental Engineering at the University of Cincinnati, Cincinnati, Ohio in September 2001. After one quarter, in January 2002, he transferred to Department of Civil Engineering at the North Carolina State University, Raleigh, North Carolina. He worked at the Constructed Facilities Laboratory of the NC State University as a graduate research assistant with Dr. Amir Mirmiran. In Spring 2003, he successfully passed his oral exam and received his Master of Science degree.

After that, Mr. Wu continued his research and worked on the National Cooperative Highway Research Program project 12-64 related to High-strength concrete with Dr. Amir Mirmiran as well as Dr. Sami Rizkalla. His research is expected to have significant impact on the bridge design codes in the U.S.

ACKNOWLEGEMENTS

I would like to thank the sponsors of this project, the American Association of State Highway and Transportation Officials in cooperation with the Federal Highway Administration. I also would like to thank the Transportation Research Board of the National Research Council who administered National Cooperative Highway Research Program Project 12-64.

I have been fortunate to have Dr. Amir Mirmiran and Dr. Sami Rizkalla as my graduate advisor for the last four years. I would like to convey my deepest appreciation for their guidance throughout my studies. They spent numerous hours to make an impact on my life and to craft me into a better researcher.

I would like to thank Dr. Paul Zia for all his constructive advices and comments throughout this study. His brilliant ideas and thoughts enhanced my point of view and served as new sources of inspiration.

I would like to recognize Dr. Eric Klang and thank him for serving on my advisory committee.

TABLE OF CONTENTS

LIST OF FIGURES

LIST OF TABLES

1 INTRODUCTION

1.1 Problem Statement

Development of high-strength concrete dated back to Yoshida (1930), who first reported concrete strengths above 14 ksi using compaction with high pressure. Later, Menzel developed cement pastes with strengths at about 18 ksi using autoclave curing. Freyssinet also reported developing 14 ksi high-strength concrete at about the same time (Zollman, 1980). These early developments were economically prohibitive for practical applications.

In the 1960's, super plasticizers were developed in Japan and Germany as efficient admixtures to enable the reduction of the water-to-cement ratio of concrete, while maintaining its workability. In the 1970's, the combined use of super-plasticizers and ultra-fine materials such as silica fume, finely ground granulated blast furnace slag or anhydrous gypsum led to further improvement of concrete performance including its strength. By the mid-1980's, high-strength concrete has gained popularity in both precast and cast-in-place construction for either reinforced or prestressed members. Table 1.1 shows some of the early applications of high-strength concrete in highway bridges. In Japan, concrete strengths as high as 11.4 ksi were used in the 1970's for railway bridges (ACI 363R-92, 1997).

In the early 1990's, the Federal Highway Administration (FHWA) sponsored the use of High Performance Concrete in several demonstration projects. Since 1993, a number of High Performance Concrete bridges have been constructed across the country. The FHWA

compilation project (Russell et al., 2003) reports on 19 such bridges in 14 states. While the highest design concrete strength in these bridges was reported as 14 ksi in Texas, the achieved strength at the design age reached as high as 15.9 ksi in South Dakota. The several High Performance Concrete showcases workshops by FHWA and state DOTs have shown that the use of high-strength concrete leads to more efficient structural designs, longer spans, shallower sections, and higher load-carrying capacities. However, as the design pushes the envelope at different limit states, the specifications should be closely examined against physical test data to allow for continued safety and efficiency.

Table 1-1 Early Applications of high-strength concrete in Highway Bridges (ACI 363R-92, 1997)

Bridge	Location	Year	Maximum Span (ft)	Maximum Design Concrete Strength (ksi)
Willows Bridge	Canada	1967	158	6
Nitta Highway	Japan	1968	98	8.5
San Diego-Coronado	California	1969	140	6
Fukamitsu Highway	Japan	1974	85	10
Linn Cove Viaduct	North Carolina	1979	180	6
Huntington/Proctor ville	West Virginia, Ohio	1984	900	8
Tower Road	Washington	1987	161	9

Some of the design codes in the US, e.g., the AASHTO LRFD Bridge Design Specifications, limit their applicability to a maximum concrete strength of 10 ksi. This limitation reflects the lack of research data at the time when the specification was developed, rather than the inability of the material to perform its intended function. The present study addresses the need for better understanding of the behavior of high-strength concrete under pure flexure and axial- flexural loading.

1.2 Research Objectives and Scope

The main objective of the research program is to study the behavior of high-strength concrete members under pure flexure and axial-flexural loading. Research and analysis focused on the following objectives:

1. Examine the usable ultimate strain of unconfined concrete, ε_{cu};
2. Investigate the adequacy and accuracy of using stress block parameters (α_1, β_1) to determine the flexural resistance of beams and beam-columns;
3. Validate methods of predicting the cracking moment and crack widths in high-strength concrete beams;
4. Investigate the adequacy and accuracy of using the current AASHTO LRFD Specifications (2004) equations in predicting the mid-span deflection at service level;
5. Verify the applicability of beam theory to high-strength concrete member under pure flexure and axial flexural loading; and
6. Study the curvature ductility of concrete members as a function of concrete strength and reinforcement ratio.

The research program, as part of NCHRP Project 12-64, was comprised of experimental and analytical work. The experimental work included pure flexure tests, axial-flexural tests and material property tests for three levels of high-strength concretes with target strengths of 10, 14 and 18 ksi. In the analytical part, behavior of high-strength concrete members was analyzed and verified by test data as well as data from literature. Finite element method was also used in this study.

1.3 Research Methodology

A total of eighteen specimens were cast and tested in the Constructed Facilities Lab at NC State University. Thirteen specimens were tested in pure flexure loading and five were tested under axial-flexural loading. The specimens were instrumented so that the strain profile, deflection and crack widths could be recorded during the test. Also, the level of axial load was recorded and maintained in testing beam-columns.

The following analytical methods were used:

1. The ultimate strains of concrete with concrete strength between 0 and 18 ksi were analyzed statistically to determine a lower boundary for design.
2. Nominal resistances were calculated for all tested specimens and specimens from literature using stress block factors in the current AASHTO LRFD Specification (2004) as well as the one proposed from NCHRP 12-64 Project (Mertol, 2006). Predicted nominal resistances and test data were compared. Conclusions were made based on statistical study.
3. The measured cracking load from the present study was compared with the predictions using the code equation. Measured crack width was also compared with predictions of the Frosch's model (2001).
4. Analytical model for calculating the moment-curvature relationship was verified against the test results and the model was used to study the curvature ductility.
5. The study of deflection was divided into two parts. In the first part, deflections were predicted for specimens tested in this project using AASHTO LRFD Specifications (2004), integration of the moment-curvature response, and computer program

Response2000 (Bentz and Collins 2000). Predicted results were compared with test data. Data from the literature was also included for a general comparison. In the second part, a finite element analysis was performed using ANSYS to investigate the effect of bond on the deflection of high-strength concrete.

1.4 Organization of the Dissertation

This dissertation consists of six chapters. Chapter 1 (this chapter) highlights the problem statement, and the significance, objectives and methodologies of the research undertaken in this study. Chapter 2 presents a literature review of the previous work related to the research objectives of this study. Chapter 3 provides detailed information about the experimental work and summarizes some of the test results. Chapter 4 is devoted to the analysis of the data from literature as well as those obtain from the experimental program. Chapter 5 presents the finite element analysis, which is focused on the prediction of the load-deflection response of high-strength concrete beams. Chapter 6 summarizes the research undertaken in this study, and provides findings and conclusions of the research.

2 LITERATURE REVIEW

2.1 Introduction

In this chapter, a thorough review and synthesis of past research on various aspects of the flexural behavior of high-strength concrete is presented, including ultimate strain of unconfined concrete, stress block parameters, cracking moment and crack width, deflection at service load, and ductility.

2.2 Ultimate Strain of Unconfined Concrete

The ultimate strain of unconfined concrete is a function of various factors, including mix proportions, type of cement and cementitious materials, type of admixtures, and type and grading of aggregates. Other factors that influence the strength of concrete, e.g., curing procedure, specimen type and size, moisture content and boundary conditions of test specimens, specimen age at the time of testing, and rate of loading, potentially affect the ultimate strain of concrete, as well.

In the U.S., all design codes suggest a value of 0.003 for the ultimate strain of concrete, whereas some of the foreign codes (e.g., Belgium, Sweden, Germany, and Canada) use 0.0035. Code in the U.K. uses an ultimate strain of 0.0036 for a concrete compressive strength of 1.8 ksi, but it is gradually reduced to 0.0028 for a concrete compressive strength of 7.3 ksi. Recognizing that ultimate strain of concrete has an inverse relationship with its compressive strength, this issue has a profound effect on the ductility requirements and the

reinforcement limits of flexural members. ACI 441-R96 (1996) indicates that the strain limit of 0.003 is quite satisfactory for both high-strength concrete and normal-strength concrete, although it may not be as conservative for high-strength concrete (Mansur, 1997). Figure 2-1 shows the ultimate strains in high-strength concrete beams as the average over the constant moment region. The figure confirms the findings of the ACI 441-R96 (1996). Except for one data point, which is from an over-reinforced beam without any stirrups (Mansur, 1997), all others show an ultimate strain greater than 0.003. The average measurements of the ultimate strain in beams ranged between 0.0034 and 0.0041 at the peak strength, and between 0.004 and 0.005 at the time of failure. Some reported local strains as high as 0.022 for a beam with a relatively short constant moment region.

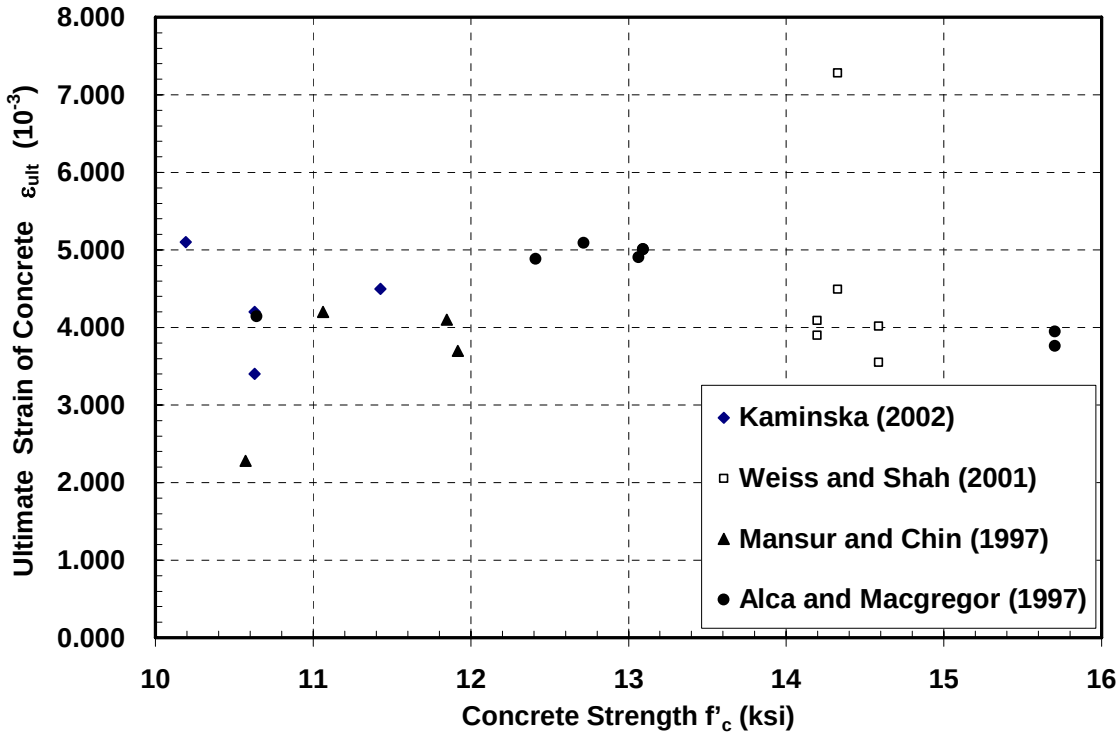

Figure 2-1 Effect of Concrete Compressive Strength on the Ultimate Compressive Strain in Flexural Members

2.3 Flexural resistance of Beams

The databank for high-strength concrete beams includes 16 different beam test projects with a total of 174 test data. The variables in the high-strength concrete beam tests include compressive strength of concrete f'_c, yield strength of steel reinforcement f_y, span length L and the distance between the load points L_c, width of the section b, depth of tension steel d, shear span to depth ratio a/d, reinforcement ratio for tension steel ρ in percentage as well as a fraction of the balanced reinforcement ratio ρ_b, the reinforcement ratio for compression steel ρ', and transverse steel reinforcement ratio ρ_s in the constant moment region. It is important to note that for flexure-critical failure, the amount of stirrups in the constant moment region is not expected to affect the flexural resistance of the member significantly, unless a large amount of stirrups is used so that the concrete in the compression zone is well confined. However, the amount of stirrups may affect ductility of the member. Table 2-1 shows the range of test variables in the high-strength concrete beam databank.

Table 2-1 Range of Test Variables in the Databank for HIGH-STRENGTH CONCRETE Beams

Test Variable	f'_c	f_y	L	L_c	b	d
	ksi	ksi	in	in	in	in
Range	10 - 18	53 - 125	32 - 285	6 - 120	4 - 13	4 - 20

Test Variable	a/d	ρ	ρ / ρ_b	ρ'	ρ_s
		percent		percent	percent
Range	1.0 - 8.4	0 - 8	0 - 1.7	0 - 0.1	0* - 3.5

* Of the 174 beam tests in the high-strength concrete databank, 143 beams (82 percent) did not have any stirrups.

Of the data obtained on high-strength concrete beams, a total of 35 specimens were reported with unusually low capacities (Ahmad and Lue, 1987). This may be attributed to the

anchorage failure of the reinforcement near the support for some of the specimens and shear failure in others. These tests were excluded from the data synthesis in Chapter 4. Flexural failure has been reported for all other test data irrespective of the *a/d* ratio.

It is important to examine the distribution of test variables in the database. Figure 2-2 shows the distribution of the beam tests based on the strength of concrete. Majority of the tests correlate to concrete compressive strengths below 14 ksi; and only 4 percent of the beams have concrete compressive strength over 16 ksi. Figure 2-3 shows the distribution of the beam tests based on the amount of reinforcement and the type of failure. In general, test data for over-reinforced concrete beams are scarcer than for under-reinforced beams. Only 18 percent of the specimens failed in compression control as over-reinforced beams; whereas the clear majority involved tension-control failure of under-reinforced beams.

Figure 2-4 shows the distribution of the beam tests based on the shape of the cross section. About 85 percent of the beams had a square section, while 5 percent of the beams were circular, 6 percent were triangular, and only 4 percent included flanged sections. There is only one research publication (Kahn and Meyer, 1995) that addressed flexural specimens with a triangular or circular compression zone. These members were designed as over-reinforced sections. It is important to note that even in the flanged sections tested, the compression zone remained in the flange. Therefore, there is a lack of test data on the high-strength concrete beams with flanged sections when neutral axis falls in the web area. Since it is unlikely for the bridge deck to be comprised of high-strength concrete above the limits prescribed by the current AASHTO LRFD Specifications (2004), the most typical

application of the flanged section will be in the negative moment region of prestresssed concrete girders over the support, if the girders are continuous, or where girders are spliced.

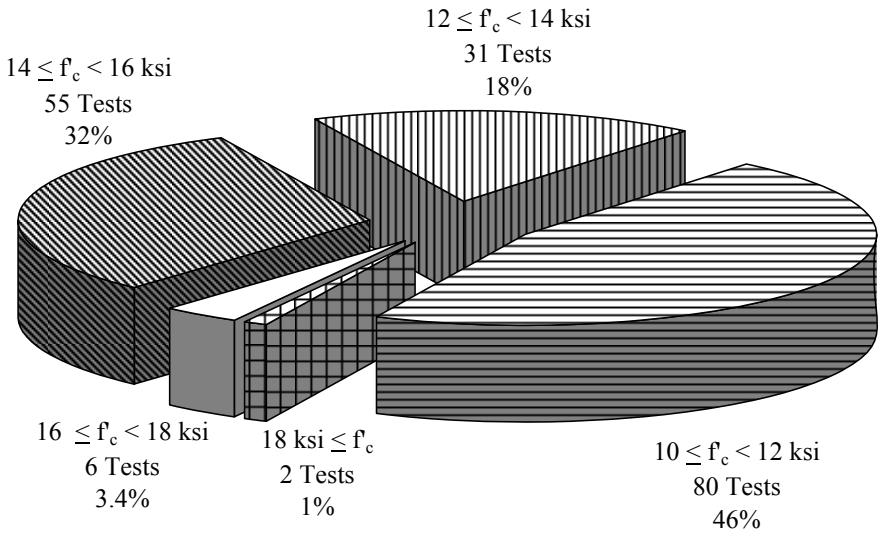

Figure 2-2 Distribution of Concrete Strengths in 174 Beam Tests with f'$_c$ > 10 ksi

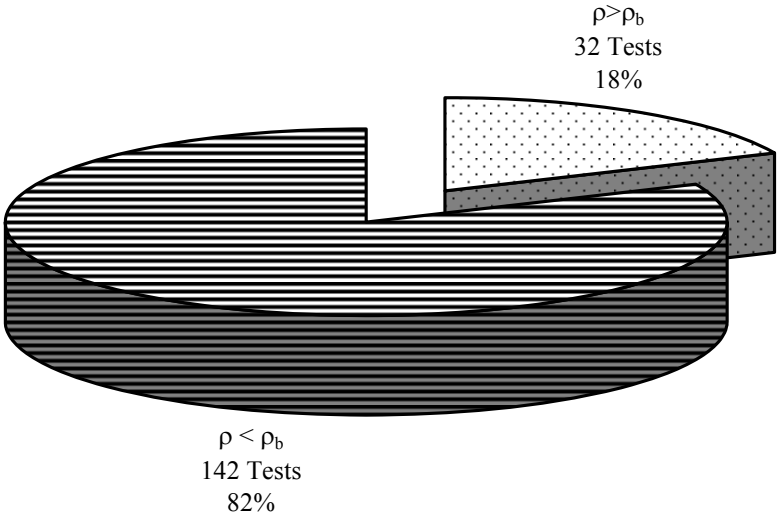

Figure 2-3 Distribution of Reinforcement Ratios in 174 Beam Tests with f'$_c$ > 10 ksi

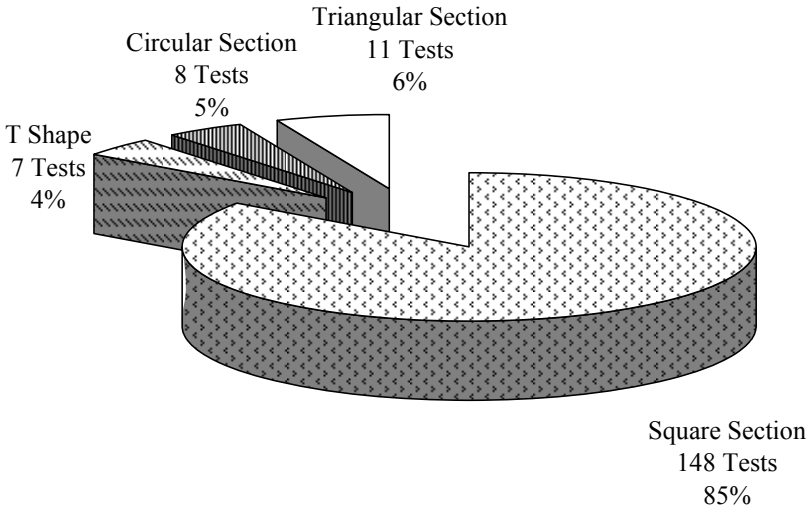

Figure 2-4 Distribution of Section Types in 174 Beam Tests with $f'_c > 10$ ksi

Ultimate Strength Design Method was first included in ACI 318-56 from October 1955. Majority of the research on flexural behavior of normal-strength concrete specimens carried out before 1950's. Test data from 14 projects, with a total of 150 specimens (Mattock, 1961) is used in this project for comparison with high-strength concrete.

Both AASHTO LRFD and ACI 318-05 determine the flexural resistance of a beam using stress block parameters. A generalized stress block is defined by three parameters, k_1, k_2 and k_3, as shown in Figure 2-5. The parameter k_1 is defined as the ratio of the average compressive stress to the maximum compressive stress. The parameter k_2 is the ratio of the depth of the resultant compressive force to the depth of neutral axis. The parameter k_3 is the ratio of the maximum compressive stress to the compressive strength of concrete cylinder f'_c.

The design values of the stress block parameters are determined at the ultimate strain ε_{cu}, which corresponds to the maximum flexural resistance of the section. These parameters were originated from the eccentric bracket tests performed by Hognestad et al. (1953). The k_1k_3 value and the k_2 value can be obtained from the equilibrium of the external and internal forces, as follows:

$$P_n = k_1 k_3 f'_c bc + A_s' f_{su} + A_s f_{su} \quad \text{(Equation 2-1)}$$

$$M_n = k_1 k_3 f'_c bc(d - k_2 c) + A_s' f_{su}(d - d') \quad \text{(Equation 2-2)}$$

The three-parameter generalized stress block can be reduced to a two-parameter equivalent rectangular stress block, by keeping the resultant of the compression force at the mid-depth of the assumed rectangular stress block. The two parameters of α_1 and β_1 can be defined as:

$$\alpha_1 = \frac{k_1 k_3}{2k_2} \quad \text{(Equation 2-3)}$$

$$\beta_1 = 2k_2 \quad \text{(Equation 2-4)}$$

The nominal axial and flexural resistance of the section can then be shown as:

$$P_n = \alpha_1 \beta_1 f'_c bc + A_s' f_{su} + A_s f_{su} \quad \text{(Equation 2-5)}$$

$$M_n = \alpha_1 \beta_1 f_c' bc\left(d - \frac{\beta_1 c}{2}\right) + A_s' f_{su}(d - d') \quad \text{(Equation 2-6)}$$

It is generally agreed that flexural resistance of under-reinforced beams is not significantly affected by the exact shape of the stress block, so long as the internal lever arm for moment resistance is chosen properly. This is mainly due to the fact that strength of under-reinforced

beams is controlled by the yield strength of the reinforcement. In over-reinforced concrete beams, where failure is controlled by compression, the flexural resistance of the member is affected more profoundly by the shape of the stress block. The latest tentative edition of AASHTO LRFD Specifications (2005) allows the design of over-reinforced beams with partial prestressing ratio (PPR) less than 50 percent, which was prohibited in previous editions. However, test data on over-reinforced high-strength concrete beams is rare.

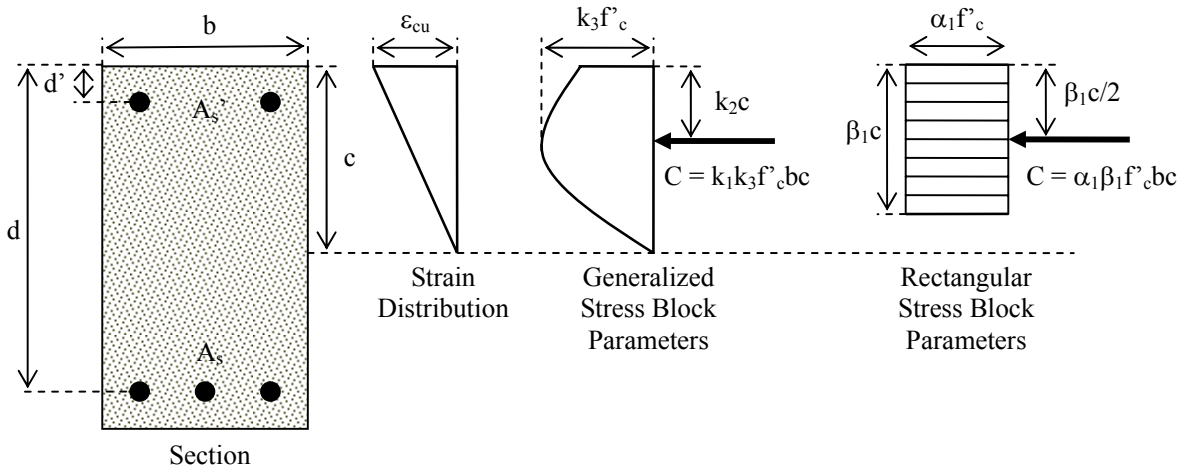

Figure 2-5 Stress Block Parameters for Rectangular Sections

The amount of compression reinforcement is an important factor in calculating the flexural resistance of the section. The presence of compression steel further increases the reinforcement limit for tension steel (Pam, 2001). It also enhances the rotational capacity of a section, especially if adequate transverse reinforcement is provided. However, no physical test data is available from the literature on doubly reinforced high-strength concrete beams.

The amount of transverse reinforcement may have an effect on the flexural resistance of high-strength concrete beams. However, only eight beam tests were found in the literature with stirrups in the constant moment region. Of these, the amount of stirrups in three (3) of the beams were not reported. Mansur (1997) reported that ultimate strength and ductility are enhanced when using stirrups in over-reinforced members. This may be attributed to the confinement effect of stirrups in the compression zone.

The ratio of the experimental flexural resistance M_{Exp} to that predicted using the LRFD Specifications M_{LRFD}, is shown as a function of concrete compressive strength f'_c in Figure 2-6. The latter is calculated based on Equation (5.7.3.2.2.1) of the LRFD Specifications, using β_1 of 0.65, because the concrete strength exceeds 10 ksi. All calculations are based on the actual yield strengths of the flexural reinforcement, if measured. Otherwise, nominal yield strengths were used instead. No strain hardening was considered in the analysis. Plain concrete beams and reinforced concrete beams with reported premature shear failure (Ahmad and Lue, 1987) were excluded from this comparison. The 125 data points in the figure are broken down into three categories: 22 over-reinforced rectangular sections, 84 under-reinforced rectangular sections, and 19 other shapes. No general trend can be observed in relation to the concrete compressive strength. It can be seen, however, that test data above 15 ksi (103 MPa) are quite rare to make a valid judgment as to the applicability of the AASHTO LRFD Specifications. It should be noted that only one research publication (Kahn and Meyer, 1995) has addressed flexural specimens with a triangular or circular compression zone. These members were designed with over-reinforced sections. The flexural resistance of other sections was calculated similar to the procedure for rectangular sections. Even though

the assumption of the rectangular stress block is not valid for other shapes, it seems that the flexural resistance of the member is not greatly affected.

Figure 2-7 shows the M_{Exp}/M_{LRFD} ratio with respect to the shear span a/d ratio. All data points reflect flexural mode of failure, as the specimens were heavily reinforced to avoid shear failure. The figure shows no clear trend, indicating same level of accuracy for the AASHTO LFRD Specifications for majority of the flexure-critical beams.

The 2004 and earlier versions of AASHTO LRFD Specifications limit the c/d_e ratio to 0.42 to distinguish between under-reinforced and over-reinforced beams. Even though in the 2005 Interim version of LRFD, this was replaced by limiting the tensile strain of the longitudinal reinforcement, the two limitations are essentially same. Figure 2-8 shows the ratio of the measured flexural resistance of high-strength concrete beams in the databank to that predicted using the equations in the LRFD Specifications, as a function of the c/d_e ratio. The line drawn at c/d_e of 0.42 identifies the previous LRFD threshold of over-reinforced and under-reinforced beams. Test data marked as other shapes refer to beams with triangular or circular compression zone (Kahn and Meyer, 1995). It is noteworthy that no value below 0.8 was observed in the literature for either over-reinforced or under-reinforced high-strength concrete beams that were carefully detailed to avoid shear or bond failure. The figure also shows that the use of rectangular stress block parameters in the current LRFD Specifications could be improved to avoid over-estimating the flexural resistance of the section in high-strength concrete beams.

Figure 2-9 shows the same data in terms of the reinforcement ratio as a fraction of the so-called balanced reinforcement ratio that is defined as the amount of reinforcement for which steel yields at the same time that concrete reaches its ultimate strain ε_{cu} of 0.003. Note that a balanced reinforcement ratio corresponds to a c/d_e ratio to 0.60, and a strain limit of 0.005 in steel; whereas the limit of 0.42 for the c/d_e ratio corresponds to 70 percent of the balanced reinforcement ratio. While majority of the tests have been carried out on under-reinforced beams, no clear trend can be observed in the figure regarding the accuracy of the AASHTO LRFD Specifications for either over-reinforced or under-reinforced beams.

In summary, the flexural resistance of rectangular sections is of great significance and of high priority in this study. There is adequate test data to establish the necessary parameters described above. However, due to large scatter of the available test data and the scarcity of data for concrete compressive strengths above 14 ksi, validation tests such as eccentric bracket tests and large-scale flexural members are needed. Unless the experiments show the existing relationship to be unreliable, only the stress block parameters need to be calibrated. To the extent possible, a seamless transition would be suggested between the normal strength concrete and high-strength concrete. The detailed analysis and discussion for collected data would be provided in Chapter 4.

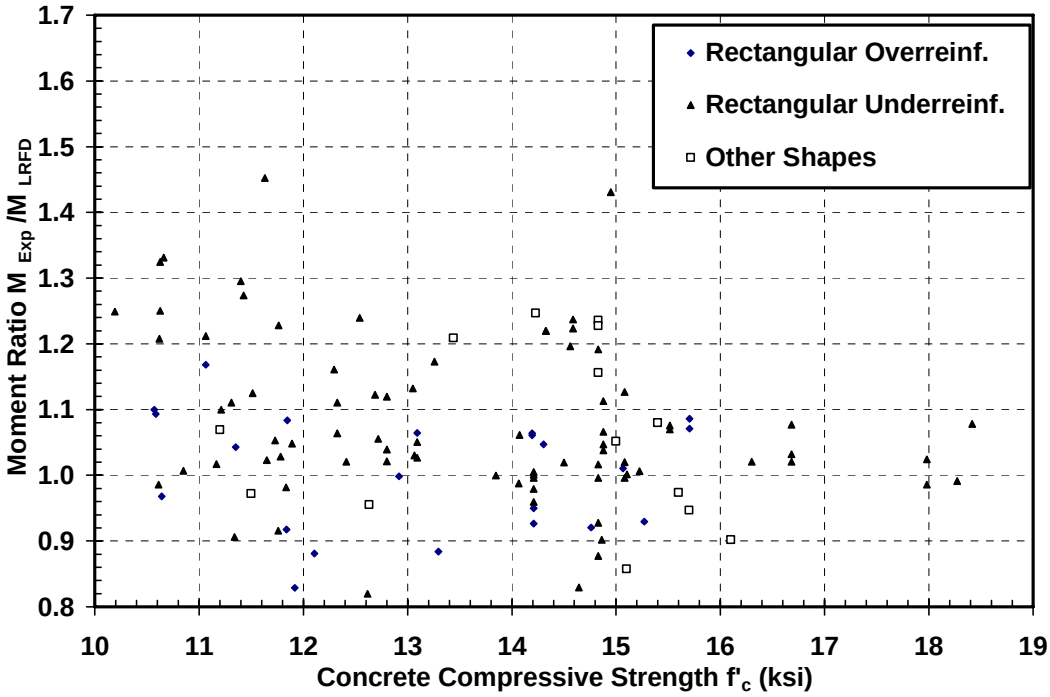

Figure 2-6 Comparison of the Experimental and Predicted Values of Flexural Resistance Using the LRFD Specifications

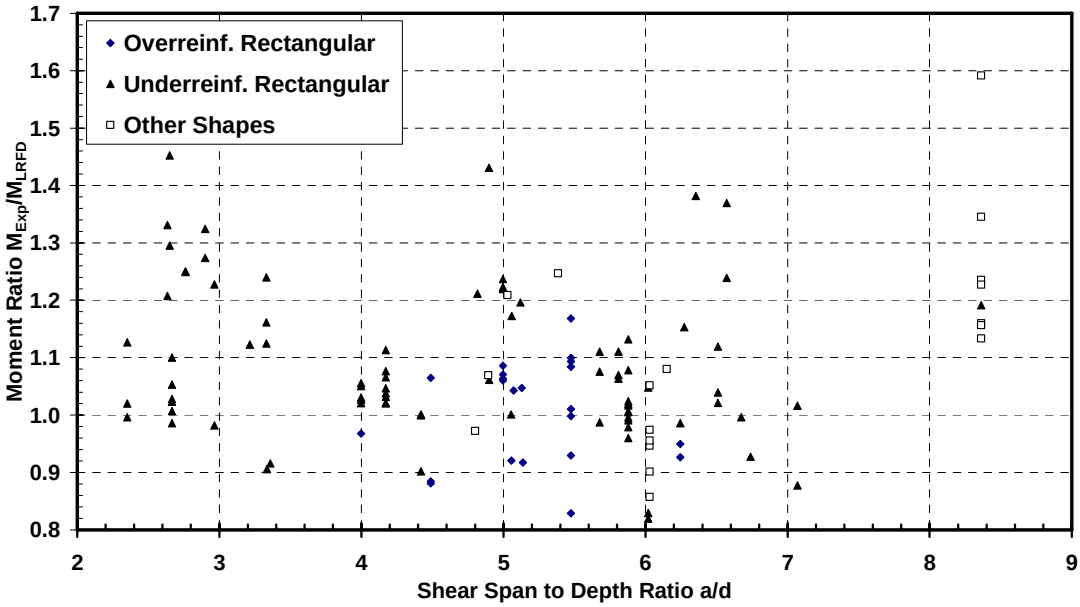

Figure 2-7 Effect of Shear Span to Depth Ratio on Flexural Resistance

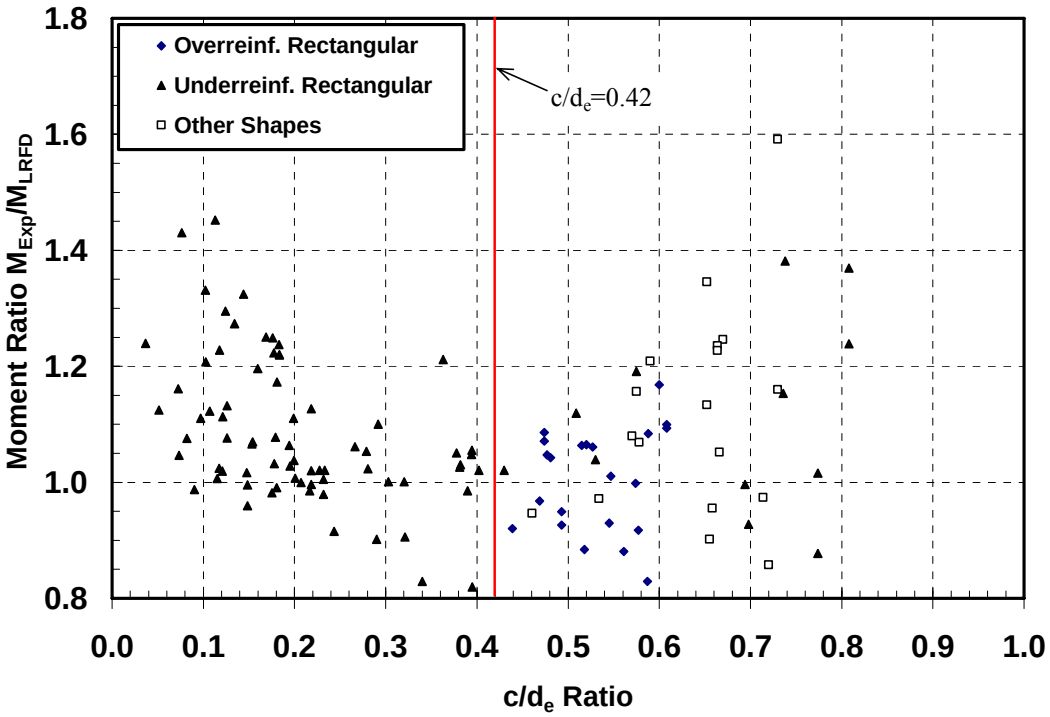

Figure 2-8 Comparison of the Experimental and Predicted Values of Flexural Resistance Using the LRFD Specifications as Function of c/d_e Ratio

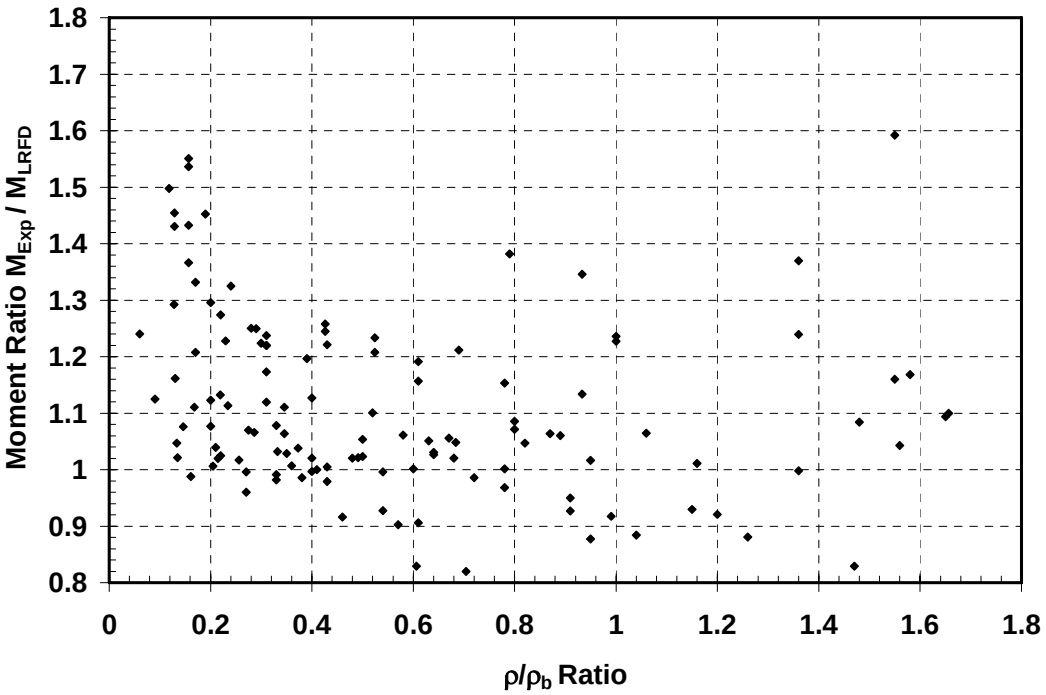

Figure 2-9 Comparison of the Experimental and Predicted Values of Flexural Resistance Using the LRFD Specifications as Function of ρ/ρ_b Ratio

2.4 Cracking Moment and Crack Width

Cracking moment is generally written as function of modulus of rupture and section modulus. Significant research efforts have been put on the determination of the modulus of rupture. The literature review suggests values for the modulus of rupture of high-strength concrete in the range of $0.24\sqrt{f'_c}$ to $0.38\sqrt{f'_c}$ ksi. Carrasquillo et al. (1981) suggested the higher value of $0.37\sqrt{f'_c}$ for concrete compressive strengths of up to 12 ksi.

ACI 363-R92 (1997) indicates that for high-strength concrete members, there is sufficient experimental evidence to merit an increase in the allowable tensile stresses to a higher factor of $\sqrt{f'_{ci}}$ or $\sqrt{f'_c}$ than is currently specified, due to higher modulus of rupture of high-strength concrete. On the other hand, it has been established that autogenous shrinkage strain for high-strength concrete is larger than that of normal strength concrete, which makes the effect of restrained shrinkage for high-strength concrete members a more significant issue. To take this effect into account, a factor has been introduced in some foreign codes (Australian Standard for Concrete, AS3600). Due to the co-existence of tensile creep and slippage between the concrete and reinforcement, the mechanism of the restrained shrinkage is very complicated and the current methods of determining the generated stresses are not accurate.

Control of crack width is important primarily for both aesthetics and durability of the structure. Due to the complexity of this issue and scatter of the data, the AASHTO LRFD Specifications do not provide an explicit equation for calculating crack width. In the 2004

and previous editions, a crack width parameter Z was used, and the tensile stress of the mild steel reinforcement was limited to $0.6f_y$. In the 2005 Interim edition, crack width control was performed by limiting the spacing of mild steel in the layer closest to the tensile face, which is based on a physical crack model (Frosh, 2001).

2.5 Deflection at Service Level

It is well established that deflection of concrete beams under service load is determined using elastic analysis. For beams subjected to four-point bending, the deflection at mid-span can be expressed as:

$$\Delta_c = \frac{Pa}{48E_cI_{eff}}(3L^2 - 4a^2) \qquad \text{(Equation 2-7)}$$

where P is the total applied load, L is the span of the beam, a is the shear span, E_c is the modulus of elasticity of concrete, and I_e is effective modulus of inertia. This method assumes the section has an average effective moment of inertia (I_e), which takes into account the effect of cracking. Various expressions are proposed for I_e over the years. However, it seems that all researchers have agreed that the lower bound of I_e is the moment of inertia of the cracked section, which is determined from force equilibrium of the section.

The most commonly adopted method to determine the effective moment of inertia was proposed by Branson (1963) and adopted in ACI 318-71. A statistical study of short-term deflection of simply-supported beams by ACI Committee 435 in 1972 reported that for controlled lab conditions there is a 90 percent confidence that deflections fall within -20 percent to +30 percent of the calculated value. However, Branson's equation seems to

under-estimate the deflection for high-strength concrete members. Rashid and Mansur (2005) summarized test data for high-strength concrete from seven projects, which include 71 beam tests. They reported that the current method underestimates the deflection for majority of the cases for high-strength concrete members, and attributed this discrepancy to the difference in the elastic modulus of the concrete.

2.6 Ductility

Test data on ductility of high-strength concrete beams is quite limited. A total of 55 high-strength concrete beam tests have been reported in six different research publications, three of which used curvature ductility (Weiss and Shah, 2001, Sarkar and Adwan, 1997, and Suzuki, 1996), two used displacement ductility (Pam and Kwan, 2001, and Bernhardt and Fynboe, 1986), and only one reported rotation ductility (Alca and Macgregor, 1997). All beams were of rectangular section, and were tested in four-point bending. Only the specimens by Pam and Kwan (2001) included stirrups. Test results indicate that in the absence of confinement in the constant moment region, the dominant factor in determining the load-deflection curve of the member is the c/d_e ratio. Ductility of the member is greatly reduced, as this ratio increases.

Figures 2-10 and 2-11 show the measured curvature and displacement ductility as functions of c/d_e ratio, respectively. Weiss and Shah (2001) considered failure of the specimen at 25 percent strength reduction, whereas Sarkar and Adwan (1997) used 30 percent strength reduction to signify failure. Suzuki (1996) considered the actual collapse of the beam. Although not shown in the graphs, rotation ductility of beams tested by Alca and Macgregor

(1997) ranged between 1.5 and 2.8 for the c/d_e ratios between 0.38 and 0.47.

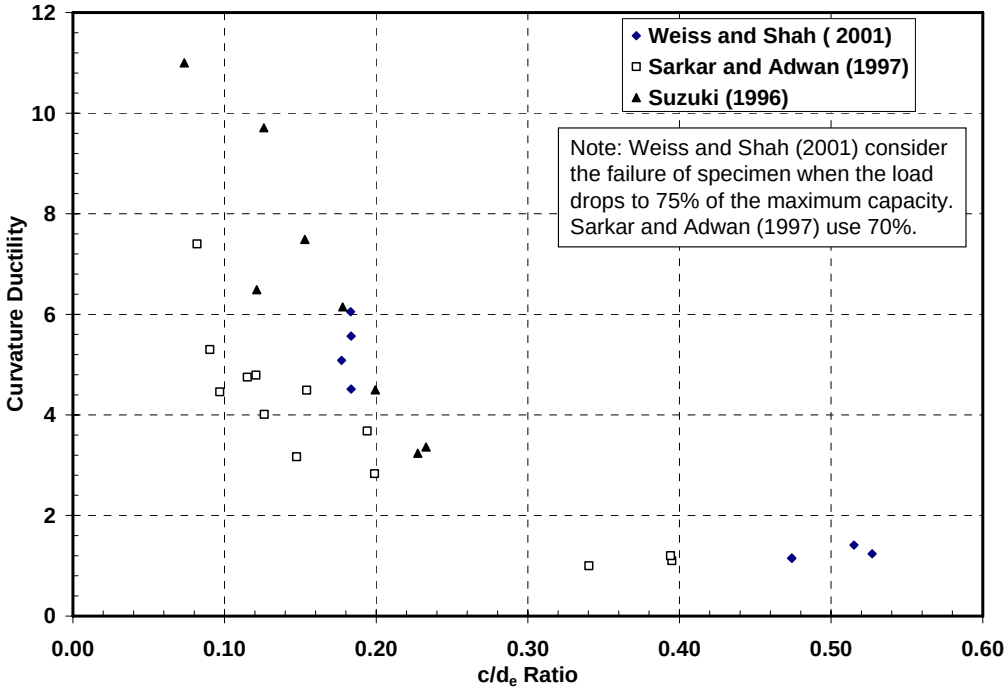

Figure 2-10 Effect of c/d_e Ratio on Curvature Ductility

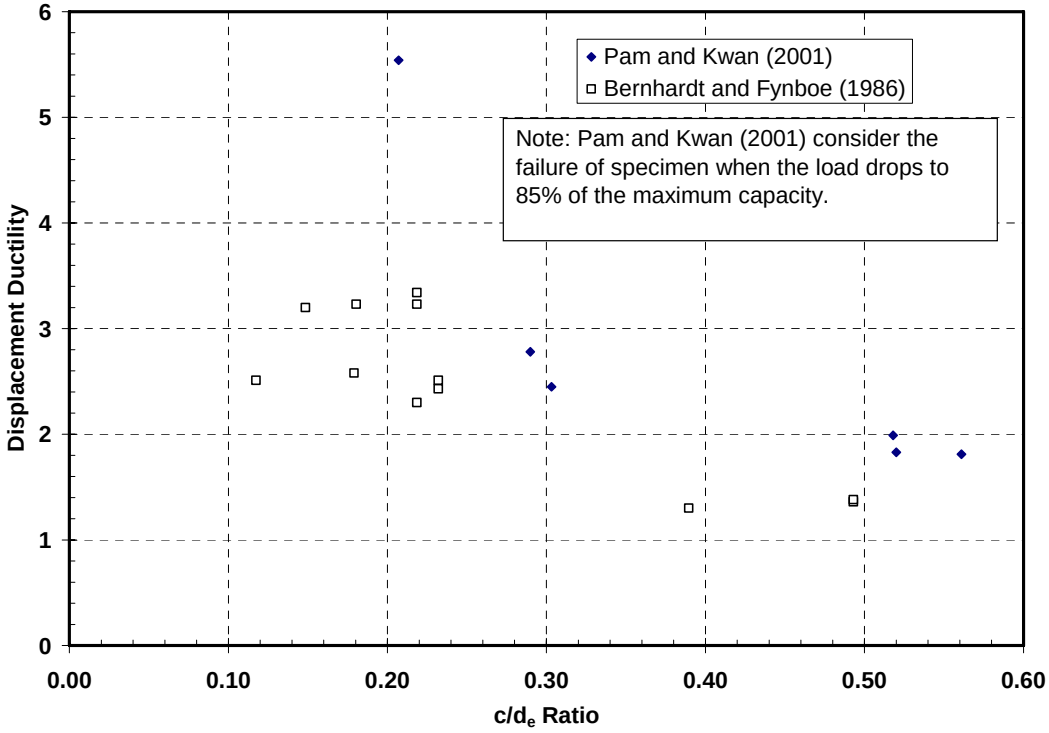

Figure 2-11 Effect of c/d_e Ratio on Displacement Ductility

3 EXPERIMENTAL PROGRAM

3.1 Test Plan

A detailed experimental program was carried out with the following three different components to evaluate the behavior of high-strength concrete members under pure and axial-flexural loading:

1) Pure flexure tests: A total of fourteen specimens were tested under monotonic loading in four-point flexure to achieve the following objectives:
    1. Determine the ultimate compressive strain of the high-strength concrete beams;
    2. Investigate the flexural resistance of beams in pure flexure and validate the stress block parameters for flexural members;
    3. Evaluate the serviceability of high-strength concrete beams for cracking and deflections;
    4. Verify the applicability of analytical models typically used for prediction of moment-curvature and load-deflection responses to high-strength concrete members in pure flexure;
    5. Investigate ductility of high-strength concrete beams.
2) Axial-flexural tests: A total of five specimens were tested under monotonic loading in four-point flexure with a constant axial load to achieve the following objectives:
    1. Determine the ultimate compressive strain of the high-strength concrete beam-columns;
    2. Investigate the flexural resistance of beam-columns under axial-flexural loading and validate the stress block parameters; and

3. Verify the applicability of analytical models typically used for prediction of moment-curvature and load-deflection responses to high-strength concrete members subjected to axial-flexure loading.

3) Ancillary material property tests: The main objective of these tests was to provide material properties for analysis. Three 4 in. x 8 in. cylinders and three 6 in. x 6 in. x 20 in. plain concrete beams were tested after each testing of beam or beam column specimens to obtain the concrete compressive strength and the modulus of rupture, respectively. Reinforcement bars were tested under monotonic tensile loading (ASTM 496) to obtain the stress-strain relationship of the steel. Cores were taken from some of the specimens after testing to examine the difference in material properties between the concrete cylinders and the flexural specimens.

3.2 Pure Flexure Tests

3.2.1 Test Specimens

The overall test matrix for pure flexure tests is shown in Table 3-1 Thirteen high-strength concrete beams were cast in five batches, named as follows; the first two digits of the specimen name identify the target concrete strength; the letter "B" representing beam specimens; the last two or three digits indicating the percentage of reinforcement ratio,. The compressive strength of each beam, shown in the table, is based on the average compressive strength of three 4 in. x 8 in. inch concrete cylinders. These cylinders were kept beside the specimen, subjected to the same curing condition and tested on the same day of testing the specimen. This is believed to better represent the true concrete strength than the cylinder

tested at 28 day. Modulus of rupture, reinforcement ratio, cross section and effective depth of reinforcement for each specimen are also shown in this table.

Test parameters include concrete strength, shape of cross section, and reinforcement ratio. The following parameters were included for the purpose of developing the test matrix for these tests:

- **Concrete Compressive Strength**: Three target strengths of 10, 14, and 18 ksi were used. It was decided that three mixes would provide a more realistic spread within the range without much overlap. The achieved concrete strength at date of testing for each specimen is shown under column "f'_c" in test Matrix in Table 3-1. It should be noted that the three specimens in the group of Cast 3 were designed to achieve a compressive concrete strength with 18 ksi. Due to their lower strength achieved, they were considered as duplicates for specimens with concrete strength of 14 ksi. Unfortunately, concrete in Cast 4 did not reach 18 ksi either.
- **Longitudinal Reinforcement**: In order to investigate the under-reinforced and over-reinforced conditions as well as the acceptable strain limits, three different reinforcement ratios were considered; $½\rho_b$, ρ_b, and $1.2\rho_b$, where ρ_b represents the balanced reinforcement ratio to develop a strain of 0.002 in the extreme layer of tensile reinforcement, simultaneously with the crushing strain of 0.003 in the extreme compression fiber in concrete at the time of failure. All reinforcement was of Grade 60 ksi steel.
- **Specimen Size and Shape**: All specimens were originally designed to have 9 in. x 12 in. rectangular sections, and to be tested with a flexural span of 120 in. Actual

lengths of the specimens were 2 ft. longer than the designed flexural span. The cross section was originally selected to correspond to the specimens in pure compression, so that the moment-thrust interaction diagram could be developed for this cross section. After testing the first two batches of specimens with concrete strengths of 10 ksi and 14 ksi, it was found the measured values of α_1 and β_1 factors determined from the eccentric bracket specimens were higher than the code value. Meanwhile, the measured ultimate strain of concrete was also higher than 0.003. As a result, the longitudinal reinforcement yielded before crushing of concrete for all the specimens with rectangular sections. To achieve the goal that the specimen crushed before yielding of the longitudinal reinforcement, it was found necessary to redesign the pure flexure specimen with target strength of 18 ksi. Specimens with inverted T-section were made to accommodate the need for enclosing the high amount of reinforcement. To reduce the shear demand, the span was increased from 10 feet to 13 feet. The same inverted T-sections were used for the repeated specimens to study the behavior of over-reinforced sections for the 10 ksi and 14 ksi target strengths.

- **Transverse Reinforcement**: All specimens were reinforced to avoid shear failure. The amount of transverse reinforcement in a member was calculated based on AASHTO LRFD specification requirement and the shear demand. However, no transverse reinforcement was used in the constant moment region in the middle third of the span length. All transverse reinforcement was No. 4 ties of Grade 60 ksi steel.
- **Cover Concrete**: Specimens with rectangular cross section were made with 1/2 in clear cover to the transverse reinforcement. For specimens with inverted T-section,

the clear cover at the bottom was controlled by the size of the hoop reinforcement in the flange and was greater than 2.5 inches.

3.2.2 Specimen Fabrication

Figure 3-1 shows typical formwork for pure flexure specimens. Figure 3-2 shows reinforcement details. No stirrup or compression reinforcement was provided within the constant moment zone. A small piece of No.4 rebar was tied to the steel cage as spacer to maintain a clear cover of 1/2 in.

The cross-section of the formwork for the inverted T-beams is shown in Figure 3-3. These specimens were cast upside down for ease of placement. Figure 3-4 provides an overview of the inverted T-beams before casting. The reinforcement details for an over-reinforced specimen, with a reinforcement ratio of 17.7 percent, are shown Figure 3-5. Steel spacers were used to position the longitudinal reinforcement. The steel cages were tied directly inside the formwork.

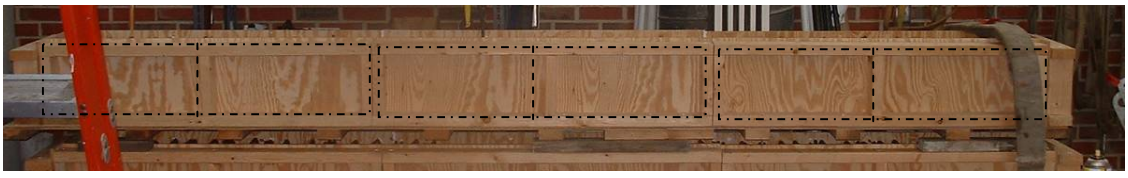

Figure 3-1 Formwork for the Pure Flexure Specimens

Table 3-1 Test Matrix for the Pure Flexure Specimens

Cast	Specimen No.	f'_c (ksi)	f_r (psi)	ρ (%)	Rebar Size and Number	d (in)
Cast 1	10B2.1	11.4	618	2.1	2 No.9	10-3/8
	10B4.3	11.5	603	4.3	2 No.9	10-3/8
					2 No.8	7-3/4
	10B5.7	11.2	607	5.7	2 No.10	10-3/8
					2 No.9	7
Cast 2	14B3.3	13.1	865	3.3	2 No.11	10-3/8
	14B7.7	13.4	858	7.7	2 No.11	10-3/16
					2 No.11	7-1/2
	14B12.4	14.2	836	12.4	2 No.14	10-1/8
					2 No.14	7-1/4
Cast 3	14B7.6	15.4	1475	7.6	3 No.9+2 No.8	10
	14B12.7	15.0	1498	12.7	5 No.11	10-3/16
	14B17.7	15.6	1413	17.7	7 No.11	10-3/16
Cast 4	18B5.9	15.7	963	5.9	2 No.9+2 No.8	10
	18B12.7	16.1	936	12.7	5 No.11	10-3/16
	18B17.7	15.1	965	17.7	7 No.11	10-3/16
Cast 5	10B10.2	12.6	812	10.2	4 No.11	10-3/16

Figure 3-2 Formwork and Steel Cage for the Pure Flexure Specimens

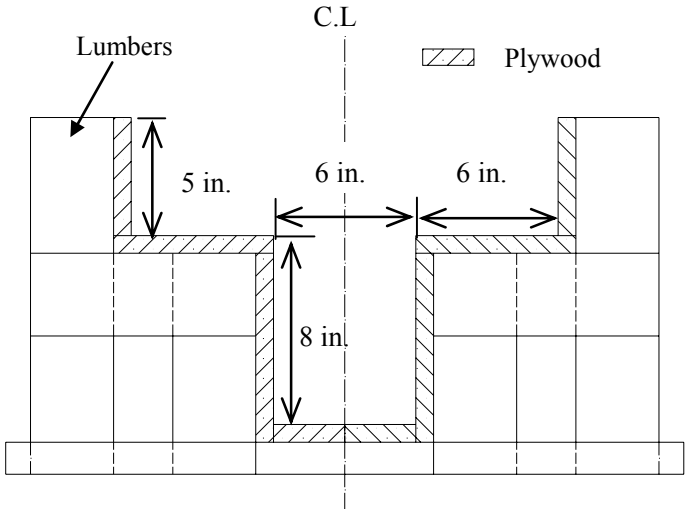

Figure 3-3 Cross-section of Formwork for Specimens with Inverted T-beams

Figure 3-4 Formwork for the Pure Flexure Specimens with Inverted T-Section

Figure 3-5 Reinforcement Details for Over-reinforced Pure Flexure Specimens

Concrete was placed directly from a ready-mixed delivery truck, and was consolidated using an immersion type vibrator. After casting, the top surfaces were covered with polystyrene sheets to maintain a moist environment for 2 hours. Specimens were demolded one day after casting and then covered with burlap for 7 days. Ice was used for curing in summer. After 7 days of moist curing, specimens in the first 2 casts were air cured in the lab until the day of testing. Specimens with inverted T-sections were kept outside of the lab. Specimens in cast 4 and 5 were prepared in fall 2005. Even though for the majority of the time, temperature is above freezing and there was no snow in winter 2005 in Raleigh, these specimens experienced a few freeze and thaw cycles during that winter.

3.2.3 Instrumentation

The primary objective of the instrumentation for the pure flexure specimens was the strain distribution profile as well as the deflection at mid-span. The strain of concrete at the extreme compressive fiber was measured over the entire constant moment zone to examine the ultimate strain of concrete. Deflections were also measured under the loading points and

at the supports.

Two types strain measurement devices were used: strain gauge type transducer and electrical resistance strain gauges. Strain gauge type transducer, which is also called pi-gauge, (TML, Tokyo Sokki Kenkyujo Co.), was used to measure the average strain of concrete surface over the gage length. The gauge lengths of 4 in. or 8 in. were used, which were deemed sufficient for minimizing the effect of a localized strain near cracks. Gauges were calibrated using a caliber (Mitutoyo Corporation) with an accuracy of 1/2500 in every time before testing. A 4 in. pi-gauge and the calibration kit are shown in Figure 3-6. The accuracy of pi-gauges was within ± 5 percent. Figure 3-7 shows the instrumentation on top surface of the beams. Pi-gauges were also attached to the sides and bottom of the specimens to measure the strain profile of the section at mid-span. Pi-gauges were also used with demec points, which were tack welded to the longitudinal reinforcement to measure the average longitudinal strain of the steel rebars, as shown in Figure 3-8. Two, 1-1/4 in long No4 reinforcing bars were tack welded to the longitudinal rebars, about 9 in. apart from each other. The two bars were then covered with styro-foam to separate them from the surrounding concrete. It is generally acknowledged that there is localized strain of steel reinforcement near the tensile cracks of the concrete. As a result, the reading of strain gauge directly attached to the longitudinal rebars may not be representative and can only be used as a reference. The benefit of using the demec points is that they provide an average strain of the steel between the two points. However, fabrication of this type of demec point is not simple and quality control is hard to achieve. Moreover, the demec point creates a weak section and affects the crack pattern of the section. As a result, this type of instrumentation was used only for the beams with

rectangular sections.

Electrical resistance strain gauges (TML, Tokyo Sokki Kenkyujo Co.) were also used to measure the strains. The major concern for choosing the gauge length was that it would to be long enough to represent the behavior of concrete as a composite material rather than the aggregates or the mortar alone. Since the maximum aggregate size in the concrete is 3/8 in, strain gauges with 2.4 inches length (TML, PFL-60-11-3L) were selected to measure the compressive strain of concrete. In a few specimens, gauges with 0.2 in length (TML, YFLA-5-3L) were used to measure the strain of longitudinal reinforcement. Gauge factors, as provided from the manufacture, were used in the data acquisition system without calibration.

Two types of instruments were used to measure mid-span or support deflections; cable-extension transducers (wire potentiometers) with 15 in stroke (PT-100 Series by Ametek Transducer Products, Inc.), and potentiometers with 3 in maximum stroke (BEI Duncan Electronics Division Sensors & Systems company), as shown in Figure 3-9. Deflection transducers were calibrated every time before testing using the calibration kit (Mitutoyo Corporation) shown in Figure 3-10. There is no substantial difference between the two types of the transducers. The cable-extension transducers were mainly used for measuring the deflections at mid-span, especially when the expected deflection was equal or greater than 3 in. as shown in Figure 3-11. On the other hands, the potentiometers were mainly used to measure smaller deflection such as those at the supports, as shown in Figure 3-12.

Figure 3-6 Pi-gauge and Calibration Kit

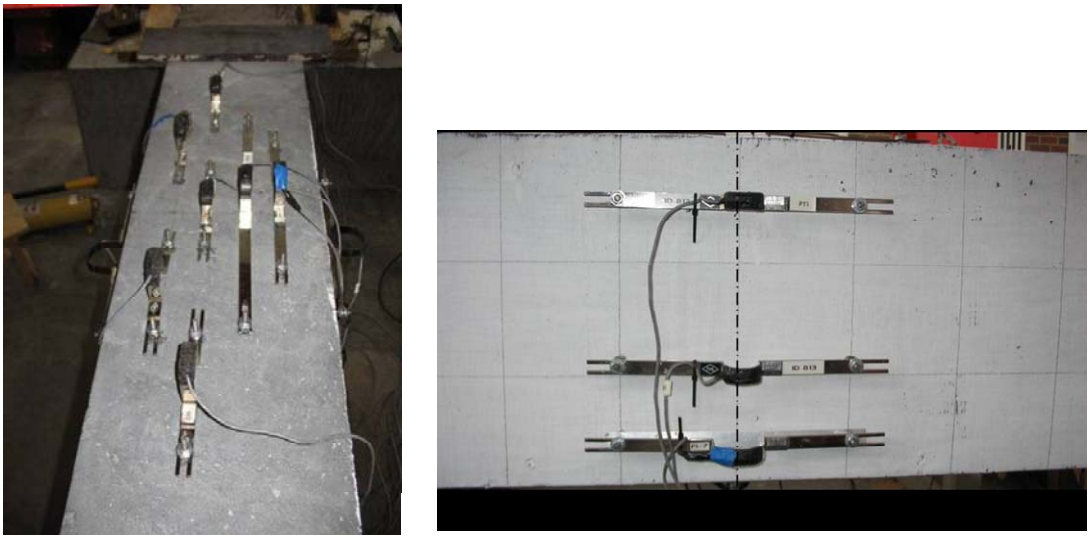

Figure 3-7 Pi-gauge and Instrumentation on the Beam

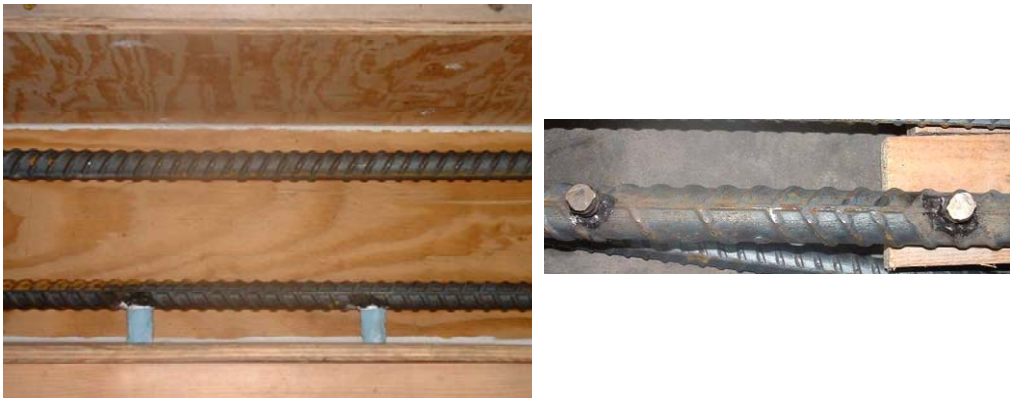

Figure 3-8 Demec Points to Measure Longitudinal Strains in Reinforcing Steel

Figure 3-9 Cable-extension Transducers (Left) and Potentiometer (Right)

Figure 3-10 Calibration Kit for Cable-Extension Transducers and Potentiometers

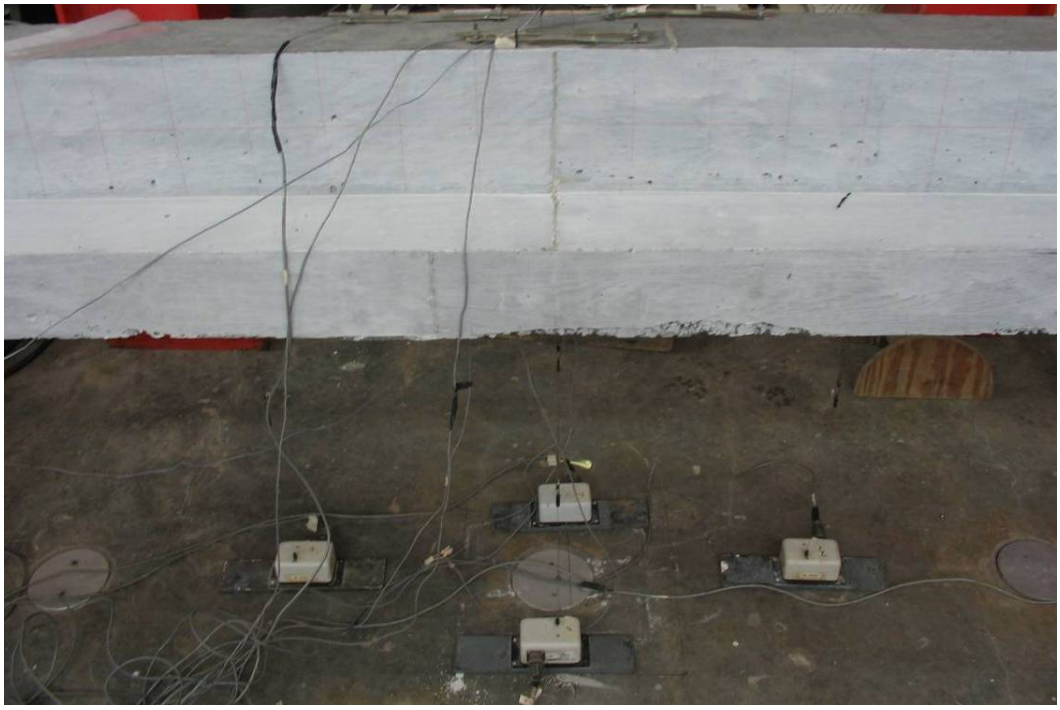

Figure 3-11 Wire Potentiometers to Measure Deflection at Mid-span

Figure 3-12 Potentiometers for Measuring the Support Subsidence

A computer controlled high-speed OPTIM Megadac data acquisition system was used throughout the testing program. During each test, electronic signals from instrumentation were transferred by the data acquisition system and stored in the computer using an excel sheet.

3.2.4 Test Setup and Procedure

The pure flexure specimens were tested using a MTS hydraulic actuator (MTS Systems Corporation) with a maximum capacity of 220-kips as shown in Figure 3-13. The test frame was tied to a 2 1/2 ft strong floor with a pretensioned force at each of its supporting steel columns. The applied load was measured using a built-in load cell with an accuracy of 50 lbs.

Figure 3-13 MTS Hydraulic Actuator and Testing Frame

Figure 3-14 shows a typical setup for testing of pure flexure specimens with rectangular sections. A 4 1/2 ft long steel spreader beam was used to distribute the load, as shown in Figure 3-14. The spreader beam was fixed to the bottom of the actuator; and loaded the beam with a constant-moment zone of 33 1/4 in. Specimens with rectangular cross-section were set on a pair of steel hinge-roller support with clear span of 10 ft. In testing of specimens with inverted T-section and 13 ft flexural span, neoprene plates were used in lieu of the steel rollers to support the 18-in. wide flange, as shown in Figure 3-15.

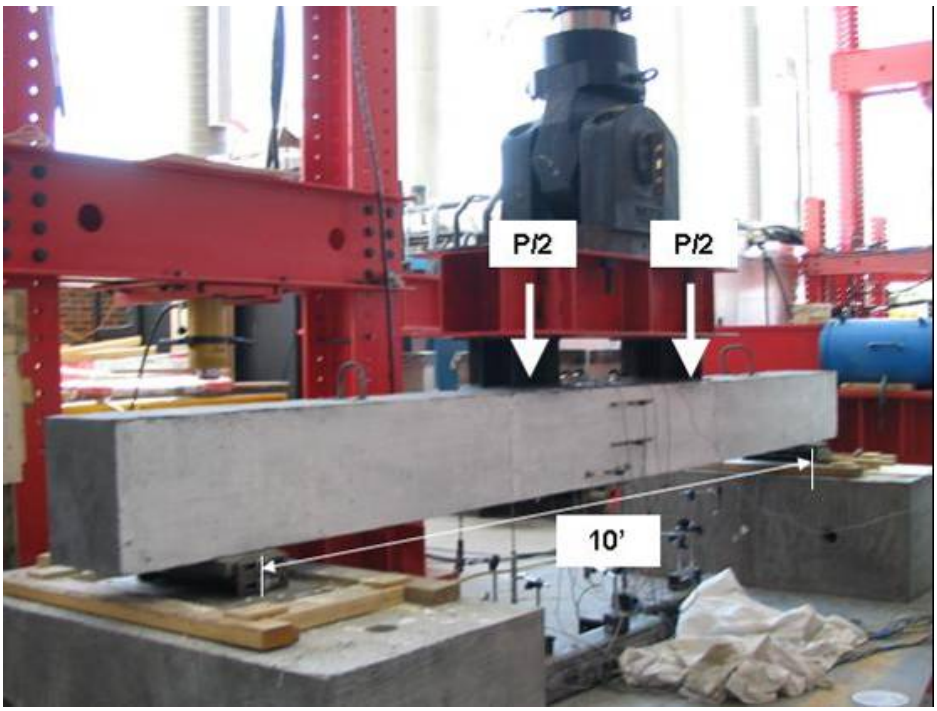

Figure 3-14 Test Setup for Pure Flexure Specimens with Rectangular Section

After placing and positioning of each specimen on the support, side surfaces were painted white using latex paint, and were then grid-marked to facilitate mapping the cracks patterns. Steel studs were attached to the specimens using epoxy and cured for 24 hours before mounting the calibrated transducers.

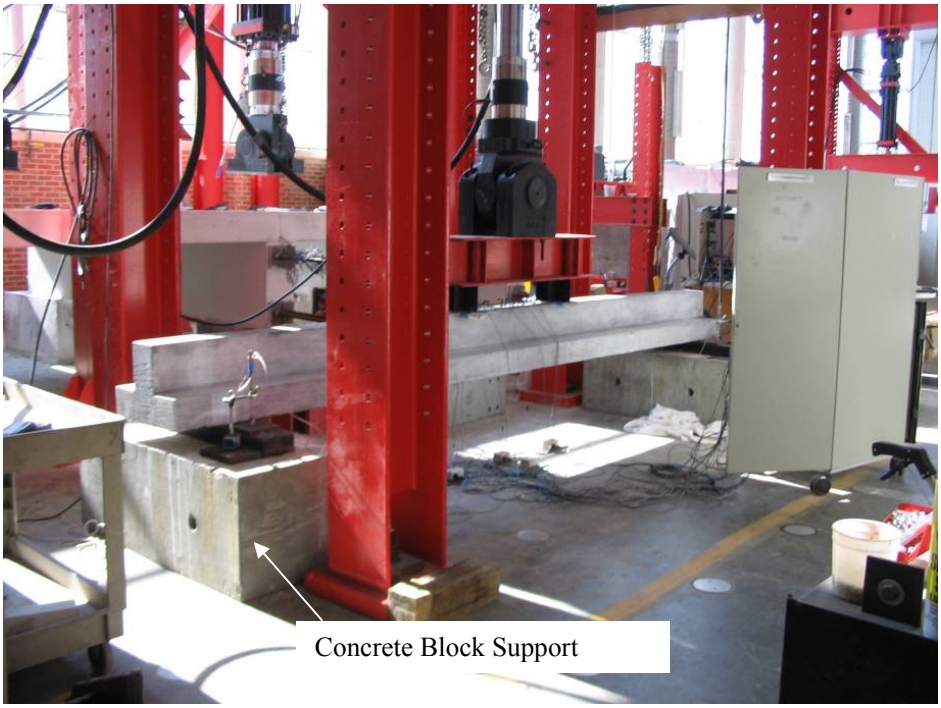

Figure 3-15 Test Setup for Pure Flexure Specimens with Inverted T-section

MTS hydraulic actuator was operated in the displacement control mode. An initial displacement rate of 0.02 in/min was applied before the first cracking of the beam, after which it was increased to a constant rate of 0.04 inch/min. Each specimen was tested in less than an hour to minimize the potential creep effect. Test was paused for 5-10 seconds after 10 kip of load was applied to allow checking the stability of the entire loading system. Visual inspection and marking of the cracks were carried out up to 80 percent of the predicted failure load. Tests were terminated after crushing of concrete at the constant moment zone.

3.2.5 Test Observations and Failure Modes

After white latex paint was applied to the surface of the specimens, some hair-line cracks were noticed in a few of specimens before testing. These cracks were attributed to the

autogenous shrinkage of concrete and were marked accordingly.

Two types of cracks were observed during the tests; vertical flexural cracks and diagonal flexure-shear cracks. Flexural cracks were observed from the early stage of the loading, usually around 10-15 percent of the ultimate load. The cracks were spaced between 3 inches and 6 inches, with an average of about 4 inches. Spread of these cracks was affected by the reinforcement ratio, as specimens with higher reinforcement ratio tend to have a deeper compression zone. For over-reinforced specimens, all flexural cracks stopped propagating upward after they reach a certain level, somewhere below the neutral axis. For the under-reinforced specimens, the cracks shifted further upward after the yielding of longitudinal reinforcement, along with shifting of neutral axis. Cracks in shear span were also observed and marked during the test. Since the specimens were heavily reinforced to avoid shear failure, diagonal shear cracks were relatively few and minor.

Figure 3-16 shows the failure mode of an under-reinforced specimen (10B2.1) with a rectangular cross section. Figure 3-17 shows failure of a beam due to crushing of concrete (10B5.7). Prior to failure, crushing of concrete occurred in the top 4 in. as shown in this figure using dashed lines. Due to the absence of stirrups, which could restrain the propagation of the cracks, crushing of the entire test zone followed immediately. The crushing of concrete was sudden and explosive, as shown in Figure 3-18, which is a snapshot at the moment of crushing of concrete for an over-reinforced specimen (14B12.4). The two diagonal cracks propagated downward until they intersected each other (see Figure 3-18), or when they were restrained by the longitudinal reinforcement (see Figure 3-17). This was the

typical failure mechanism for all tested beams.

The cracking pattern and failure mode of the specimens with inverted T-section were similar to those of the specimens with the rectangular sections. Typical mode of failure observed from one of the 14 ksi specimens is shown in Figure 3-19.

Tests were terminated after crushing of concrete near the top surface accompanied by sudden drop in the applied load. After the actuator was lifted up and the load was removed, some residual deflection was observed for the under-reinforced specimens.

Figure 3-16 Typical Failure Mode for Under-reinforced Specimens (10B2.1)

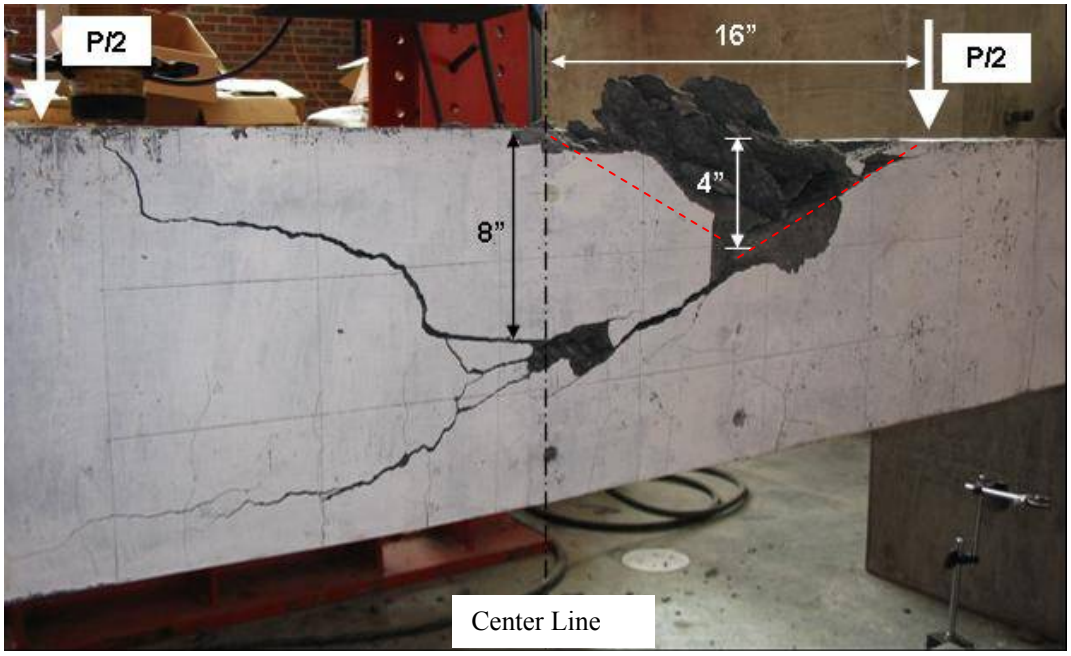

Figure 3-17 Typical Shape of Failure Zone for Over-Reinforced Specimens (10B5.7)

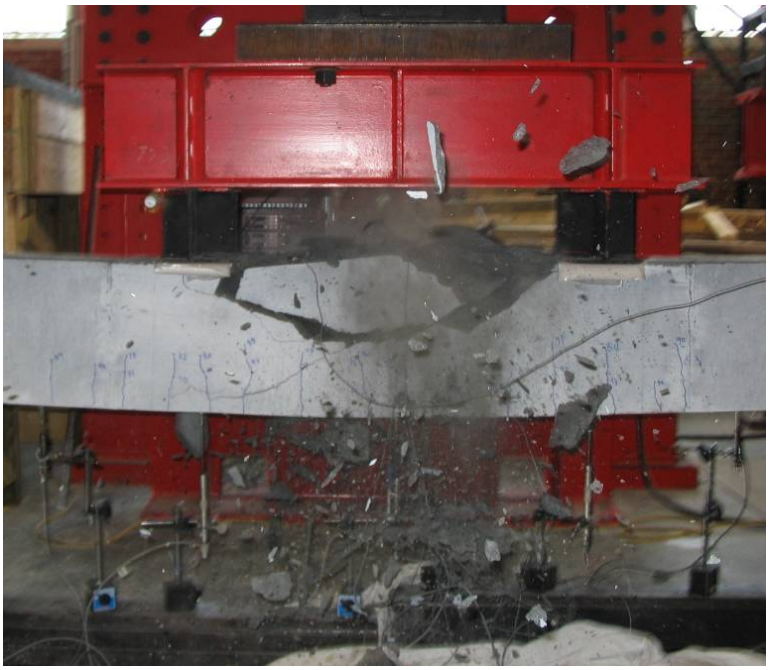

Figure 3-18 Typical Failure Mode for Over-Reinforced Specimens (14B12.4)

Figure 3-19 Typical Failure Mode of Flexural Specimens with Invert T-Section (18B12.7)

3.2.6 Test Results and Discussions

In this section, test results for various aspects of the pure flexure specimens are presented and discussed.

3.2.6.1 Ultimate Compressive Strain of Concrete

In the AASHTO LRFD Specifications, “maximum usable strain of concrete” refers to the strain at which concrete crushes. Meanwhile, this strain is also used for determining the strain profile and ductility of a section. For over-reinforced specimens, the strain profile is also critical in determining the nominal resistance of the member. If a member is tested in displacement control mode, as such in the present study, there is a small time lag between peak load and the crushing of concrete. Therefore, the compressive strain of concrete at these

two stages of the loading, are reported separately, in Figures 3-20 and 3-21.

At least three pi-gauges were attached to the top surface of each specimen to monitor the compressive strain of concrete during the test. The measured strain values depended on the location of the gauge relative to the failure region. If a gauge was right above of the zone where concrete was crushed, it provided the largest strain readings. Only the largest reading of each specimen is reported here. It should be noted that as the pi-gauges were mounted about ½ in above the concrete surface, their original readings were adjusted accordingly based on the measured strain profile.

It can be seen from Figures 3-20 and 3-21 that the ultimate strain of concrete is more or less independent of the strength of concrete. When the specimen reaches it is peak resistance; all but one under-reinforced specimen had concrete strain reading greater than 0.003. Even for this particular specimen, the strain reached 0.0037 when concrete crushed.

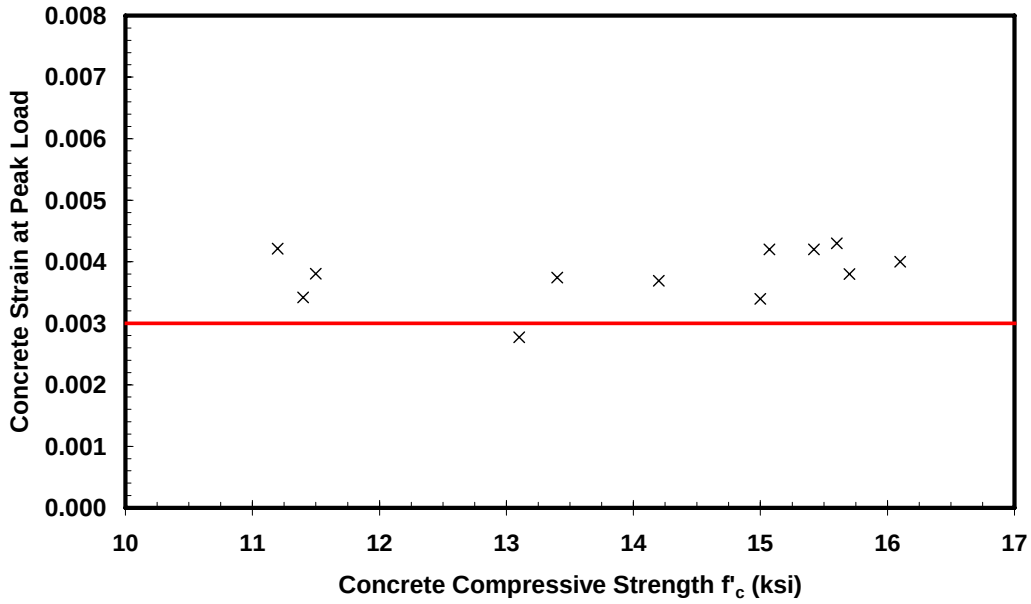

Figure 3-20 Compressive Strain of Concrete at Peak Resistance for Pure Flexure Specimens

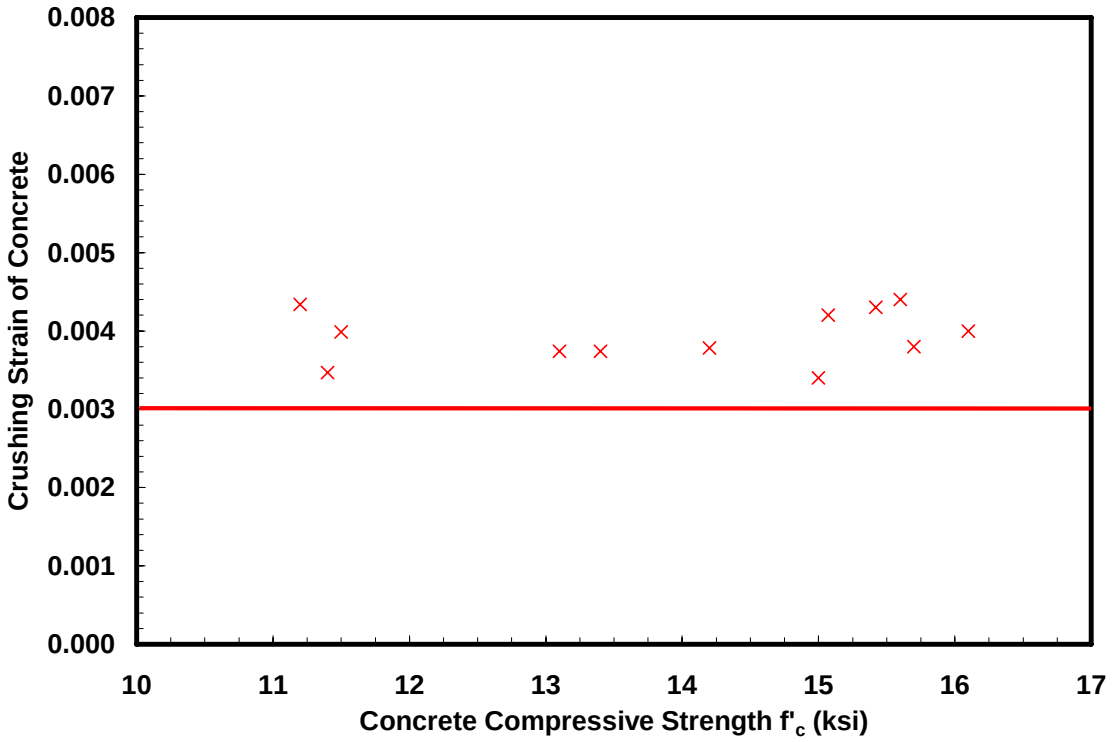

Figure 3-21 Crushing Strain of Concrete at the for Pure Flexure Specimens

3.2.6.2 Moment-Curvature Response

The moment-curvature response at mid-span for the pure flexure specimens are shown in Figures 3-22 to 3-26. Curves are grouped together for specimens in the same cast of concrete to facilitate the comparison.

Derivation of the curvature at mid-span required regression analysis of the measured strain data. Even though each pi-gauge was carefully calibrated and attached to the specimen before testing, their readings were quite sensitive to the cracks close to the steel studs. The cracks would compromise the bond between the steel stud and concrete surface. The original data from the pi-gauges were checked before using for regression analysis. The readings of each gauge were first plotted to check for consistency. Also, one reading of each gauge was extracted and plotted at every 10 kips of loading. The strain profile could be located by comparing the readings from a series of Pi-gauge at different depth. Those pi-gauges (usually 1 or 2 for each specimen) with apparent erroneous or inconsistent data relative to the overall strain were discarded.

At each particular load level, moment-curvature response was derived based on the "linear regression" results of readings of a set of 4-5 pi-gauges attached to the top, bottom and side of the specimens. For all but one specimen (18B5.9), the square of Pearson correlation coefficient was greater than 0.98, which indicated good linearity and that the assumption of "plane sections remain plane" was valid at mid-span. For Specimen 18B5.9, with bad pi-gauge readings, strain gauge readings of the longitudinal reinforcement were used, instead. Theoretically, the slope of the moment-curvature curve reduces after cracking. This trend,

however, was not detected in all tested specimens, possibly because some specimens were cracked before testing. The curves present good linearity after cracking up to the yielding of the bottom layer of reinforcement for under-reinforced specimens. A cursory review of the curves indicates that as the reinforcement ratio increases, the capacity and stiffness of the section both increase, but the ultimate curvature decreases. However, once the reinforcement ratio is higher than the balanced ratio, additional reinforcement does not enhance the stiffness very much. This trend can be observed in Figures 3-25 and 3-26 by comparing the behavior of Specimen 14B12.7 with 14B17.7, and 18B12.7 with 18B17.7. Similarly, strength of the specimen hardly benefited from additional reinforcement once the reinforcement ratio exceeded the balance ratio. It can be seen in Figure 3-26 that Specimen 18B12.7 has a higher resistance than specimen 18B17.7. This is not a surprise, because the strength of the specimen is dominated mainly by the strength of concrete for over-reinforced members; and concrete in Specimen 18B12.7 has a higher compressive strength.

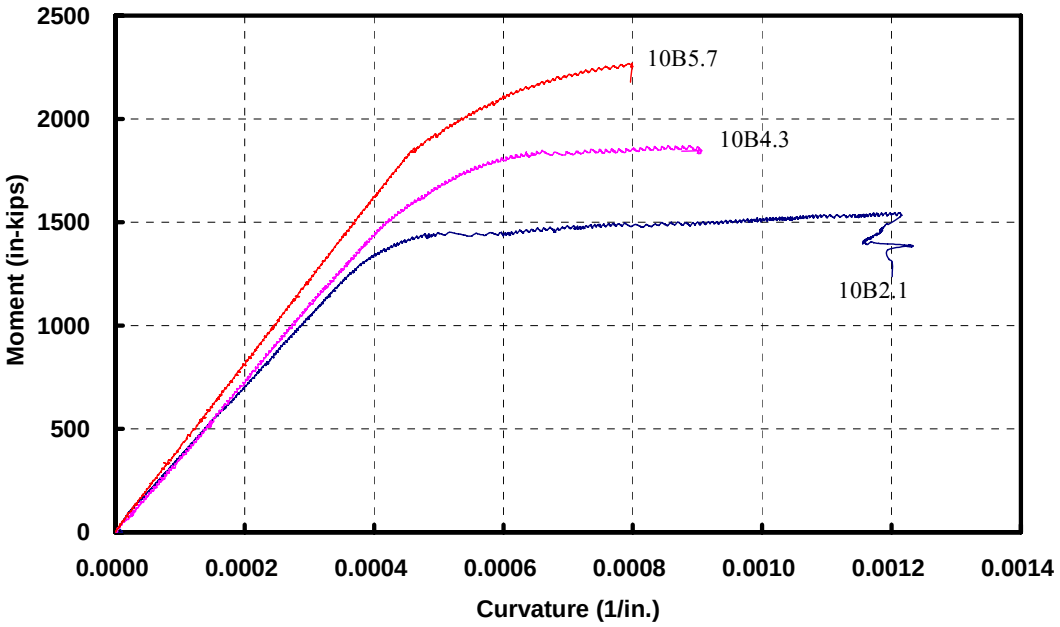

Figure 3-22 Moment-Curvature Response for Pure Flexure Specimens with Rectangular Section and Target Strength of 10 ksi

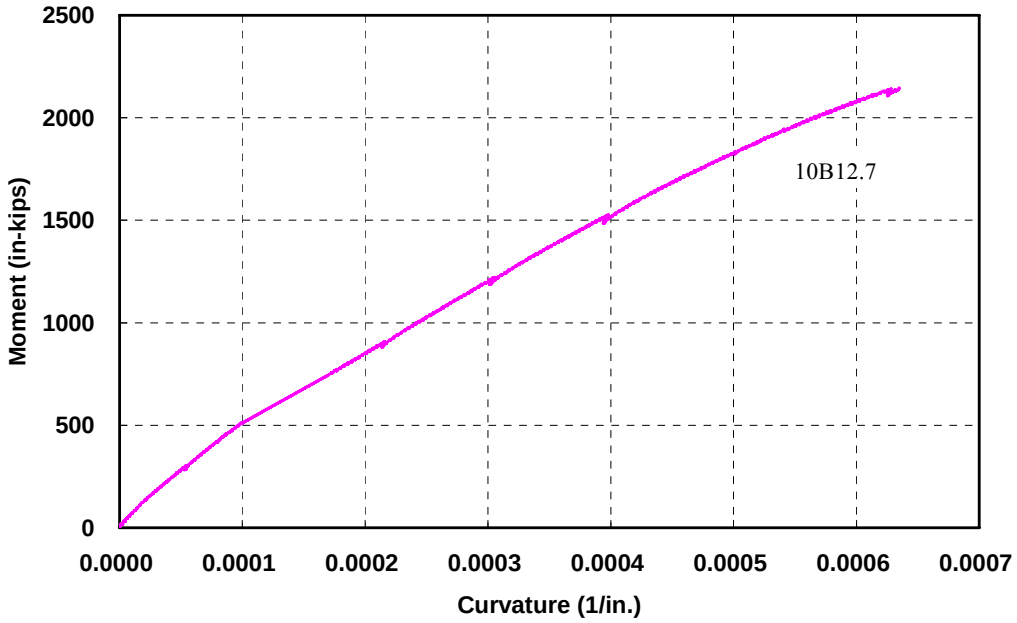

Figure 3-23 Moment-Curvature Response for Pure Flexure Specimens with Inverted T-Section and Target Strength of 10 ksi

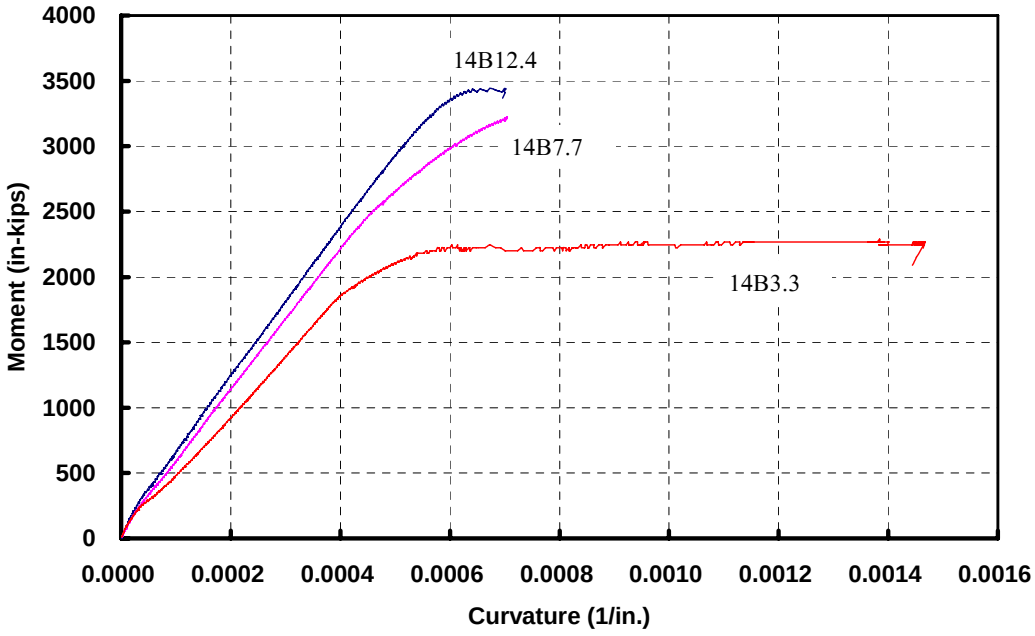

Figure 3-24 Moment-Curvature Response for Pure Flexure Specimens with Rectangular Section and Target Strength of 14 ksi

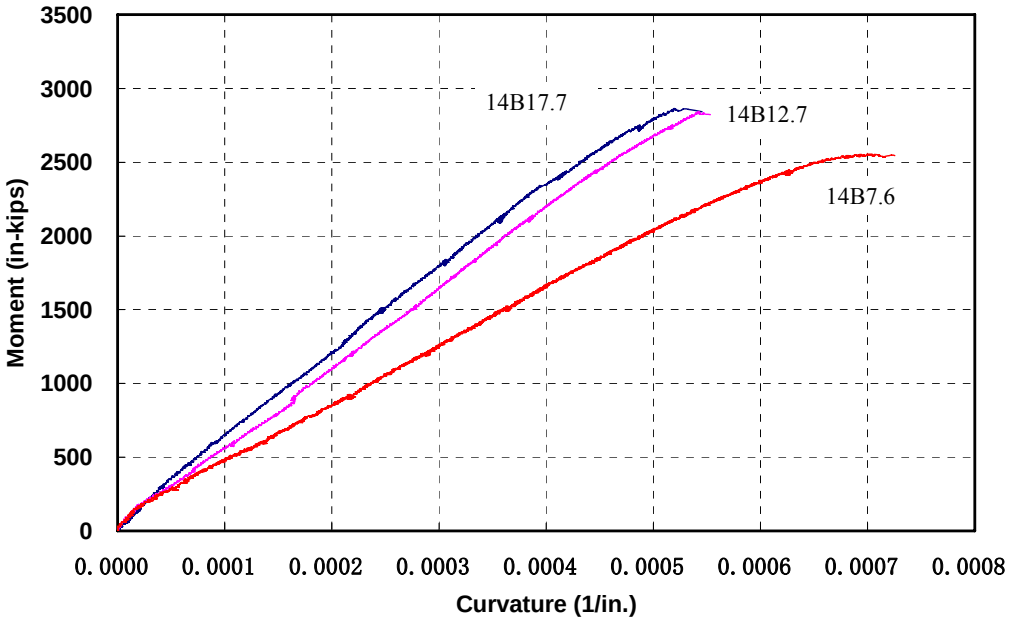

Figure 3-25 Moment-Curvature Response for Pure Flexure Specimens with Inverted T-Section and Target Strength of 14 ksi

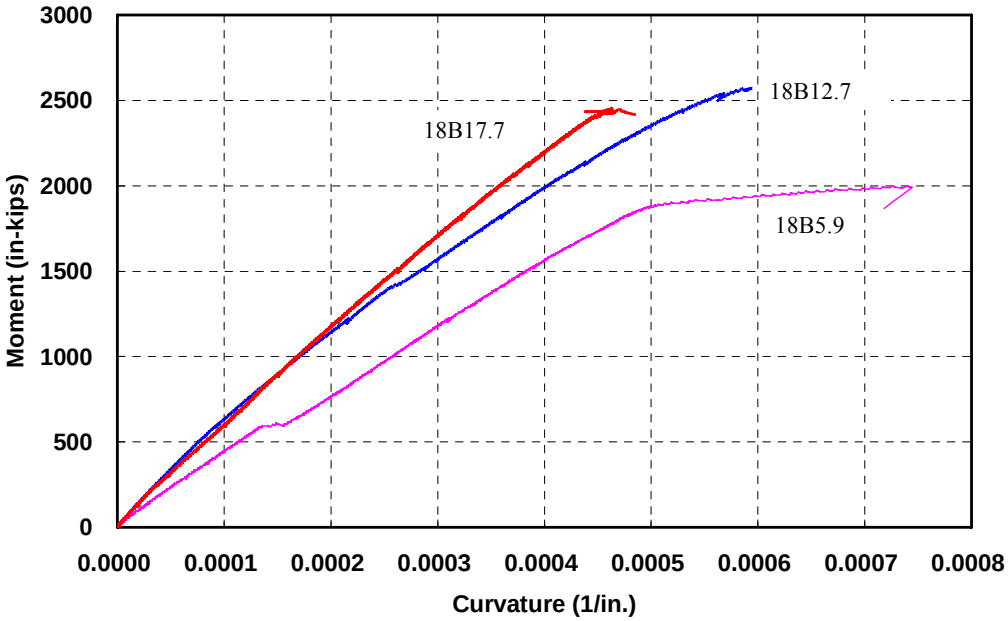

Figure 3-26 Moment-Curvature Response for Pure Flexure Specimens with Inverted T-Section and Target Strength of 18ksi

3.2.6.3 Depth of Neutral Axis

Depth of neutral axis for each cast of specimens is plotted against measured load in Figures 3-27 to 3-31. The depth of neutral axis is analyzed based on the same group of pi-gauges which were used to determine the curvature using a similar regression analysis. In general, the depth of neutral axis increased with the reinforcement ratio. The initial part of the curves has high fluctuations, mainly due to the errors from the initial setting of the instrumentation as well as the effect of initial cracking. Because the stress-strain curve of high-strength concrete is almost linear up to its peak stress, the cracked section at mid-span behaves elastically, and the depth of neutral axis remains almost constant after cracking. Neutral axis shifts upward after yielding of the longitudinal reinforcement for under-reinforced beams, as observed in Specimen 10B2.1 shown in Figure 3-27. For over-reinforced beams, specimens fail before the reinforcement yields. If the stress of concrete drops, neutral axis may shift downward, as observed in Specimen 10B10.2 shown in Figure 3-29 or Specimen 18B12.7 shown in Figure 3-31. In this study, most of over-reinforced specimens failed suddenly when neutral axis was almost constant, possibly because concrete crushed upon reaching its peak stress.

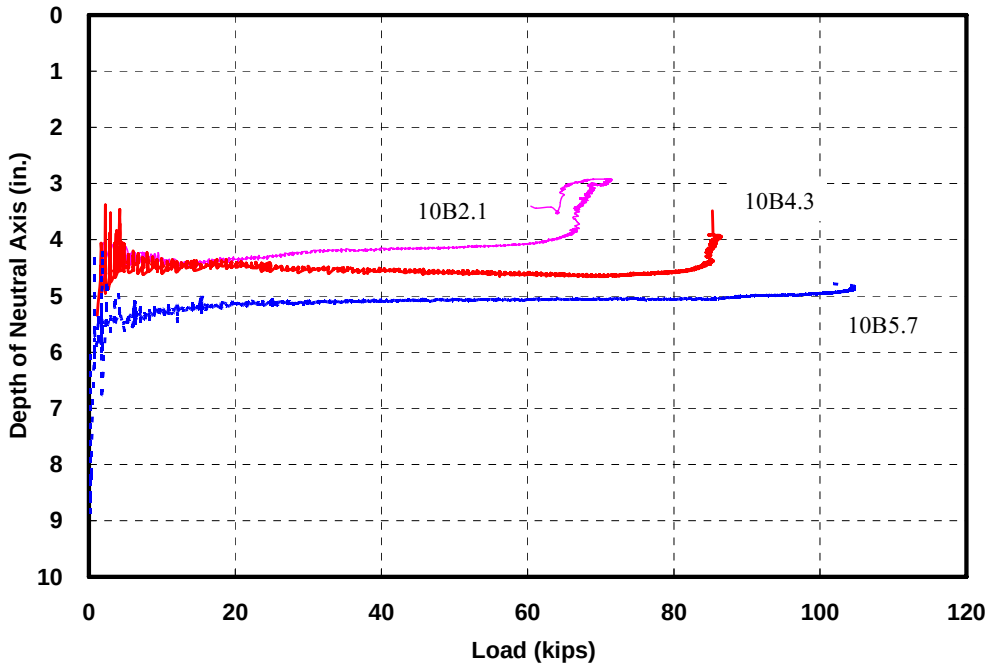

Figure 3-27 Depth of Neutral Axis vs. Load for Pure Flexure Specimens with Rectangular Section and Target Strength of 10 ksi

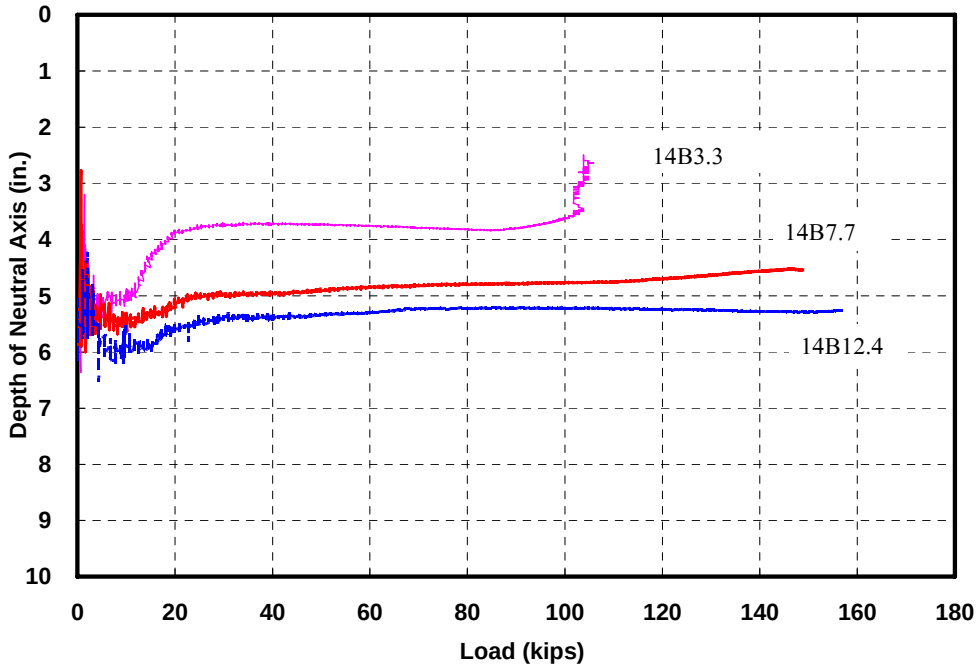

Figure 3-28 Depth of Neutral Axis vs. Load for Pure Flexure Specimens with Rectangular Section and Target Strength of 14 ksi

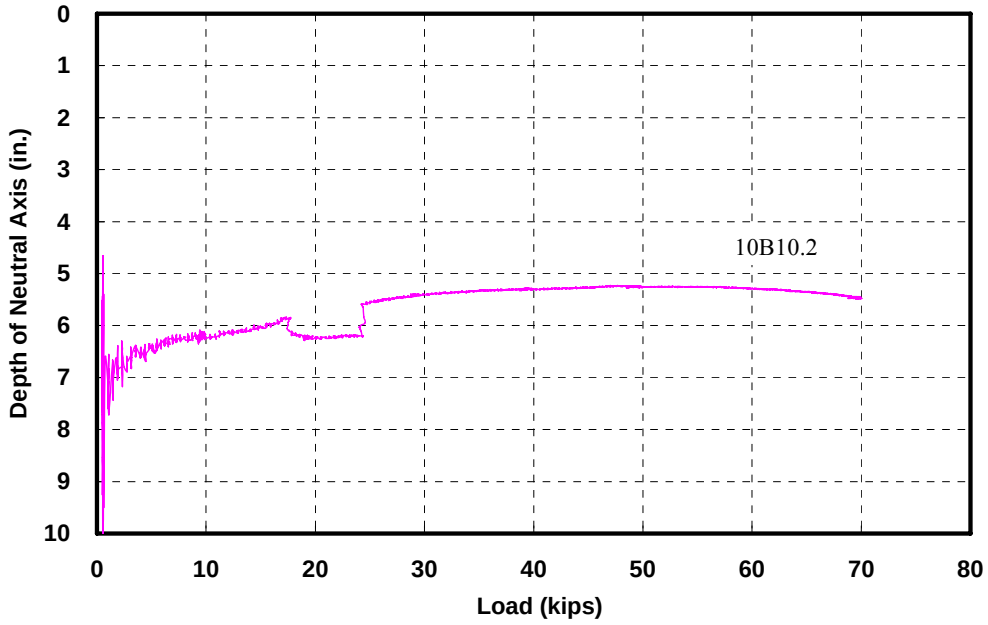

Figure 3-29 Depth of Neutral Axis vs. Load for Pure Flexure Specimens with Inverted T-Section and Target Strength of 10 ksi

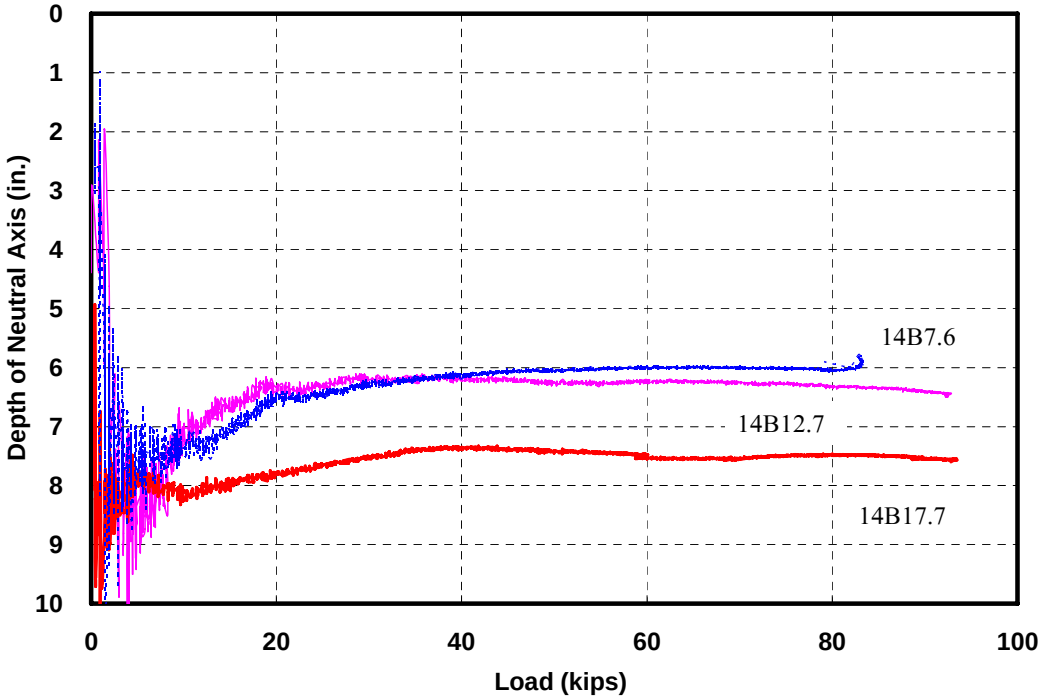

Figure 3-30 Depth of Neutral Axis vs. Load for Pure Flexure Specimens with Inverted T-Section and Target Strength of 14 ksi

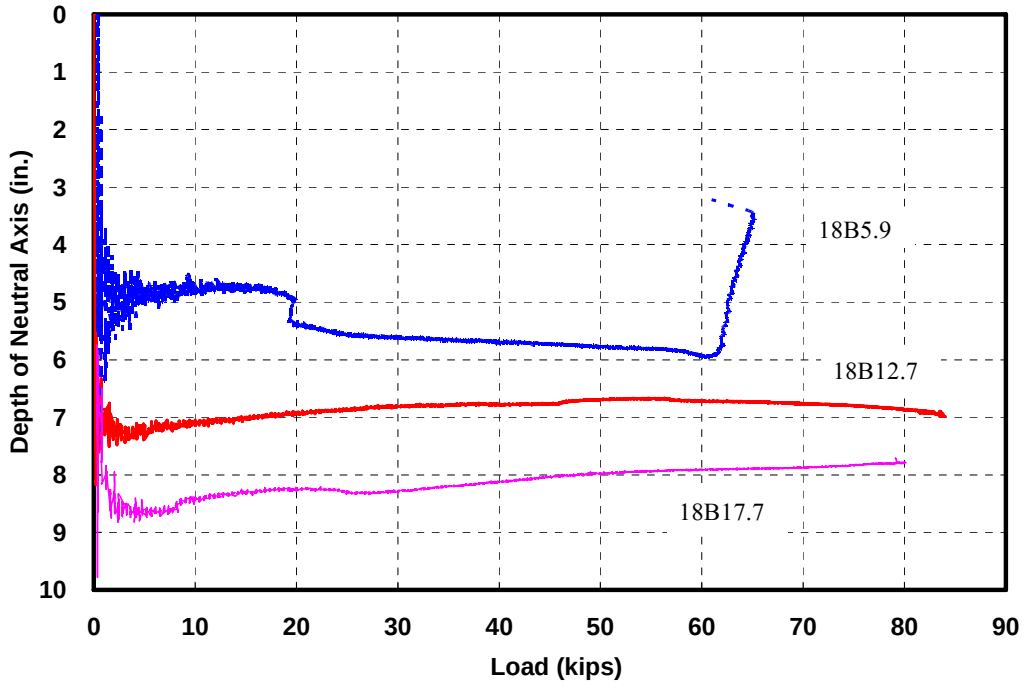

Figure 3-31 Depth of Neutral Axis vs. Load for Pure Flexure Specimens with Inverted T-Section and Target Strength of 18 ksi

3.2.6.4 Load-Deflection Response

Load-deflection curves for each cast of specimens are shown in Figures 3-32 to 3-36. The deflections shown are the averages of the two potentiometers or wire transducers at mid-span. Subsidence of the support measured by the two potentiometers were also averaged and subtracted from the measured mid-span deflections. Readings of the two potentiometers compared very well for all specimens tested in this project, with a difference of less than 2 percent.

Because some specimens cracked beforehand, not all cracking moments can be clearly identified from the response. The behavior of the high-strength concrete beams is generally the same as normal-strength concrete beams. For an under-reinforced beam, as the reinforcement ratio increases, the capacity and stiffness of the section both increase, but the

ultimate deflection decreases. For an over-reinforced specimen, this is sometimes not true as the resistance is mainly controlled by the compressive strength of concrete. The load-deflection curves generally remain linear after cracking. The over-reinforced specimens failed at their peak load; while the under-reinforced specimens showed a more ductile failure.

Due to the low concrete strength achieved, none of the specimens with the inverted T-section showed a clear ductile response. Specimens with target strength of 18 ksi had higher cylinder strength but did not achieve as high a flexural resistance as expected. This is possibly due to the curing method of the specimens, as they were cured outside during the winter, and experienced a few freeze and thaw cycles.

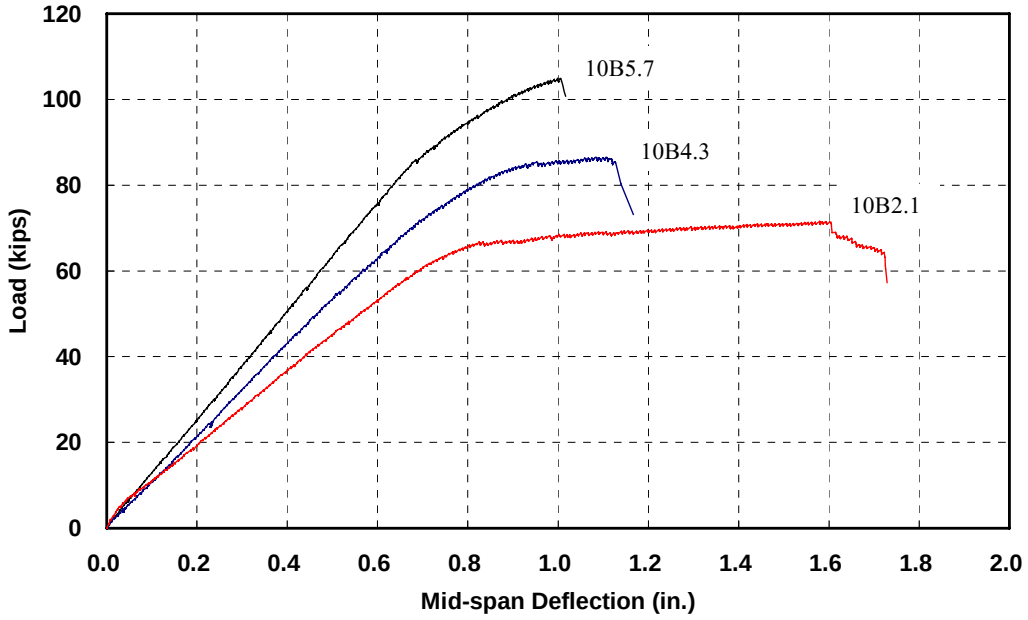

Figure 3-32 Load-Deflection Response at Mid-span for Pure Flexure Specimens with Rectangular Section and Target Strength of 10 ksi

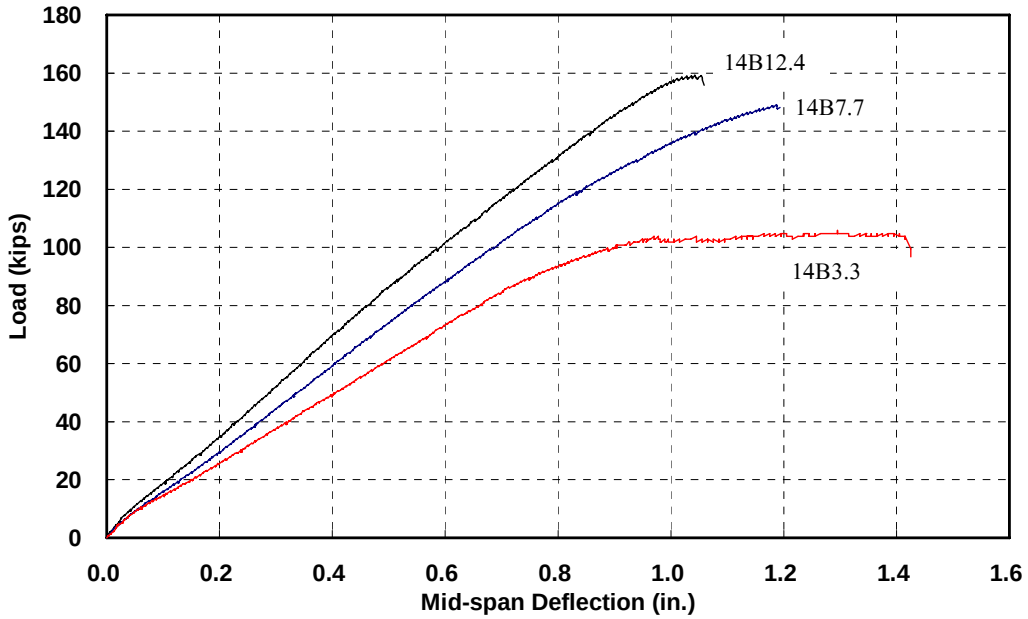

Figure 3-33 Load-Deflection Response at Mid-span for Pure Flexure Specimens with Rectangular Section and Target Strength of 14 ksi

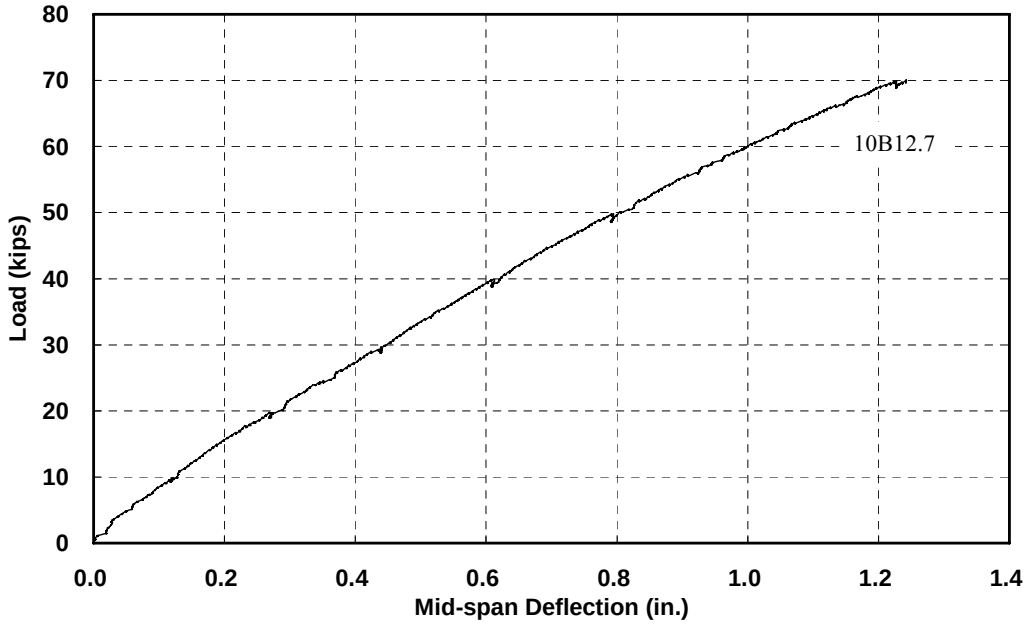

Figure 3-34 Load-Deflection Response at Mid-span for Pure Flexure Specimens with Inverted T-Section and Target Strength of 10 ksi

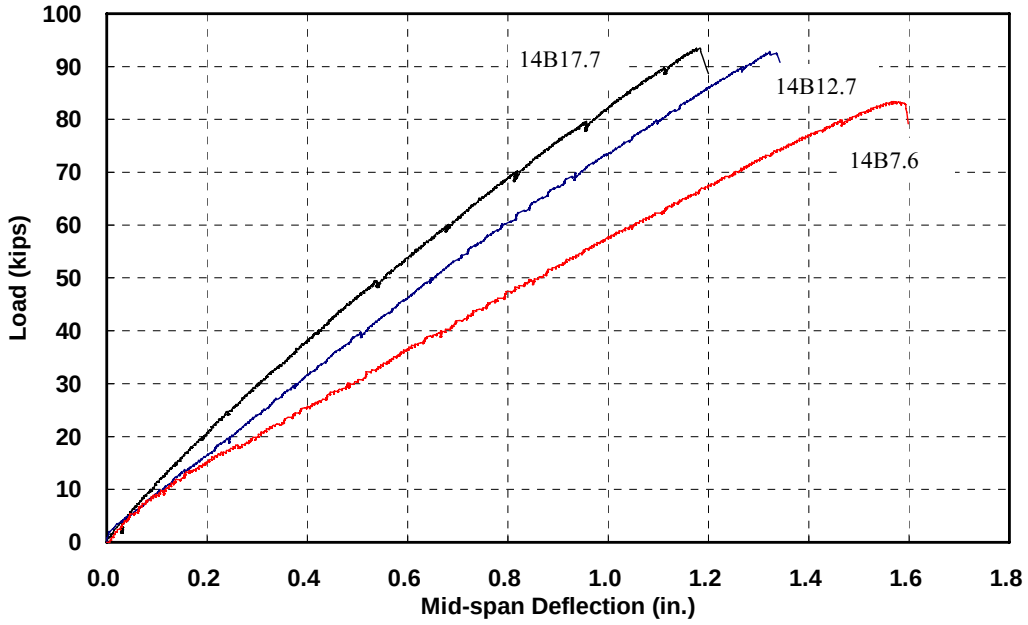

Figure 3-35 Load-Deflection Response at Mid-span for Pure Flexure Specimens with Inverted T-Section and Target Strength of 14 ksi

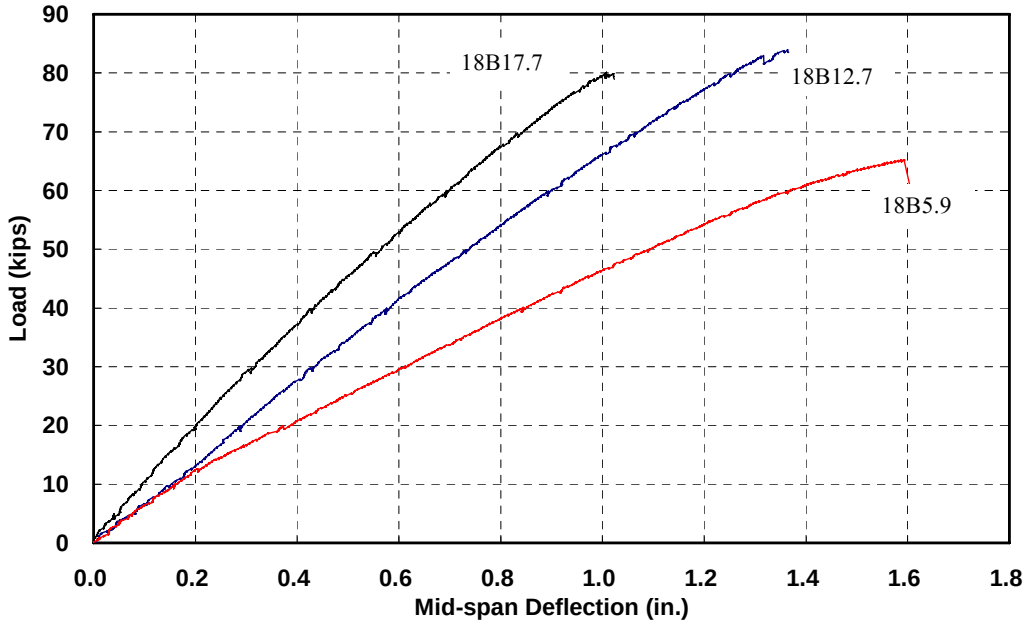

Figure 3-36 Load-Deflection Response at Mid-span for Pure Flexure Specimens with Inverted T-Section and Target Strength of 18 ksi

3.3 Axial-Flexural Tests

3.3.1 Test Specimens

The overall test matrix for axial-flexural specimens is shown in Table 3-2. Five high-strength concrete beam-column specimens were cast together with the pure flexure specimens, as indicated in the first column. Specimens are named under the same rules as the pure flexure specimens; except that the letters "BA" represent beam-columns subjected to axial-flexural loads. The last letter "R" stands for duplicated specimens. The compressive strength of each beam-column specimen shown in this table is based on the average compressive strength of three 4 in. x 8 in. concrete cylinders tested on the same day as the specimen. Modulus of rupture, reinforcement ratio, specimen geometry and effective depth of reinforcement are also shown in the table.

The affecting test parameters include concrete strength, shape of cross section, reinforcement ratio and applied axial load. The following parameters are included for the purpose of developing the test matrix:

- **Concrete compressive strength**: Three target strengths of 10, 14, and 18 ksi were used. The same as pure flexure specimens.
- **Longitudinal Reinforcement**: All specimens had reinforcement ratio of 4 percent. Longitudinal reinforcement was arranged in three layers, same as other axial-flexural specimens tested in NCHRP Project 12-64. All reinforcement was Grade 60 ksi steel.
- **Specimen Size and Shape**: All specimens were originally designed to have 9 in. x 12 in. rectangular section, and were designed to be tested with a flexural span of 120 in. The size of specimen was reduced to 7 in. x 9 in. rectangular section to match the

column specimens in Casts 3 and 4; and the length of the specimen was reduced to 108 in. All specimens had end blocks which were 6 in. wider to facilitate the application of axial load. Actual length of each specimen was 3 ft. longer than its designed flexural span.

- **Transverse Reinforcement**: All specimens included transverse reinforcement to avoid shear failure. The amount of transverse reinforcement was calculated based on the AASHTO LRFD Specifications requirement and the shear demand. Spacing of transverse reinforcement in the constant moment region was 4 1/2 in., which was half of the maximum spacing of the lateral reinforcement required for columns. All transverse reinforcement was No. 4 ties of Grade 60 ksi steel.
- **Axial Load**: The axial load level was chosen to be between 6 percent and 10 percent of the nominal axial resistance, and below the level of balanced failure load. When testing the first axial-flexural specimen (10BA4), it was noticed that axial load increased up to 20 percent with the increase of lateral deflections. This problem was solved using a pressure-relief valve, which enabled manual control of the axial load level. Specimen 10BA4 was replaced with an identical specimen 10BA4R.

3.3.2 Specimen Fabrication

Fabrication of formwork, casting and curing for axial-flexural specimens were the same as those for pure flexure specimens with rectangular section. The only difference is that axial-flexural specimens had a heavily reinforced end blocks on each side to facilitate the application of axial load.

Table 3-2 Test Matrix of the Axial-Flexural Specimens

Cast No.	Specimen No.	f'_c (ksi)	f_r (psi)	Axial Load (kips)	ρ (%)	Rebar size and number	d(in.)
Cast 1	10BA4	11.7	596	87	4.1	2 No. 8	1.5
Cast 2	14BA4	15.2	850	108		2 No. 7	6
Cast 5	10BA4R	12.8	807	79		2 No. 8	10.5
Cast 3	14BA4R	15.1	1457	93	4.1	2 No. 6	1 3/8
						2 No. 6	4.5
Cast 4	18BA4	15.3	963	56		2 No. 6	7 5/8

* Note the arrangements of reinforcement for Casts 1,2 and 5 were same, for Cast 3 and 4 were same

3.3.3 Instrumentation

The primary objective of the instrumentation of the axial-flexural specimens was to obtain the strain distribution as well as the deflection in the constant moment zone. Besides, axial load was monitored using a load cell as shown in Figure 3-37. Load cells with capacity up to 150 kip were used. Load cells were calibrated on an annual basis with tracing back to the National Institute of Standards and Technology (NIST).

Fig 3-37 Load Cells for Monitoring of Axial Loads

3.3.4 Test Setup and Procedure

Figure 3-38 shows an overview of the test setup. Lateral loading was applied the same as testing of the pure flexure specimens. A self-reacting frame was used for the application of axial load. The frame consists of an ENERPAC hydraulic jack with a 60 ton capacity and a pressure-relief valve, a load cell, two sets of roller supports to allow the end of the beam to rotate freely, two steel spreader beams, and eight 1 in. diameter ASTM 193 Grade B7 high strength alloy steel coarse threaded rods of about 10 ft. in length. The two steel spreader beams were placed at each end of the beam-column and were connected by threaded rods to form a self-reacting frame, as shown in Figures 3-37 to 3-39. The axial load was applied using the hydraulic jack, as shown in Figure 3-39. Axial load was transferred to the specimen through a roller support at each end of the specimen, which allows the ends to rotate, as also

shown in Figure 3-39. The roller supports were designed and aligned in a way that the centroid of the axial force would always pass through the centroid of the cross-section. The load cell was placed at the other end of the specimen to measure the axial load, as shown earlier in Figure 3-37. A steel plate was embedded in each of the two end blocks of the specimen to provide a smooth loading surface in the axial direction. As the threaded rods required in for system were longer then the available commercial length, they were coupled in the middle.

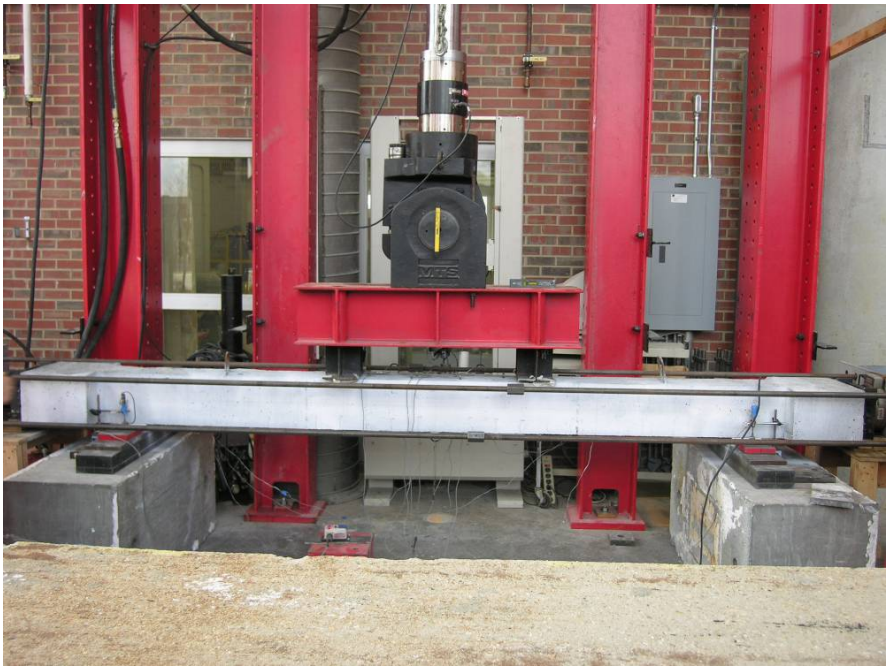

Figure 3-38 Test Setup for Axial-Flexural Specimens

Figure 3-39 Hydraulic Jack, Roller Support and Self-Reacting Frame

After the axial load reached the predetermined value, the specimens were loaded transversely in four-point bending the same way as the pure flexure specimens. Once the axial load changed by more than 2 percent of the expected value, the pressure relief valve (see Figure 3-40) or hand pump were used to manually adjust the axial load. The axial load was kept within ± 3 percent of the designed value.

After reaching the peak load, the axial load dropped quickly and it became very hard maintain. Therefore, it was fully released, for safety purposes, once the transverse load started to decline. Test was terminated when the observed deflection at mid-span reached about 4 in., again for safety purposes.

Figure 3-40 Pressure Relief Valve

3.3.5 Test Observations and Failure Modes

The axial-flexural specimens behaved very similar to the under-reinforced specimens tested in pure flexure. However, the failure mode is quite different. Unlike the sudden and explosive failure observed in testing of pure flexure specimens, the failure of axially loaded specimens was slow and progressive. This is mainly due to the presence of lateral reinforcement within the constant moment zone. Upon reaching the peak load, failure was initiated by crushing of concrete cover at the extreme compression fiber, accompanied by a sudden drop of the load, as shown in Figure 3-41. The loss of flexural resistance was quickly stabilized by the confinement effect, which was provided by the lateral reinforcement within the compression zone. With larger deflection, concrete cover within the compression zone gradually crushed or spalled, as shown in Figure 3-42. After the test was terminated and the load was removed,

all the specimens showed large plastic deformation, as shown in Figure 3-43

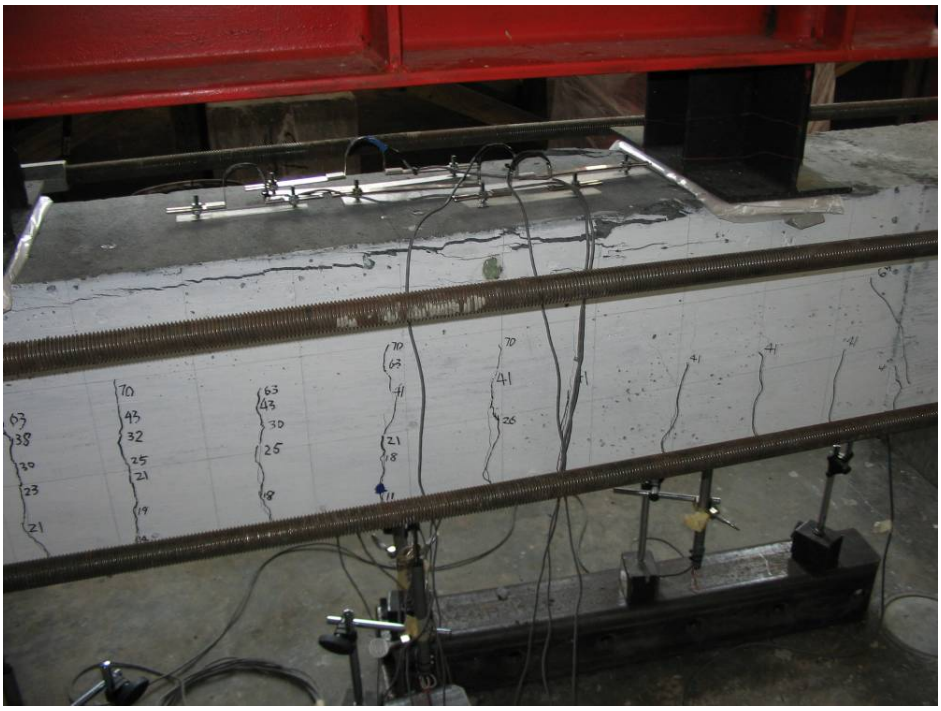

Figure 3-41 Concrete Cover Spalling of Axial-Flexural Specimen (10BA4)

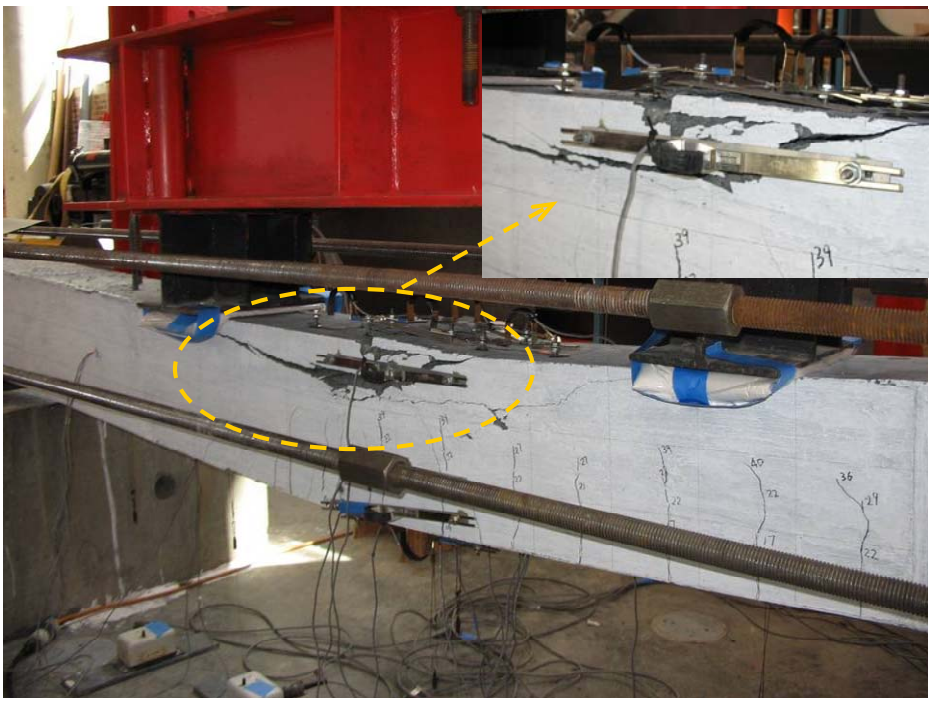

Figure 3-42 Typical Failure Mode of Axial-Flexural Specimen (14BA4R)

Figure 3-43 Typical Failure Mode of Axial-Flexural Specimen (10BA4)

3.3.6 Test Results and Discussions

In this section, test results for various aspects of the axial-flexural specimens are presented and discussed.

3.3.6.1 Ultimate Compressive Strain of Concrete:

The data of ultimate strain for axial-flexural tests were synthesized much the same way as those of the pure flexure specimens.

The failure of axial-flexural specimens was very progressive and ductile. After crushing of concrete cover, specimens usually maintained their resistances due to confinement effect.

However, the strain value after the peak load was not of interest in the present study. The strain readings at peak load and at crushing concrete cover are shown in Figures 3-44 and 3-45, respectively. Of the five tested specimens, all strain readings shown here exceed 0.003 at peak load.

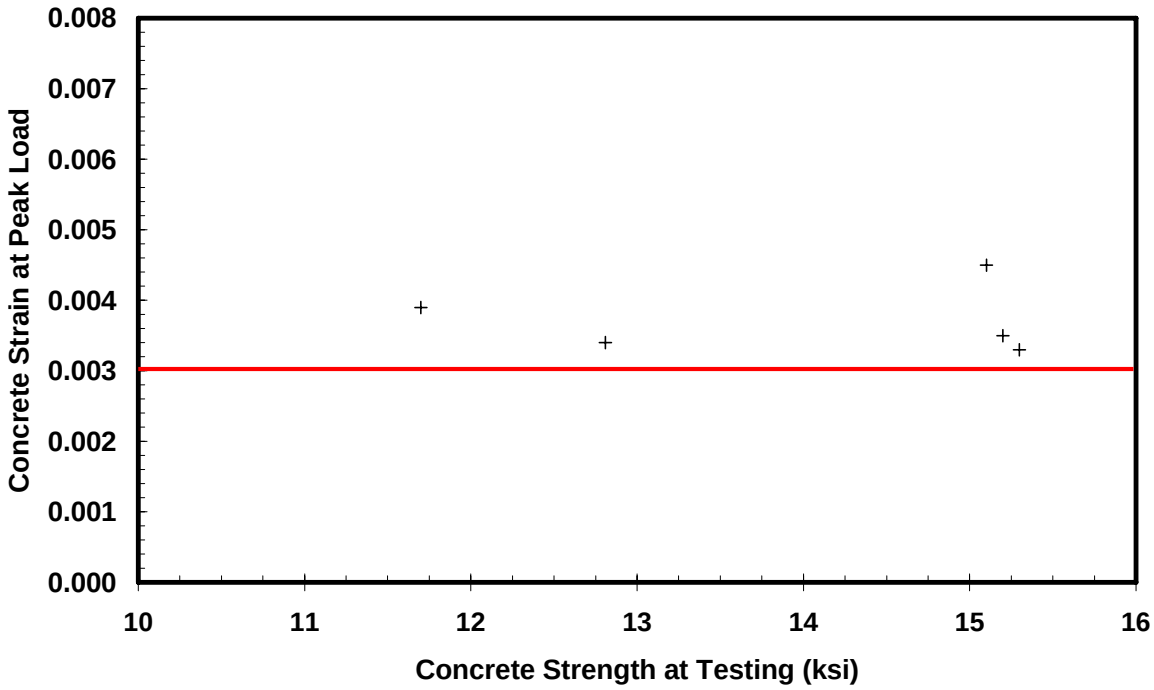

Figure 3-44 Compressive Strain of Concrete at Peak Load for Axial-Flexural Specimens

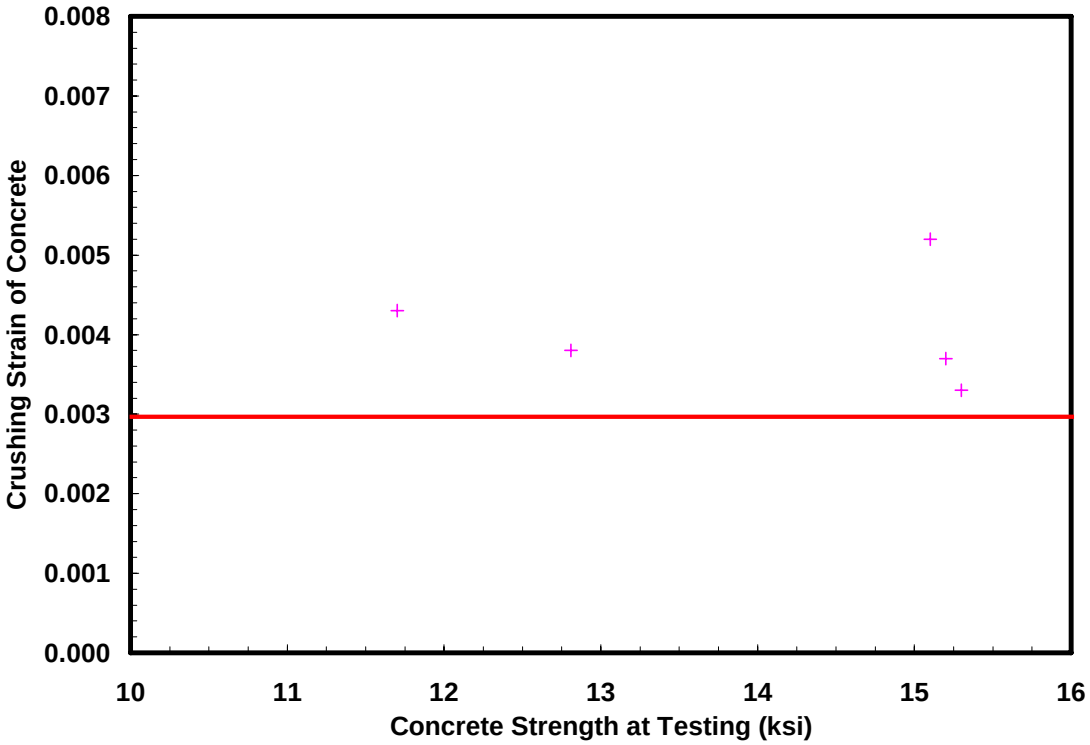

Figure 3-45 Compressive Strain of Concrete at Crushing of Top Cover for Axial-Flexural Specimens

3.3.6.2 Moment-Curvature Response

The moment-curvature curves at mid-span for axial-flexural specimens are shown in Figures 3-46 and 3-47. Curves are grouped together for specimens with the same cross section.

In calculating the moment at mid-span, the primary moment and secondary moment were combined together. Primary moment refers to the moment form lateral loads. Secondary moment is the product of the axial load and the deflection at mid-span. Similar to the pure flexure specimens, strain data from axial-flexural tests were examined. Curvature at mid-span was calculated using regression analysis and the best-linear fit.

It can be seen from these two figures that specimens with same cross section have very

similar capacity and stiffness, mainly because all tested specimens are under-reinforced and have the same the reinforcement ratio and cross-section. The moment-curvature responses have a tri-linear shape up to the peak load. Before first cracking, the section behavior is linear with highest stiffness. The point of first change in the slope reflects the cracking of the section. Due to the axial load, the cracking moments for the axial-flexural specimens are generally higher than the pure flexure specimens. The second change in the slope reflects the yielding of the bottom layer of the longitudinal reinforcement. As the reinforcements were placed in three layers, the second layer of the longitudinal reinforcement remained elastic and contributed to the capacity of the section until the concrete cover on the compression side crushed when a sudden drop of load and curvature was observed for all specimens.

In testing Specimen 18BA4, the frame for applying axial load lost its stability after yielding of the longitudinal reinforcement, but concrete at the top did not crush. The specimen was re-aligned and the test was repeated. However, as the longitudinal reinforcement at the bottom layer had yielded during the first test, the beam curled-up due to the residual strains in the longitudinal reinforcement. In the second test, the initial moment-curvature response was different, but the two curves approach each other at higher load levels. For this specimen, the pi-gauges on the sides of the specimen lost their bond with concrete surface as soon as the top concrete crushed, and therefore no further curvature reading was available.

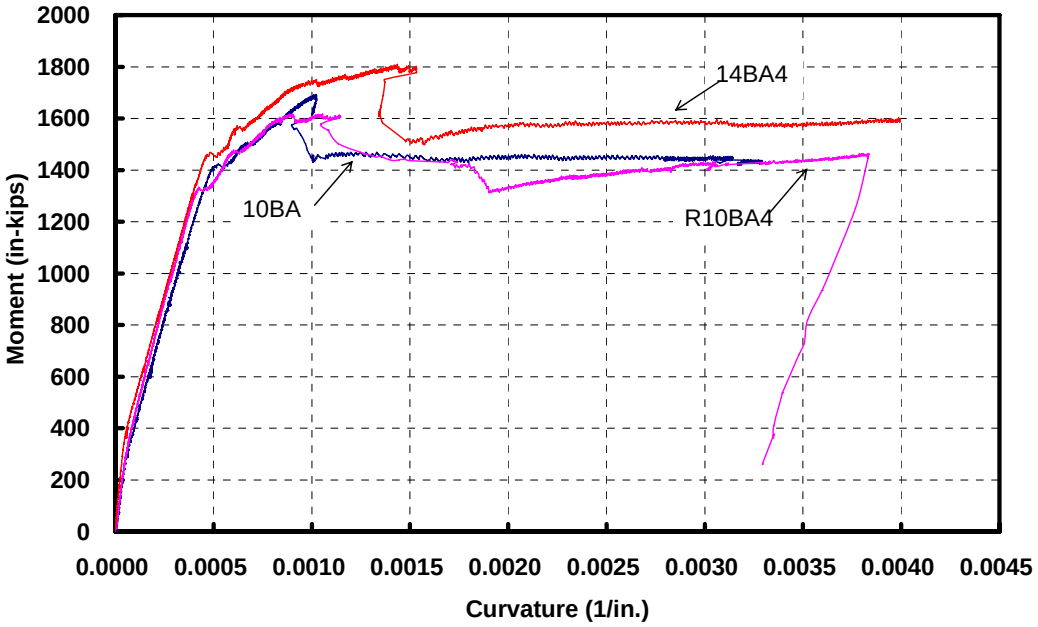

Figure 3-46 Moment-Curvature Response for Axial-Flexural Specimens with 9 in. x 12 in. Rectangular Section

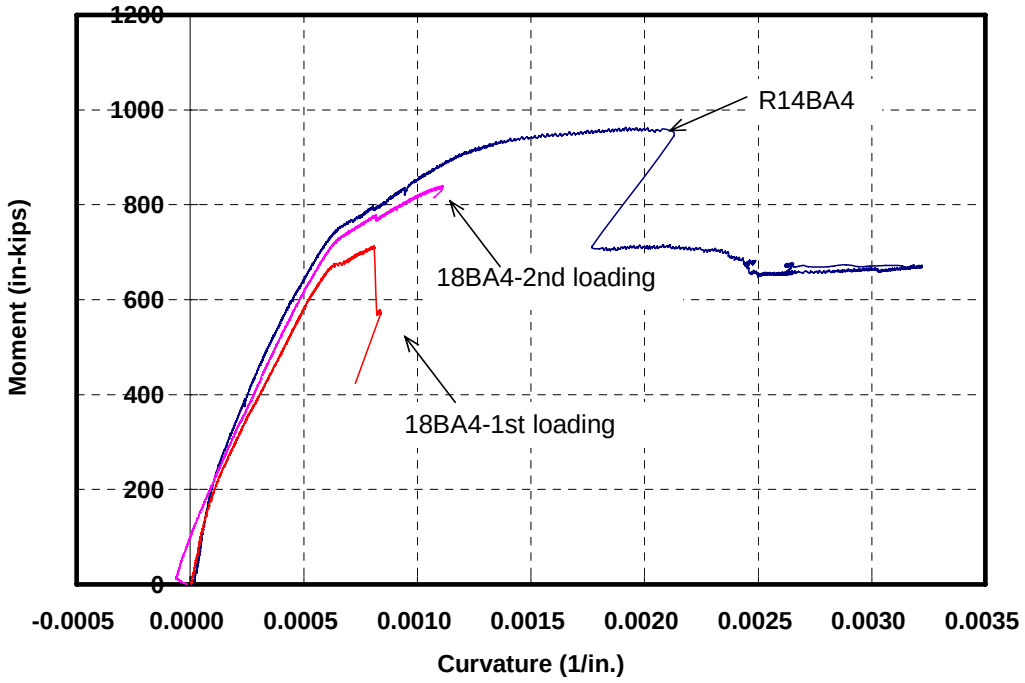

Figure 3-47 Moment-Curvature Response for Axial-Flexural Specimens with 7 in. x 9 in. Rectangular Section

3.3.6.3 Depth of Neutral Axis

The depth of neutral axis is plotted against the measured load in Figures 3-48 and 3-49. Depth of neutral axis was calculated based on the readings of the same group of pi-gauges used to determine the moment-curvature response. A regression analysis was performed to determine the depth of neutral axis.

Since the axial load was applied at the centroid of the cross-section, the theoretical depth of neutral axis was infinite before lateral load was applied. The neutral axis shifted upward as more lateral load was applied. In some of the specimens (R14BA4 and 18BA4), neutral axis seemed to stabilize at the applied lateral load greater than 50 percent of the peak load, similar to what was observed for pure flexure specimens. For other specimens, this trend was not very clear. The yielding of the bottom layer of the longitudinal reinforcement created a discontinuity in the curve and the shifting of neutral axis become irregular. Neutral axis quickly moved upward after the peak load due to the crushing of top concrete cover.

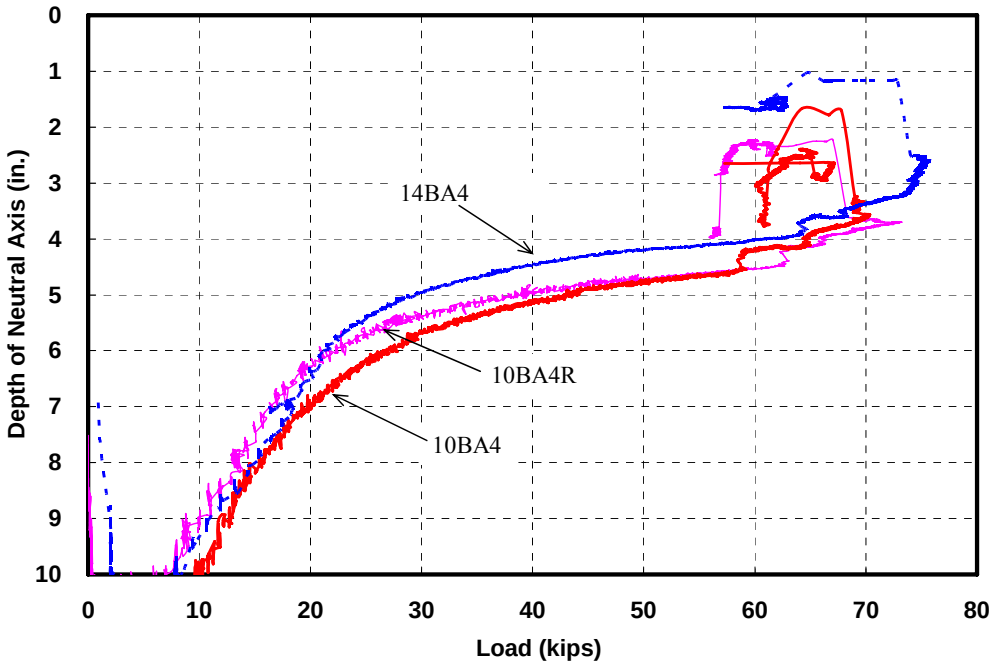

Figure 3-48 Depth of Neutral Axis vs. Load for Axial-Flexural Specimens with 9 in. x 12 in. Rectangular Section

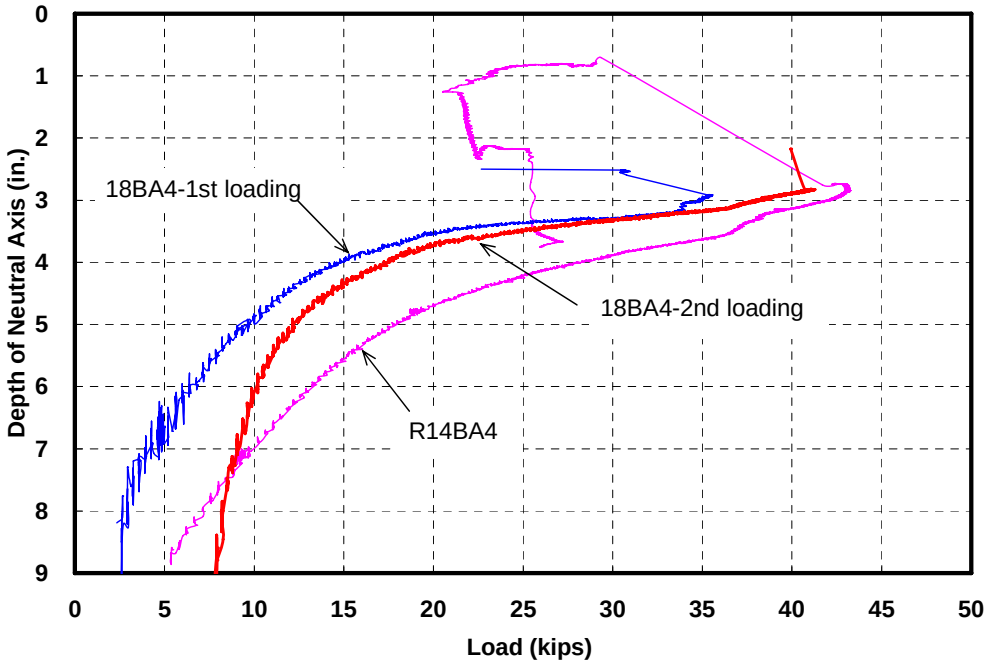

Figure 3-49 Depth of Neutral Axis vs. Load for Axial-Flexural Specimens with 7 in. x 9 in. Rectangular Cross-Section

3.3.6.4 Load-Deflection Response

Load-deflection responses for all tests are shown in Figures 3-50 and 3-51. The deflections shown are the average values of the two potentiometers or wire transducers at mid-span. The two readings generally compared very well for all the specimens tested in this project, within 2 percent of each other. The displacements of the steel roller support were monitored in one of the tests and found to be negligible.

The load-deflection curves demonstrate a tri-linear relationship before the peak load, except for the second test on Specimen 18BA4, which had cracked before loading. The first change in the slope reflects the cracking of the section, while the second is the yielding of the bottom layer of longitudinal reinforcement. The loss of capacity after the peak load was mainly due to the crushing concrete cover. For Specimens 10BA4, R10BA4, 14BA4, about 20 percent of the capacity was lost at that point. After that, all specimens showed some ductility and some limited gain of strength due to confinement. For specimens R14BA4, 18BA4, the load drop was more significant because the concrete cover has a larger influence in a smaller cross-section.

It needs to be reiterated here that except for Specimen R14BA4, which failed due to the loss of stability of the self-reacting frame, all the other tests were terminated due to large deflection and safety concern. It is very likely that the specimens may have been able to sustain even larger deflections.

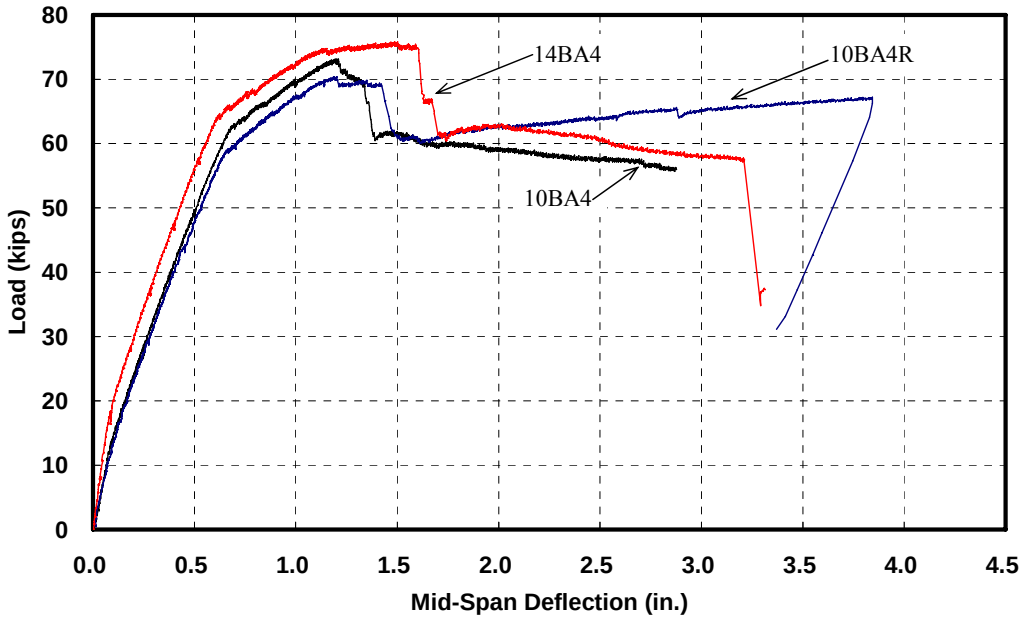

Figure 3-50 Load-Deflection Responses at Mid-span for Axial-Flexural Specimens with 9 in. x 12 in. Rectangular Section

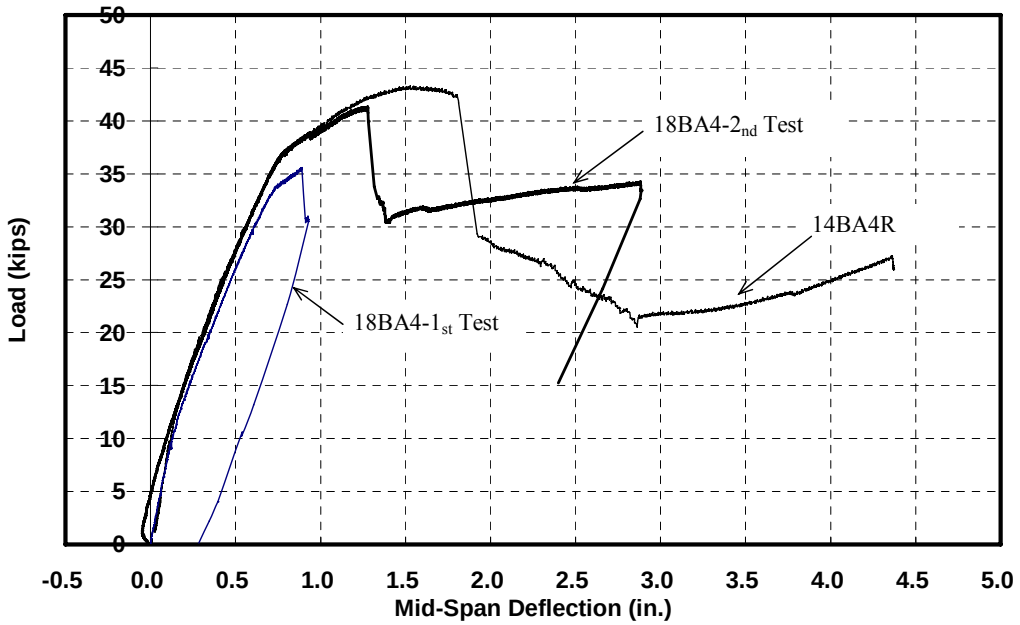

Figure 3-51 Load-Deflection Responses at Mid-span for Axial-Flexural Specimens with 7 in. x 9 in. Rectangular Section

3.4 Ancillary Material Property Tests

3.4.1 Concrete Cylinders Test

Three 4 in. x 8 in. cylinders were cast for each beam or beam-column specimens using plastic molds in accordance with AASHTO T23 (ASTM C31). Cylinders were demolded 1-2 days after casting and cured beside the specimens in the same condition.

All cylinders used for tests were first prepared by grinding both end surfaces to remove irregularities on the surfaces and to ensure that the ends were perpendicular to the sides of the specimen. Grinding the end surfaces was accomplished with a rotary grinding machine shown in Figure 3-52.

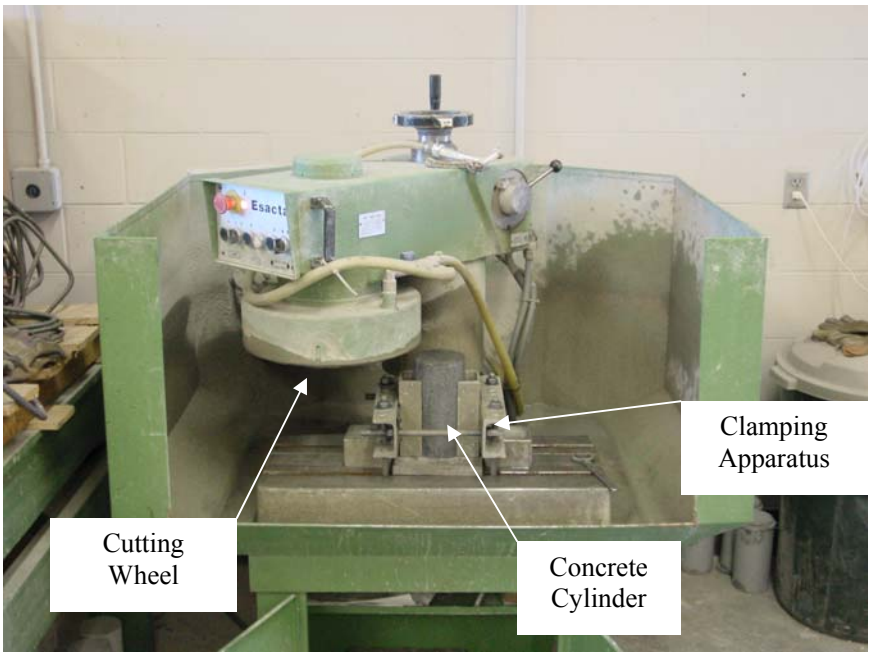

Figure 3-52 Grinding Machine

The cylinders were tested using a 500 kip compression machine (Forney). For the first 3 casts

of concrete, only concrete strength was measured. The elastic modulus of concrete of these casts was measured by Logan (2005). Two types of instrumentation were used, as shown in Figure 3-53. The apparatus in Figure 3-53 (a), called compressometer-extensometer, consisted of two aluminum rings attached the cylinders with screws. Axial strains were calculated from deflections measured using potentiometers attached to the two aluminum rings. The instrumentation shown in Figure 3-53 (b) consists of two 4 in. pi-gauges attached to each side of the cylinders to measure axial strains. There is no substantial difference between the two types of instrumentation. Majority of the cylinders were tested using the setup shown in Figure 3-53 (a). The setup shown in Figure 3-53 (b) was use mainly for testing the cores, which were not long enough to fit into the compressometer-extensometer. Results indicated that elastic modulus measured using the two types of instrumentation were very close for 4 in. x 8 in. cylinders

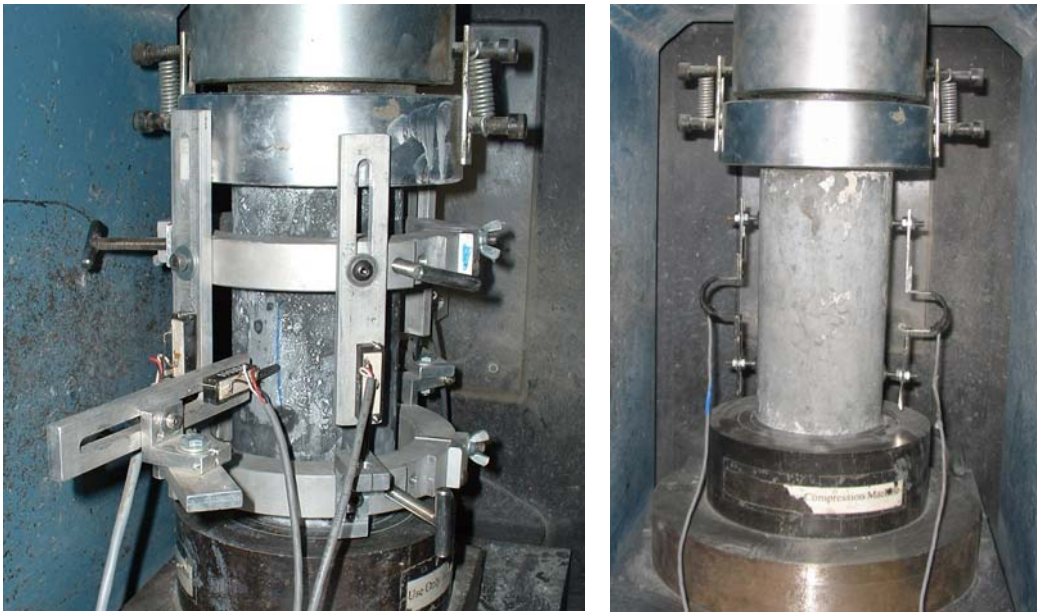

(a) (b)

Figure 3-53 Instrumentation for Measuring the Elastic Modulus

The elastic modulus of the 4 in. x 8 in. cylinders was determined in accordance with ASTM

C 469. The cylinders were loaded 3 times. The first cycle consisted of loading up to 40 percent of the anticipated capacity, and was only intended to seat the gauges and the specimen. The second and third loading cycles were similar, but with measurements taken. After removal of the instrumentation, the cylinders were loaded up to failure in accordance with ASHTO T 22 (ASTM C 39). Per ASTM C 39, the loading rate should be 35+/-7 psi/sec. The rate used in this project was approximately 40 psi/sec. Data was recorded using an Optim Megadac high-speed data-acquisition system at 1 scan/ second.

Similar to normal-strength concrete, typical failure mode of high-strength concrete cylinders was conical, as shown in Figure 3-54. However, in contrast to normal-strength concrete, upon reaching the peak load, failure was sudden and hardly any post-peak.

Figure 3-54 Typical Failure Mode of High-Strength Concrete Cylinders

3.4.2 Concrete Cores

The core tests were not in the original test plan and were added after analytical work on the results of the first three casts showed that all measured deflections at service load were larger than the predicted values. It has been proved experimentally that concrete strength in large-scale specimen is statistically lower than its respective cylinder. It has not been reported whether a similar difference exists for the elastic modulus. To investigate this possibility, cores were taken from the undamaged beam ends after testing.

To make sure that cored areas were free of reinforcement, a rebar detector was used prior to the drilling operation. The location of the stirrups was marked on both sides of the specimens. To avoid large longitudinal reinforcements in the flanges, cores were taken horizontally through the web of the inverted T-beams, which limited the length of the core to only 6 in. The size of the cores was also limited by the clear spacing of the stirrup, which was only 3 ½ in. at the end of the beam. Considering the tested cylinders have an aspect ratio of 2, cores was taken with diameter of about 3 in. to maintain the same aspect ratio. Due to the thickness of the blade, the clean core diameters were all approximately 2 ¾ in.

The ends of the cores were prepared with a rotary grinding machine before testing, similar to the cylinders. The cores were instrumented similar to the cylinder tests, as shown in Figure 3-53(b). Two 4 in. pi-gauges were attached on opposite sides of the core to measure the axial strain. Possibly due to the size effect, the failure modes of the cores were somewhat different from the 4 in. x 8 in. cylinders. Failure was initiated by vertical spitting cracks, and cores were exploded into pieces upon failure.

The compressive strength of each specimen is given previously in Tables 3-1 and 3-2. The reported results are based on the average of 3 tested cylinders. However, if one of the cylinders was more than ± 25 percent from the average of the cast, it was excluded.

The compressive strength and elastic modulus from the core tests are summarized and compared with other test data, including those by Logan in Figure 3-55. For specimens with target strength of 18 ksi, the compressive strength of the cores seems to be lower than the value from 4 in. x 8 in. cylinders. After taking out two extreme readings (the largest and the smallest), the four cores indicate an average concrete strength of only 12.2 ksi, approximately 80 percent of the measured strength of 4 in. x 8 in. cylinders. On the other hand, the average and standard deviation of the elastic modulus are 6045 ksi and 358 ksi; respectively, which is slightly higher than but close enough to that measured from the 4 in. x 8 in. cylinders. For specimens with target strength of 10 ksi, strength of cores was very close but the elastic modulus of core is slightly higher than the cylinders.

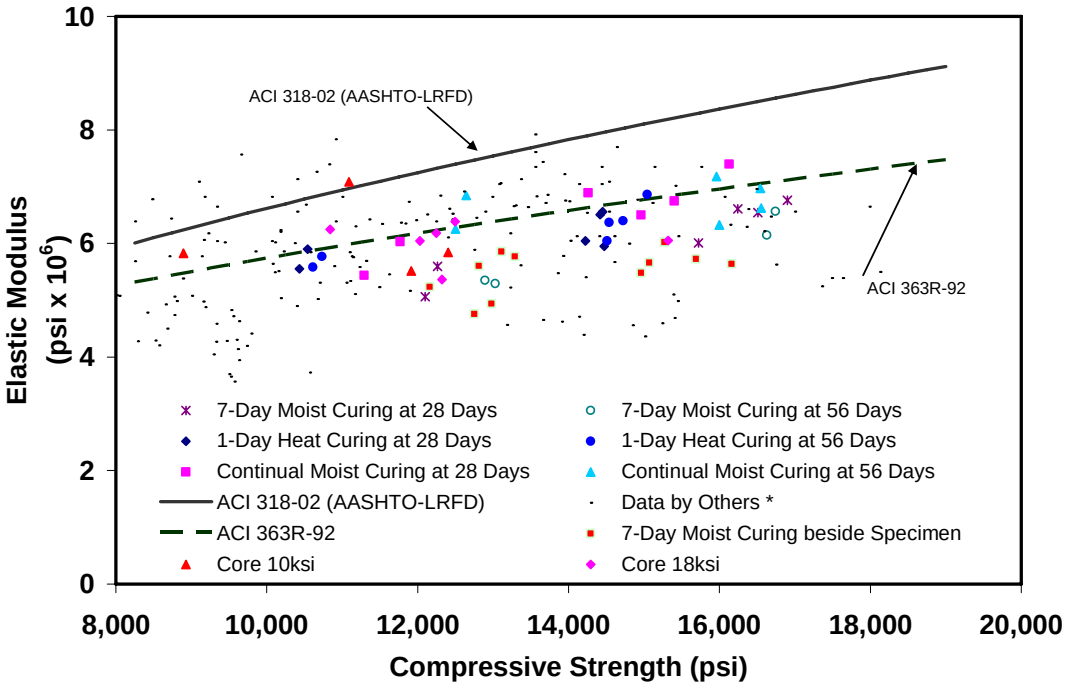

Figure 3-55 Comparison of Elastic Moduli of Concrete Cylinders and Cores

3.4.3 Modulus of Rupture Beam

The modulus of rupture beams are cast using 6 in. x 6 in. x 20 in. steel molds, and in general accordance with AASHTO T 23 (ASTM C 31) except for consolidation. The concrete was discharged from the truck directly into the molds. The molds were filled until overflowing. Each mold was consolidated with a 1 in. diameter concrete vibrator. Next, the excess concrete was struck off and the top surface was smoothed with a trowel. The specimens were then placed in their respective curing locations. Finally, wet burlap was placed on the exposed concrete surface and then plastic sheets were placed over the tops of the specimens to prevent moisture loss.

Before testing, irregularities caused by the seams in the beam molds protruding above the

plane of the loading surfaces of the specimen were removed by hand using a grinding stone. Next, marks were made on the specimen to align it with the supports and the two loading points. The specimen was then placed in the testing frame (See Figure 3-56) and oriented so that the specimen on its side with respect to its position in the mold as specified in ASTM C 78. A 90 kip hydraulic jack mounted inside a structural steel test frame applied the load. A load cell measured the applied load. Below the load cell, there was a spherical head and a plate/roller assembly to distribute the load evenly to the two loading points on top of the specimen. The span length of the specimen was 18 in. and the spacing between supports and the nearest loading point as well as the space between the two loading points was 6 in. The load was applied at a rate of approximately 1800 lb/min such that the stress at the extreme bottom fiber of the specimen increased at a rate of about 150 psi/min. Load readings from the load cell were recorded using a data acquisition system. After the test, the dimensions of the fractured surface were measured. Three measurements were taken in each direction (height and width). The average value in each direction was later used to calculate the stress at the extreme bottom fiber of the beam. Results from modulus of rupture tests will be discussed in Section 4.4.1.

Figure 3-56 Modulus of Rupture Test Setup (Logan, 2005)

3.4.3 Steel Reinforcement Coupons

Steel rebar coupons of 32 in length were ordered from manufacturer for material testing for each size of rebar used in this project. Since No. 14 rebars were larger than the machine grip, 4 in. from each end of the rebar was grind smaller to fit the grip.

The rebars were tested using MTS hydraulic machine with a maximum capacity of 200 kips. Test setup is shown in Figure 3-58. Before testing, bottom side of the rebar was first gripped to the predetermined pressure. Then the top part of the rebar was gripped, while the testing machine was in operation with load control is to guarantee that no axial force was introduced to the specimen during the gripping process. A potentiometer (MTS) with a gauge length of 2

in. was attached to measure the axial strain using rubber bands.

Figure 3-57 Test Setup to Measure Tensile Strength and Elastic Modulus of Reinforcement

The test was conducted in accordance with AASHTO A370 and in displacement control. For a specimen with a clear testing length of 20 in., a rate of 0.01 in/minute was selected so that the rebar would yield in approximately 5 minutes. After yielding of the reinforcement was observed from the data-acquisition, the rate was increased to 0.05 in/minute. Test was terminated when the strain reached 2 percent to 3 percent, which is much larger than the strains of reinforcement reached in the flexural tests.

The measured stress-strain curves of the steel reinforcement are shown in Figure 3-59. The measured yield stresses were between 62 ksi and 76 ksi, and the strain hardening started between 0.7 percent and 1.5 percent of strain. All but No. 14 rebars were tested beyond the yield point. Due to the limited gripping pressure, No. 14 rebars were only tested to measure

the elastic modulus. The stress-strain curves presented some non-linearity near the yield point, especially for large size rebars. This was attributed to the residual stress from the manufacturing process. The measured elastic modulus for each size of the rebar is reported in Table 3-3, which is based on the linear regression of the stress-strain data between 20 percent and 75 percent of the yield point.

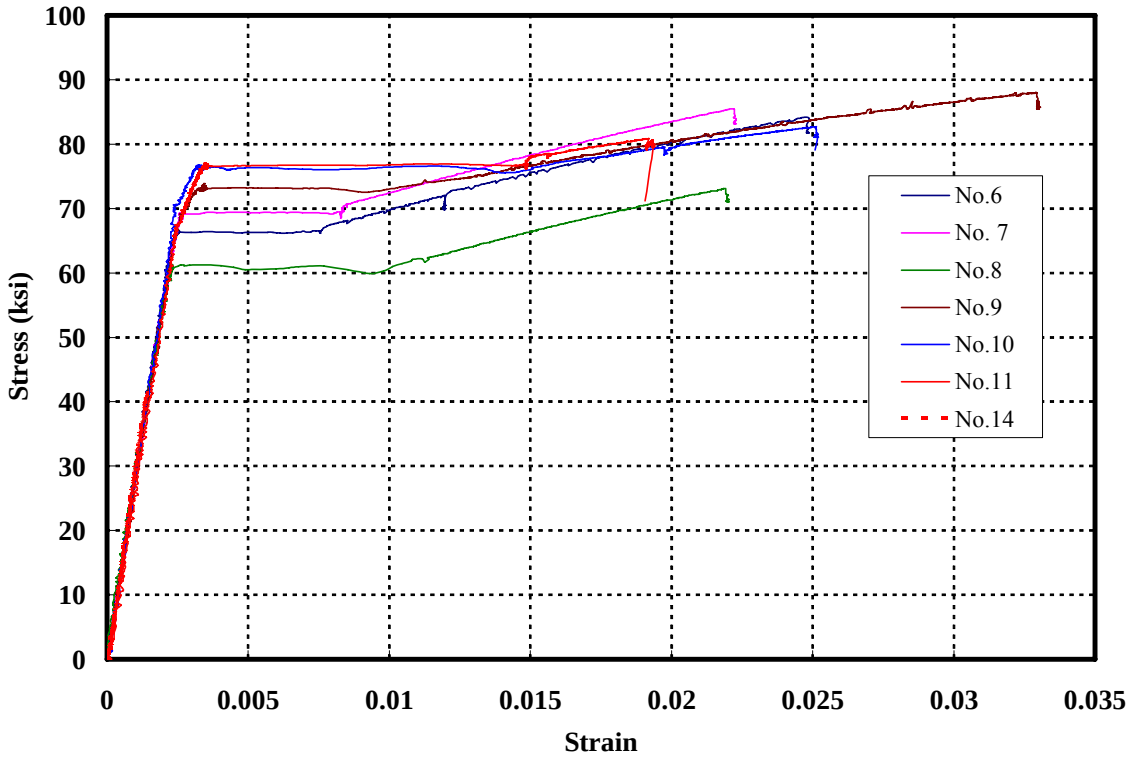

Figure 3-58 Stress-strain Curves of Reinforcement

Table 3-3 Measured Yield Stress and Elastic Modulus of the Steel Reinforcement

Rebar Size	6	7	8	9	10	11	14
f_y (ksi)	66.0	69.2	60.8	75.4	76.1	76.6	NA
E (10^3ksi)	28.8	28.3	26.3	28.1	28.3	28.9	29.8

4 ANALYSIS AND DISCUSSION OF TEST RESULTS

4.1 Introduction

In this chapter, data acquired from present study and those from the literature were combined together for a comprehensive study on the behavior of high-strength concrete under pure flexure and axial-flexural loading. Each section in this chapter focuses on one of the research objectives, and the sections are arranged in the same sequence of the research objectives, as listed in Chapter 1.

4.2 Ultimate Strain of Concrete

Data on the ultimate strain were collected from the literature for both normal-strength concrete and high-strength concrete. The data are presented together with those test results of the present study (NCHRP 12-64 Project). A statistical study was then carried out to examine the ultimate strain of high-strength concrete.

The reported ultimate strain of concrete from beam tests alone is relatively scarce. Therefore, data were collected from various types of tests including cylinders, C-shape specimens, prestressed girders and columns. Data from both normal-strength concrete and high-strength concrete specimens were collected for a comprehensive statistical study. It should be noted that the reported ultimate strains of concrete have two meanings: it could either reflect the strain at which concrete is crushed; or the strain at which load dropped to 85 percent of the peak load. Data were examined before included in this review. Specifically, strain readings

were excluded from this research, when they were affected by cover-spalling or lateral confinement.

The ultimate strain values are plotted against concrete strength in Figure 4-1. Test data from the present study is marked differently than the data from literature review. The six data points of NCHRP Project 12-64, which has concrete strength below 10 ksi are from testing of prestressed girders (Choi, 2006). It can be seen from this figure that the data from this project and those collected from literature are in the same range. The maximum ultimate strain value of 0.0072 was reported by Weiss et al. (2001) in their study on the effect of damage localization. This extremely high value is attributed to the loading condition, where the two plates are so close to each other that they provide high confinement for the concrete within. This data point was deemed as an outlier and was only shown in the figure; but not included in statistical analysis. Overall, majority of the data points in this figure fall above 0.003. However, no clear trend can be seen from this figure as a function of concrete strength.

The average and standard deviation of the data for various concrete strengths are shown in Table 4-1. The average ultimate strain for concrete strength between 6-10 ksi is slight smaller than that for other concrete strengths. This is possibly due to the smaller sample size. Otherwise, the average and the standard deviation of ultimate strain for each range of concrete strengths are very close to each other for both high-strength concrete and normal-strength concrete. The average ultimate strain value for high-strength concrete is slightly higher than that of normal-strength concrete and the standard deviation is slightly

smaller. It can also be seen that the value of 0.003, which is adopted by major design codes in US, seems to be one standard deviation below the average for both the high-strength concrete and the normal-strength concrete. Meanwhile, the value of 0.0035, which is used in the design codes of Belgium, Sweden, Germany, and Canada, is very close to the average value.

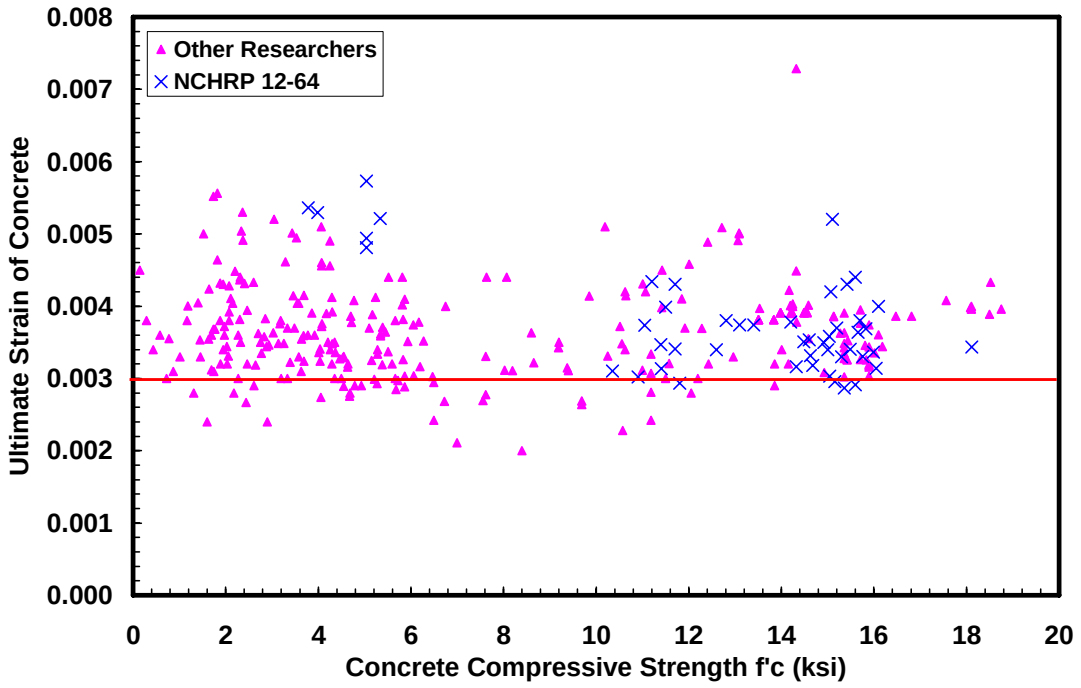

Figure 4-1 Ultimate Strain of Concrete for Various Concrete Strengths

The distribution of the ultimate strain for normal-strength concrete and high-strength concrete are also plotted in the format bar charts, as shown in Figures 4-2 and 4-3, respectively. The frequency of occurrence for each range of strain values is also given above each bar.

Distribution of the ultimate strains for normal-strength concrete has a bell-shape. For normal-strength concrete, 26 out of 190 specimens (15 percent) have an ultimate strain below

0.003. The percentage of high ultimate strain values (greater than 0.0042) are 19 percent, which is higher than the reported low values (less than 0.003), making the distribution is slightly skewed to the high values.

Table 4-1 Average and Standard Deviation of the Data for Ultimate Strain of Concrete

f'_c (ksi)	Sample size	Ultimate Strain of Concrete	
		Average	Standard Deviation
0-2	33	0.00376	0.00071
2-4	62	0.00381	0.00068
4-6	67	0.00363	0.00067
6-8	15	0.00317	0.00062
8-10	13	0.00324	0.00062
10-12	31	0.00367	0.00062
12-14	29	0.00385	0.00060
14-16	72	0.00363	0.00046
>16	15	0.00379	0.00032
Normal-Strength Concrete (0-10ksi)	190	0.00365	0.00070
High-Strength Concrete (>10ksi)	147	0.00370	0.00060

Distribution of the ultimate strains for high-strength concrete is quite different. Data is clustered in the range between 0.003 and 0.0042. Therefore, standard deviation is lower for high-strength concrete. Only 9 out of 147 data (6 percent) falls below 0.003. It is to be noted that about 30 percent of reported values fall into the range of 0.0038 and 0.0042, which is much higher than the number of points for normal-strength concrete in this range. Meanwhile the number of reported values above 0.0042 is significantly less than that of normal-strength concrete.

ACI 363-R92 states that “While high-strength concrete reaches its peak stress at a compressive strain slightly higher than that for lower-strength concrete, the ultimate strain is

lower for high-strength concrete, both in uniaxial compression tests and in beam tests." However, the observed trend from this research seems contradictory to this statement, even though test data in ACI 363-R92 report were also incorporated in this data analysis.

Based on the mean, standard deviation and the sample size, the mean value of the ultimate strain for normal-strength concrete and high-strength concrete are compared. For a significance test, the statistical z-value is only 0.7, which is a relatively small value. In other words, there is no significant difference in the ultimate strain between normal-strength concrete and high-strength concrete.

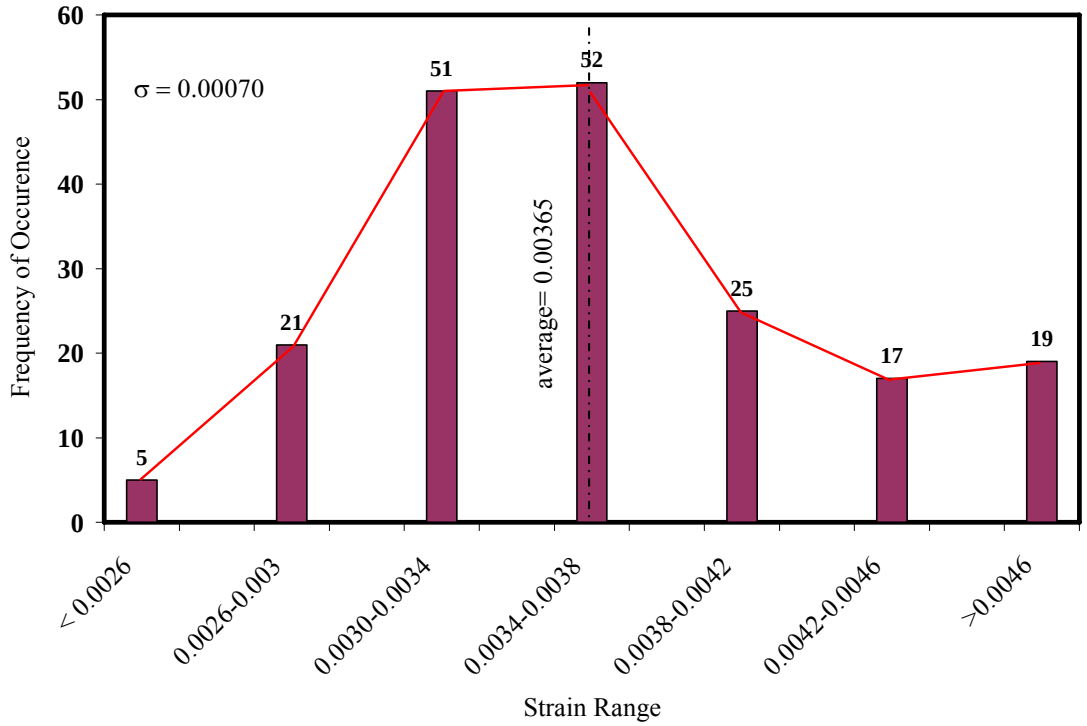

Figure 4-2 Distribution of Ultimate Strain of Concrete for Normal-Strength Concrete

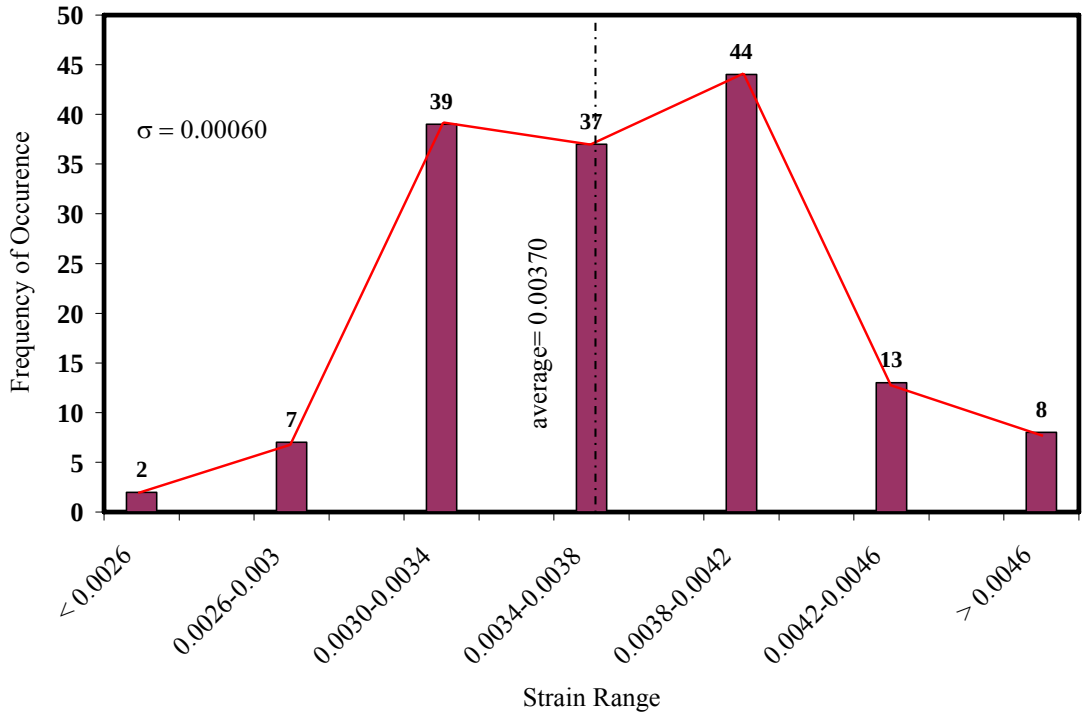

Figure 4-3 Distribution of Ultimate Strain of Concrete for High-Strength Concrete

To investigate the effect of strain gradient on the ultimate strain of concrete, the collected data were divided into two categories, and compared in Figure 4-4. Beams and C-shape specimens are considered as specimens with “large eccentricity”, where the neutral axis is within the section. On the other hand, cylinders and columns are categorized together as specimens with “small eccentricity”, where the neutral axis is way outside the section.

No clear trend can be observed in Figure 4-4 between the two categories. For a total of 241 specimens with “large eccentricity”, the average ultimate strain is 0.00359 and the standard deviation is 0.00066. Meanwhile the average and standard deviation are 0.00386 and 0.00049 respectively, for a total of 96 specimens with “small eccentricity”. Significance test was conducted for the two categories of data and the statistical z-value was found to be 4.13,

which is quite significant. In other words, there is more than 99 percent confidence that specimens with small eccentricity have larger ultimate strain. Many researchers seem to believe that specimens subjected to strain gradient have higher ultimate strain values. It needs to be reiterated here that any column test data which involved cover-spalling or confinement effect were excluded in this analysis. The result of the statistical significance test indicates that the reported low ultimate strain values is more likely due to the cover-spalling rather than the absence of strain gradient.

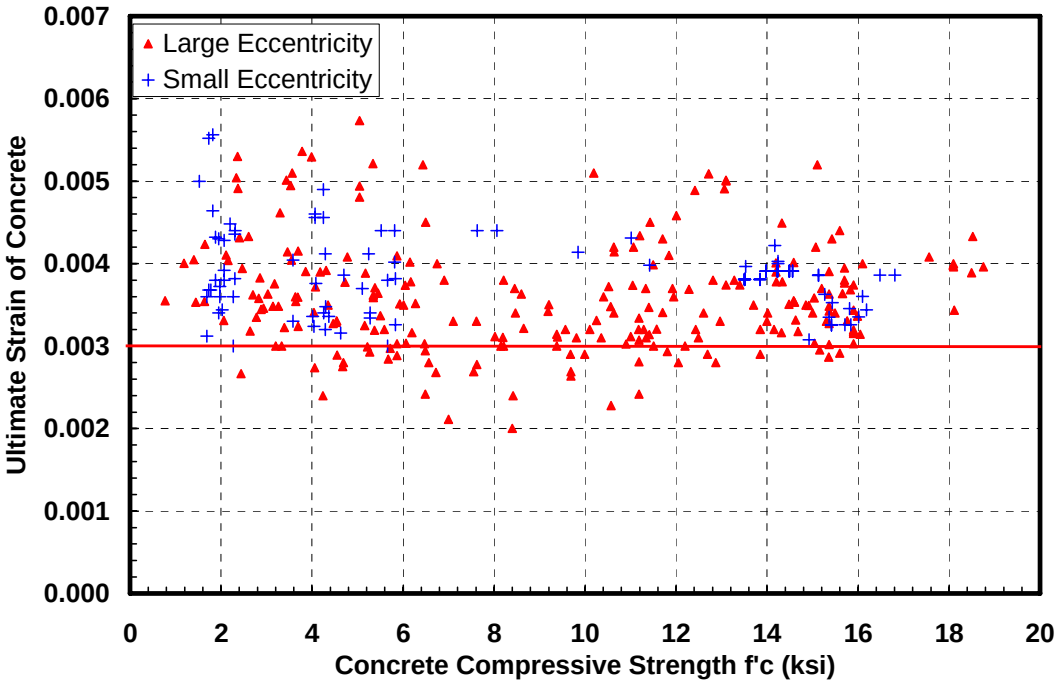

Figure 4-4 Ultimate Strain of Concrete, Small Eccentricity vs. Large Eccentricity

It is believed that the issue is actually more complicated than it appears. Before further discussion, it is necessary to clarify the definition of the ultimate strain of concrete. In most of US design codes, the ultimate strain of concrete refers to the strain at which concrete is crushed.

However, in an actual experiment with multiple instruments applied, it is not clear as to which measurement is the true ultimate strain. Test results from specimen (10B5.7) are used here to demonstrate this quandary. Figure 4-5 shows a typical failure mode which is observed for many specimens tested in pure flexure. The loading point, center-line as well as the dimension of the failure zone are marked on the graph. During the test, it was observed that the 16" wide, 4" deep triangular zone crushed first, which was instantly followed by the failure of the specimen. Figure 4-6 shows the instrumentation on the top surface, which included 7 pi-gauges in the constant moment zone. Measured values of the gauges were adjusted based on the measured strain gradient and are shown in Figure 4-7. Out of the five 4 in. pi-gauges, the gauge No."100d" didn't function at all. As the gauges were all in the constant moment zone, theoretically, the strain readings should be same. However, the measured values were apparently quite different. At the time of failure, the measured ultimate strain values were 0.00379, 0.00296, 0.00407, 0.00434 for pi-gauge 100a, 100b, 100c, 100e, respectively. The readings of pi-gauge number 200 and were 0.00393 and 0.00371, respectively. The gauge right above the failure zone, i.e., 100e had the largest strain reading, which is 0.00434 at the time when concrete crushed. The gauge 100b had smallest reading from the beginning of the test, possibly because of its closeness to the edge. The other gauges had measurements somewhere in between. From this comparison, it is believed that the readings of gauge 100e should be taken for the ultimate strain. Some may argue that any of these readings would be acceptable, except for gauge "100b". However, using the value of 0.00371 or 0.00434 could make a huge difference in the statistical analysis.

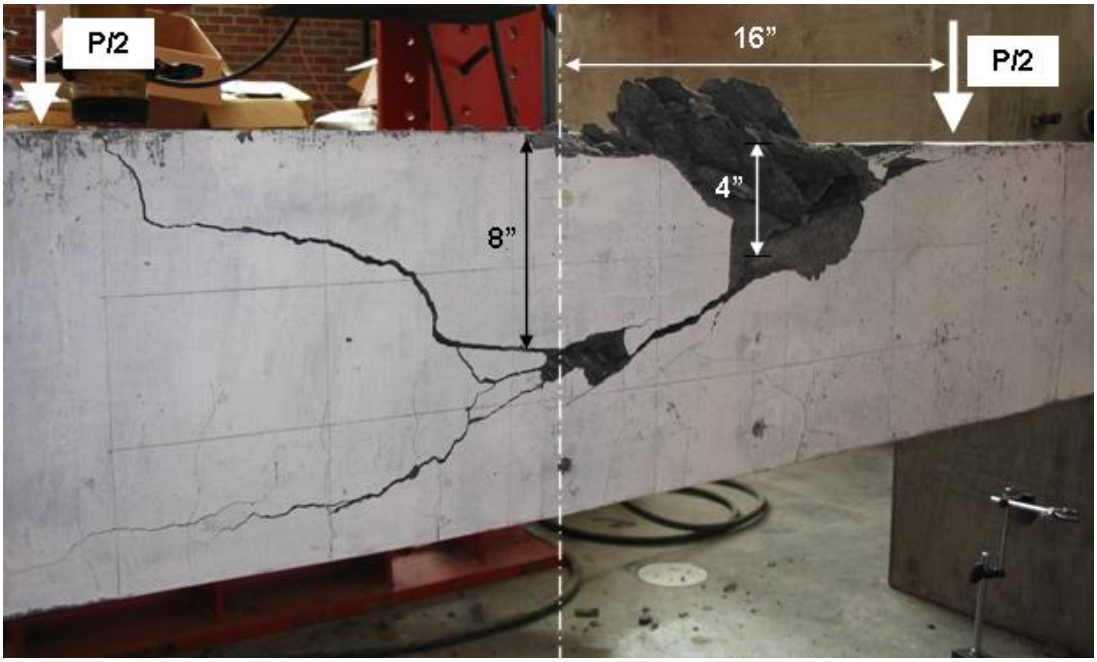

Figure 4-5 Typical Failure Mode of the Pure Flexure Specimen (10B5.7)

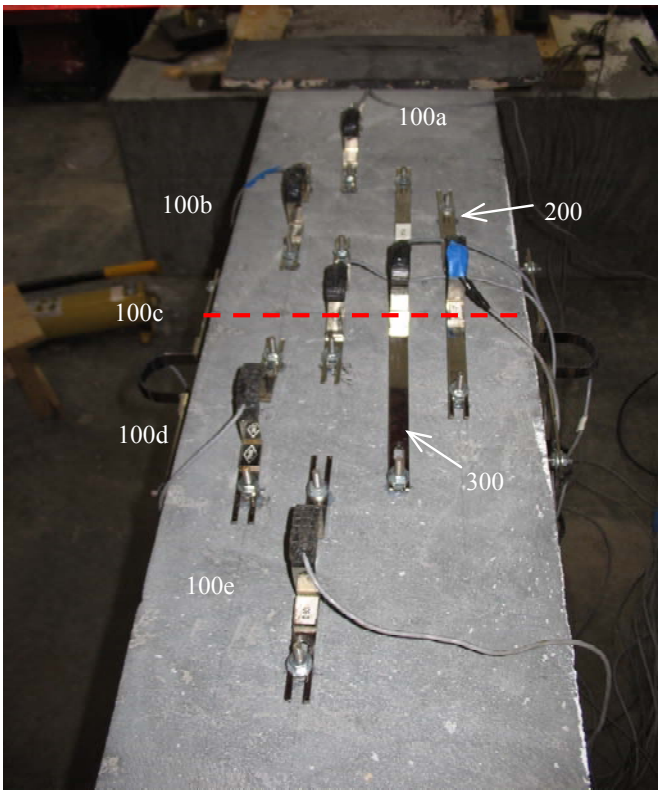

Figure 4-6 Instrumentation of the Pure Flexure Specimen (10B5.7)

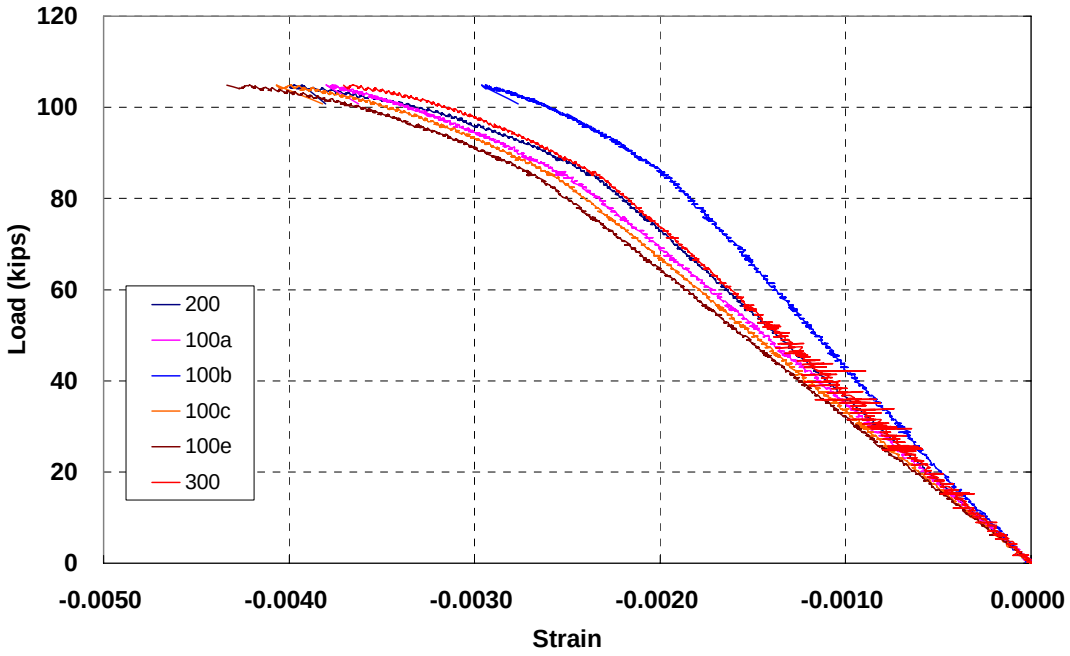

Figure 4-7 Strain Readings on the Pure Flexure Specimen (10B5.7)

The difference of measurements between the pi-gauges in the constant moment area was observed practically in all tested specimens, even though the overall difference is not very significant. Similar "strain localization" was reported by Weiss et al. (2001). The effect of strain localization makes it very difficult to identify the peak strain when concrete crushed. In this regards, the selection of gauge length is very critical. If the gauge length is too long, the localized strains may be missed. On the other hand, if the gauge is too short, the difference in material property between the aggregate and the mortar may affect the measured strain value. It is also important to instrument the entire area where failure may occur. When the constant moment area is long, it requires a large amount of instrumentation as well as a good, multi-channel data acquisition system to catch the readings of all instrumentation at the same time.

In many cases, it may be cost prohibitive to instrument the entire constant moment area. In some cases, identifying the maximum strain is not the primary research interest. For example, research papers concerned with the stress-strain curve of concrete may focus on the average strains in the testing zone. In many of such studies, the researchers only instrument the mid-span.

One assumption in the statistical analysis is that the reported data in the literature have the same accuracy, which is probably not true. Many data points, particularly those for normal-strength concrete, were collected from the studies in the 1950's and 1960's, when computers and high-speed data acquisition system were not available. In such cases, the entire stress strain curve of concrete is usually characterized by less than 10 points; while these days, a curve usually consists of thousands of points and the data is recorded at high frequencies.

The ultimate strain may also be affected by the stiffness of the testing machine as well, particularly for cylinders. Machines with higher stiffness help detect the post-peak behavior of concrete better. However, this is often hard to distinguish from research papers.

In summary, it is not possible to conclude whether normal-strength concrete or high-strength concrete has a higher ultimate strain. However, the value of 0.003 seems to be a reasonable lower bound for design purpose for both normal-strength concrete and high-strength concrete.

On the other hand, some of the design codes in the countries (e.g. Germany DIN Fachberricht

101) distinguish between the normal-strength concrete and high-strength concrete for their ultimate strain. As part of NCHRP Project 12-64, Mertol (2006) proposed the following equation for the ultimate strain of concrete based on 188 tests on C-shape specimens:

$\varepsilon_{cu}=0.0038 - 0.00004 \times f'_c$ (Equation 4-1)

where ε_{cu} is the ultimate strain and f'_c is the strength of concrete.

4.3 Flexural Resistance of Beams

4.3.1 Current AASHTO LRFD Specifications

The measured flexural resistance M_{Exp} is compared to the predicted value M_{LRFD} from the current AASHTO LRFD equations in Figure 4-8 for all tested beams in the present study, as well as data from literature with concrete strengths over 10 ksi. For under-reinforced beam under pure flexure loading, the predicted value is based on the AASHTO LRFD Specifications (2004) Equation. 5.7.3.2.2.1, using the current value of 0.85 for α_1, 0.65 for β_1, and the measured material properties. For over-reinforced specimens or the axial-flexural specimens, flexural resistance is determined by solving the two equations based on force equilibrium and strain compatibility. An ultimate strain of 0.003 is assumed in the analysis, and plane sections are considered to remain plane. No strain hardening is considered for steel reinforcement; also tensile strength of concrete is neglected. Plain concrete beams or reinforced concrete beams with reported premature shear failure (Ahmad and Lue, 1987) were excluded from this comparison.

When the M_{Exp}/M_{LRFD} ratio is less than 1 in Figure 4-8, the design code is un-conservative.

This figure seems to indicate more over-reinforced specimens fall below the line, hence un-conservative.

As part of the NCHRP Project 12-64, Mertol (2006) proposed a reduced α_1 factor for high-strength concrete, while keeping the β_1 factor the same as that in the current per AASHTO LRFD Specifications (2004), as shown in Figure 4-9. The flexural resistance is determined using the proposed stress-block factors. The predicted value M_{Prop} is compared with the measured value M_{Exp} in Figure 4-10.

Comparing the results presented in Figures 4-8 and 4-10 indicates that using the proposed α_1 leads to a more conservative prediction of the nominal flexural resistance for all specimens tested in this project. Table 4-2 shows the statistical information of the predicted values of M_{LRFD} and M_{Prop} versus the measured values M_{Exp} for a total of 143 specimens collected from the literature (including those tested in NCHRP Project 12-64). It can be seen that the predictions using the proposed α_1 factor is more realistically conservative, especially for the over-reinforced beams.

Mattock (1961) collected test data from 150 normal-strength concrete beams and calculated their nominal flexural resistance using the same method as that prescribed in the current AASHTO LRFD Specifications (2004). Comparison of test results and predictions are shown in Figure 4-11. Some statistical information about his study is also shown in Table 4-3.

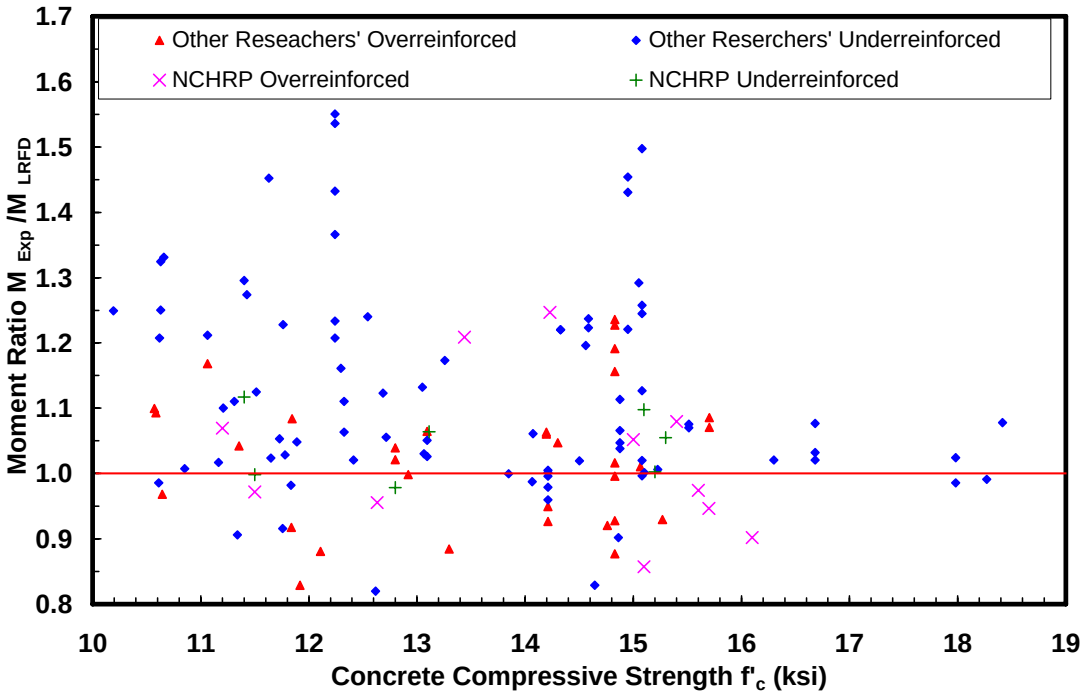

Figure 4-8 Comparison of the Experimental and Predicted Values of Flexural Resistance using the Current AASHTO LRFD Specifications (2004)

Table 4-2 Statistical Data for Over-Reinforced and Under-Reinforced High-Strength Concrete Beams

Type	No. of Specimens	M_{Exp}/M_{LRFD}				
		<1	Min	Max	Avg.	σ
Over-Reinf.	52	19	0.83	1.59	1.07	0.15
Under-Rein.	91	16	0.82	1.55	1.12	0.15
		M_{Exp}/M_{Prop}				
Over-Reinf.	52	12	0.86	1.59	1.11	0.14
Under-Rein.	91	11	0.83	1.55	1.13	0.15

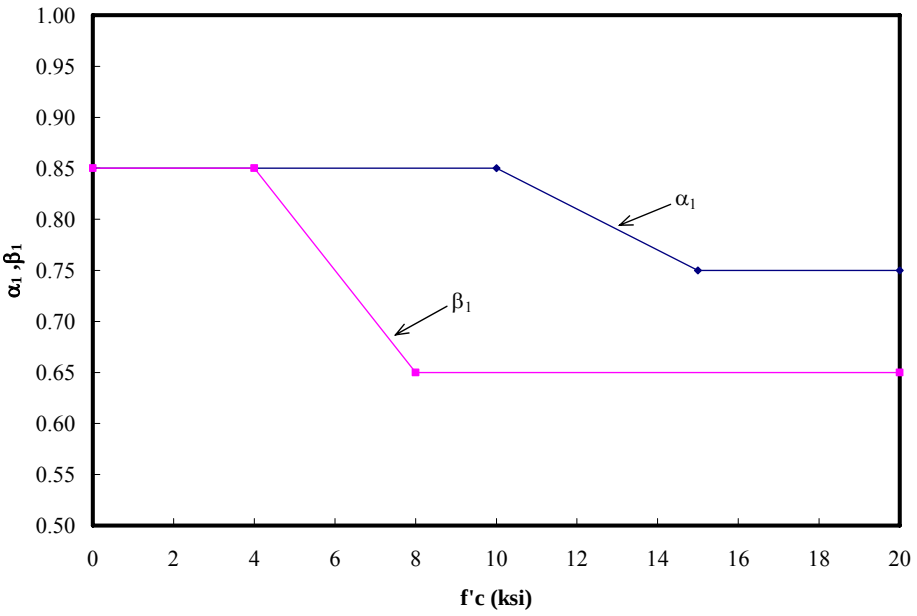

Figure 4-9 Proposed α_1 Factor from NCHRP Project 12-64

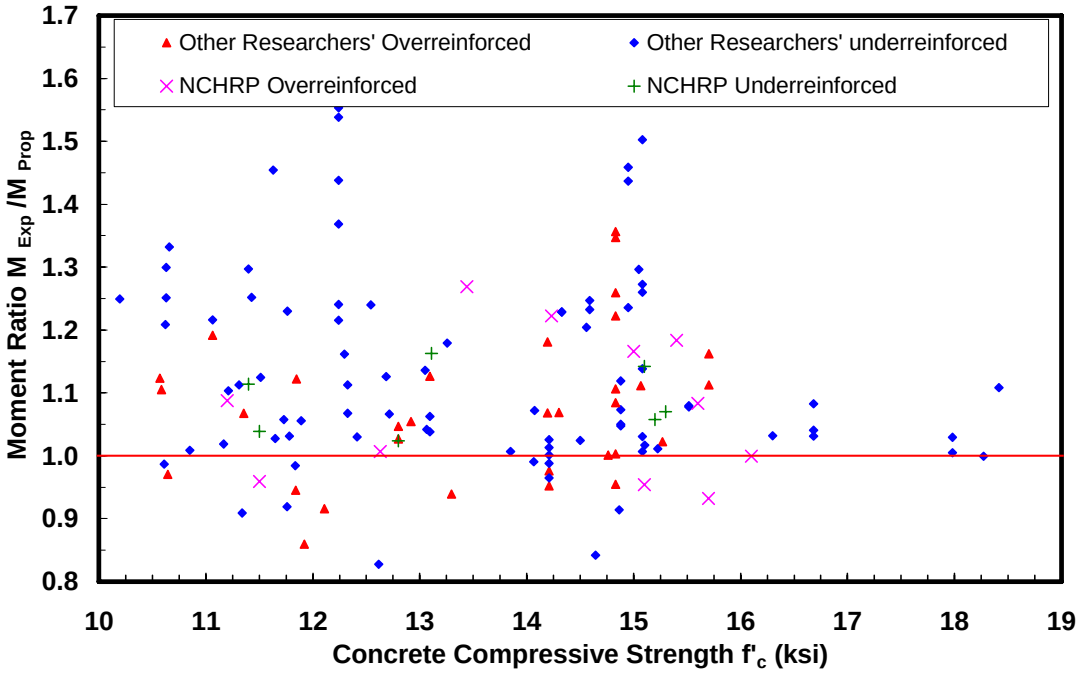

Figure 4-10 Comparison of the Experimental and Predicted Values of Flexural Resistance Using the Proposed Stress Block Factors

Comparing the statistical results in Tables 4-2 and 4-3, it seems that for under-reinforced beams, the accuracy of the current code equations and stress block factors to determine the nominal moment resistance for high-strength and normal-strength concretes is approximately the same. This is expected since flexural resistance of under-reinforced beams is not significantly affected by the exact shape of the stress block, so long as the internal lever arm for the moment is chosen properly.

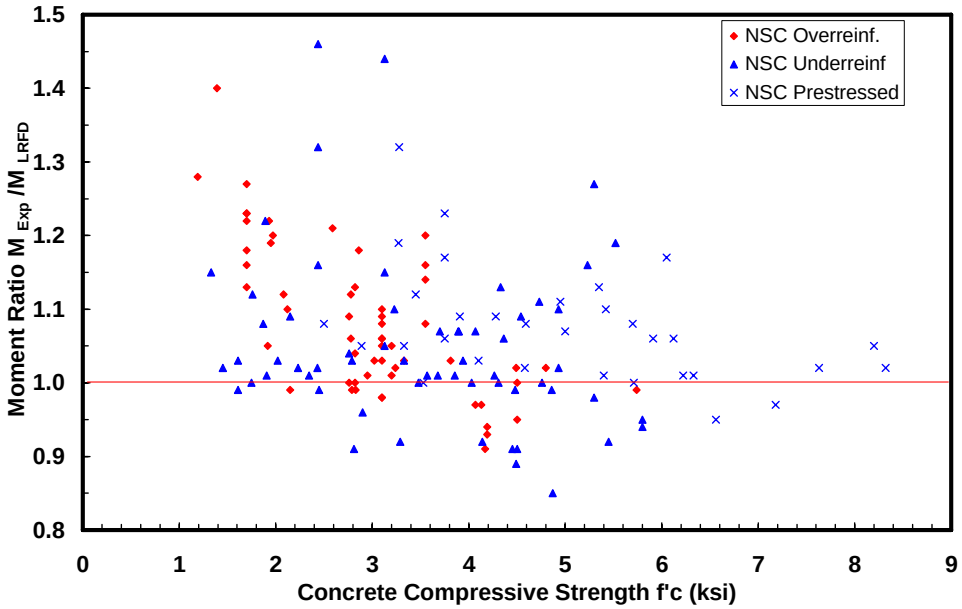

Figure 4-11 Comparison of the Experimental and Predicted Values of Flexural Resistance for Normal-Strength Concrete Specimens

Table 4-3 Statistical Data for Over-Reinforced and Under-Reinforced Normal-Strength Concrete Beams (Mattock, 1961)

Type	Total Number of Specimens	M_{Exp}/M_{LRFD}				
		<1	Min	Max	Avg.	σ
Over-Reinf.	57	12	0.91	1.40	1.08	0.10
Under-Rein.	93	18	0.85	1.28	1.07	0.09

However, when comparing the flexural resistance of over-reinforced beams, code equations

and stress block factors are less conservative for high-strength concrete than for normal-strength concrete beams. Nominal flexural resistance is overestimated in 21 percent of the normal-strength concrete beams; while for high-strength concrete beams, 36.5 percent of the cases were overestimated. When using the proposed stress block factor by Mertol (2006), overestimation drops down to 23 percent for over-reinforced high-strength concrete beams, which is similar to the normal-strength concrete (Mattock, 1961).

The distribution of the M_{Exp}/M_{LRFD} ratio is shown using bar chart in Figures 4-12 and 4-13 for normal-strength concrete and high-strength concrete specimens, respectively. The distribution of the M_{Exp}/M_{Prop} ratio is shown in Figure 4-14 for high-strength concrete specimens. The current LRFD equations predict the nominal flexural resistance for normal-strength concrete members reasonably accurate and conservative. 102 out of 150 (approximately 70 percent) predictions fall within ± 10 percent. The overall distribution of ratio for normal-strength concrete specimens is a bell shape, skewed to the right, which indicates the predictions tend to be safer.

For high-strength concrete, prediction of nominal flexural resistance using the current LRFD equations is less conservative and less accurate, as shown in the Figure 4-13. Using proposed stress block factor (α_1) by Mertol (2006) would improve the prediction for high-strength concrete beams and beam columns.

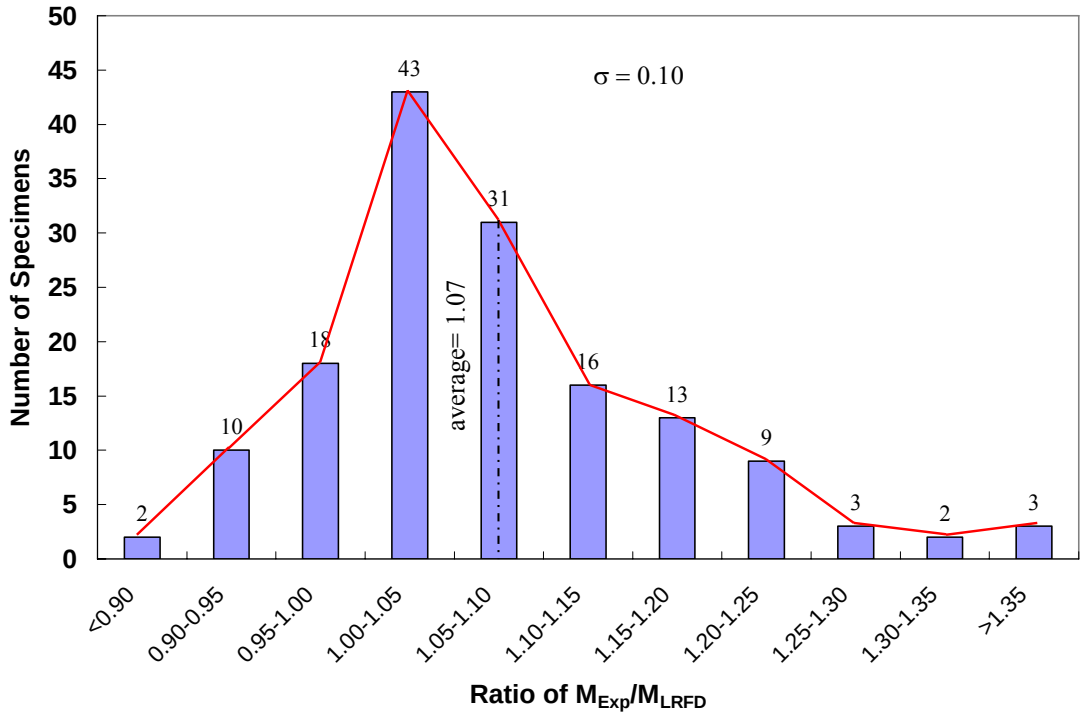

Figure 4-12 Distribution of M_{Exp}/M_{LRFD} for Normal-Strength Concrete Specimens

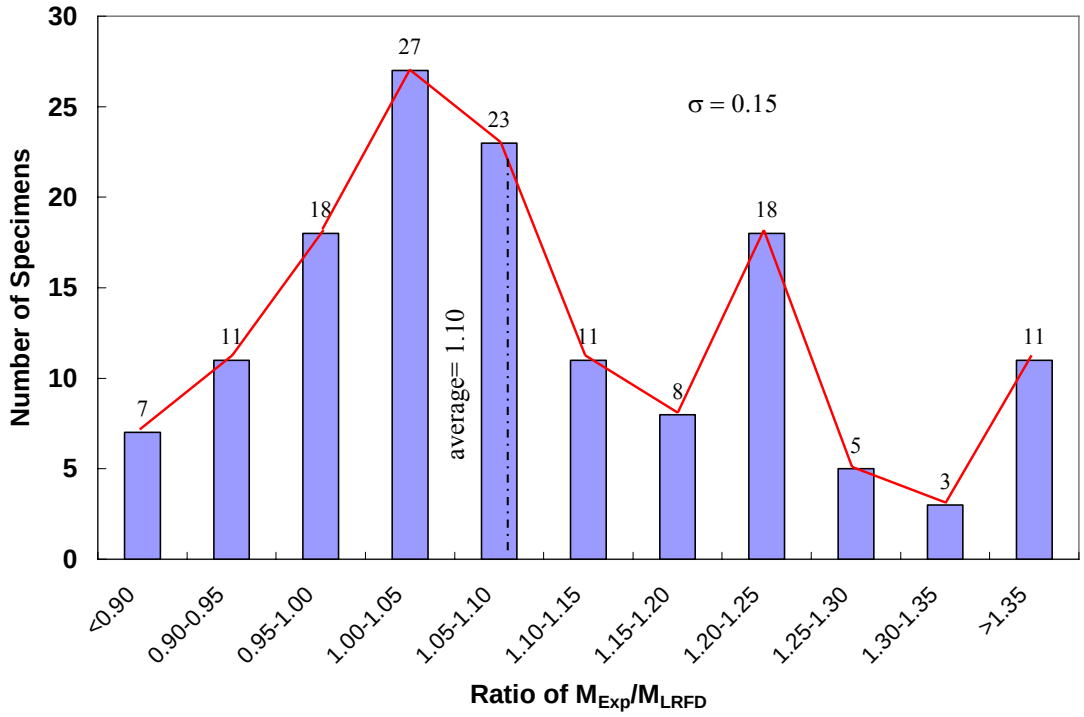

Figure 4-13 Distribution of M_{Exp}/M_{LRFD} for High-Strength Concrete Specimens

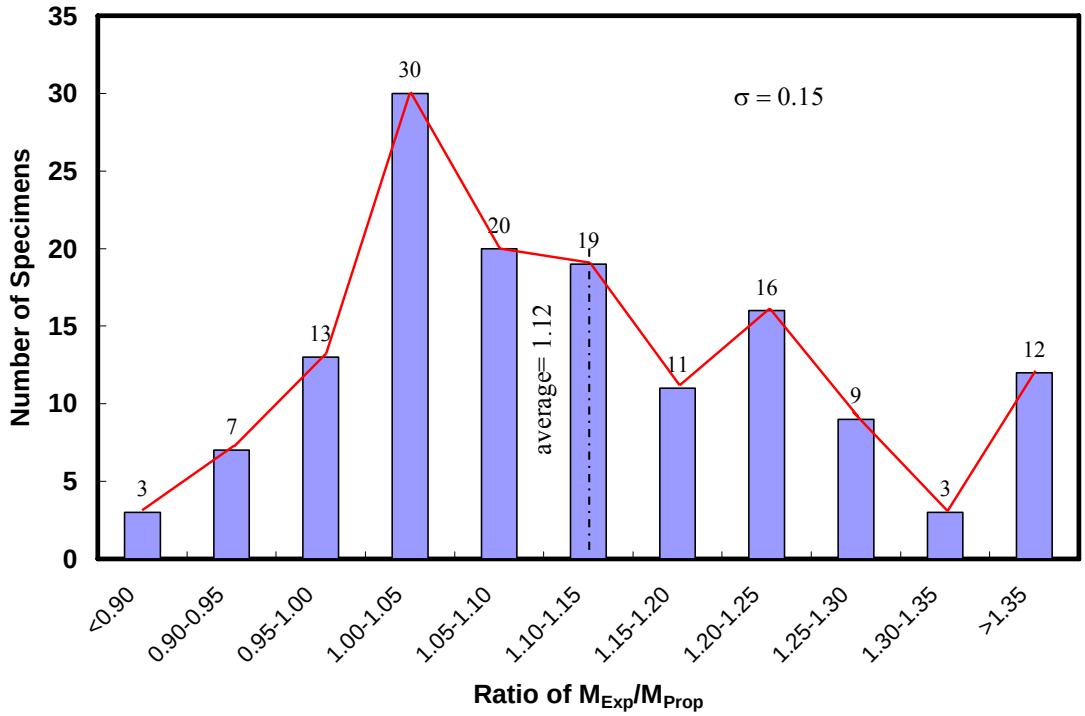

Figure 4-14 Distribution of M_{Exp}/M_{Prop} for High-Strength Concrete Specimens

4.3.2 Sensitivity Analysis on Stress Block Factors

A sensitivity analysis was carried out to determine how the effect of stress block factors would affect the nominal resistance. For under-reinforced members, the longitudinal reinforcement yields at the time concrete crushed. The nominal flexural resistance of a member with rectangular section can be derived by solving the equilibrium equations as:

$$M_n = A_s f_y d(1 - \frac{\rho f_y}{2\alpha_1 f_c'}) \qquad \text{(Equation 4-2)}$$

where A_s and f_y are the area and the yield strength of longitudinal reinforcement, respectively, d is the effective depth of the section, α_1 is the stress block factor, f'_c is the compressive strength of concrete, and ρ is the reinforcement ratio. Taking ω as $\rho\frac{f_y}{f_c}$, the nominal flexural

resistance can be further simplified as:

$$M_n = A_s f_y d(1 - \frac{\omega}{2\alpha_1}) \qquad \text{(Equation 4-3)}$$

Assuming the steel reinforcement ratio is constant in a given under-reinforced cross-section, and the nominal resistances calculated using two different stress block factors, α_1^a and α_1^b, are M_n^a and M_n^b respectively, then ratio of M_n^a to M_n^b can be expressed as:

$$\frac{M_n^a}{M_n^b} = \frac{1 - \frac{\omega}{2\alpha_1^a}}{1 - \frac{\omega}{2\alpha_1^b}} = \frac{\alpha_1^b(2\alpha_1^a - \omega)}{\alpha_1^a(2\alpha_1^b - \omega)} \qquad \text{(Equation 4-4)}$$

It can be seen from the above equation that for under-reinforced beam with rectangular cross-section, neither stress block factor β_1 nor the ultimate strain of the concrete ε_{cu} affects the normal flexural resistance.

For an over-reinforced member, the reinforcement does not yield at the time concrete reaches its ultimate strain. The nominal flexural resistance is calculated by solving the force equilibrium and strain compatibility equations:

$$M_n = A_s f_s (d - \frac{\beta_1 c}{2}) \qquad \text{(Equation 4-5)}$$

$$\alpha_1 \beta_1 f_c' bc = A_s f_s \qquad \text{(Equation 4-6)}$$

$$f_s = \varepsilon_s E_s = E_s \varepsilon_{cu} \frac{d - c}{c} \qquad \text{(Equation 4-7)}$$

where A_s, f_s and E_s are the area, stress and elastic modulus of longitudinal reinforcement, respectively, and c is the neutral axis depth.

To demonstrate the effect of changing the stress-block factor α_1 on the nominal resistance, a 9”x12” cross-section is assumed and effective depth of is 10” for all cases. The parameters involved in this study are given below:

1. Compressive strength of concrete, with values of 10ksi, 14ksi and 18ksi;
2. Reinforcement ratio, with values ranging from 1 percent to 16 percent; and
3. Stress block factor α_1, with values ranging from 0.85 to 0.75.

The calculated nominal flexural resistances are normalized with respect to the value using the current code α_1 value of 0.85. Normalized results are shown in Figures 4-15 through 4-17 for concrete strength of 10ksi, 14ksi and 18ksi, respectively.

It can be seen from these figures that the nominal resistance of the member reduces as α_1 factor reduces. The reduction is more significant for members with higher reinforcement ratio and lower compressive strength of concrete. There is an approximately 10 percent reduction of normalized resistance for assumed sections with concrete strength of 10 and 14ksi, and reinforcement ratio of 8 percent. However, for a member with concrete strength of 18ksi and same reinforcement ratio, the reduction is only about 3 percent because the balanced reinforcement ratio for 18ksi concrete specimen is greater than 8 percent.

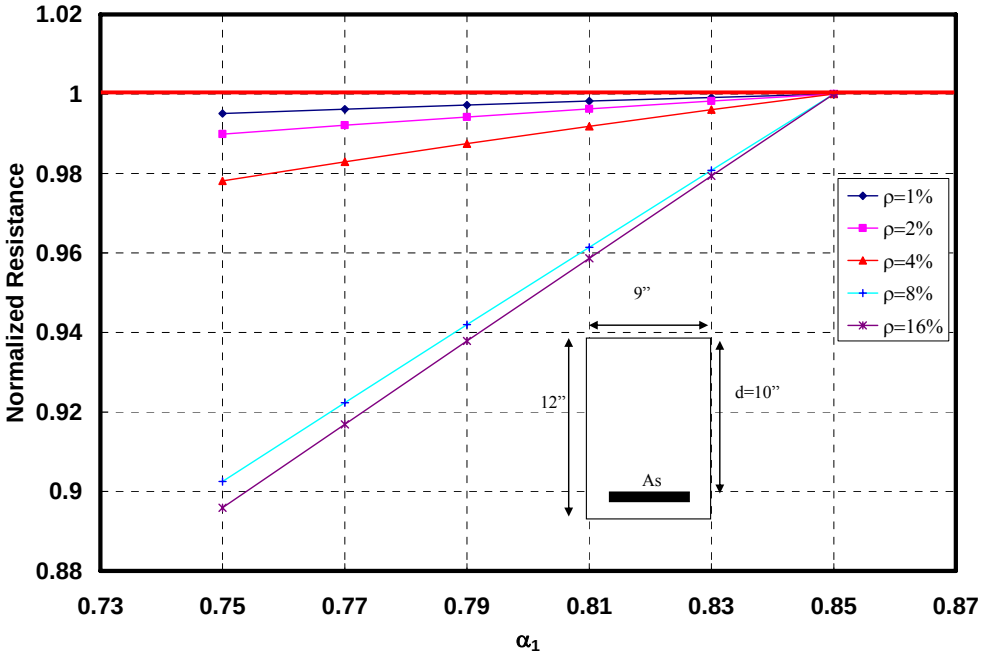

Figure 4-15 Effect of α_1 on the Flexural Resistance for Concrete Strength of 10 ksi

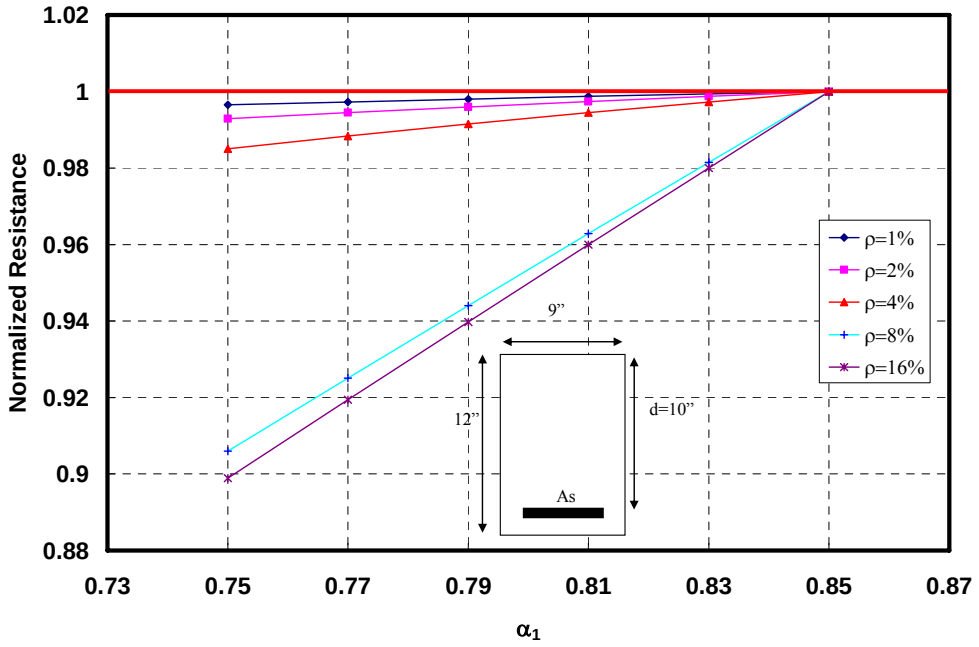

Figure 4-16 Effect of α_1 on the Flexural Resistance for Concrete Strength of 14 ksi

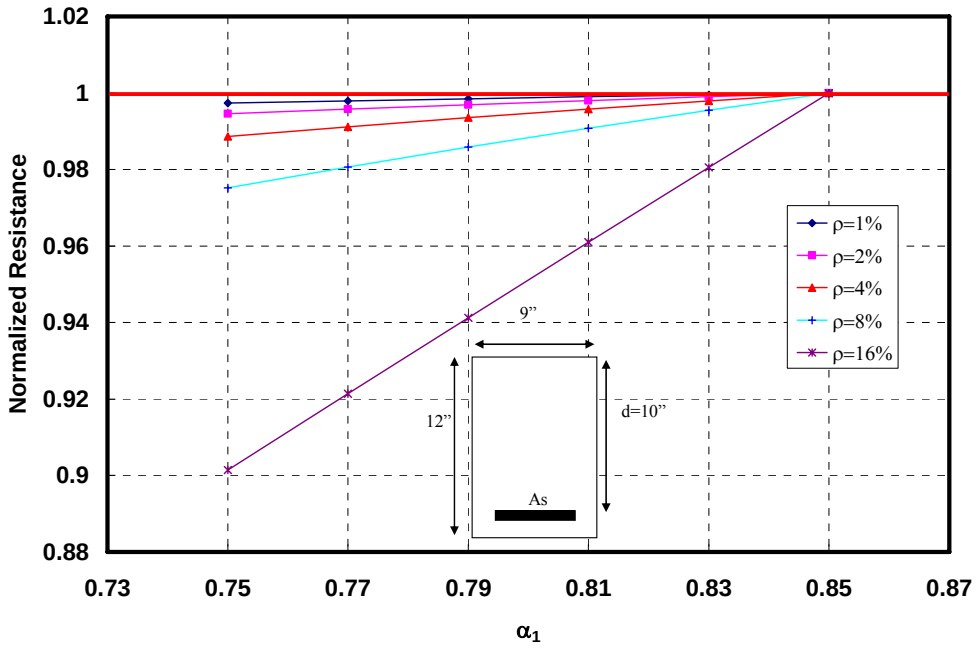

Figure 4-17 Effect of α_1 on the Flexural Resistance for Concrete Strength of 18 ksi

A similar methodology was used to study how the change of stress-block factor β_1 affects the nominal resistance of a cross-section. The parameters involved in this study are given below:

1. Compressive strength of concrete with values of 10ksi, 14ksi and 18ksi;
2. Reinforcement ratio with values of 10 percent and 16 percent; and
3. Stress block factor β_1 ranging from 0.65 to 0.85.

For under-reinforced specimens, changing of β_1 does not affect the nominal resistance of the section. Therefore, only two high reinforcement ratios, ρ=10 percent and 16 percent were selected so that for the selected range of concrete strengths, the section remains over-reinforced for most cases. The flexural resistance of the cross section was calculated in each case using the current α_1 value 0.85. Results were then normalized with respective to the value calculated using $\beta_1 = 0.85$, as shown in Figure 4-18 and Figure 4-19, respectively.

It can be seen from Figure 4-18 and Figure 4-19 that the nominal resistance of the member reduces if the β_1 factor reduces for all the over-reinforced members. In Figure 4-18, there is about 10 percent reduction when β_1 is reduced from 0.85 to 0.65 for all three sections with reinforcement ratio of 16 percent. In Figure 4-19, when reinforcement is 10 percent; the reduction is also about 10 percent for concrete strength of 10 ksi and 14 ksi. For the assumed section with concrete strength of 18 ksi and reinforcement ratio of 10 percent, section becomes under-reinforced when the β_1 is greater than 0.7; therefore change of β_1 has no effects.

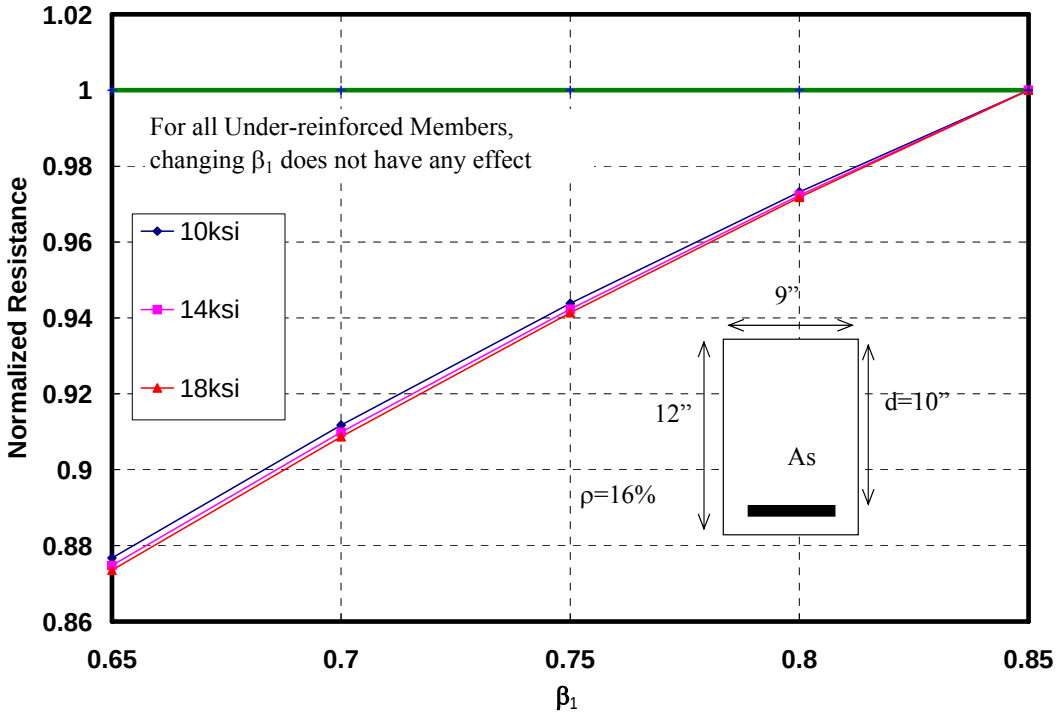

Figure 4-18 Effect of β_1 on the Flexural Resistance for Reinforcement Ratio of 16 percent

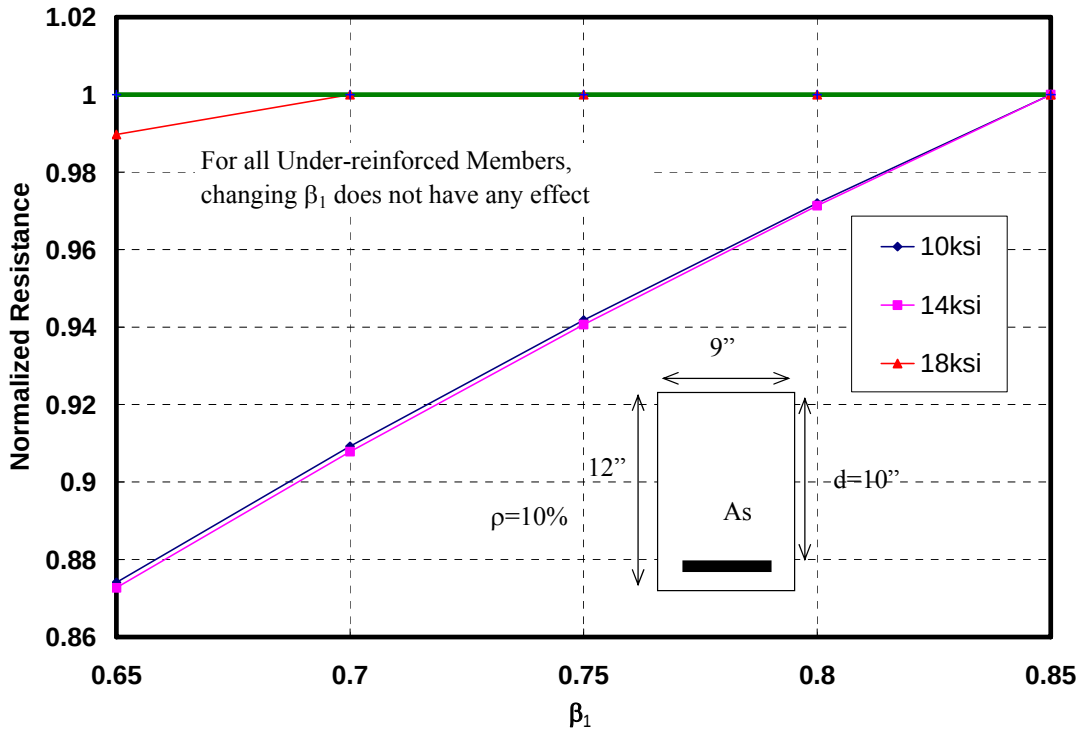

Figure 4-19 Effect of β_1 on the Flexural Resistance for Reinforcement Ratio of 10 percent

The ultimate strain of concrete ε_{cu}, also affects the flexural resistance of an over-reinforced member as well. To explore this issue, the same section with three concrete compressive strengths, 10 ksi, 14 ksi and 18 ksi are selected and a constant reinforcement ratio of 16 percent was used so that the section remains over-reinforced. The nominal resistance of the cross section are calculated using the $\alpha_1 = 0.85$ and $\beta_1 = 0.65$ as in the current AASHTO LRFD Specifications. The results are then normalized with respect to the value calculated using $\varepsilon_{cu} = 0.003$ and are shown in Figure 4-20. It can be seen from this figure that the nominal resistance of the member is reduced along with the reduction of the ultimate strain of concrete ε_{cu}, for all the 3 assumed over-reinforced sections. The reduction in the resistance of the section is slightly higher for higher concrete strengths. However, reduction is all less than 5 percent.

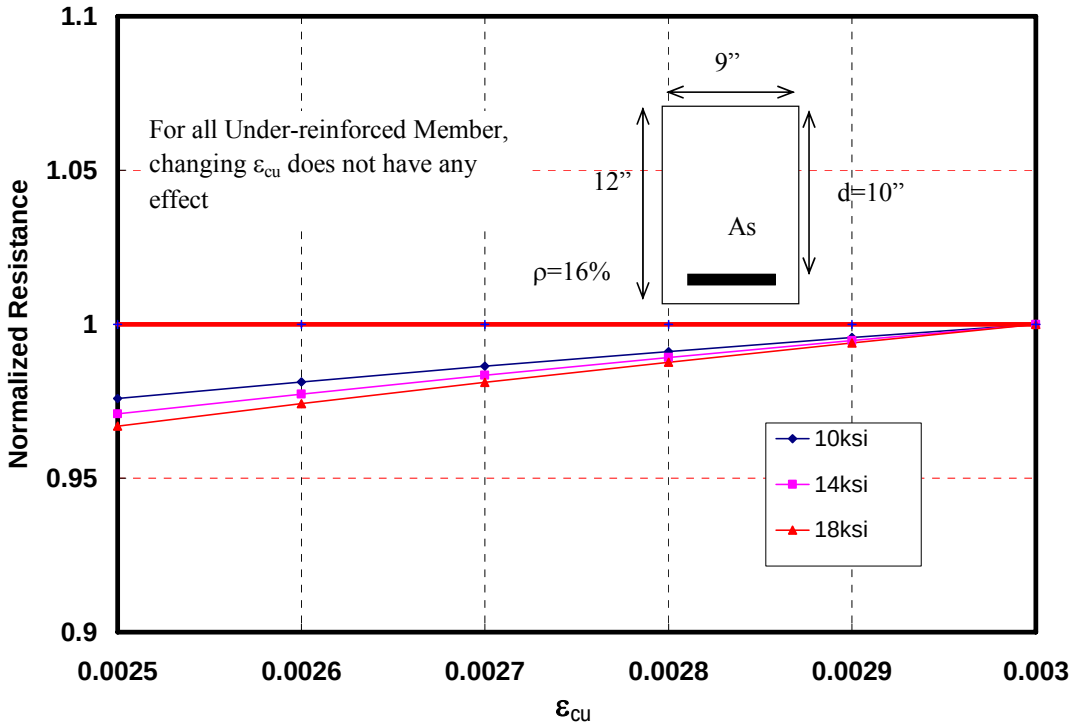

Figure 4-20 Effect of ε_{cu} on the Flexural Resistance for Reinforcement Ratio of 16 percent

4.4 Cracking Moment and Crack Width

4.4.1 Cracking Load/Moment

In the AASHTO LRFD Specifications (2004), the cracking moment is used mainly for two purposes:

1. To calculate deflection at service load, from equation (5.7.3.6.2-2) and,
2. To determine the minimum reinforcement ratio from equation (5.7.3.3.2-1).

As part of NCHRP Project 12-64, the applicability of current expression of modulus of rupture f_r to the high-strength concrete was mainly investigated by Logan (2005). Measured modulus of rupture values from his data and from the data available in the literature are

shown in Figure 4-21, along with test data of modulus of rupture specimens accompanied with the beams and beam-columns in this study.

Logan (2005) reported that ACI 363R-92 provides a better estimate for the modulus of rupture of continually moist cured specimens; while for those cured for only 7 days, AASHTO LRFD provides a better estimate. It should be noted that the modulus of rupture value is very sensitive to the moisture content of the specimen at the time of testing. Most of the data from this study falls within the range of other 7-day moist cured specimens. However, there are fours specimens with high moduli of rupture, which correspond better to the ACI 363R-92 equation. This is mainly due to the fact that these four specimens were kept outside and the rain in summer 2005 resulted in high moisture content.

The observed as well as calculated cracking load are summarized and compared in Table 4-4. The observed cracking load data are from two sources: test observation and the measured load-deflection curves. The cracking load of a specimen was noted down during the test, when the first vertical crack was observed. These loads are listed under column titled "@ testing". Some of the specimens have cracks on the surface before loading, possibly due to drying shrinkage. In these cases, data is marked as NA. Meanwhile, the cracking load can be estimated from the measured load deflection curve at mid-span. Theoretically, upon the first cracking, the stiffness of the cross-section is significantly reduced. These loads are reported under column titled "From P-Δ".

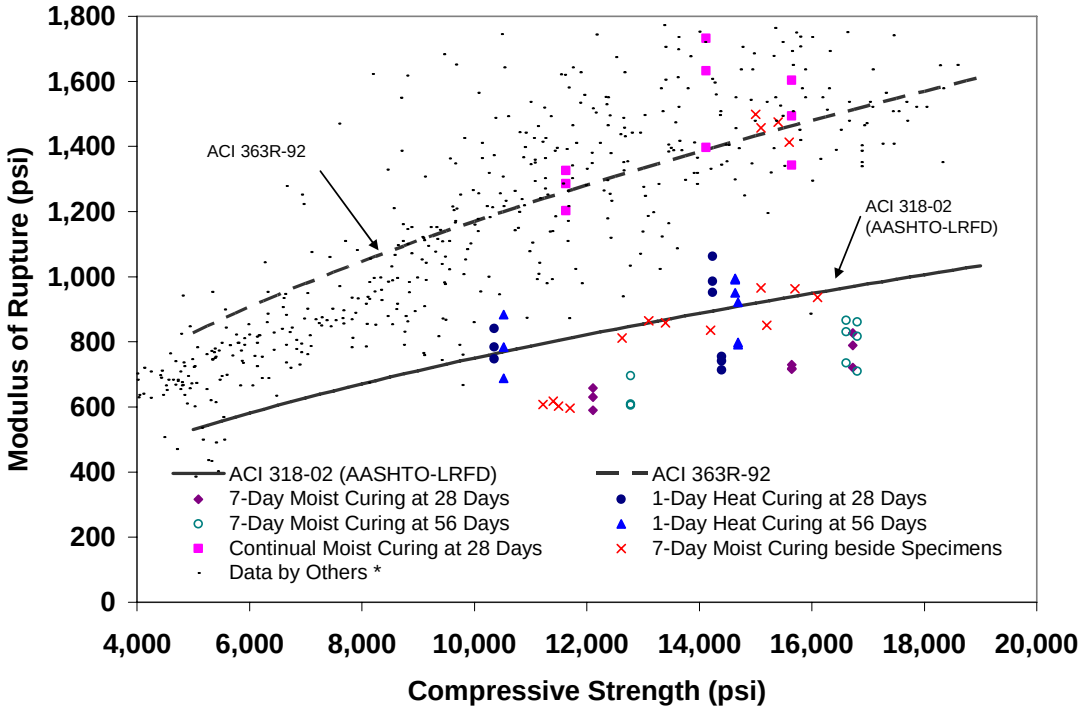

Figure 4-21 Modulus of Rupture vs. Concrete Compressive Strength

The cracking load for each specimen is also calculated using AASHTO LRFD equation (5.7.3.6.2-2). Two expressions are used for the modulus of rupture: current LRFD equation and the measured f_r value. It should be noted that LRFD provides two modulus rupture values: one for calculating deflection and the other for the determination of the minimum reinforcement ratio. The smaller value of the two, equation for calculating the deflection and camber is used here, which is: $f_r = 0.24\sqrt{f'c}$ (ksi).

Overall, the observed value and the predicted value do not always match very well. This is attributed to inaccuracies from both observed and predicted data. The inaccuracy from observed data may come from the following sources:

1. The first cracking could not be recognized until it propagated to the surface of the specimen. Also, the crack might be so small that it would take some time to be noticed. Therefore, it is believed that the reported value is usually slightly over-estimated.
2. The cracking load from the load-deflection curve is not very accurate either. This is because the development of micro-cracks in the mortar is gradual. As a result, the change in the slope is gradual and not distinctive.

The predictions are not accurate either, and mainly because:

1. The change of moisture content affects the modulus rupture specimens and the flexural specimens differently. As mentioned earlier in this section, all specimens were kept outside during the summer and subjected to high humidity. However, the size of modulus rupture beams is much smaller compared to the beam and beam column specimens. As a result, the increase of moisture content for modulus rupture beams is likely to be more significant. In other words, it is likely that the measured f_r value from modulus of rupture beam is not representative of the actual f_r of the flexural members.
2. Using the modulus of rupture alone to determine the cracking moment is merely an approximation: The modulus of rupture beams are plain concrete specimens, while the flexural members are reinforced. The shrinkage of concrete, when restrained by the reinforcement, generates tensile stresses in concrete, which in turn would lower the cracking moment. In this study, it was observed that several specimens cracked even before loading. The effect of restrained shrinkage is taken into account in the

Australian code (Australian Standard for Concrete AS3600).

Table 4-4 Summary of Cracking Load Data

Specimen No.	f'_c @ Testing Day (ksi)	f_r(psi)		Cracking Load (kips)			
		LRFD	Measured	Observed		Predicted	
				@Tesing	From P-Δ	Code f_r	Using Measured f_r
10B2.1	11.4	810	618	11	6.5	7.9	6.2
10B4.3	11.5	814	603	7	NA	8.1	6.0
10B5.7	11.2	803	607	10	12.2	8.0	6.0
10B10.2	12.6	853	812	NA	4.5	10.3	9.8
10BA4	11.7	821	596	11	14.3	14.6	12.6
10BA4r	11.5	814	807	13	12.8	15.2	15.3
14B3.3	13.1	869	865	13	10.0	8.5	8.6
14B7.7	13.4	879	858	16	8.0	8.6	8.6
14B12.4	14.2	904	836	15	13.0	8.9	8.4
14B7.6	15.4	942	1475	NA	6.0	11.2	17.8
14B12.7	15.0	930	1498	15	7.0	11.1	18.0
14B17.7	15.6	948	1413	NA	8.0	11.3	17.0
14BA4	15.2	936	850	22	18.0	19.0	18.3
14BA4r	15.1	933	1457	10	9.0	12.1	14.8
18B5.9	15.7	951	963	NA	12.0	11.3	11.6
18B12.7	16.1	963	936	NA	10.0	11.5	11.3
18B17.7	15.1	933	965	4	15.0	11.1	11.6
18BA4	15.3	939	963	NA	9.5	9.4	9.3

4.4.2 Crack Width

In the present study, crack widths were measured using pi-gauges installed on the bottom

surface of the specimens. Readings were adjusted based on measured strain gradient to reflect the crack width at the extreme tension fiber of concrete. The reported values are the readings at 45 percent of the measured peak load, which is generally considered to represent the service load.

The measured crack widths for the tested pure flexure specimens are shown in Figure 4-22. A crack width of 0.017 in., which is representative of crack width specified for class 1 exposure condition, is also shown in the same figure. It is to be noted that comparing the crack width at the stress level of $0.6f_y$ for the longitudinal reinforcement with the limit of 0.0017 in. is not appropriate for over-reinforced specimens, because the stress level could be well below $0.6f_y$ at the time of failure. Since all the specimens tested in this project utilized mild steel reinforcement with spacing less than that allowed LRFD Eq.5.7.3.4.1, all of the measured crack widths were expectedly less than 0.017 in.

The current LRFD equations in control of cracking are based on a physical crack model (Frosch 2001) rather than the statistically-based model used in previous editions of the specifications. Measured crack widths are compared with the predicted values using Frosch's model (Frosch 2001) in Figure 4-23. In calculating the crack width, the measured steel strains were used. It can be seen that Frosch's model over-predicts the crack widths for the majority of the beams tested in this study. The crack widths of three over-reinforced beams were under-predicted by Frosch's model, in which the stress in steel at service load was much below $0.6\ f_y$.

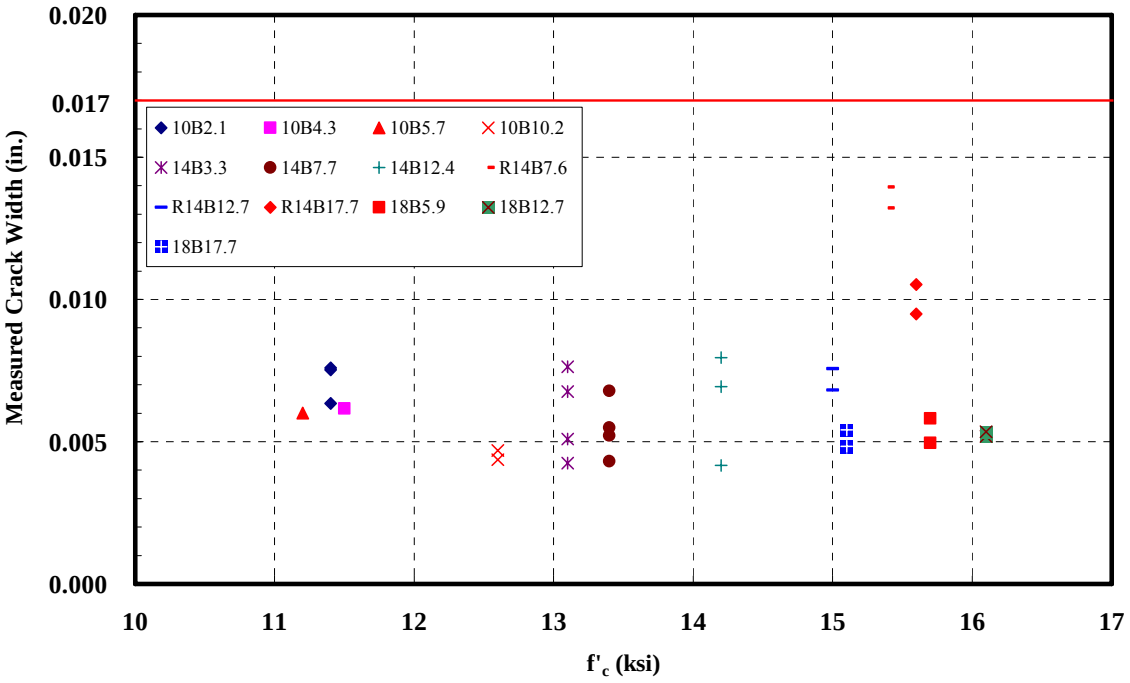

Figure 4-22 Measured Crack Width for Various Concrete Compressive Strength

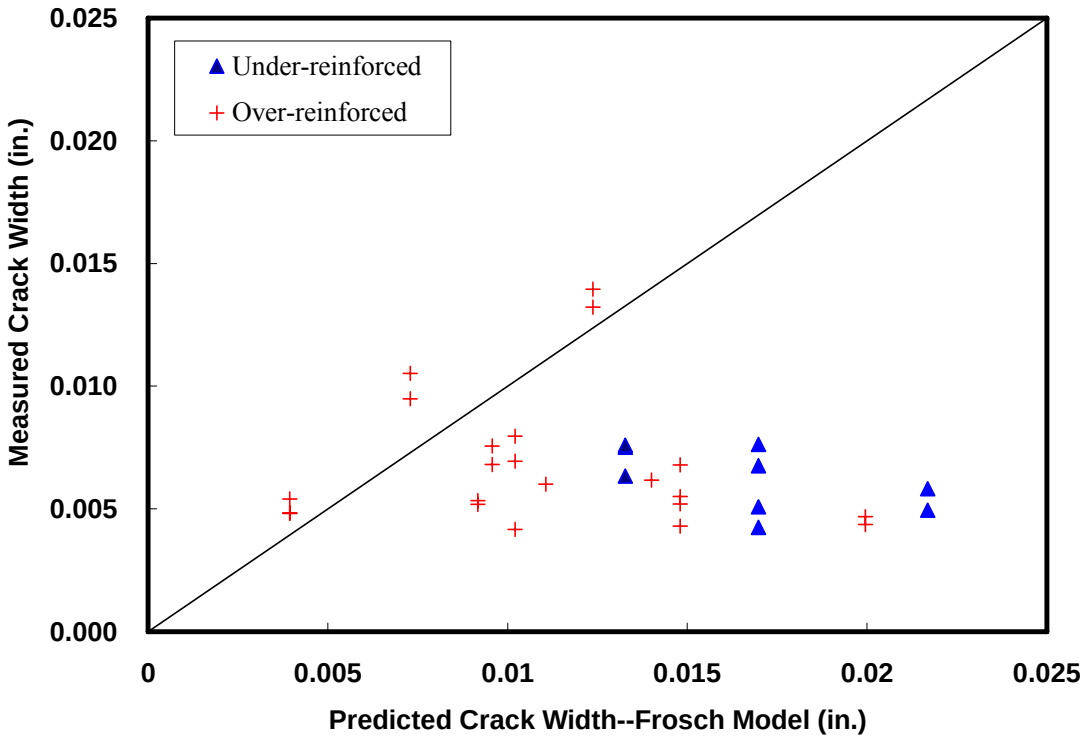

Figure 4-23 Measured Crack Width vs. Predicted Value Using Frosch's Model

4.5 Moment-Curvature Response at Mid-span

4.5.1 Introduction

While moment curvature response is not directly addressed in ACI 318 code or AASHTO LRFD specifications, it is necessary for finding the curvature ductility of the section as well as for the full load-deflection response.

The moment-curvature response at mid-span is calculated using two computer programs in the present study: a VBA program using excel sheet written by the author, and Response2000 (Bentz and Collins 2000).

4.5.2 The VBA program

Moment-curvature can be derived using sectional analysis with the following assumptions:

1. Plane sections remain plane after loading;
2. No slippage occurs between concrete and reinforcement, i.e., strain compatibility;
3. Tensile stress of the concrete is assumed to be zero after cracking;
4. Concrete crushed upon reaching the ultimate strain value, which is measured from the present study;
5. Lateral reinforcement has no impact on the moment-curvature response; and
6. No confinement effect is considered.

The steel reinforcement is modeled using bi-linear stress-strain relationship, with the measured yield stress and elastic modulus for each particular specimen. After the steel yields, the stress is assumed to be constant, i.e., strain hardening effect is neglected.

Stress-strain relationship of concrete used in the analysis is proposed by Mertol (2006), which is a modified model from Popovics (1973) to represent the behavior of high-strength concrete better, as:

$$f_c = f_c^{'} \times \frac{\varepsilon_c}{\varepsilon_{co}} \times \frac{n}{n-1+(\varepsilon_c / \varepsilon_{co})^{nk}}, \qquad \text{(Equation 4-8)}$$

where f_c is the general stress in concrete; ε_c is the general strain in concrete; ε_{co} is the strain at peak stress. As the value of ε_{co} could not be obtained directly from the flexure tests, the suggestion from Mertol (2006) is used, as:

$\varepsilon_{co} = 0.0033\text{-}0.00002 f'_c$ (Equation 4-9)

and n and k in Equations 4-10 and 4-11, are the coefficients in this model, which are also suggested by Mertol (2006) as:

$n = 0.31\ f'_c + 0.78$ (Equation 4-10)

$k = 0.10\ f'_c + 1.20$ (Equation 4-11)

The overall difference between the modified model by Mertol and the original Popovics' model is very small. The relationship of ε_{co} and f'_c proposed by Mertol is the best-fit results from 21 tested C-shape specimens. The concrete material used by Mertol (2006) is from the same batch of what is used in this study. It should be noted that the expression of ε_{co} proposed by Mertol is contradictory to the research finding by ACI 363-R92 report (1992), which indicates that strain at maximum stress (ε_{co}) increases as concrete strength increases.

The algorithm in the VBA program is shown in Figure 4-24. In this program, the strain of concrete at the extreme compressive fiber ε_c was increased linearly up to the measured

ultimate strain in 100 sub-steps. Within each sub-step, a neutral axis depth was assumed, resulting a unique strain profile. The tensile force (F_s) from steel was calculated based on this strain profile. The concrete in compression zone was discretized into 500 integration strips. The compressive force in each strip (dF_c) was calculated based on the stress-strain relationship and geometry. Summation of force in each strip (F_c) was compared with the tensile force of steel (F_s). If it was greater, the assumed neutral axis depth was reduced in the next integration cycle; otherwise, neutral axis depth would be increased. This trial and error procedure is automated using "loop" function in the VBA code. Force equilibrium was considered satisfactory when the difference between the two forces (F_c and F_s) was less than 100 lbs. Then, the moment and the corresponding curvature were calculated, and the strain in the extreme compression fiber of concrete was increased for the next sub-step.

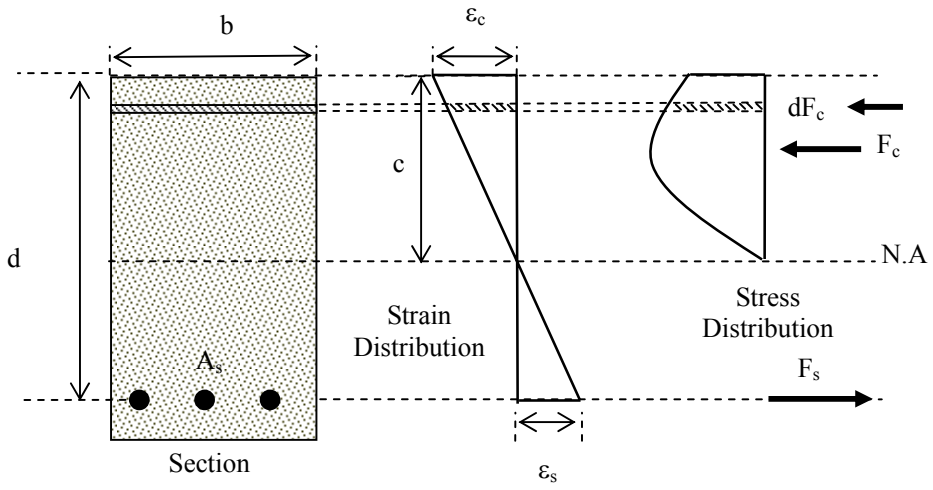

Figure 4-24 Methodology in Section Analysis

4.5.3 Response2000 Program

This section provides a brief description on Response2000 program, which was also used in

predicting moment-curvature as well as full load-deflection response later in this chapter. Response2000 (Bentz and Collins 2000) provides 2-dimensional analysis for reinforced as well as prestressed concrete members. Assumptions adopted in this program are as follows:

1. Plane sections remain plane;
2. No significant transverse clamping stress acts through the depth of the beam; and
3. Modified compression field theory (MCFT) is used for biaxial stress-strain response of concrete throughout the depth of the section.

Response2000 takes into account the effect of tension stiffening using a model proposed by Bentz (1999). This is the major difference between this program and the VBA program. The stress-strain relationship of concrete used in Response2000 is Popovics' model (1973), which is only slightly different from what was used in the VAB program.

4.5.4 Results and Discussions

4.5.4.1 Pure Flexure Specimens

The predicted moment-curvature curves using the two aforementioned programs are compared with test results in Figures 4-25 to 4-37 for all pure flexure specimens tested in this study. The best-fit curve from measured strain data, prediction using Response2000 program and prediction using the VBA program are referred to as "Test Data", "Response2000", "VBA" curves in the figures, respectively.

The predicted responses from Response2000 and the VBA program are very close. The difference between the two programs is mainly contributed to the tension stiffening effect. As

a result, the predicted response from Response2000 program shows a smooth transition before and after cracking and with a slightly higher stiffness. On the other hand, the VBA program shows a sudden drop of load after cracking.

A brief review of the predicted curves indicates that predictions match well with the best-fit curves from the measured data, for the under-reinforced specimens. For the over-reinforced specimens with rectangular cross-section, the predictions are still reasonable except for specimen 14B7.7, which is mainly due to the underestimation of the concrete strength in the specimen. For over-reinforced specimens with inverted-T section, both programs underestimate the curvature, which may be explained as follows:

1. Behavior of over-reinforced specimens is controlled by the material properties of concrete. On the other hand, behavior is controlled by the reinforcement for under-reinforced specimens. Strength of concrete measured from testing of cylinders may be different from flexural specimen, as the two are different in volume and compacting method.
2. "Test Data" is directly not measured, but is rather a best-fit curve of the strain readings from pi-gauges. When pi-gauges are attached to the surface of concrete, their readings are inevitably affected by the cracks within the gauge length. As a result, measured strain values are less accurate. Accordingly, confidence level for these "measured curves" is slightly lower, compared to the measured deflections at mid-span.

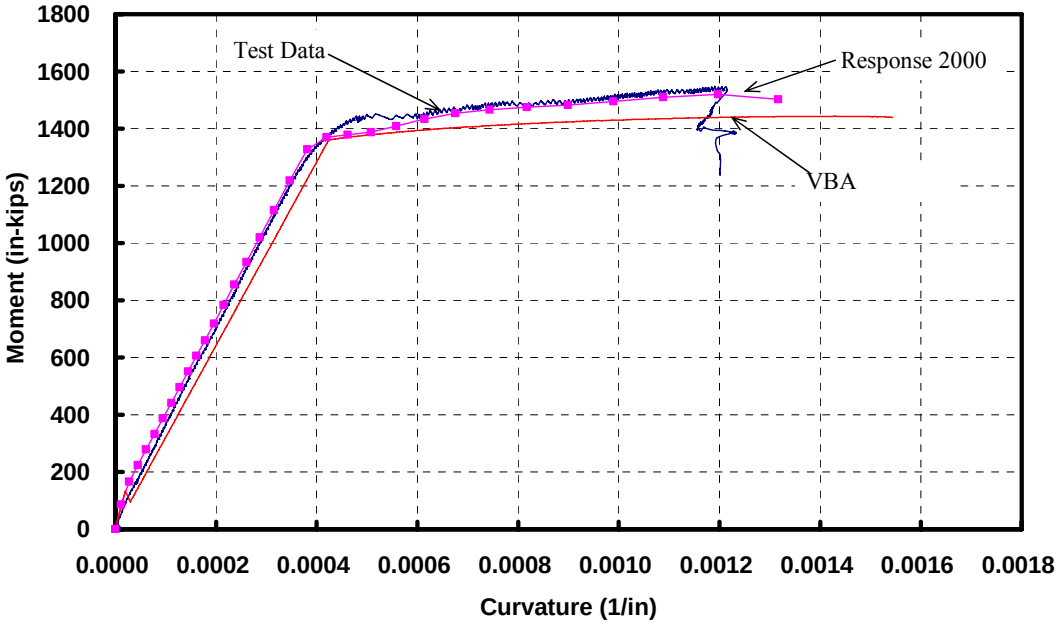

Figure 4-25 Comparison of Measured and Predicted Moment-Curvature Response for Specimen 10B2.1

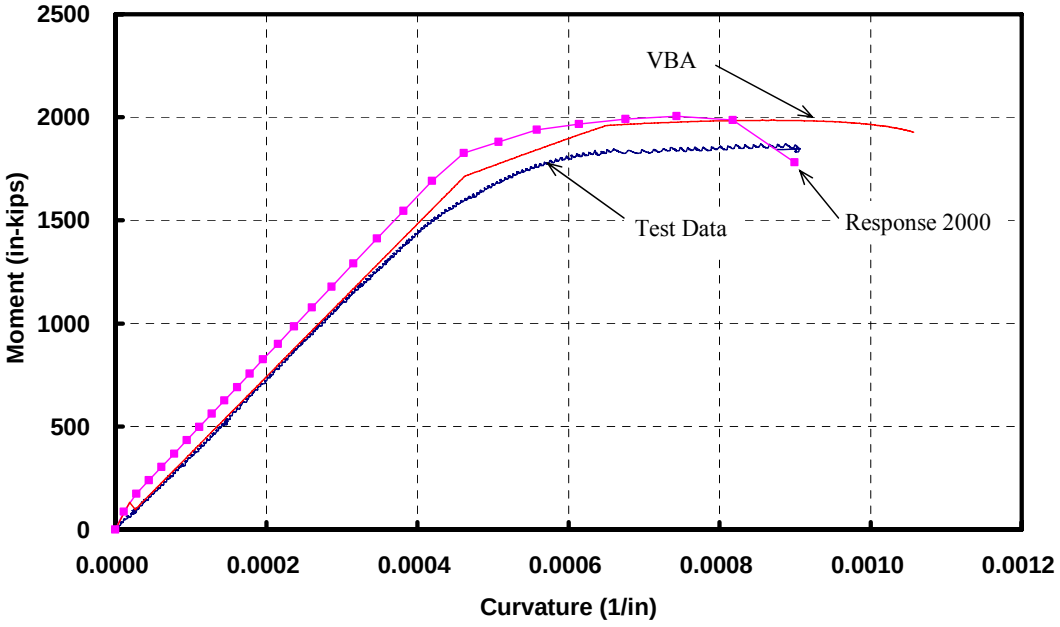

Figure 4-26 Comparison of Measured and Predicted Moment-Curvature Response for Specimen 10B4.3

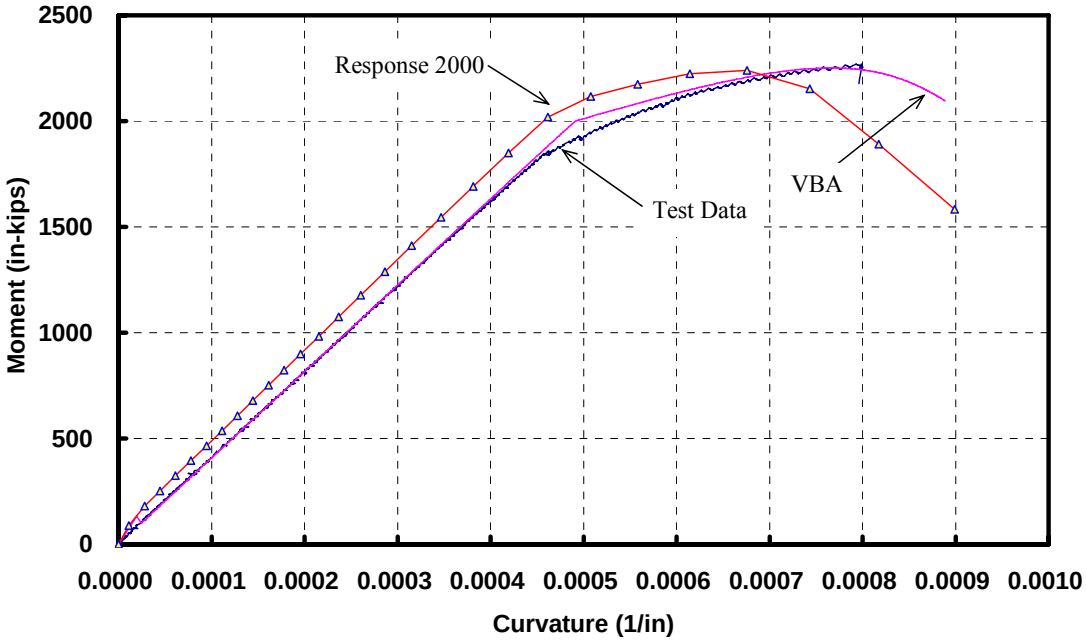

Figure 4-27 Comparison of Measured and Predicted Moment-Curvature Response for Specimen 10B5.7

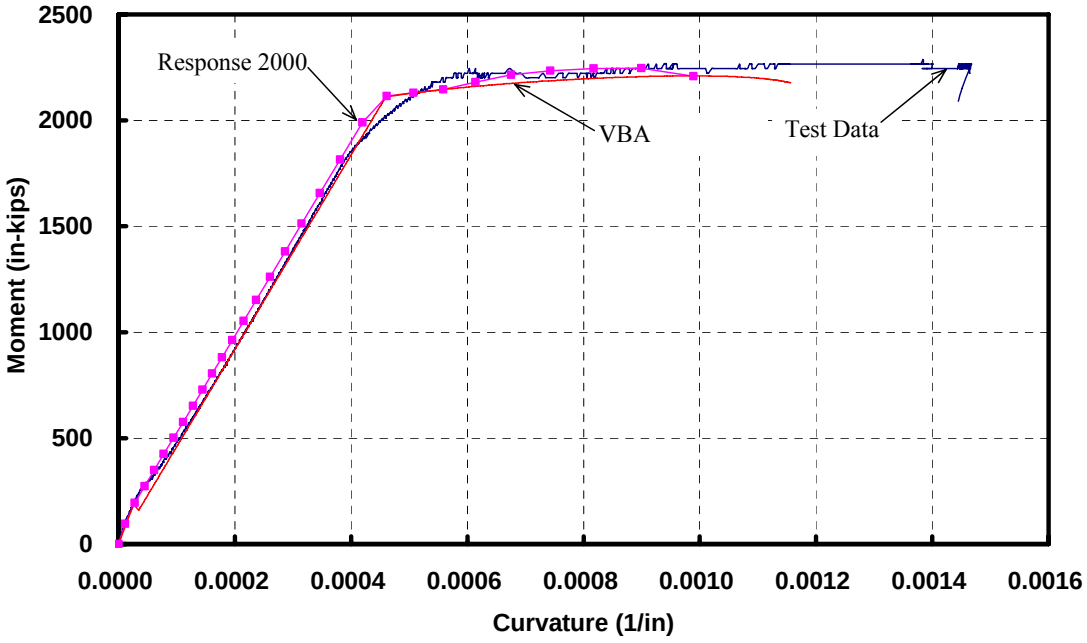

Figure 4-28 Comparison of Measured and Predicted Moment-Curvature Response for Specimen 14B3.3

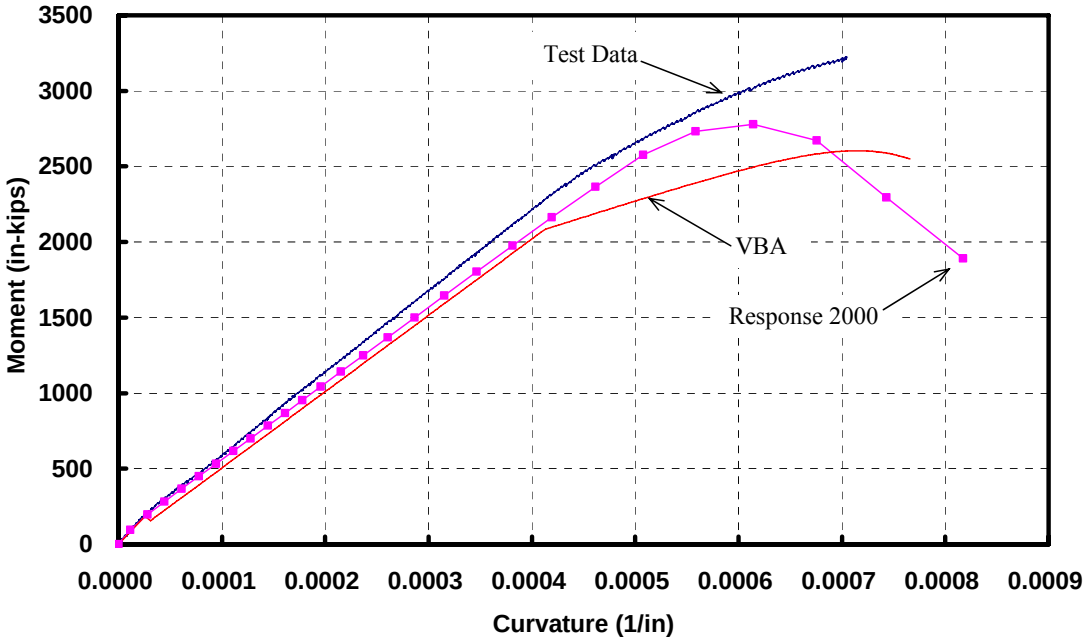

Figure 4-29 Comparison of Measured and Predicted Moment-Curvature Response for Specimen 14B7.7

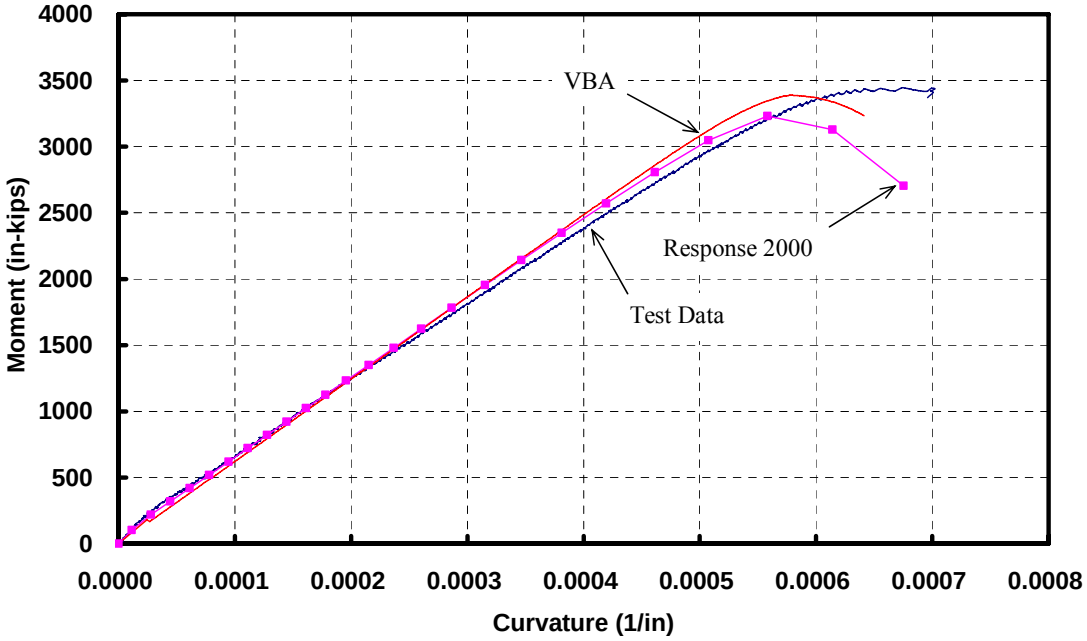

Figure 4-30 Comparison of Measured and Predicted Moment-Curvature Response for Specimen 14B12.4

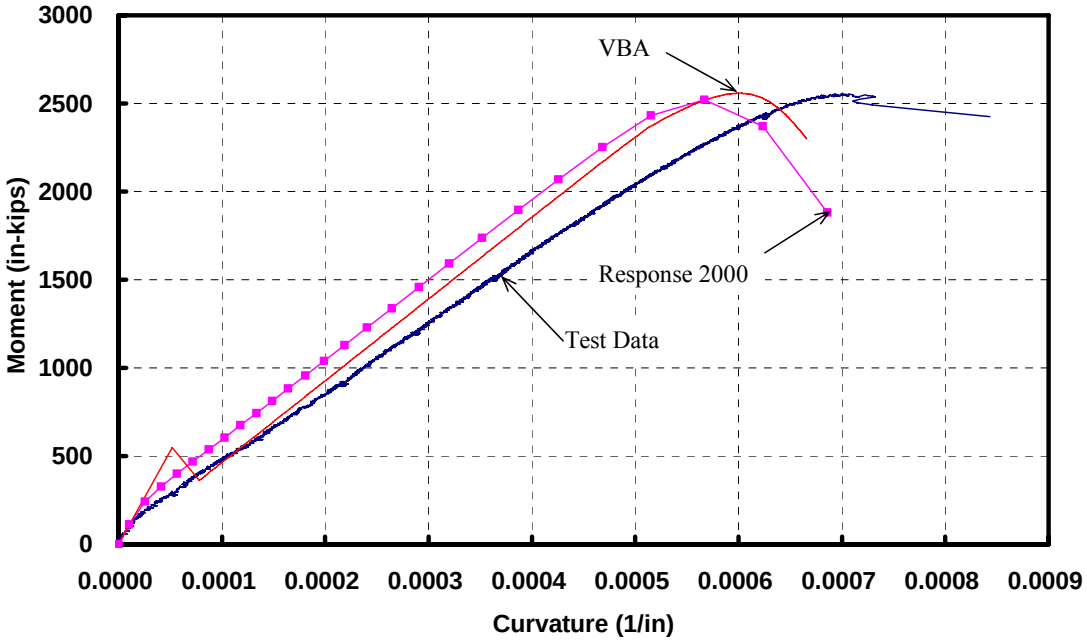

Figure 4-31 Comparison of Measured and Predicted Moment-Curvature Response for Specimen 14B7.6

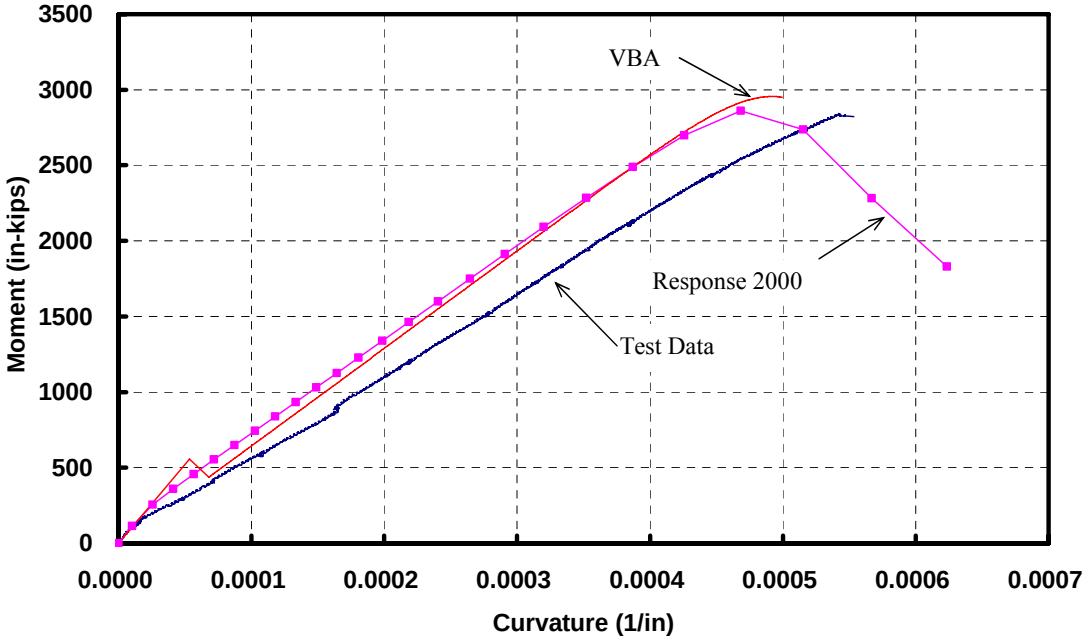

Figure 4-32 Comparison of Measured and Predicted Moment-Curvature Response for Specimen 14B12.7

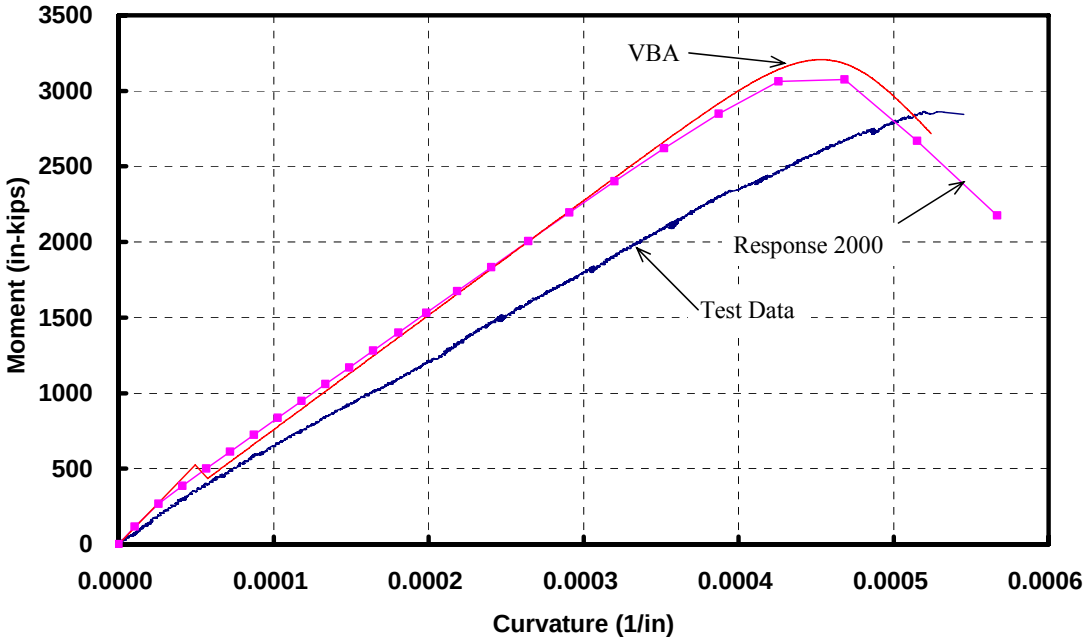

Figure 4-33 Comparison of Measured and Predicted Moment-Curvature Response for Specimen 14B17.7

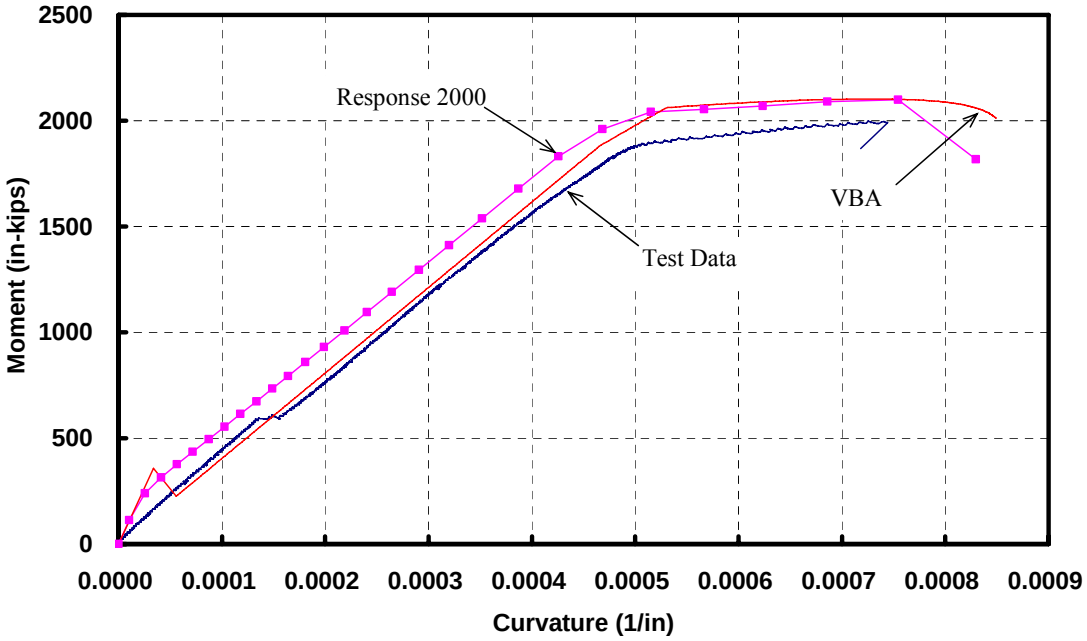

Figure 4-34 Comparison of Measured and Predicted Moment-Curvature Response for Specimen 18B5.9

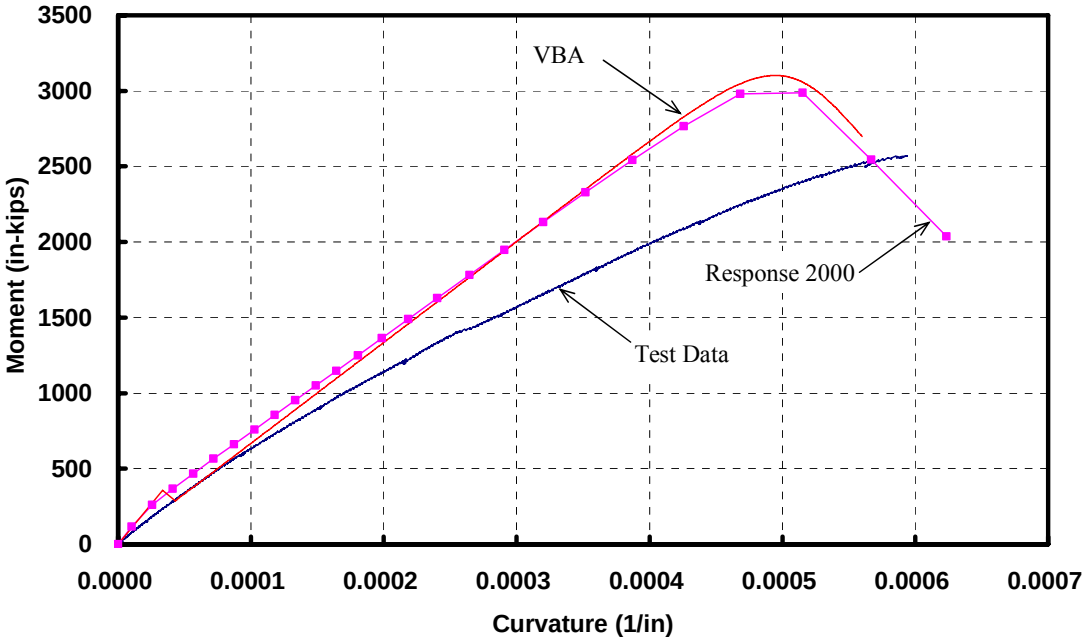

Figure 4-35 Comparison of Measured and Predicted Moment-Curvature Response for Specimen 18B12.7

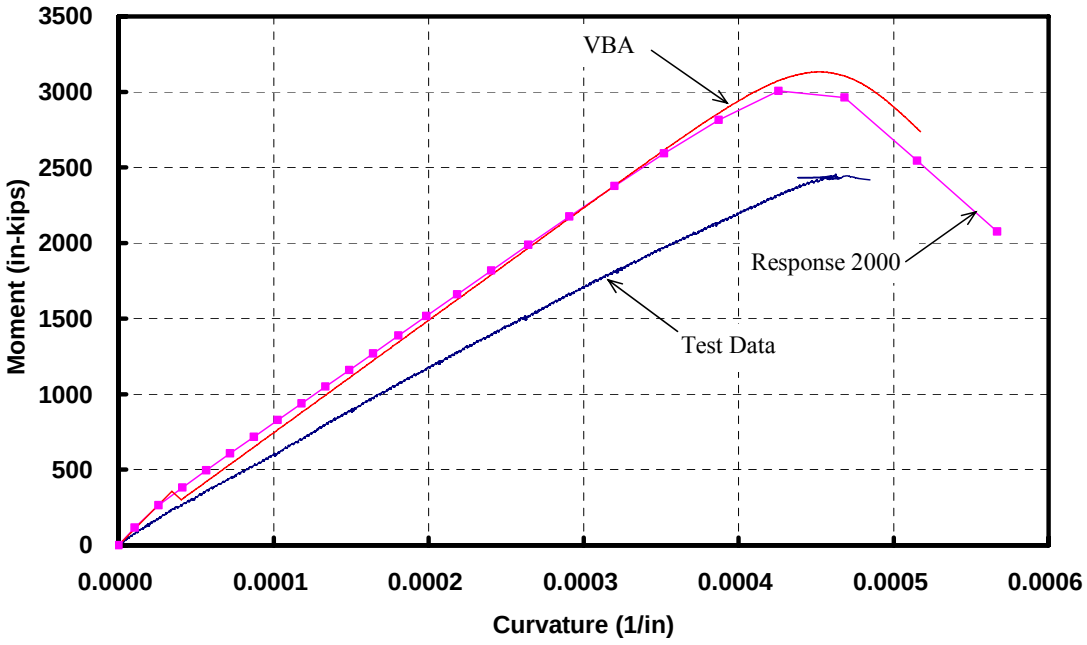

Figure 4-36 Comparison of Measured and Predicted Moment-Curvature Response for Specimen 18B17.7

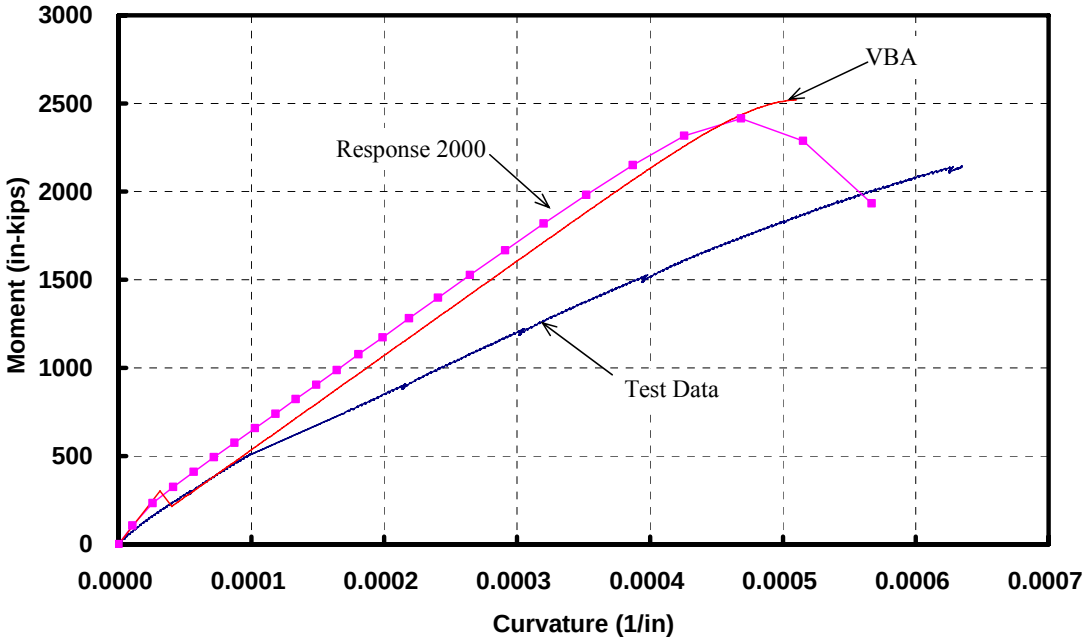

Figure 4-37 Comparison of Measured and Predicted Moment-Curvature Response for Specimen 10B10.2

4.5.4.2 Axial-Flexural Specimens

The predicted moment-curvature curves are compared with test results in Figures 4-38 to 4-41 for axial-flexural specimens tested in this study. Specimen 10BA4 was excluded from this analysis due to the increase of axial load during the test. The test was repeated using an identical specimen, 10BA4R. In remaining tests, axial load was controlled using a pressure relief valve within ±3 percent of the predetermined level. Specimen 18BA4 was tested twice due to the loss of the stability of the axial loading system. It should also be noted that the secondary moment is accounted for in the test result to reflect the true moment at the mid-span.

Overall, all predicted curves match test data reasonably well up to the peak resistance.

Unlike the pure flexure specimens, the axial-flexural specimens had stirrup in the constant moment zone, which helped confine the core concrete. The confinement contributed to the ductility of the section. However, this confinement effect was not included in the VBA program or Response2000 program.

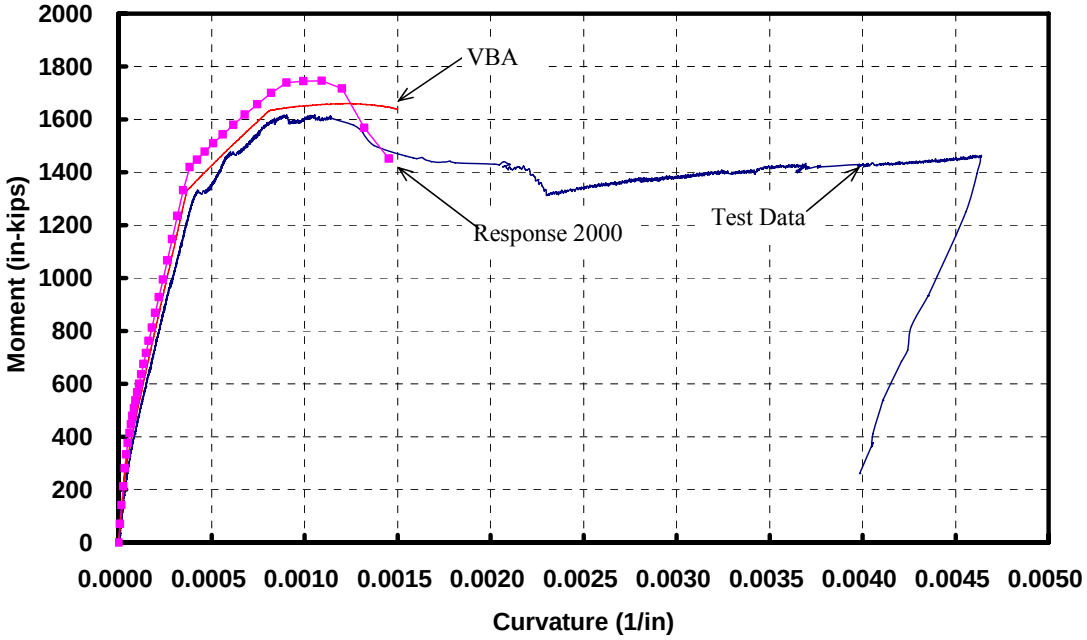

Figure 4-38 Comparison of Measured and Predicted Moment-Curvature Response for Specimen 10BA4R

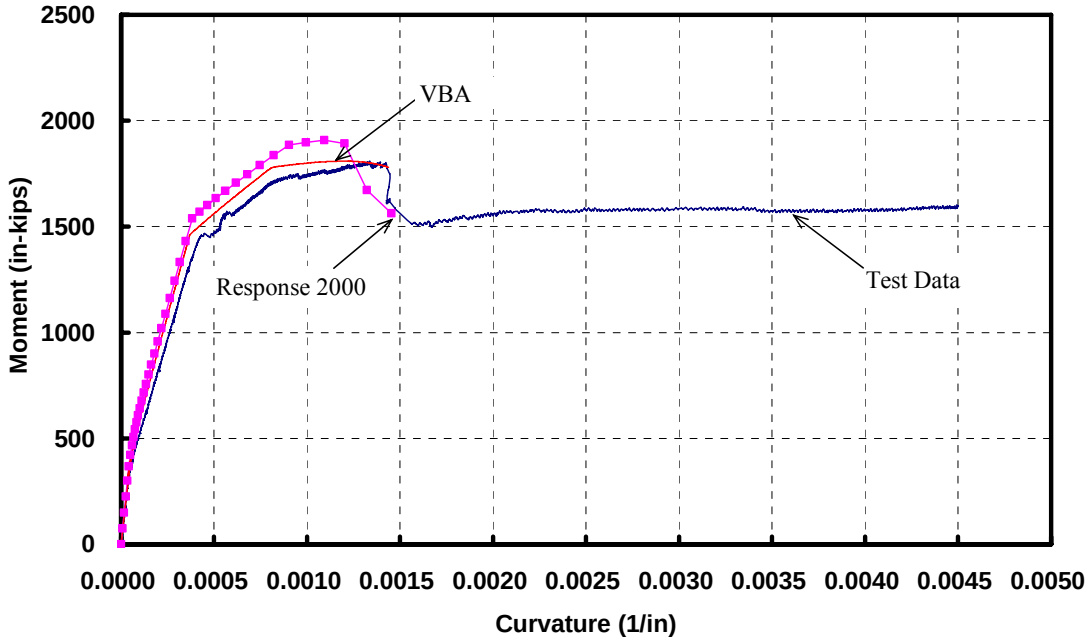

Figure 4-39 Comparison of Measured and Predicted Moment-Curvature Response for Specimen 14BA4

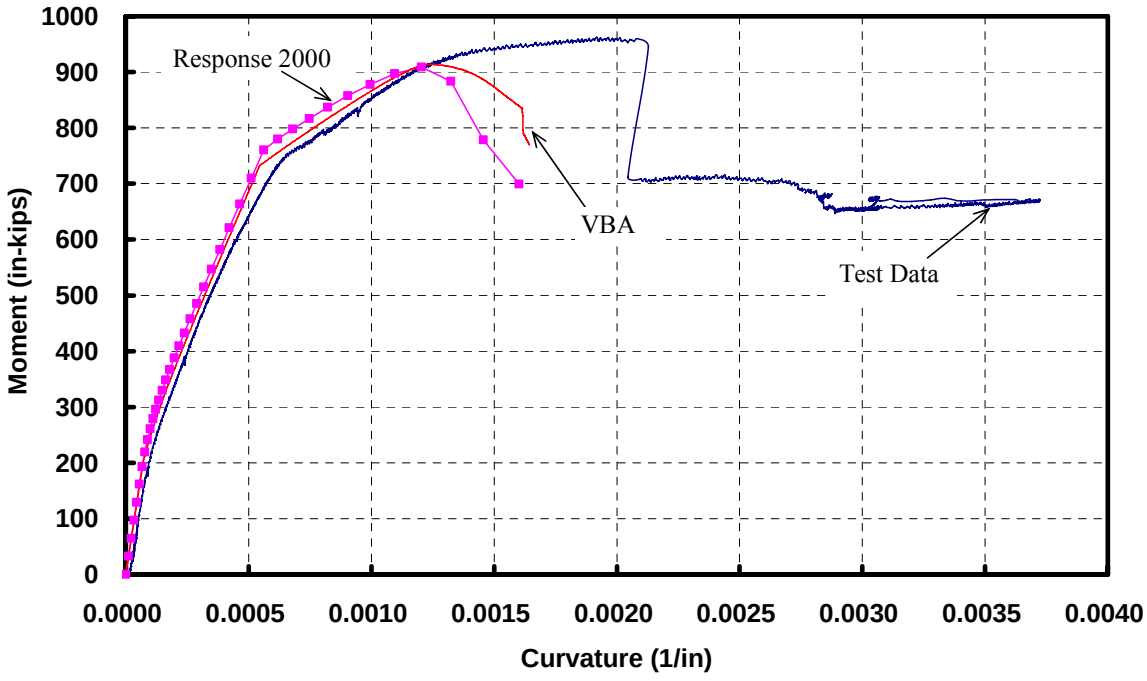

Figure 4-40 Comparison of Measured and Predicted Moment-Curvature Response for Specimen 14BA4R

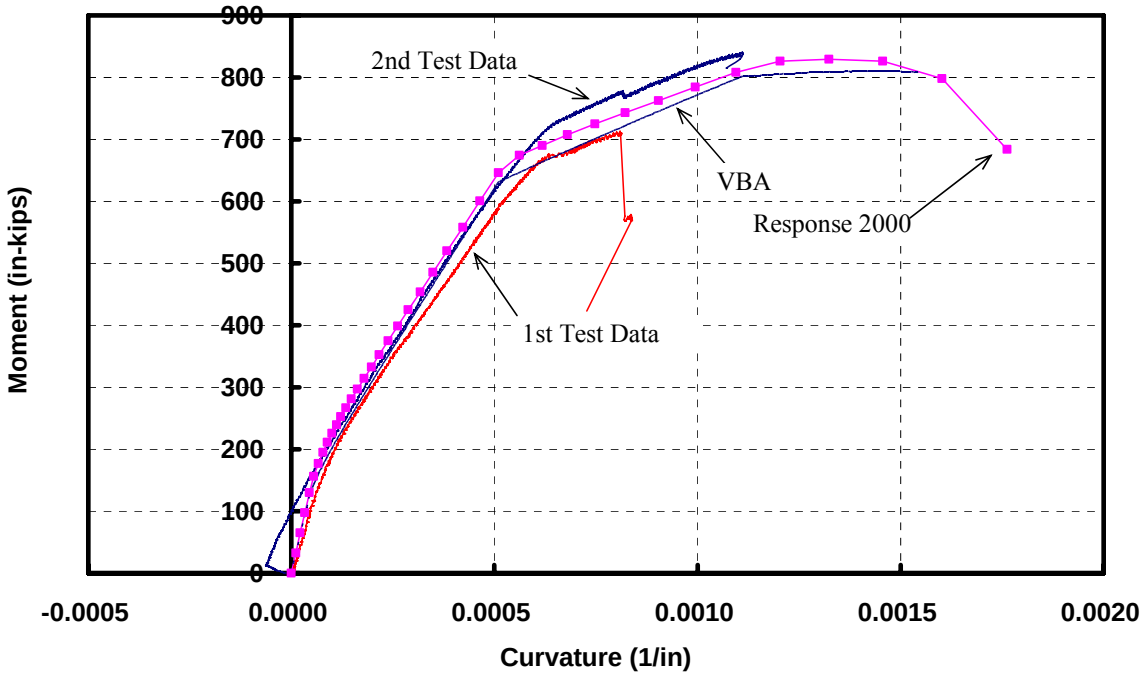

Figure 4-41 Comparison of Measured and Predicted Moment-Curvature Response for Specimen 18BA4

4.6 Deflections

4.6.1 Selection of Service Load Level

An appropriate service load level needs to be selected before investigating the deflection at this level. In the AASHTO LRFD Specifications (2004), the general requirement for all components and connections in a structure is expressed as:

$$\sum \eta_i \gamma_i Q_i \le \phi R_n \qquad \text{(Equation 4-12)}$$

where η_i is the load modifier with values between 0.95 and 1; γ_i is the load factor, which is a statistically-based multiplier applied to the force effect; Q_i is the force effect; Φ is the resistance factor, which is a statistically-based multiplier applied to the nominal resistance; and R_n is the nominal resistance.

A total of eleven different states are specified in the AASHTO LRFD Specifications (2004), out of which nine are related to earthquake, wind or other non-gravity loads. The other two strength limits are as follows:

Strength Limit 1 is the basic load combination relating to the normal vehicular use of the bridge without Wind, where the load and resistance factor is given as:

1. $\gamma_p = 1.25$, for dead load (D);
2. $\gamma = 1.75$, for live load (L); and
3. $\phi = 0.9$ for reinforced member subjected to flexure

Equation 4-12 can then be rearranged as:

$$R_n \geq \frac{\sum \eta_i \gamma_i Q_i}{\phi} = \frac{1.25(D) + 1.75(L)}{0.9} = 1.39(D) + 1.94(L) \qquad \text{(Equation 4-13)}$$

Two special cases are considered to determine the relationship between the applied load and nominal resistance:

1. If the live load (L) is dominant and the effect of dead load is negligible, then service load will be approximately 50 percent of the nominal resistance.
2. Assuming the live load contribution at failure is twice that of dead load, which is assumed by Pastor (1984), then service load will be 57 percent of the nominal resistance

Strength limit 4 is the load combination relating to very high dead load to live load force effect ratios, where $\gamma_p = 1.5$, for dead loads (D) and the effect of transient loads is negligible since the dead dominant in this case, and $\phi = 0.9$, for reinforced members under flexural loading.

Substituting in the load factors above, and service load will be 60 percent of the nominal

resistance.

Based on the derivations above and to be reasonably conservative, it is assumed that service load constituted 45 percent of the measured ultimate resistance.

4.6.2 Elastic Analysis

In the present study, all the pure flexure specimens were tested under 4-point bending. Therefore, deflection at mid-span is given by:

$$\Delta_c = \frac{Pa}{48EI_e}(3L^2 - 4a^2) \qquad \text{(Equation 4-14)}$$

where Δ_c is the mid-span deflection; P is the total applied load; L is the span of the beam; a is the shear span; E is the elastic modulus of concrete and I_e is the effective moment of inertia, given by LRFD Specification equation (5.7.3.6.2.1) as:

$$I_e = (1 - (\frac{M_{cr}}{M_a})^3)I_{cr} + (\frac{M_{cr}}{M_a})^3 I_g \qquad \text{(Equation 4-15)}$$

where M_{cr} is the cracking moment, M_a is the applied moment, I_{cr} is the moment of inertia of the cracked section, and I_g is the gross moment of inertia of the uncracked section.

The mid-span deflections at service load of the 13 beams tested in this project are compared with the predicted values from the LRFD equations in Table 4-5. The elastic modulus equation from ACI 363 report, together with the value from the current LRFD equation and the measured elastic modulus were used in the calculation of deflections in Table 4-5. It is worth noting that the moment of inertia of the cracked section is affected by the elastic modulus of concrete as well. Therefore, it needs to be re-calculated each time the elastic

modulus is revised.

It can be seen from Table 4-5 that the current LRFD Specifications underestimates the deflection for all tested specimens in this project. The measured elastic modulus from testing of cylinders provides the closest prediction, probably because it best reflects the elastic modulus of the concrete, which is lower than the value from the code expression. Similar results have been reported in the literature as summarized by Rashid and Mansur (2005) in Table 4-6, which is updated to include test results of the NCHRP 12-64 Project for comparison.

Table 4-5 Comparison of Measured and Predicted Mid-span Deflections at Service Load for the Pure Flexure Specimens

Specimen No.	$\frac{\Delta_{Predicted}}{\Delta_{Measured}}$ using E from		
	LRFD	ACI363	Measured
10B2.1	0.84	0.88	0.91
10B4.3	0.81	0.86	0.90
10B5.7	0.89	0.94	0.98
10B10.2	0.75	0.82	0.93
14B3.3	0.77	0.82	0.82
14B7.7	0.81	0.86	0.88
14B12.4	0.79	0.85	0.88
14B7.6	0.81	0.88	0.88
14B12.7	0.75	0.83	0.82
14B17.7	0.77	0.85	0.85
18B5.9	0.69	0.76	0.84
18B12.7	0.66	0.73	0.83
18B17.7	0.78	0.87	0.99
Average	0.78	0.84	0.89
Std. Dev.	0.060	0.054	0.056

Table 4-6 Statistical Information on Service Load Deflection from Literature

Researchers	No. of Beams	f'_c (ksi)	ρ (percent)	Measured/Predicted	
				Average	σ
Rashid and Mansur (2005)	16	6.2 – 18.3	1.3 – 5.3	1.26	0.08
Ashour (2000)	9	7.1 – 14.8	1.2 – 2.4	1.17	0.07
Lin and Hwang (1992)	9	3.9 – 10.0	2 – 3.7	1.27	0.12
Lambotte and Taerwe (1990)	5	4.9 – 11.7	0.5 – 1.5	1.17	0.12
Paulson and Nilson (1989)	9	5.4 – 13.2	1.5	1.37	0.14
Shin (1986)	23	3.9 – 14.5	0.4 – 3.6	1.56	0.27
Pastor and Nilson (1984)	12	3.8 – 9.3	1.1 – 5.3	1.09	0.08
NCHRP 12-64	13	11.4-16.1	2.1-17.7	1.29	0.10

The difference between the predicted and measured curve may be attributed to two issues: overestimation of cracking moment and stiffness, and will be discussed below:

1. Overestimation of Cracking Moment

As mentioned in section 4.4, cracks were observed on the surface of many specimens before testing. Even though the cracking moment can be also estimated from load-deflection curve, it can not be determined accurately from the load-deflection graph.

Analytically, a smaller M_{cr} in Equation 4-15 will reduce I_e, and will make it closer to I_{cr} at a lower load level. In the present study, the service load is taken as 45 percent of the ultimate resistance, which is much higher than the cracking moment. Table 4-7 shows the ratio of the applied moment (M_a) to cracking moment (M_{cr}) at service load, and demonstrates how this ratio affects the deflection when using Equation 4-15 to determine the effective moment of

inertia (I_e). It can be seen that all pure flexure specimens tested in this project, except for one, have the ratio of M_a/M_{cr} greater than three. Accordingly, the difference between the I_e and I_{cr} from the Equation 4-15 is almost negligible. Therefore, reducing M_{cr} would hardly improve the prediction.

2. Overestimation of Stiffness

By re-arranging Equation 4-15, the average flexural stiffness of the member, EI_e, can expressed as:

$$EI_e = \frac{Pa}{48\Delta_c}(3L^2 - 4a^2) \qquad \text{(Equation 4-16)}$$

In Equation 4-16, a and L are known parameters of from the test setup; P/Δ_c is assessed directly from the best-fit of the measured load-deflection curve. Therefore, stiffness of the section can be back-calculated from the measured load-deflection curve and is compared with the stiffness of the cracked section EI_{cr}, as shown in Table 4-8. The correlation R^2 for P and Δ_c is also shown in the table. It is worth noting that the slope of the load-deflection curve was taken at 30 percent to 45 percent of the peak resistance. At this load level, correlation R^2 is close to unit for all tested specimens, which indicates the measured load-deflection curves are very closed to straight lines in this range.

In Table 4-8, specimens cast in the same batch of concrete are grouped together and are distinguished from each other. It can be seen that within each group of specimens, the stiffness increases as the reinforcement ratio increases. However, the calculated stiffness from the measured load-deflection curve is always less than the predicted stiffness of the cracked section. This is contradictory to the elastic theory, in which, the lowest stiffness a

section could have is EI_{cr}.

Table 4-7 Effect of M_a/M_{cr} Ratio on Effective Moment of Inertia

Specimen No.	**M_a/M_{cr}**	**I_{cr} / I_{eff}**
10B2.1	4.18	0.98
10B4.3	4.80	0.99
10B5.7	5.04	0.99
10B10.2	3.06	0.96
14B3.3	5.51	0.99
14B7.7	7.85	1.00
14B12.4	8.60	1.00
14B7.6	3.29	0.95
14B12.7	3.72	0.98
14B17.7	3.67	0.99
18B5.9	2.55	0.88
18B12.7	3.24	0.97
18B17.7	3.20	0.98

Rashid and Mansur (2005) recommended reducing elastic modulus by 50 percent in calculating deflections and reported that using the reduced elastic modulus improves the accuracy of prediction. In order to test this possibility, cores were drilled from some of the specimens, as discussed previously in section 3.4. Test results for cores indicate that there is no significant difference in the elastic modulus between the concrete of the cylinders and the cores of the specimens, which is against the assumption of Rashid and Mansur (2005). Their method may be a good numerical simulation, but is not justified in the present study.

Other factors may cause the low stiffness for the specimen, e.g., geometric tolerances. However, fabrication tolerances are random and should not cause under-estimations of deflection in all members.

The bar slippage at the crack compromises the strain compatibility between concrete and steel reinforcement. This in turn could affect the stiffness of the specimen. This possibility is explored using the finite element method; and will be discussed in Chapter 5.

Table 4-8 Comparison of Measured Stiffness with Predicted Cracked Section Stiffness

Mix & Batch No	Specimen #	Measured from 30%-45% of the peak load		Ratio of Measured EI from P-Δ curve/ EI_{cr}		
		EI_{eff}	R^2	LRFD	ACI363	Measured
		in^2-kips	-----			
Cast 1	10B2.1	2786689	0.997	0.79	0.82	0.84
	10B4.3	3291651	0.992	0.78	0.82	0.85
	10B5.7	3884073	0.997	0.83	0.82	0.91
Cast 5	R10B10.2	4102595	0.991	0.64	0.69	0.79
Cast 2	14B3.3	3837821	0.997	0.74	0.78	0.79
	14B7.7	4829986	0.999	0.82	0.88	0.9
	14B12.4	5658308	0.999	0.81	0.87	0.9
Cast 3	14B7.6	4122082	0.995	0.77	0.83	0.83
	14B12.7	5129431	0.996	0.68	0.75	0.75
	14B17.7	6105157	0.998	0.69	0.77	0.77
Cast 4	18B5.9	3285188	0.998	0.70	0.75	0.83
	18B12.7	5104693	0.997	0.66	0.72	0.83
	18B17.7	6597295	0.994	0.75	0.82	0.93

4.6.3 Load-Deflection Response for Pure Flexure Specimens

The load-deflection curve could be derived by integrating the moment-curvature along the shear span. A small program is developed by the author for this purpose. The algorithm is summarized in the following steps:

1. Discretize the entire beam into 1000 elements;

2. At the level of applied load, find the moment for each element;
3. Find the curvature for each element using the moment-curvature response;
4. Apply a virtual force at the mid-span and calculate the virtual moment for each element;
5. Add the products of the area under the curvature curve and virtual load along the entire span; and
6. Repeat the above steps for the next load level until failure.

The limitations in this method are as follows:

1. Shear deflection is ignored;
2. Prediction is only up to the peak resistance, and no post-peak response is calculated;
3. Slippage of rebars is neglected;
4. The moment-curvature relationship in this study is calculated without considering the effect of tension stiffening. Therefore it shows a load drop upon cracking. When load is increased monotonically, this part of load drop is not taken into consideration in the program. As a result, for an element which has a moment value slightly above the cracking moment, the curvature will be deemed doubled or even tripled, which will create a plateau in the load-deflection curve.

Response2000 (Bentz and Collins 2000) was also used to calculate the load-deflection response of each specimen. It should also be noted that in the Response2000 program, there is no input for the modulus of rupture. Instead, the program uses the terminology “tensile strength of concrete” as a parameter in the “modified compression field theory”. This

parameter is not available from the measured test results therefore system default value is used.

The predictions using the aforementioned two methods are compared with the test results for all the pure flexure specimens in Figure 4-42 to Figure 4-54. Predictions using the current AASHTO LRFD equation are also plotted in each figure for up to approximately 50 percent of the measured peak load.

It can be seen that the predictions using the VBA program and Response2000 are very similar for all the pure-flexure specimens tested in this study, even though the algorithms of the two programs are significantly different. The predictions by both two programs are better than the prediction using the AASHTO LRFD equations, except for specimens 10B2.1 and 14B12.4, for which predictions are almost the same. On the other hand, except for specimens 10B5.7 and 14B7.7 with a good match, both programs underestimate the deflections. Two of the specimens, 10B2.1 and 18B12.7 would be modeled and analyzed further using the finite element method in Chapter 5.

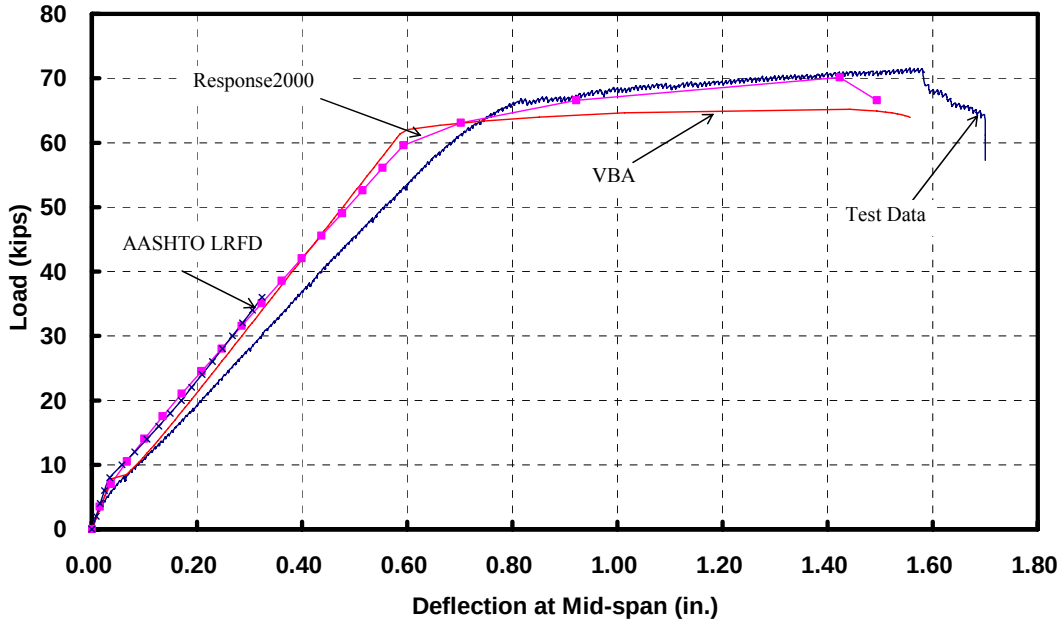

Figure 4-42 Comparison of Measured and Predicted Load-Deflection Response for Specimen 10B2.1

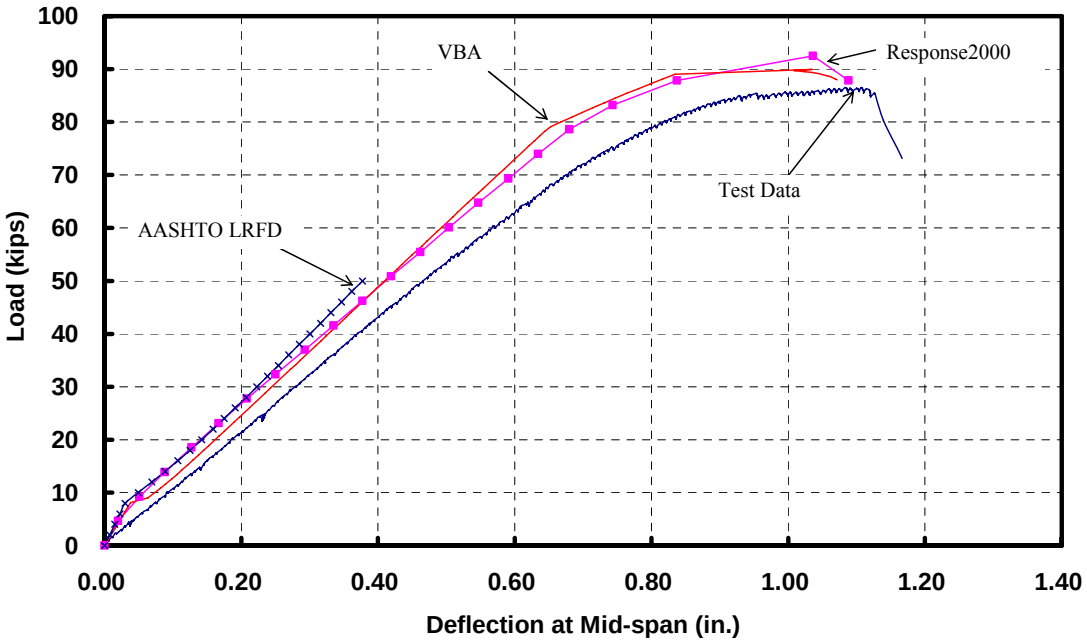

Figure 4-43 Comparison of Measured and Predicted Load-Deflection Response for Specimen 10B4.3

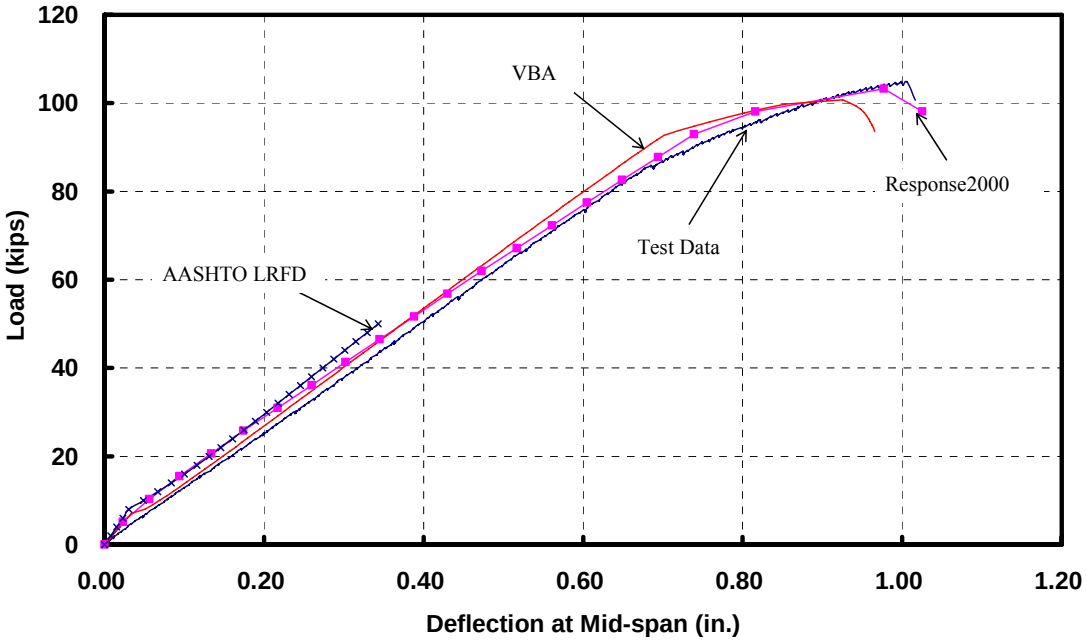

Figure 4-44 Comparison of Measured and Predicted Load-Deflection Response for Specimen 10B5.7

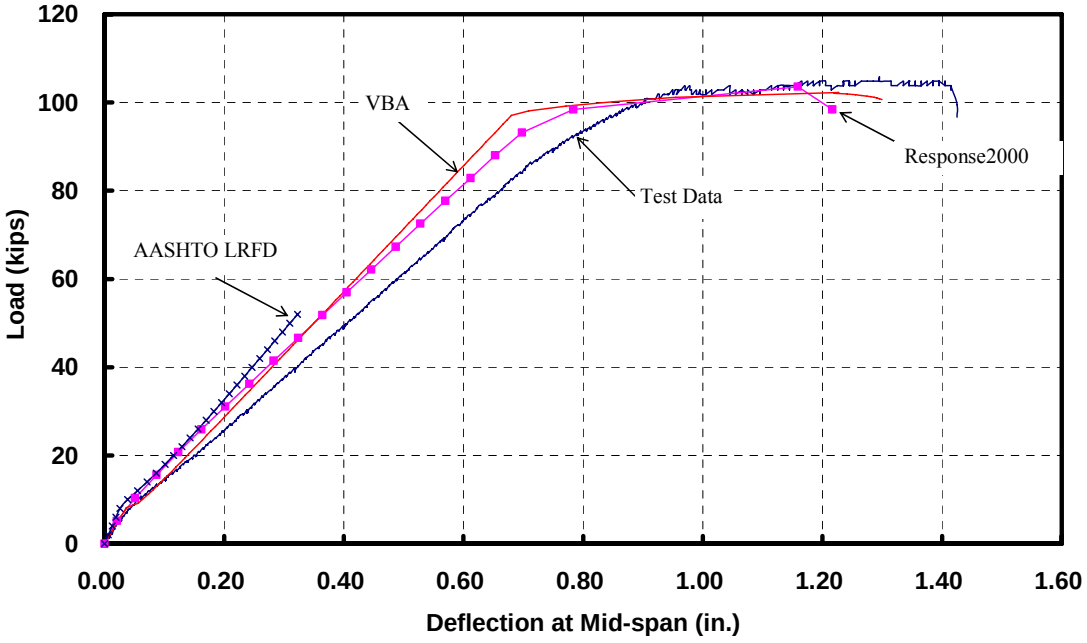

Figure 4-45 Comparison of Measured and Predicted Load-Deflection Response for Specimen 14B3.3

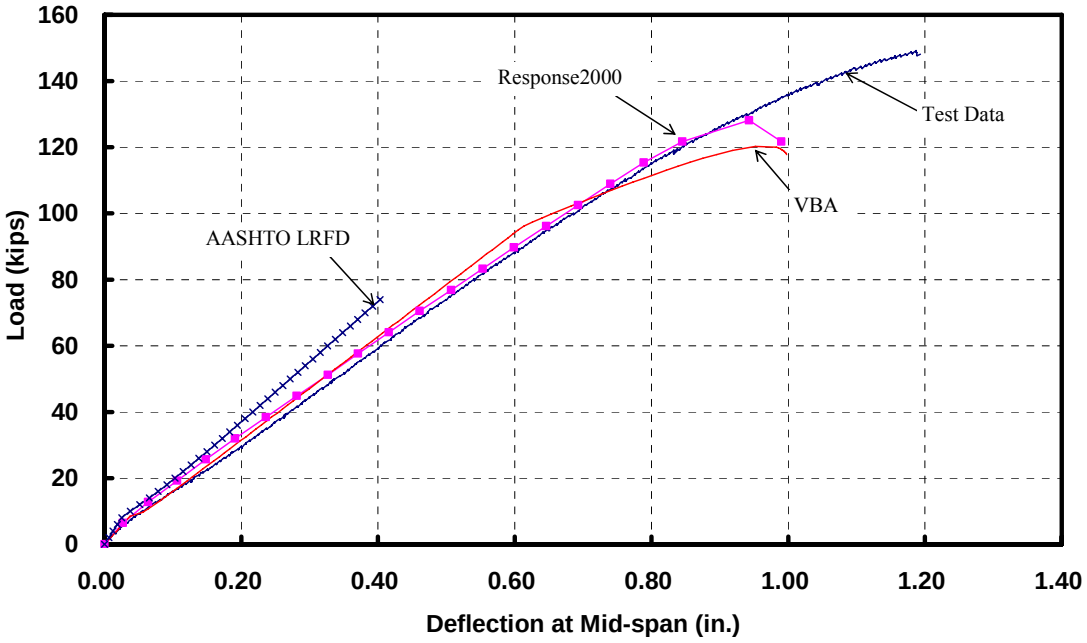

Figure 4-46 Comparison of Measured and Predicted Load-Deflection Response for Specimen 14B7.7

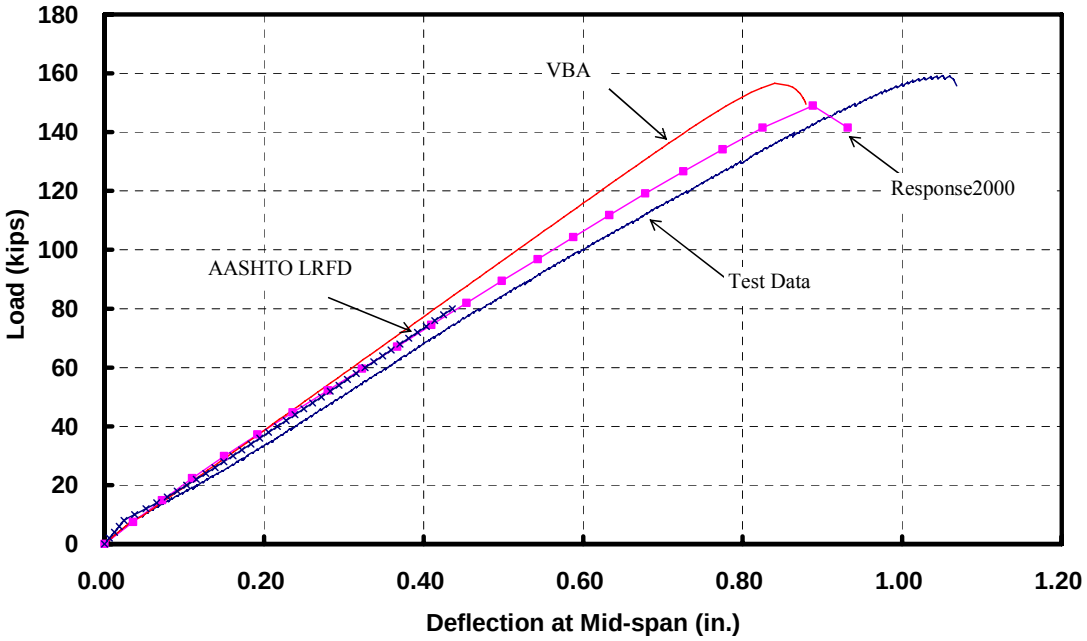

Figure 4-47 Comparison of Measured and Predicted Load-Deflection Response for Specimen 14B12.4

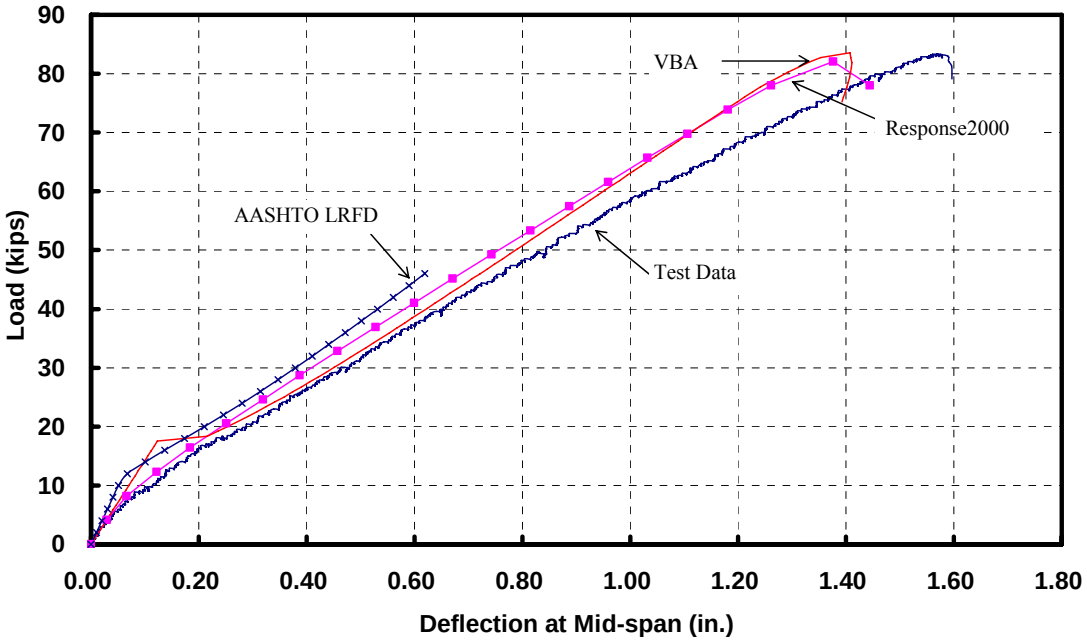

Figure 4-48 Comparison of Measured and Predicted Load-Deflection Response for Specimen 14B7.6

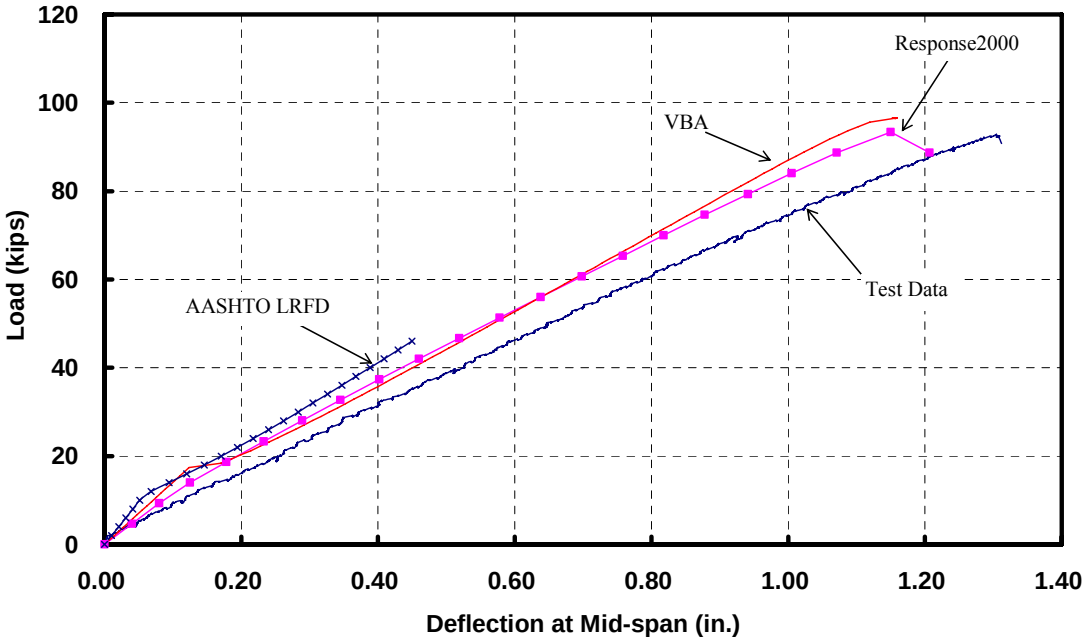

Figure 4-49 Comparison of Measured and Predicted Load-Deflection Response for Specimen 14B12.7

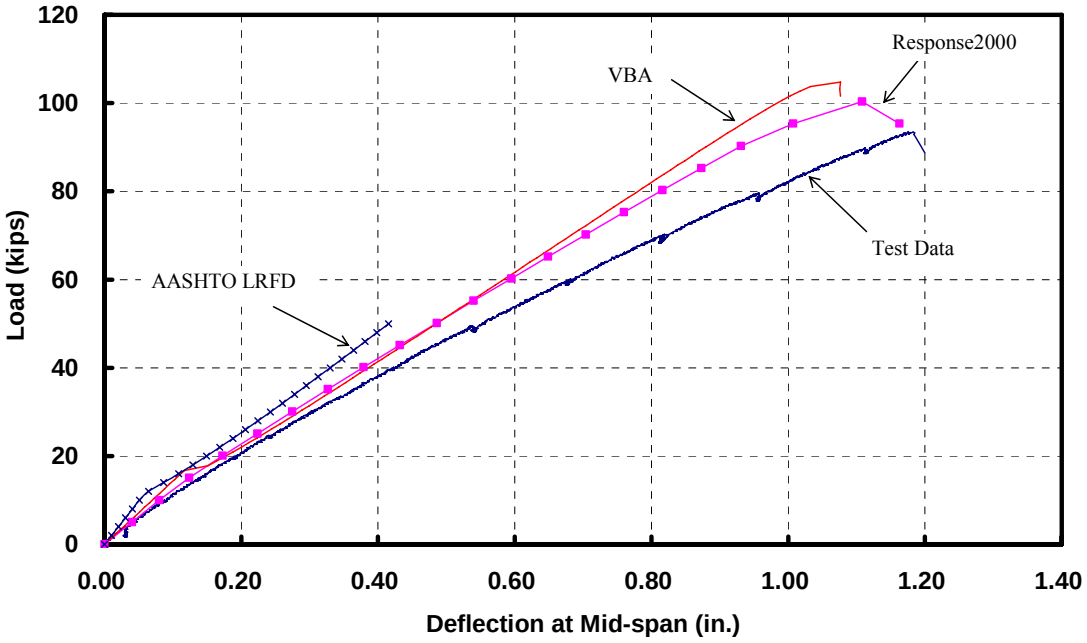

Figure 4-50 Comparison of Measured and Predicted Load-Deflection Response for Specimen 14B17.7

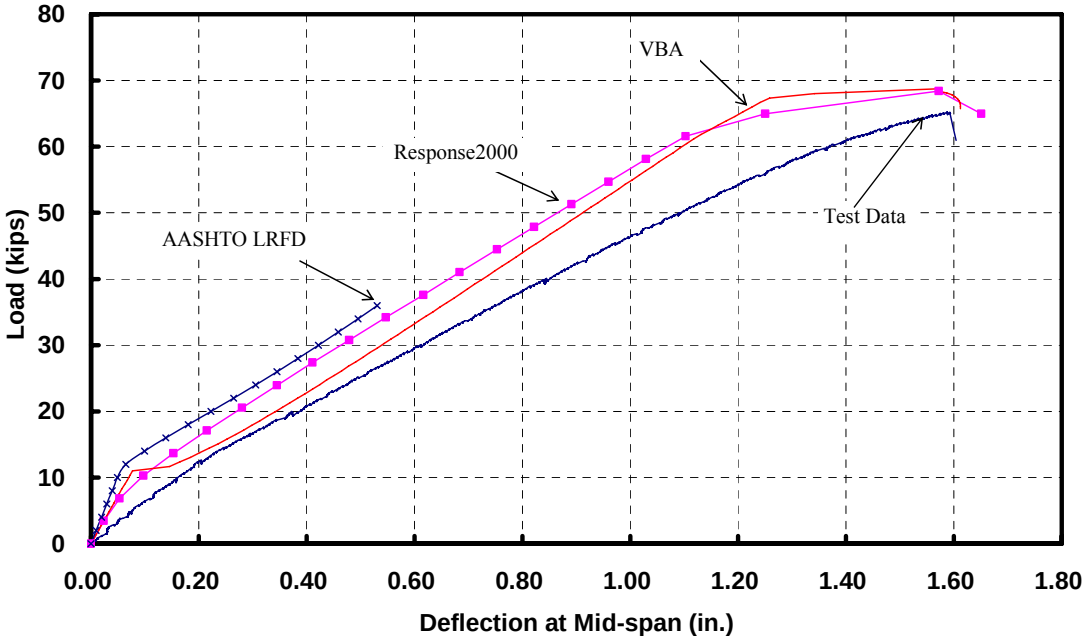

Figure 4-51 Comparison of Measured and Predicted Load-Deflection Response for Specimen 18B5.9

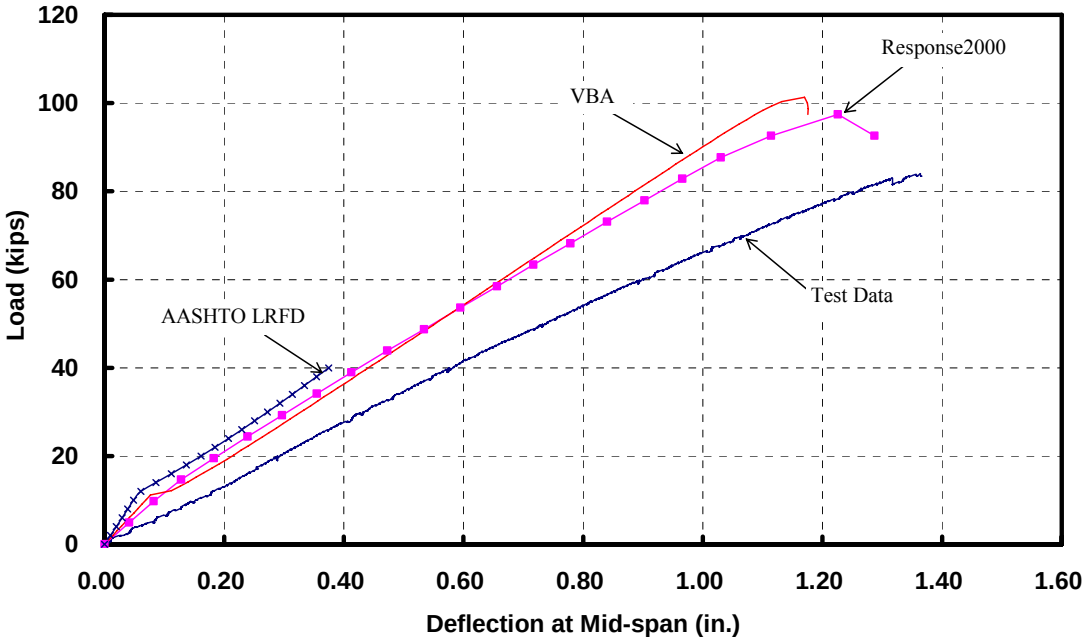

Figure 4-52 Comparison of Measured and Predicted Load-Deflection Response for Specimen 18B12.7

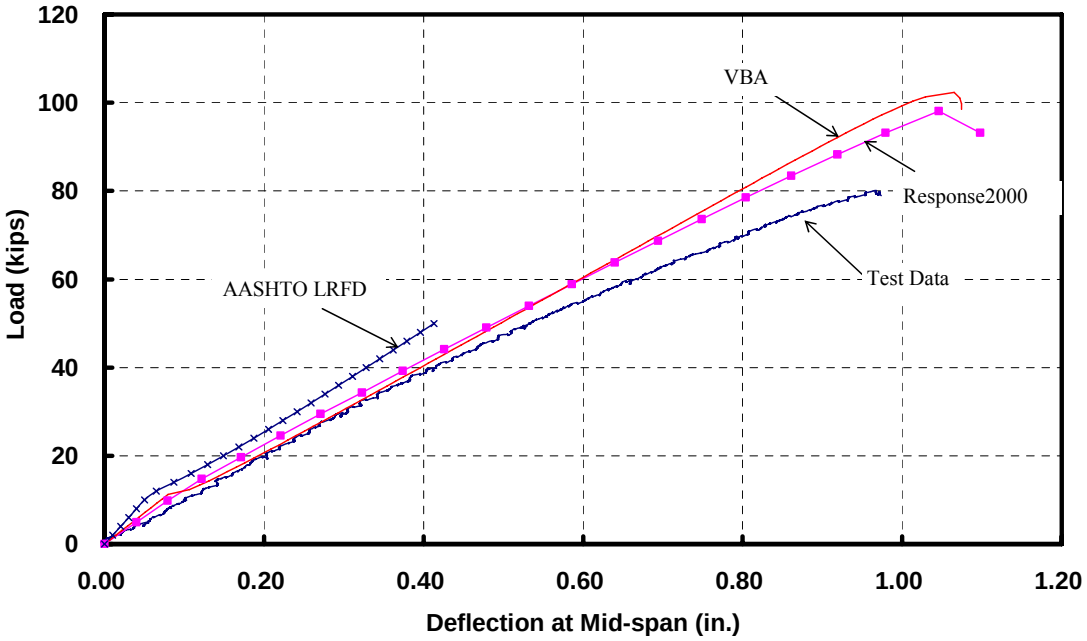

Figure 4-53 Comparison of Measured and Predicted Load-Deflection Response for Specimen 18B17.7

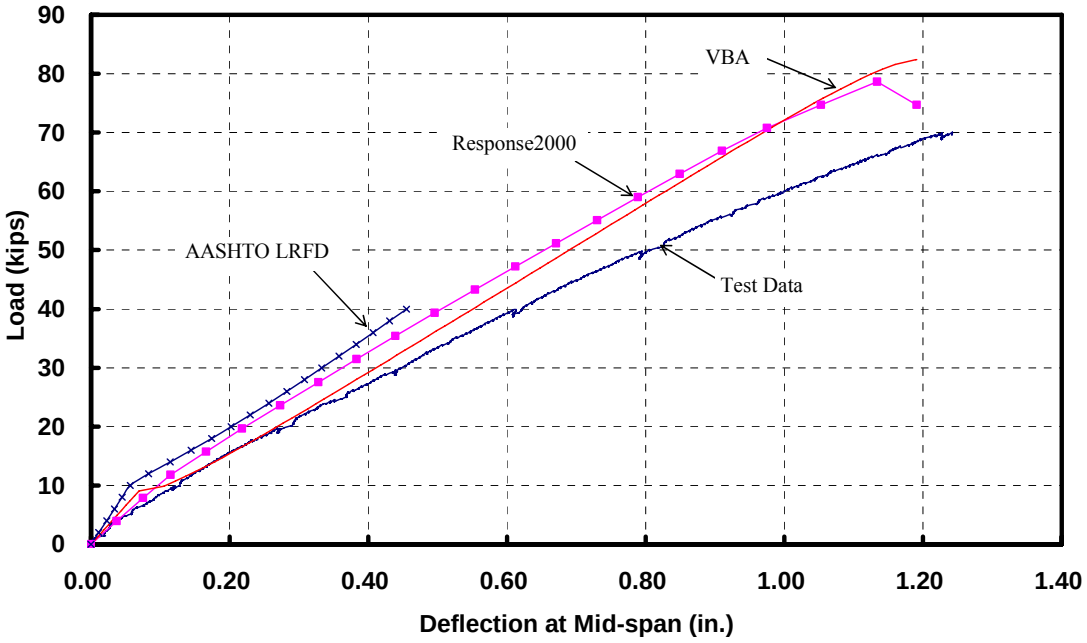

Figure 4-54 Comparison of Measured and Predicted Load-Deflection Response for Specimen 10B10.2

4.6.4 Load-Deflection Response for Axial-Flexural Specimens

The VBA code developed in this study was also used here. The output of the program is then modified to account for slenderness effect, using a series of equations as listed below:

$$\Delta_a = \Delta_0 \left(\frac{P / P_{cr}}{1 - P / P_{cr}} \right) \qquad \text{(Equation 4-17)}$$

where Δ_o is the deflection due to the applied lateral load, P is the applied axial load, P_{cr} is the critical Euler buckling load, as given by

$$P_{cr} = \frac{\pi^2 \cdot EI}{L^2} \qquad \text{(Equation 4-18)}$$

where L is the effective length of the specimen. For the specimens tested in this program, all beams are simply supported. Therefore, the span length is used as effective length in this study. EI is the flexural rigidity of the member and was calculated using the equations in

Section 5.7.4.3 of AASHTO LRFD Specifications to simplify the analysis. In this approach, EI is taken as the greater of the two expressions:

$$EI = \frac{\frac{E_c I_g}{5} + E_s I_s}{1 + \beta_d} \qquad \text{(Equation 4-19)}$$

$$EI = \frac{\frac{E_c I_g}{2.5}}{1 + \beta_d} \qquad \text{(Equation 4-20)}$$

where E_c is the gross modulus of elasticity of concrete as measured from testing of 4 in. by 8 in. cylinder, I_g is the gross moment of inertia of the section about its centroidal axis, E_s is the modulus of elasticity of longitudinal steel, I_s is the moment of inertia of longitudinal steel about the centroidal axis of the section, β_d is the ratio of maximum moments from the factored permanent loads to the maximum moments from the factored total loads and taken as 0.26, which is based on the load factors for strength limit 1 and an assumption of live load to dead load ratio of 2. The overall modifications using Equations 4-17 to 4-20 result in an amplification of the deflection by about 5 to 10 percent in the present study.

Response2000 program is also used in this analysis as a reference. This program did not take into account the effect of slenderness, and the output of the program is used directly in comparison without any moment magnification.

The predictions, using the aforementioned two programs are compared with the test results for axial-flexural specimens in Figures 4-55 to 4-58. As mentioned earlier, Specimen 10BA4 is not analyzed due to the increase of axial load during the test. On the other hand, Specimen 18BA4 was test twice and results from both tests are presented here.

The VBA program slightly overestimates the peak resistance (by about 10 percent) and so does the Response 2000 program. This overestimation is contributed mainly to the stress-strain model used in the analysis, but still within a reasonable range.

The author's program slightly outperforms the Response2000 program in the prediction of load-deflection response, possibly because of the including of slenderness effect. Neither program includes confinement effects or predicts the post-peak response. Overall, the predictions before the peak load match reasonably well with the measured responses.

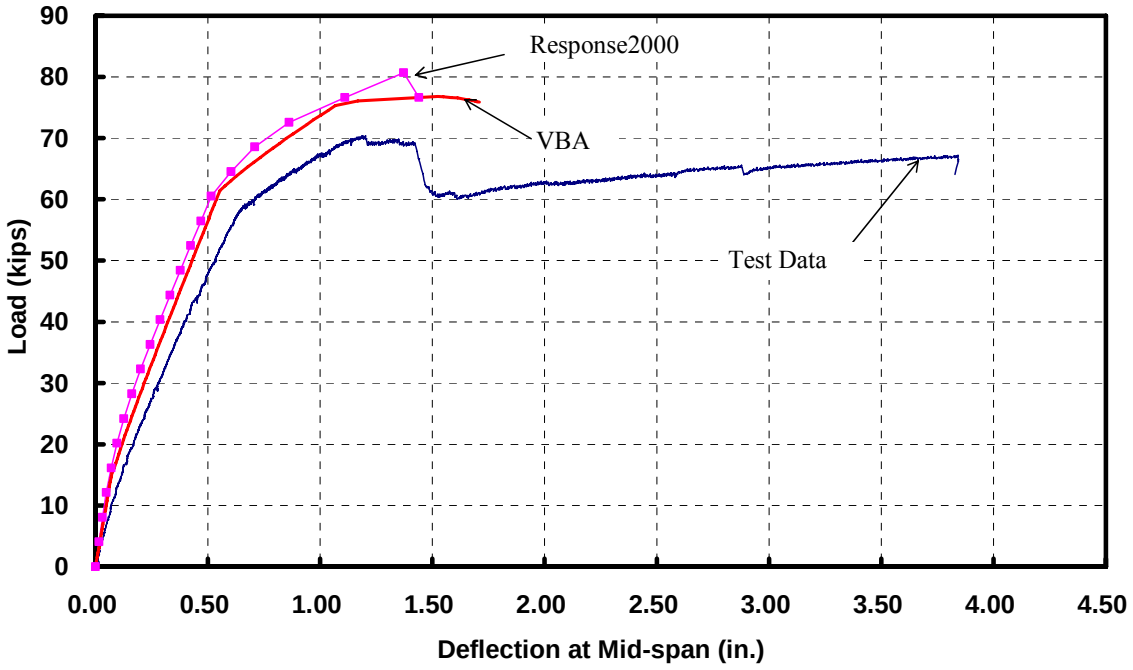

Figure 4-55 Comparison of Measured and Predicted Load-Deflection Response for Specimen 10BA4R

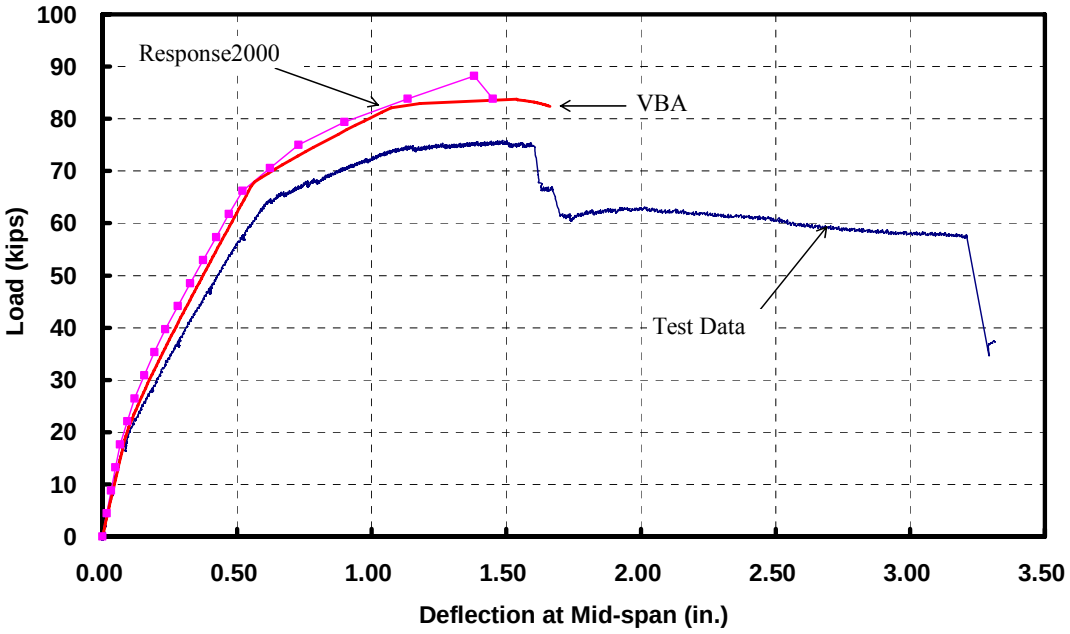

Figure 4-56 Comparison of Measured and Predicted Load-Deflection Response for Specimen 14BA4

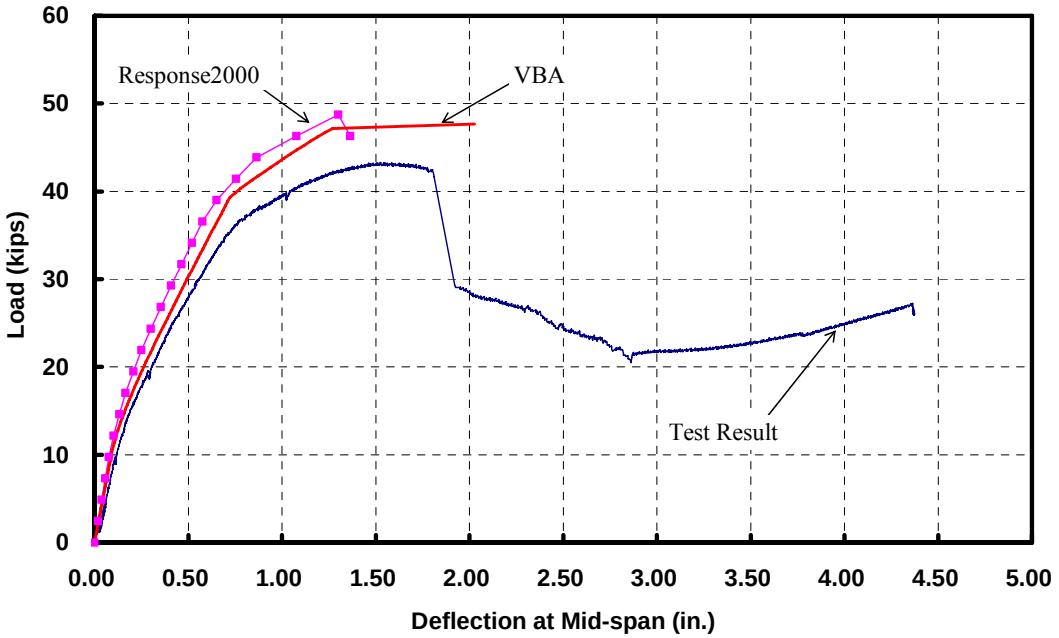

Figure 4-57 Comparison of Measured and Predicted Load-Deflection Response for Specimen 14BA4R

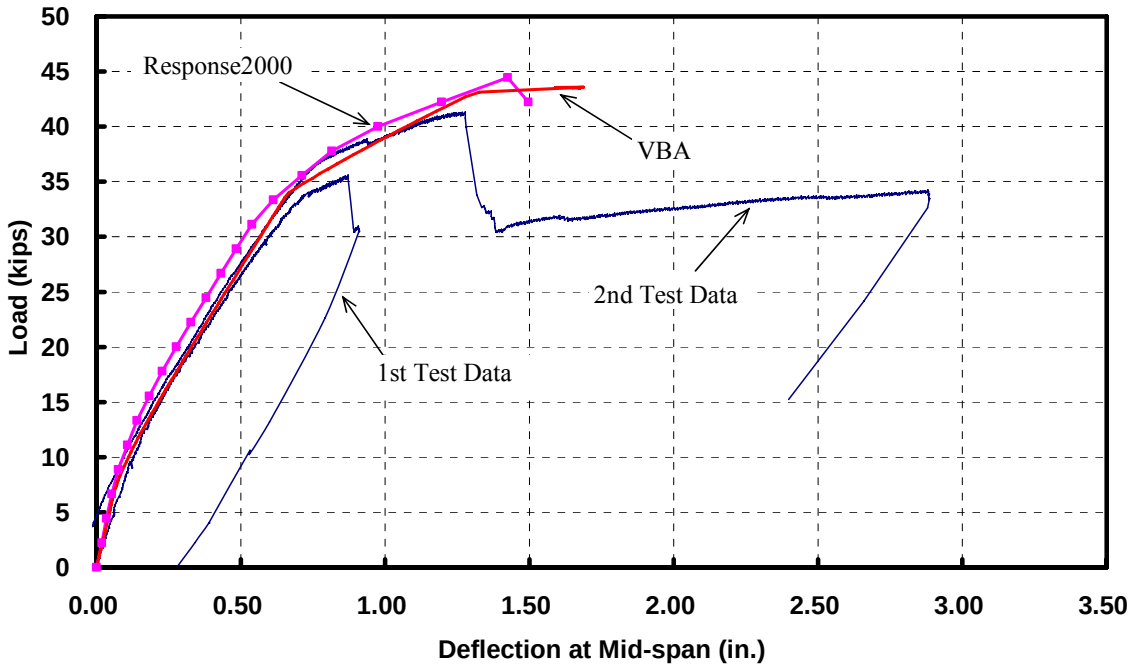

Figure 4-58 Comparison of Measured and Predicted Load-Deflection Response for Specimen 18BA4

4.7 Ductility

The term ductility is defined as the ability of the material or member to sustain deformation beyond the elastic limit, while maintaining a reasonable load-carrying capacity before total collapse. Depending on the type of material or member, the deformation measure for ductility may be strain, curvature, displacement or rotation. Displacement ductility is perhaps easiest to measure, but it would be affected by the loading conditions. As a result, displacement ductility is a more complicated issue and no generalized form of displacement ductility could be developed. On the other hand, the curvature ductility is not a function of loading or boundary condition. In this study, curvature ductility of normal-strength and high-strength concrete specimens is compared to study effect of compressive strength and reinforcement ratio on curvature ductility.

Curvature ductility is defined as:

$$\mu_\phi = \frac{\phi_u}{\phi_y} \qquad \text{(Equation 4-21)}$$

where μ_ϕ is the curvature ductility and ϕ_u and ϕ_y are the ultimate and yield curvature, respectively.

Various criteria have been used to define the curvature at failure. For example, Park and Paulay (1975) defined it as that corresponding to a strength loss of 20 percent for the specimen. Weiss and Shah (2001) considered failure of the specimen at 25 percent strength reduction, whereas Sarkar and Adwan (1997) used 30 percent strength reduction to identify failure.

For all pure flexure specimens tested in this study, no lateral reinforcement is used in the constant moment zone. As a result, concrete crushed soon after reaching the peak resistance, accompanied by sudden and complete loss of resistance. Therefore, the aforementioned criteria could not be applied. An alternative failure criterion is to use the ultimate strain of concrete at extreme compressive fiber of concrete. It is believed by many researchers that the ultimate strain of concrete (ε_{cu}) decreases as concrete strength increases. In this study, the relationship of ε_{cu} and compressive strength of concrete (f'_c) is expressed in Equation 4-1, which was proposed by Mertol (2006).

Determination of curvature ductility requires sectional analysis. Besides the assumptions in moment-curvature analysis as stated in Section 4.5, it was further assumed that:

1. Steel reinforcement is considered to have a yield strength of 60 ksi and elastic modulus of 29000 ksi,
2. Specimen fails when concrete reaches the predetermined ultimate strain, as expressed in Equation 4-1,

The stress-strain relationship of concrete used in this analysis is Equation 4-8, as that used in section 4.5. A closed-form solution for curvature ductility is not available unless the product of n and k in Equation 4-8 is an integer, which is usually not the case. As a result, curvature ductility is investigated numerically. The VBA code used in predicting the full moment-curvature response was used here to calculate the curvature ductility for a given cross-section. The program was slightly modified to incorporate the two additional assumptions as described above. In case a cross-section fails before the reinforcement yields, i.e. over-reinforced specimens, the curvature ductility is taken as equal to one.

It can be shown mathematically that curvature ductility is independent of the width as long as the cross-section is rectangular. To investigate how the effective depth of the section affects curvature ductility, a sensitivity analysis is carried out. The parameters selected in this analysis are listed as follows:

1. Effective depth: 5, 10, 20 and 100 inches;
2. Compressive strength of concrete: between 4ksi and 18ksi at every 2ksi; and
3. Reinforcement ratio: 1 percent to 7 percent at every percent.

As the curvature ductility is independent of width of the cross-section, only one value of 9 inches is used throughout. Curvature ductility was calculated for each combination of parameters. It was found that changing effective depth alone hardly affects the predicted

ductility. Although could not be proved mathematically, this indicates the correlation between the curvature ductility and the effective depth for specimen would be very low for specimens with rectangular cross-section. This is important as it means that analytical results for one hypothetical rectangular cross-section may be used to represent the behavior for all rectangular sections with reasonably high accuracy.

The results from analyzing a hypothetical 9 in. x 12 in. rectangular cross section are presented here. The effective depth is assumed to be 10 in. Other parameters used are the same as those described above in the sensitivity analysis. Predicted curvature ductility is plotted against concrete strength between 4 ksi and 18 ksi in Figure 4-59 for various reinforcement ratios. A dashed line, which indicates a series of sections failed at a longitudinal steel strain of 0.005, is also included in this figure. Predicted curvature ductility values are not plotted on the chart if they are greater than 8. The following two trends can be seen from this chart:

1. For the same concrete strength, curvature ductility decreases as reinforcement ratio increases.
2. For the same reinforcement ratio, curvature ductility increases with concrete strength, despite the fact that ultimate strain of concrete is reduced. It is to be noted that this conclusion is drawn without taking into account the effect of confinement.

The benefit from using high-strength concrete is demonstrated in this figure. High-strength concrete significantly increases the maximum amount of reinforcement that can be placed in a cross-section, while maintaining a reasonable ductility. For example, for a ductility ratio of 3, about 5 percent of reinforcement is allowed in a concrete section with compressive

strength of 18 ksi, while only about 1.6 percent is allowed for the same concrete section with compressive strength of 4 ksi. This also results in a much larger flexural resistance, in this case over three times, for the section with the high-strength concrete. Despite a number of assumptions used in this analysis, the conclusion can be generalized for the flexural members with rectangular cross-section and even members with rectangular shape above the neutral axis, such as a T-section. One of the benefits of using high-strength concrete in flexural member is to enhance the ductility for a given section with a high reinforcement ratio.

ACI 318-05 as well as many other design codes require that the strain of longitudinal steel reaches at least 0.005 at the time of failure as a measure of ductility. Therefore, it is necessary to study how this strain limit affects the curvature ductility for high-strength concrete members. In other words, for a series of specimens failed at the same longitudinal strain of steel at 0.005, are the curvature ductility values for the high-strength and normal-strength concrete specimens same?

Again, a 9 in. x 12 in. rectangular cross-section is assumed and effect depth was assumed with an effective depth of 10 in. The VBA program was used for back-calculating the curvature ductility for a series of sections failed at a longitudinal steel strain of 0.005. Figure 4-60 shows the results, where curvature ductility of each ease is normalized with respect to a value of 2.0, which is obtained from the cross-section with concrete strength of 4ksi and reinforcement ratio 2.2 percent.

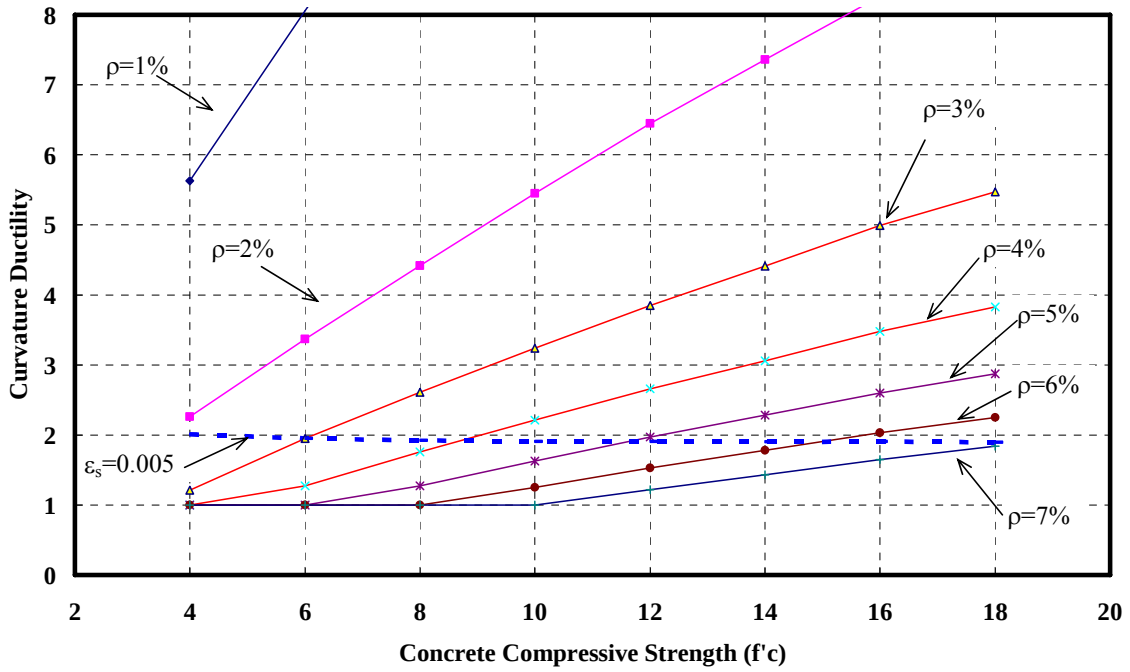

Figure 4-59 Predicted Curvature Ductility for Various Concrete Strength and Reinforcement Ratios

Each data point in this figure reflects a 9 in. x 12 in. rectangular cross-section with the reinforcement ratio and concrete strength as indicated. What this series of assumed sections have in common is that all of them failed at the tensile strain of 0.005 for longitudinal reinforcement. It can be seen from this figure that as concrete strength increases, to maintain a failure at the tensile strain of 0.005 for longitudinal reinforcement, the reinforcement ratio also needs to increase. On the other hand, the curvature ductility dropped slightly, by about 5 percent when concrete strength increases from 4 ksi to 18 ksi.

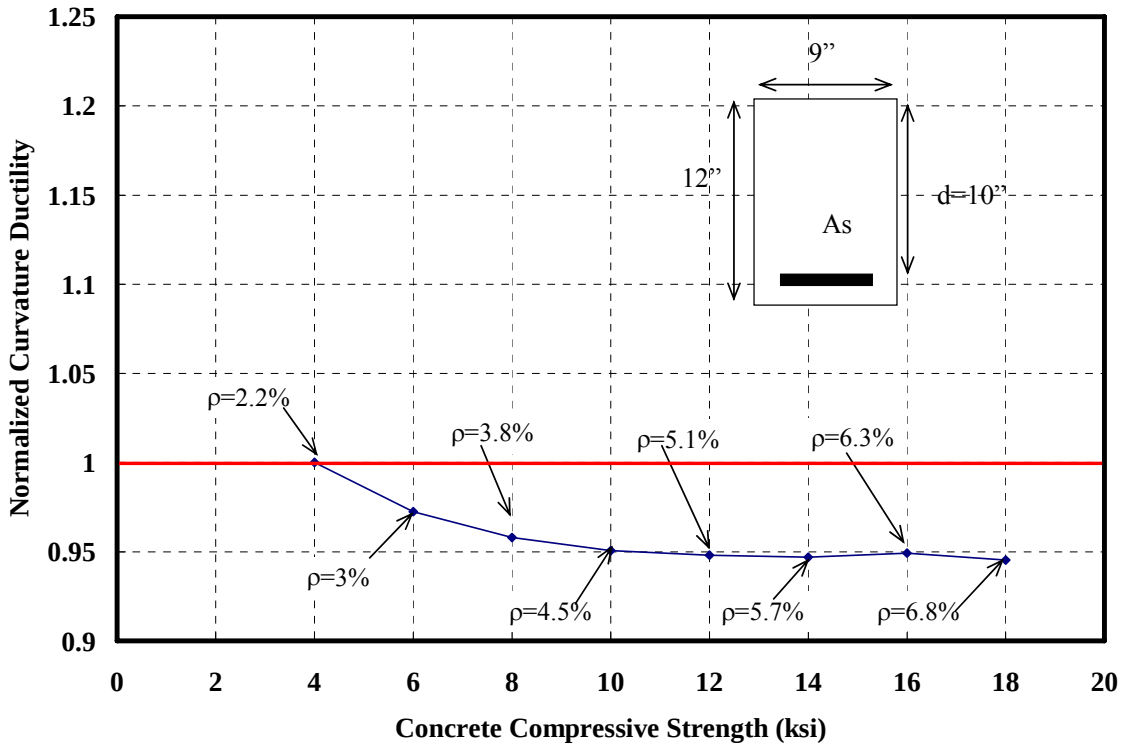

Figure 4-60 Effect of Concrete Compressive Strength on Curvature Ductility Maintaining Steel Strain of 0.005

Another way to present the above finding is to determine how the strain limit of 0.005 needs to be changed in steel reinforcement for high-strength concrete section to maintain the same curvature ductility as that of the same cross section with a compressive strength of 4 ksi. Figure 4-61 shows this comparison, indicating that the strain limit needs to slightly increase to approximately 0.0054 for 18 ksi concrete. Although design codes such as the AASHTO LRFD do not require explicit minimum curvature ductility, the above finding has design implications, in that a higher minimum strain limit in steel is required for high-strength concrete to achieve the same level of implicit ductility as that in a normal-strength concrete member.

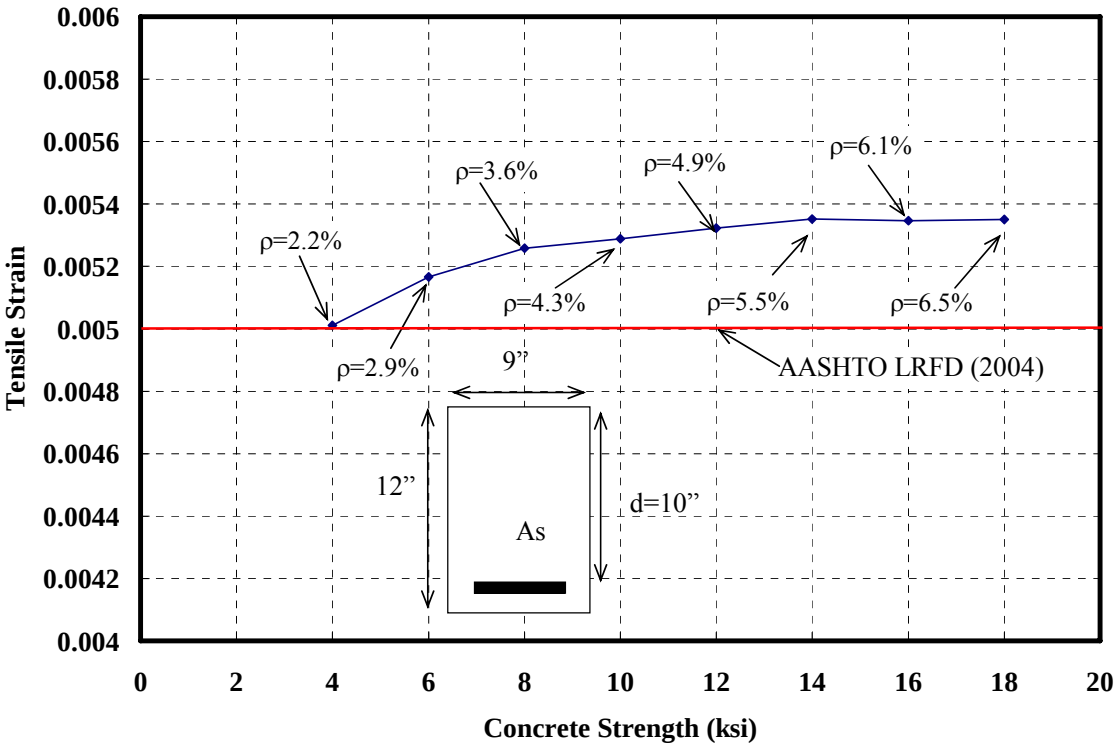

Figure 4-61 Minimum Strain Limit in Steel Reinforcement for Normal- and High-Strength Concrete

5 FINITE ELEMENT ANALYSIS

5.1 Introduction

In this chapter, a general-purpose finite element program, ANSYS Program Release 8.0 (ANSYS 2003), is used to model the flexural response of high-strength concrete beams.

As mentioned in Chapter 4, it has been reported by several researchers in the past that the deflection of high-strength concrete members at service load is generally underestimated using the current AASHTO LRFD or ACI equations. Integrating the moment-curvature curve, which is another commonly used approach, only slightly enhances the accuracy of prediction. Response2000 program (Bentz and Collins, 2000) uses the modified compression field theory (Vecchio and Collins, 1986) in calculating the deflections and takes the shear contribution and tensile stiffening into account. Unfortunately, as shown in the previous chapter, the predicted load-deflection from this program is practically the same as the one from integrating the moment-curvature response.

The difference between the test results and predictions is mainly attributed to overestimation of two key parameters in the analysis: cracking moment and stiffness of the cracked section. Overestimation of cracking moment has been addressed in some foreign design codes, e.g., AUS3600, in which the expression for cracking moment has been modified to account for the restrained shrinkage. With the reduced cracking moment, the predicted deflection will be higher, hence closer to the measured value. The overestimation in stiffness may be attributed to the following two issues:

1. Shear effects: other than Response2000 program, the aforementioned approaches did not take into account the shear contribution, which could be part of the reason for overestimation of the stiffness. It is generally accepted the behavior is dominated by shear if shear span to depth (a/d) ratio is less than 2, and dominated by flexure if shear span to depth ratio is greater than 5. In this study, the shear span to depth ratio, a/d is about 3, which is between the two limits. Thus, it is likely that shear deformation may contribute parts of the difference between tests and predictions.
2. Bond and slippage: it is well known that slippage exists between concrete and reinforcements at the cracks, which result in releasing the stress in concrete. This slippage compromises the strain compatibility between the steel and concrete, and may lower the stiffness of the section. However, it is not feasible to model slippage in sectional analysis.

It was expected that the finite element analysis using ANSYS could provide some useful information to assess one or both of above hypotheses. Two specimens tested in the experimental program were modeled in this chapter. An under-reinforced specimen, 10B2.1, was modeled to demonstrate the entire load-deflection response using the finite element program; and an over-reinforced specimen18B12.7 was modeled to assess the bond-slippage issue.

5.2 Finite Element Modeling

In the present study, finite element models are constructed using graphical user interface (GUI) in ANSYS.

5.2.1 Element Types

Two types of elements were selected for different components of the high-strength concrete beams, as follows:

1. SOLID65 elements were used to model the concrete material. This element is defined by eight nodes and has the isotropic material properties. This element is capable of cracking (in three orthogonal directions), crushing, plastic deformation, and creep. The geometry, node locations, and the coordinate system for this element are shown in Figure 5-1. Solid65 element is capable of incorporating one material property for concrete and up to three rebar materials for rebars, which are assumed to be uniformly distributed throughout the concrete element in a defined region of the FE mesh. This type of smeared reinforcement model is mainly used in analyzing structures which are large in volume of concrete, e.g., foundations.

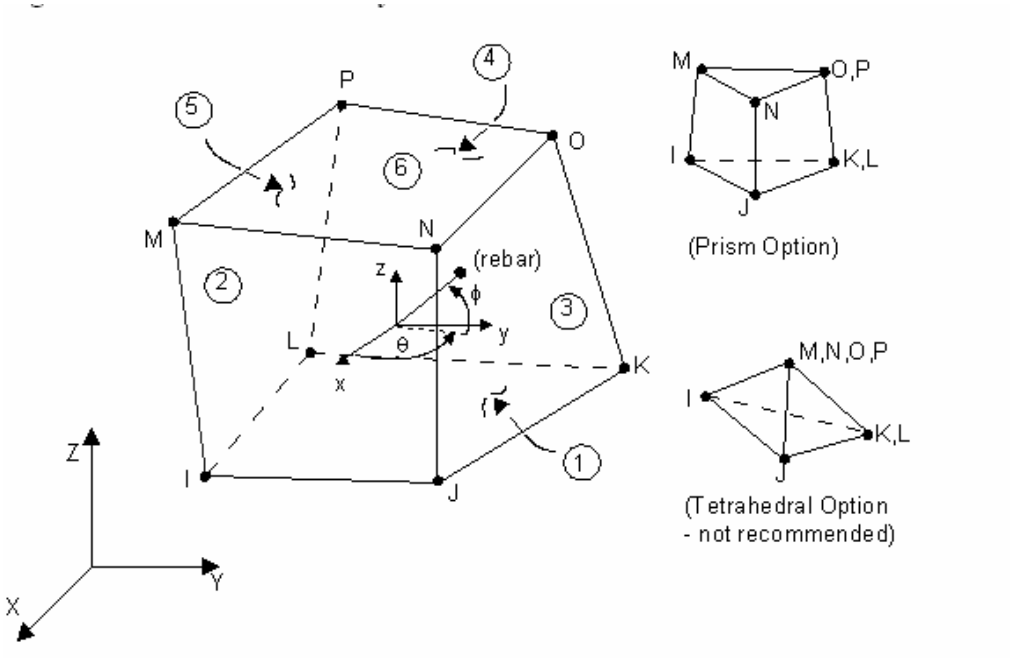

Figure 5-1 Solid65 Element (ANSYS 2003)

2. Link8 element was used to model steel reinforcement. The 3-D spar element is defined by two nodes and an isotropic material property. No bending stiffness is considered. Plasticity, creep, swelling, stress stiffening, and large deflection capabilities can be included. A schematic of this element is shown in Figure 5-2.

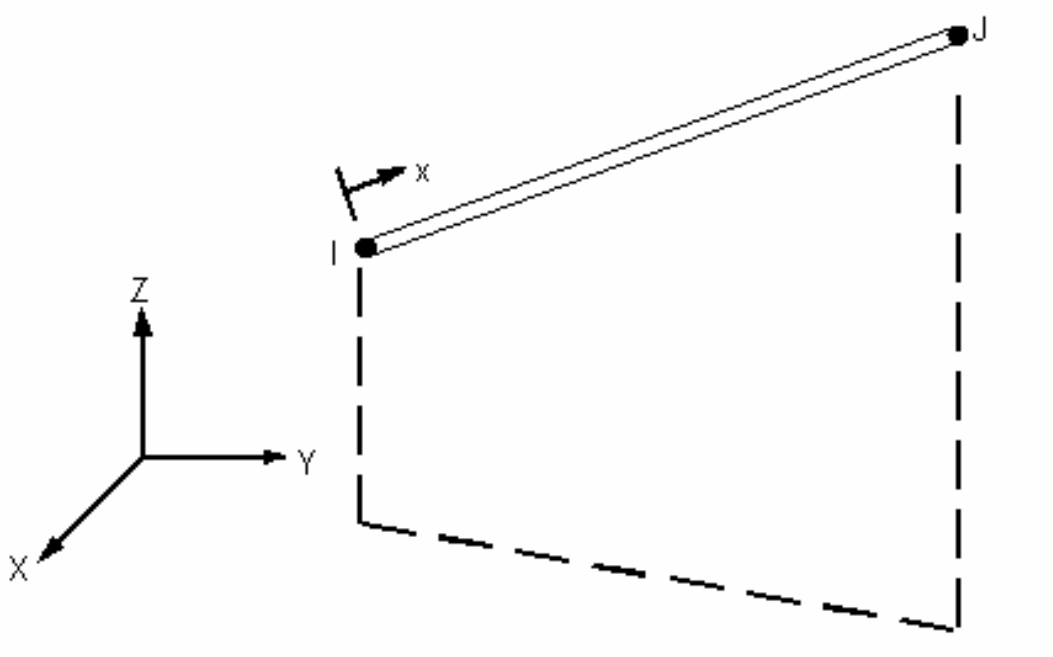

Figure 5-2 Link8 Element (ANSYS 2003)

5.2.2 Real Constants

In ANSYS GUI, real constant tables are used to input "parameters" for each element type. An example of real constant input is given in Table 5-1.

Real constant options for the Solid65 elements are used for setting up a smeared model for reinforcement. In this study, both the longitudinal and transverse reinforcements are modeled individually, and the three volume ratios in the three directions are all set as zero here.

Real constant options for the Link8 elements are used to define the area of reinforcement as

well as the initial strain of the reinforcement. Nominal area of each type of reinforcement is used in the modeling. The initial strain input is used for modeling prestressed members, hence not applicable to this study.

5.2.3 Material Properties

Setting up a material model in ANSYS generally involves in two steps:

1. Selecting appropriate material model; and
2. Input data for each selected material model.

In ANSYS GUI, this is done in Material Properties tables, such as those in Table 5-2 are used for this purpose.

Table 5-1 Example of Real Constants Input in ANSYS

Real Constant No.	Element Type		Real constant for rebar1	Real constant for rebar2	Real constant for rebar3
1	Solid 65	Material No.	1	1	1
		Volume Ratio	0.00	0.00	0.00
		Orientation Angle	0	0	0
		Orientation Angle	0	0	0
2	Link 8	Cross Section Area	1.56		
		Initial Strain	0		

For Link8 elements, the bi-linear elastic-plastic stress-strain for steel reinforcement was setup in two data tables. Elastic modulus (“EX”) and Poisson’s ratio (“PRXY”) were entered in the first table to setup a linear isotropic model, which is for the elastic range. For “Bilinear Isotropic Hardening” model used in this study, after reaching the specified yield stress (“Yield Stss”), the stress-strain curve of reinforcement continues along the second slope

defined by the tangent modulus ("Tang Mod"). It is worth noting that this tangent modulus ("Tang Mod"), should not be set as zero, as this would cause the member lose its stability upon yielding. Therefore, a very small value of 100 is used.

The material properties of Solid65 elements were input in three data tables. In the table for "Linear Isotropic" model, initial elastic modulus and Poisson's ratio of concrete were entered. In the table for "Multi-linear Isotropic Hardening" model, the uniaxial stress-strain relationship of concrete was entered with several points, which were calculated from the model proposed by Mertol (2006). It is to be noted that "Multi-linear Isotropic Hardening" model is not the only one that can be used for modeling concrete. Other more complicated models, e.g., "Multi-linear Kinematic Hardening" can be applied (Lu and Jiang 2003). However, since no cyclic loading was applied in the present study and confinement effect was considered, "Multi-linear Isotropic Hardening" model was found sufficient in this study.

A series of 9 constants needs to be specified for Solid65 element in ANSYS, as shown in the third data table ("Concrete Material Data") in Table 5-2. These constants are for the implementation of the Willam and Warnke (1974) model, as described below:

No.1 Shear transfer coefficients for an open crack:

This factor ranges from 0 to 1, with zero representing a smooth crack (i.e., complete loss of shear transfer) and one representing a rough crack (i.e., no loss of shear transfer). Unfortunately, no reference to this factor was found for high-strength concrete in the literature. Kachlakev et al. (2001) and Wolanski (2004) used 0.3 for this constant in modeling normal-strength concrete members in flexure. Wolanski (2004) reported no

deviation of the response with the change of the coefficient. A small sensitivity study in this study verified his finding, which indicates overestimating the shear transfer would not affect the flexural response. On the other hand, convergence problems repeatedly occurred when the shear transfer coefficient for an open crack dropped below 0.2, as was reported by Wolanski (2004).

No.2 Shear transfer coefficients for a closed crack:

Due to the monotonic loading scheme and boundary condition, it was found from the results that none of the concrete elements exhibited "a closed crack". Therefore, this factor actually did not affect.

No.3 Uniaxial tensile cracking stress (f_t): measured values of modulus of rupture is used.

No.4 Uniaxial crushing stress (f'_c, positive): measured values of concrete compressive strength is available, however, this constant is set to a value of -1, which turns off the crushing capability of Solid65 element as suggested by previous researchers (Wolanski, 2004, Kachlakev et al. 2001). Convergence problems have been reported if the measured concrete strength (f'c) is used.

No.5 Biaxial crushing stress (f_{cb}, positive);

No.6 Ambient hydrostatic stress state for use with constants 7 and 8 (σ^a_h);

No.7 Biaxial crushing stress (positive) under the ambient hydrostatic stress state (f_1); and

No.8 Uni-axial crushing stress (positive) under the ambient hydrostatic stress state (f_2):

Table 5-2 Example of Material Properties Input in ANSYS

<table>
<tr><th>Material Model Number</th><th>Element Type</th><th>Material Properties</th></tr>
<tr><td>1</td><td>Link8</td><td>
<table>
<tr><td colspan="2">Linear Isotropic</td></tr>
<tr><td>EX</td><td>29,000,000</td></tr>
<tr><td>PRXY</td><td>0.3</td></tr>
</table>
<table>
<tr><td colspan="2">Bilinear Isotropic</td></tr>
<tr><td>Yield Stss</td><td>68,000</td></tr>
<tr><td>Tang Mod</td><td>100</td></tr>
</table>
</td></tr>
<tr><td>2</td><td>Solid65</td><td>
<table>
<tr><td colspan="2">Linear Isotropic</td></tr>
<tr><td>EX</td><td>5,863,000</td></tr>
<tr><td>PRXY</td><td>0.2</td></tr>
</table>
<table>
<tr><td colspan="3">Multi-linear Isotropic Hardening</td></tr>
<tr><td>Point 1</td><td>0.0003</td><td>1839</td></tr>
<tr><td>Point 2</td><td>0.0006</td><td>3677</td></tr>
<tr><td>Point 3</td><td>0.0009</td><td>5514</td></tr>
<tr><td>Point 4</td><td>0.0012</td><td>7343</td></tr>
<tr><td>Point 5</td><td>0.0015</td><td>9145</td></tr>
<tr><td>Point 6</td><td>0.0018</td><td>10878</td></tr>
<tr><td>Point 7</td><td>0.0021</td><td>12465</td></tr>
<tr><td>Point 8</td><td>0.0024</td><td>13783</td></tr>
<tr><td>Point 9</td><td>0.0027</td><td>14678</td></tr>
<tr><td>Point 10</td><td>0.003</td><td>15000</td></tr>
</table>
<table>
<tr><td colspan="2">Concrete Material Data</td></tr>
<tr><td>ShrCf-Op</td><td>0.2</td></tr>
<tr><td>ShrCf-Cl</td><td>1</td></tr>
<tr><td>UnTensSt</td><td>1498</td></tr>
<tr><td>UnCompSt</td><td>-1</td></tr>
<tr><td>BiCompSt</td><td>0</td></tr>
<tr><td>HydroPrs</td><td>0</td></tr>
<tr><td>BiCompSt</td><td>0</td></tr>
<tr><td>UnTensSt</td><td>0</td></tr>
<tr><td>TenCrFac</td><td>0.6</td></tr>
</table>
</td></tr>
</table>

In the present study, default values from ANSYS, which are proposed by Willam and Warnke model (1975) are used, as below:

$f_{cb} = 1.2\ f'_c$;

$f_1 = 1.45\ f'_c$;

$f_2 = 1.725 f'_c$;

These default values are valid if hydrostatic stress $\sigma^a_h < \sqrt{3}\ f'_c$, where σ^a_h the average of the three principal stresses. No additional work is done to verify the applicability of this model for high-strength concrete. No lateral reinforcement is used in the constant moment area in this study, and therefore the confinement effect, if any, is not expected to significantly affect the overall behavior.

No.9 Stiffness multiplier for cracked tensile condition:

This constant is used to define the effect of tension stiffening, as shown in Figure 5-3. In this figure, f_t is the uniaxial tensile strength of the concrete. Upon cracking, the tensile stress drops abruptly to a fraction of it, $T_c f_t$, where T_c is a multiplier for the amount of tensile stress relaxation (ANSYS 2003). Thereafter, the tensile stress of concrete approaches to zero at a strain 6 times the cracking. T_c has value between zero and one. An input of zero stands for a complete loss of tensile stress at cracking; and a value of one means no sudden loss of tensile stress at cracking. System defaults value of 0.6 is adopted in this study.

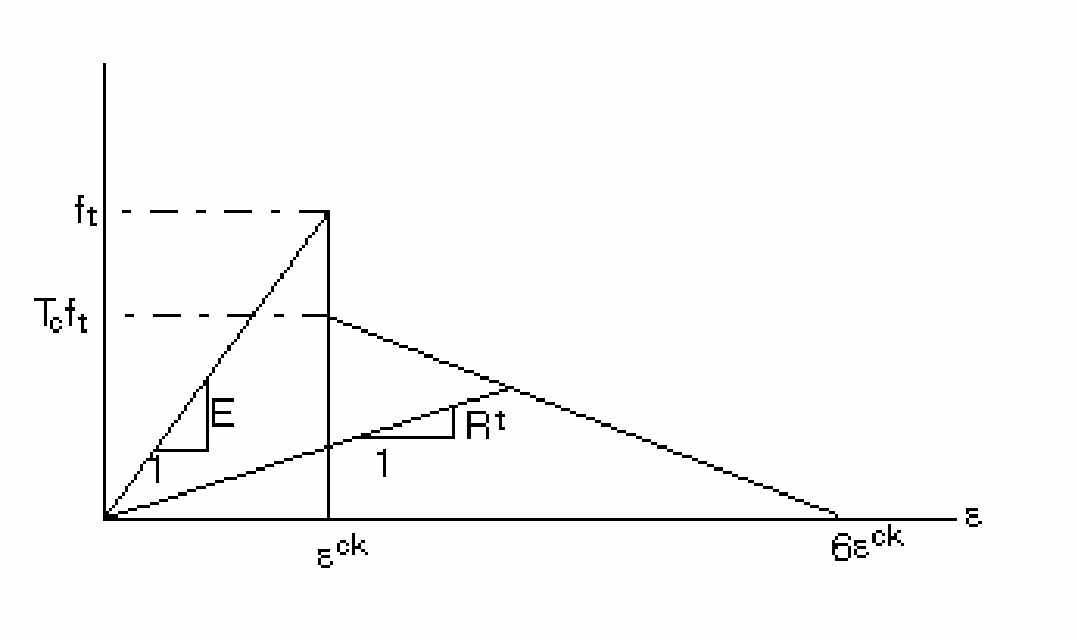

Figure 5-3 Tensile Strength of Cracked Concrete

5.2.4 Mesh Geometry

The flexural member and the loading conditions are symmetric. The two planes of symmetry are shown in Figure 5-4, using dashed-lines. Taking advantage of the symmetry, only one quarter of each beam was modeled. The meshes of the concrete elements for modeling Specimens 10B2.1 and 18B12.7 are shown in Figures 5-5 and 5-6, respectively. In these three-dimensional models, Z represents the longitudinal direction; X is the transverse direction; and Y is the direction of the height. The configuration of reinforcement for Specimen 18B12.7 is shown in Figure 5-7 as an example of how the reinforcement is modeled in this study.

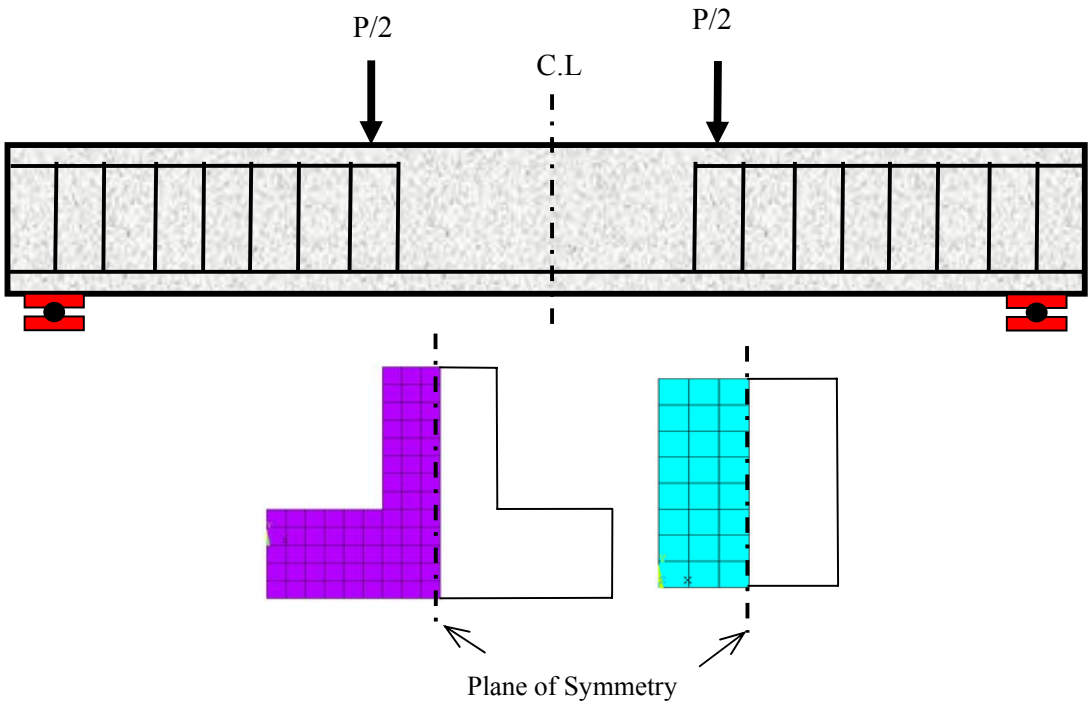

Figure 5-4 Plane of Symmetry Used in Finite Element Modeling

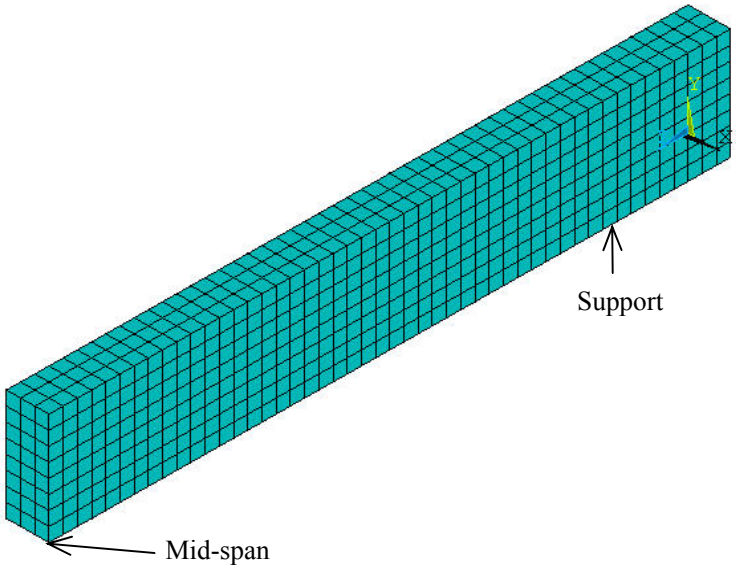

Figure 5-5 Mesh of Concrete Elements for Specimen 10B2.1

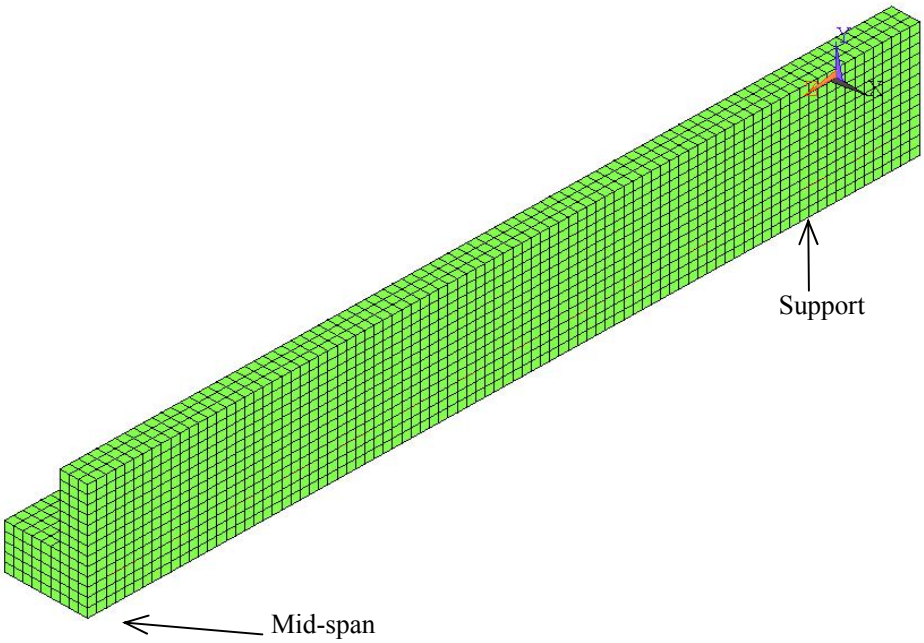

Figure 5-6 Mesh of Concrete Elements for Specimen 18B12.7

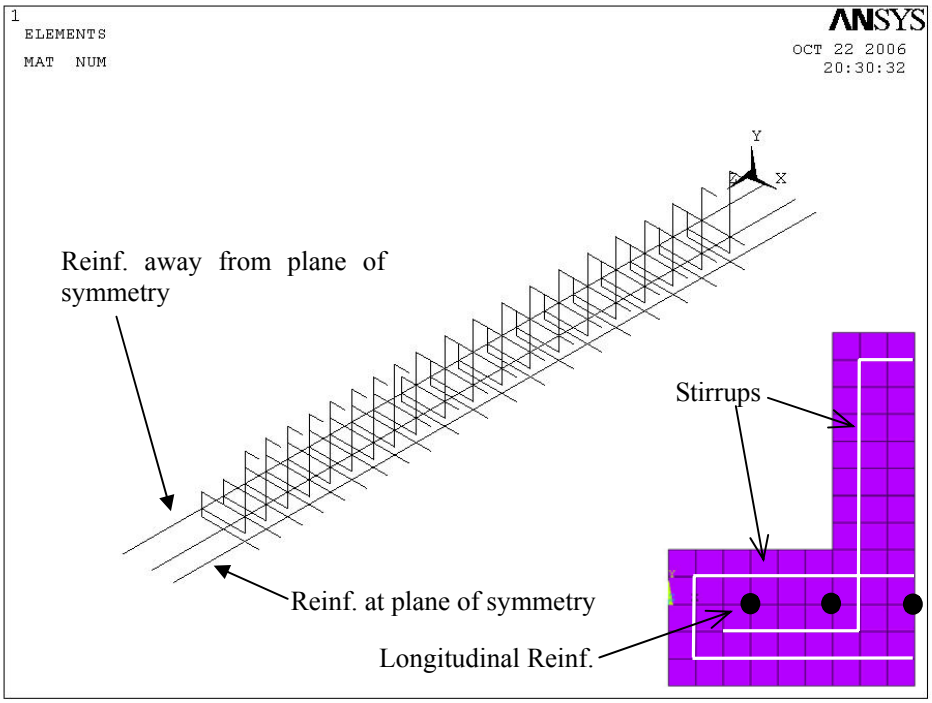

Figure 5-7 Reinforcement Configurations

The length of the longitudinal reinforcement elements was decided according to the type of model used in this study:

1. In the bonded model, the length of Link8 elements is the same as the dimension of concrete elements so that the nodes of the two types of elements can be merged together to generate the perfect bond.
2. In the debonded model, only one Link8 element is created between the support and the mid-span for the longitudinal reinforcement.

It should also be noted that due to the limit of the mesh size, location of the reinforcement is slightly different from the real specimen. The effective depth is reduced by 3/16 inch and the concrete cover is reduced by ¼ inch.

5.2.5 Load and Boundary Conditions

In the testing program of the present study, all specimens were loaded in displacement control. To simulate this loading procedure, deflection was directly applied in an incremental manner to the nodes under the loading plates in the finite element analysis.

The symmetric boundary conditions were applied to the plane of symmetry, as shown in Figure 5-4. Supports were modeled by applying "zero deflection" directly to the nodes of concrete elements. Some investigators, e.g., Wolanski (2004), used a more complicated approach to model support, in which a steel plate under the beam was modeled using Solid45 elements. The steel plate support, which acts as "cushion", was perfectly bonded with the concrete beam, and the restraint was applied to the nodes of the Solid45 elements. It was believed that the "cushion" would alleviate the stress concentration and avoid unexpected

local failure at the support (Lu, 2003). In this study, both types of model for support were attempted, i.e., with and without the "cushions". It was found that the response of the two models were practically same: no unexpected failure occurred at the support, and the predicted load-deflection response was essentially the same. Since the stress distribution at the support is not a research objective, it was decided not to model the steel cushion, which simplified the analysis.

5.2.5 Analysis Type and Solution Controls

In running non-linear analysis such as the present study, options in the "Solution Controls" options need to be set for an appropriate iteration process and output of the program.

The "Solution Controls" contain a set of related parameters, as follows:

1. Basic;
2. Transient;
3. Solution Options;
4. Nonlinearity; and
5. Advanced Nonlinearity.

Under "Basic" controls, Small Displacement Static analysis is selected from the "Analysis Options" to perform a linear static analysis, in which large deformation effects are ignored. A time value was provided at the each end of the load step. In the present study, as deflection is applied monotonically to the member, only one load step is needed. The loading history was controlled by several options as follows:

"Number of substeps" provides a measure of rate of loading. Usually, a compromise

between the number of substeps and the speed of computation is necessary. A smaller number is chosen for over-reinforced beams with their linear response. Maximum and minimum number of substeps provide thresholds for the loading option. In this study, result file at each substep were written down.

In non-linear controls, criteria for convergence were set manually. Displacement convergence criteria were set to be within 5 percent, which is the system default. The force tolerance was also set to be 5 percent, which is 10 times the system default value. Any further reduction of this value would cause non-convergence problems in the analysis after concrete starts to crack. Same criterion was adopted by previous research (Wolanski, 2004). The remaining solution control options, such as type of equation solvers were set to system defaults.

5.3 Results of Finite Element Analysis

5.3.1 General Failure Mode

As mentioned previously, the function of crushing of concrete was turned off to avoid early termination of the solution, which may due to local stress concentration. Fortunately, the equations in the current AASHTO LRFD Specifications (2004) can be used to predict the ultimate resistance of the flexural members reasonably well. In the present study, the measured peak resistance was considered as the ultimate resistance in the FEM analysis.

Results from modeling of Specimen 18B12.7 were used here to demonstrate the distribution of stress and strain in concrete at peak resistance. The predicted distribution of third principle stress (maximum compressive stress) is shown in Figure 5-8. At the extreme

compressive fiber in the constant moment zone, stress in concrete is about 16 ksi, which is approximately the compressive strength of concrete. Stress concentration is observed in a few elements near the loading area, with as high as 21ksi of stress predicted by ANSYS. The contour plot of the third principle strain (maximum compressive strain) is shown in Figure 5-9. High levels of the strain are observed under the loading plate, nearly at the same location of the stress concentration. In reality, this part of concrete under the loading plate is somehow confined, possibly due to the friction between concrete and the loading plate. Therefore, failure is very likely to initiate from the elements to left side the loading plate.

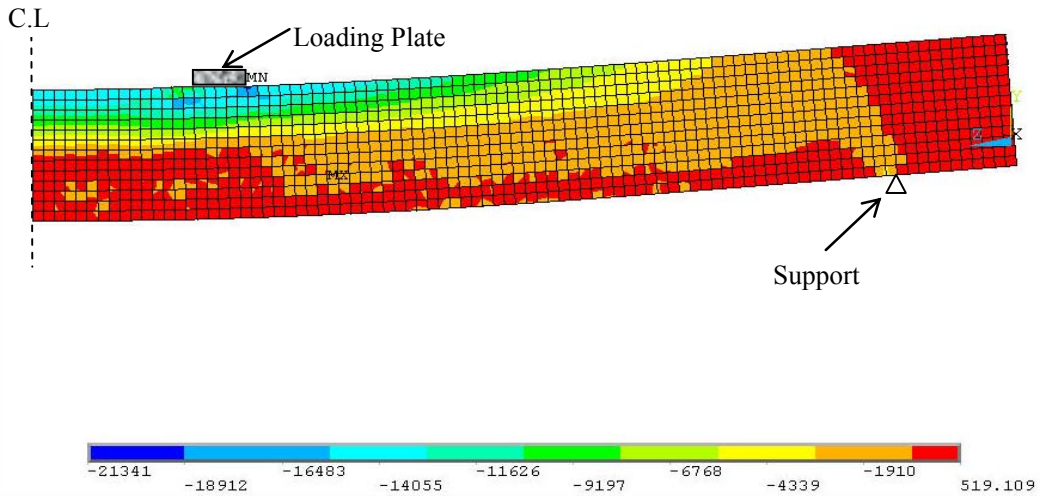

Figure 5-8 Stress Contours in Specimen 18B12.7 at Maximum Resistance

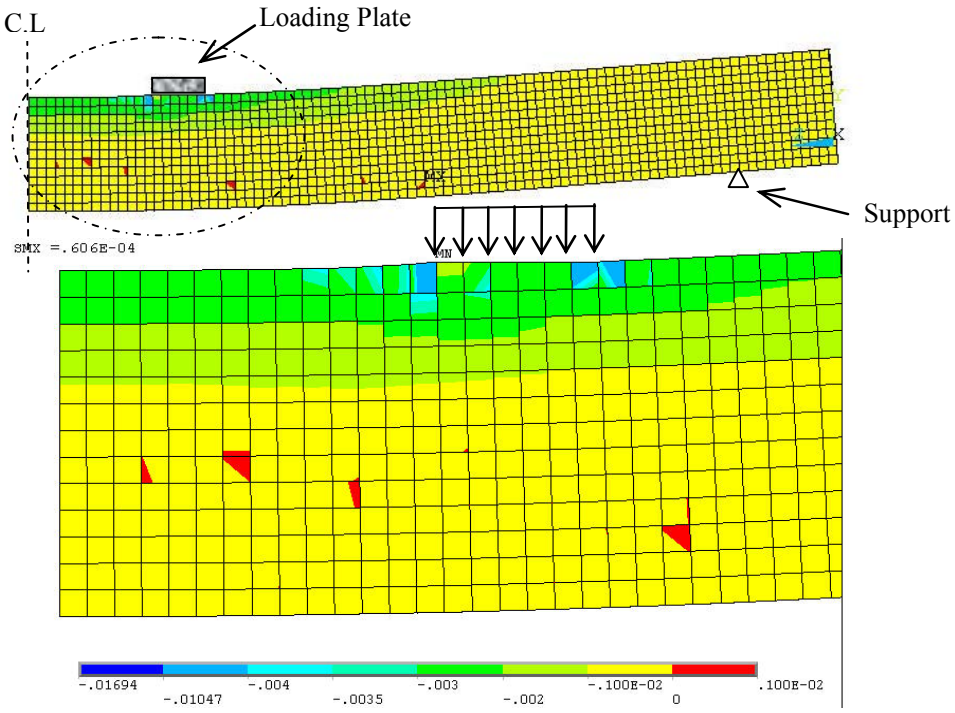

Figure 5-9 Third Principle Strain at Maximum Resistance

5.3.2 Crack Pattern

ANSYS Solid65 element output does not include prediction of crack widths. Since this issue is not a major concern in the finite element analysis, only an example of the predicted crack pattern is shown in Figure 5-10, which is from the solution of bonded model of Specimen 18B12.7. In ANSYS program, a crack is shown as a circle outline in the plane of the crack. Because the specimen is viewed from its transverse direction, for majority of the elements shown in Figure 5-10, the crack is shown just a as line, which is a projection of the cracking plane. In this figure, vertical cracks are predicted within the constant moment area, and diagonal shear cracks are predicted in the shear span, which reflects the typical crack pattern observed in the test.

The amount of cracks shown here from the ANSYS solution is much more than what is observed in the test. It is to be noted however that a crack shown in this figure does not mean there would be a crack in the beam. No more than 3 cracks can be predicted in each Solid65 element. Therefore, the amount of cracks shown is affected by the size of mesh. Using a larger mesh size for Solid65 elements would result in fewer elements and less cracks shown; vice versa, using a finer mesh size will result more elements and more cracks shown. Therefore, it is more appropriate to consider the cracks shown in Figure 5-10 as contours of where tensile stress exceeds the tensile strength of concrete. Excessive cracks may also be attributed to the bonded model in this analysis, where concrete elements and steel elements are perfectly bonded together at every one inch. In the real case, once a tensile crack is generated, tensile stress in concrete is released due to slippage between the two materials at the cracks.

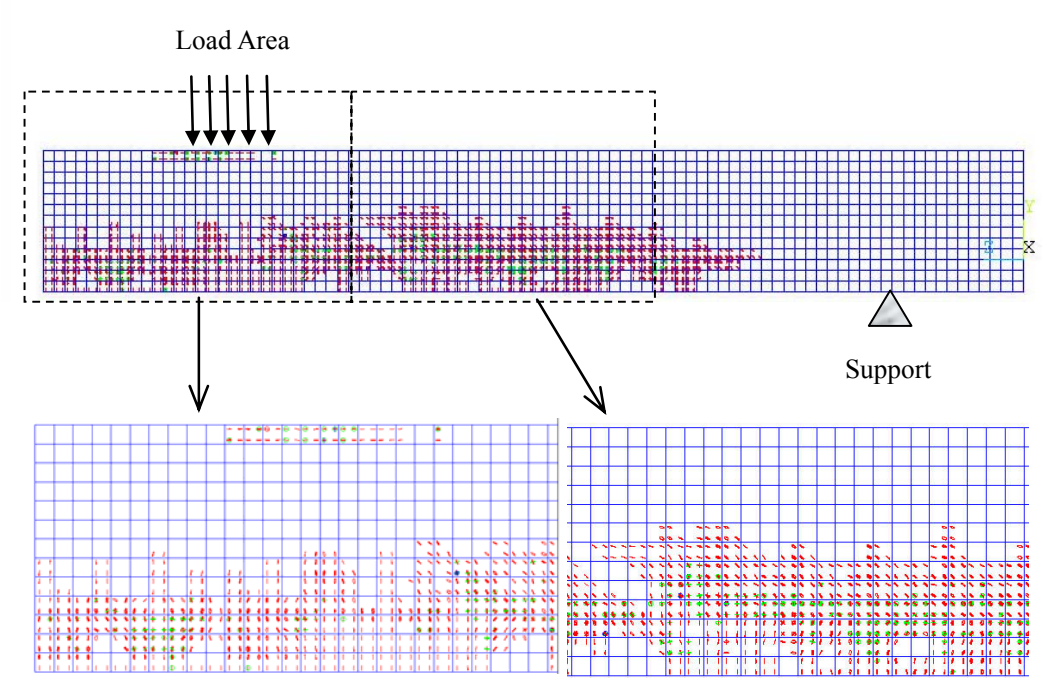

Figure 5-10 Crack Pattern for the Bonded Model of Specimen 18B12.7 at Maximum Resistance

5.3.3 Load-Deflection Response

In the present study, load-deflection solutions were generated from "Time-History Post-process" for each substep of loading. As mentioned earlier, Specimen 10B2.1 was modeled mainly to verify the capability of ANSYS in predicting the load-deflection response for under-reinforced, high-strength concrete member. The load-deflection curves from ANSYS as well as prediction using AASHTO LRFD equations are shown together with test data in Figure 5-11. The predicted curve from ANSYS almost overlaps the prediction using code equations. This is expected since the code assumes perfect bond between the materials, much the same as the bonded model in ANSYS.

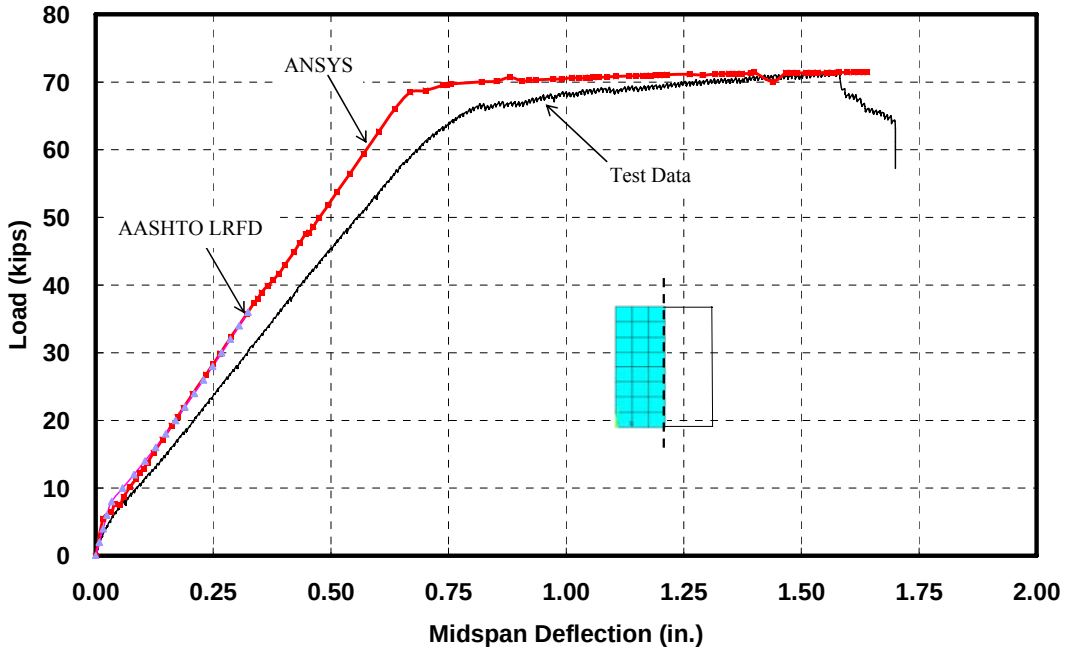

Figure 5-11 Load Deflection Response for Specimen 10B2.1

Specimen 18B12.7 was modeled in two different ways: bonded model and debonded model, as discussed in Section 5.2.4. The predicted load-deflection responses for both models are shown in Figure 5-12, along with the test data and the predicted curve using the current

AASHTO LRFD Specifications. At each level of load, predicted deflection using current AASHTO LRFD (2004) equations is the smallest. As the load increases, the stiffness of the predicted curve from the code equations remained constant as I_{eff} is practically the same as I_{cr}. However, the slope the ANSYS bonded model is decreased and the two curves deviate from each other at higher load levels.

The fully debonded model overestimates the deflection at higher level of load. But it provides closest prediction after cracking up to a load level 20 kip, in term of stiffness as well as the absolute deflection value. The test data is approximately in the middle of the two finite element models. This indicates the loss of bond between concrete and steel is a possible explanation for the underestimation of deflection and overestimation of stiffness.

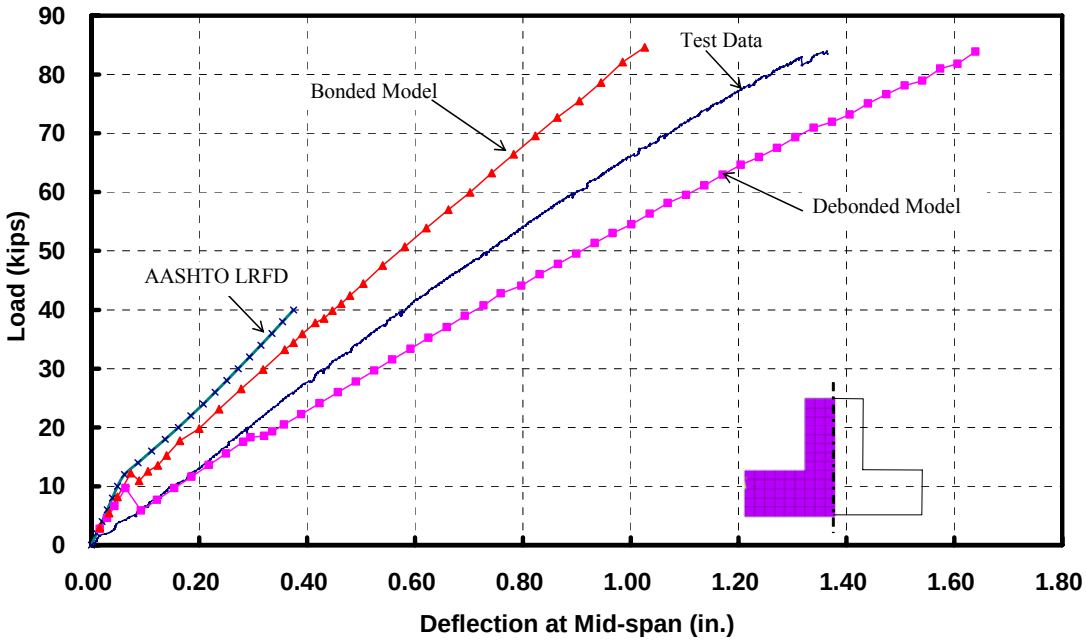

Figure 5-12 Load Vs Mid-span Deflection for Specimen 18B12.7

5.4 Discussion

5.4.1 Shear Contribution to Deflection

The difference between the stiffness of the two predictions from the bonded model and the LRFD prediction mainly reflects contribution of shear to deflection: as more cracks developed in the beam, shear stiffness reduces as well and therefore may contribute more to the deflection, which the code equations do not take into account. However, it can be seen from Figures 5-11 and 5-12 that shear contribution to deflection is not significant.

5.4.2 Effect of Shear-lag

Shear-lag refers a delay or slow response in developing shear flow reactions to the applied loads. In other words, due to the shear deformability of flange, the assumption of normal stress uniformity along the width of the flange plate is not valid for certain situations, e.g., concrete or steel box girders.

As shown previously in Figure 5-7, the longitudinal reinforcement was distributed within the flange. Therefore, there is a possible difference in the longitudinal strain between the reinforcement away from, and the one at or near the plane of symmetry. To test this possibility, longitudinal strain results from ANSYS for both models were compared. It was found that the stress of the reinforcement at the plane of symmetry is highest, while the stress of reinforcement away from it is slightly lower. The difference is highest at the initial stage of loading due to the effect of cracks. Once the load reaches the service load level, there is only 2 percent difference between the stresses of the reinforcement. Such small difference

in stress and its effect on the stiffness of section could be deemed negligible.

5.4.3 Effect of Bond and Slippage

If concrete and the longitudinal reinforcement were perfected bonded together, the cracking pattern would comprise of large number of small cracks, somewhat similar to the ANSYS predictions in Figure 5-10, but different from what is observed in the experiments. In other words, the tensile stress in concrete is released because of the slippage at the cracks between the reinforcement and the surrounding concrete. Nevertheless, the effect of this slippage is hard to quantify, experimentally as well as theoretically. Measuring the slippage requires assessment of local strain of steel as well as concrete. Due to the randomness of the crack and non-homogeneity of the material, it is very hard to measure a representative localized strain of concrete. Also, the strain of steel varies at the crack and un-cracked sections.

The strain compatibility assumption commonly used in design of concrete, is an approximation rather than a perfect simulation, especially after cracking. In other words, the best expectation of strain profile determined based on this assumption is that it would represent a smeared average strain for a small segment of the member, but not any particular localized strain at the cracked or uncracked sections. Once the bond between concrete and steel is removed completely and shear transfer between the two materials is eliminated, e.g. at the cracks, the validity of this assumption becomes questionable. Without the strain compatibility assumption, the strain of steel and concrete are decoupled and setting the force equilibrium equation as well as deflection compatibility by hand becomes very hard. As a result, it is hard to find any reference on how to quantify the slippage and its effects on the

deflections. There are no available equations in the code for predicting the deflection of an un-bonded, non-prestressed flexural member, either.

The debonded model was created to explore this issue. As described previously, nodes of the concrete and reinforcement elements were merged only at mid-span and at the support in this model. This model, even though not replicating the real case, reflected an extreme condition. In other words, there is no bond or strain compatibility between the reinforcement and concrete in the entire span of the beam. The corresponding load-deflection response brings to light, in the worse case, how much the slippage between the materials would affect the load-deflection response of the member. As shown in Figure 5-12, the debonded beam has much larger deflection at the mid-span, which indicates the slippage could have a significant impact on the deflection.

6 SUMMARY AND CONCLUSIONS

6.1 Summary

The behavior of high-strength concrete members under pure flexure and axial-flexural loading was investigated in this study. The research program, as part of NCHRP Project 12-64, was comprised of both experimental and analytical work.

The experimental work included the following pure flexure tests, axial-flexural tests and ancillary material property tests for three levels of high-strength concretes with target strengths of 10, 14 and 18 ksi:

1. Pure flexure tests: a total of fourteen specimens were tested under monotonic loading in four-point flexure.
2. Axial-flexural tests: a total of five specimens were tested under monotonic loading in four-point flexure with constant axial load.
3. Ancillary material property tests: Three 4 in. x 8 in. cylinders and three 6 in. x 6 in. x 20 in. plain concrete beams were tested for each beam or beam-column specimen to obtain the compressive strength and the modulus of rupture of concrete, respectively. Cores were taken from some of the specimens after testing to examine the difference in material properties between the concrete cylinders and the flexural specimens. Reinforcement bars were also tested under monotonic tensile loading to obtain the stress-strain relationship of the steel.

Test results from the present study, combined with collected data from the literature, were analytically evaluated with the following objectives:

1. Examine the usable ultimate strain of unconfined concrete, ε_{cu};
2. Investigate the adequacy and accuracy of using stress block parameters (α_1, and β_1) to determine the flexural resistance of beams and beam-columns;
3. Validate methods of predicting the cracking moment and crack widths in high-strength concrete beams;
4. Investigate the adequacy and accuracy of using the current AASHTO LRFD Specifications (2004) equations in predicting the mid-span deflection at service load level;
5. Verify the applicability of beam theory to high-strength concrete member under pure flexure and axial-flexural loading; and
6. Study the curvature ductility of concrete members as a function of concrete strength and reinforcement ratio.

Finite element analysis was also performed using the general-purpose ANSYS 8.0 program to investigate the effect of bar slippage on the deflection of high-strength concrete beams.

6.2 Conclusions

The present study has resulted in a number of conclusions, as outlined below:

1. The value of 0.003 seems to be a reasonable lower bound of the ultimate strain for design purposes for both normal-strength concrete and high-strength concrete.
2. Prediction of nominal flexural resistance using the current AASHTO LRFD equation is less conservative and less accurate for high-strength concrete members. Using the proposed lower stress block factor (α_1) by Mertol (2006) would improve the predictions for high-strength concrete beams and beam-columns.

3. Nominal resistance of a flexural member decreases if the stress block factor α_1 decreases. The reduction is more significant for members with higher reinforcement ratio and lower compressive strength of concrete. For over-reinforced members, nominal flexural resistance decreases if the stress block factor β_1 or ultimate strain of concrete reduces. For under-reinforced members, changing either β_1 factor or the ultimate strain of concrete does not have any impact on the flexural resistance.
4. The observed cracking moment could not be accurately predicted in the present study, owing to the inaccuracies of the measurements and the code equations.
5. All measured crack widths are less than 0.017 in, which is representative of crack width specified for class 1 exposure condition in the AASHTO LRFD Specifications (2004). Frosch's model provides conservative predictions to the crack widths for majority of the beams tested in this study.
6. Current AASHTO LRFD Specifications (2004) underestimated the deflection at service load for all tested specimens in this project. Other methods for predicting the load-deflection responses, e.g., integrating the moment-curvature response along the span or using Response2000 program, yield very similar results, in which accuracy of the predictions are slightly improved but the overall deflections are still underestimated for majority of the specimens tested in this study.
7. High-strength concrete allows larger amount of reinforcement that may be placed in a cross-section, while maintaining a reasonable ductility. As concrete strength increases, to maintain a failure at the tensile strain of 0.005 for the longitudinal reinforcement, the reinforcement ratio also needs to increase. On the other hand, the curvature ductility drops by about 5 percent, when concrete strength increases from

4ksi to 18ksi. Therefore, a slightly higher minimum strain limit in steel is required for high-strength concrete to achieve the same level of implicit ductility as that in a normal-strength concrete member.

8. Finite element analysis suggests slippage between concrete and steel reinforcement, which compromises the strain compatibility, could have a significant impact on the deflection.

REFERENCES

AASHTO LRFD Bridge Design Specifications, 3rd edition, American Association of State Highway and Transportation Officials, Washington, D.C. 2004

ACI Committee 318, "Building Code Requirements for Structural Concrete (ACI 318-02) and Commentary (318R-02)", American Concrete Institute, Farmington Hills, MI, 2002, 443 pp.

ACI Committee 363, "State-of-the-Art Report on High-Strength Concrete (ACI 363R-92)", American Concrete Institute, Detroit, 1992 (Revised 1997), 55 pp.

ACI Committee 363, "Guide to Quality Control and Testing of High-Strength Concrete (ACI 363.2R-98)", American Concrete Institute, Detroit, 1998, 18 pp.

Ahmad, S. H. and Lue, D. M., "Flexure-Shear Interaction of Reinforced High-Strength Concrete Beams", ACI Structural Journal, Vol. 84, No.4, 1987, pp. 330-341.

Alexander, A.N.,and MacGregor, J. G., "Effect of Size On Flexural Behavior of High-Strength Concrete Beams", ACI Structural Journal, Vol. 94, No.1, 1997, pp. 59-67.

ANSYS (2003). Elements Manuals Release 8.0, ANSYS, Inc.

AS3600-1994, Australian Standard for Concrete Structures, Standards Australia, Sydney, (1994)

Ashour, S.A., " Effect of Compressive Strength and Tensile Reinforcement Ratio on Flexural Behavior of High-strength Concrete Beams", Engineering Structures, V22, No. 5 2000, pp413-423

Bernhardt, C. J. and Fynboe, C. C., "High Strength Concrete Beams" ,Nordic Concrete Research, No.5, 1986, pp. 19-26.

Choi, W., "Flexural Behavior of Prestressed Girders with High-strength Concrete", Ph.D, Dissertation, Department of Civil, Construction, and Environmental Engineering, North Carolina State University, Raleigh, North Carolina, Dec 2006, 167p.

Frosch, R.J., "Flexural Crack Control in Reinforcement Concrete", ACI International SP 204 "Design and Construction Practices to Mitigate Cracking", ACI International, 2001, pp 135-153

Hognestad, E., Hanson, N.W. and McHenry, D., "Concrete Stress Distribution in Ultimate Strength Design", ACI Journal, Vol.52, No.4, 1955 pp.455-479

Kahn, L. F. and Meyer, K. F., "Rectangular Stress Block for Nonrectangular Compression Zone" ACI Structural Journal, Vol. 92, No.3, 1995, pp. 304-310.

Kaminska, M. E., "High-Strength Concrete and Steel Interaction in RC Members", Cement and Concrete Composites, Vol. 24, No.2, 2002, pp. 281-295.

Kachlakev, D.I.; Miller, T.; Yim, S.; Chansawat, K.; Potisuk, T., "Finite Element Modeling of Reinforced Concrete Structures Strengthened With FRP Laminates,"

California Polytechnic State University, San Luis Obispo, CA and Oregon State University, Corvallis, OR for Oregon Department of Transportation, May 2001.

Lambotte, H. and Taerwe, L. R., "Deflection and Cracking of High-Strength Concrete Beams and Slabs", High-strength concrete: second international symposium / Weston T. Hester, editor. Hester, Weston T.1990, pp. 109-128.

Lambotte, H and Taerwe, L.R. "Deflection and Cracking of High-strength Concrete Beams and Slabs" High-Strength Concrete, Second International Symposium, SP121, American Concrete Institute 1990, pp109-128

Leslie, K. E., Rajagopalan, K. S. and Everard, N. J., "Flexural Behavior Of High-Strength Concrete Beams", Journal of the American Concrete Institute, Vol. 73, No. 9, 1976, pp. 517-521.

Lin, C-Hung, "Flexural Behavior of High Strength Fly Ash Concrete Beams", Chung-kuo Kung Ch'eng Hsueh K'an/Journal of the Chinese Institute of Engineers, v 15, n 1, Jan, 1992, p 85-92

Lu, X. and Jiang. "Analysis for Concrete Structure under Complex Stress Condition with Solid 65 FEA Element of ANSYS", Building Structure, 33(6), 2003 pp22-24

Logan,A. "Short-Term Material Properties of High-Strength Concrete", M.S. Thesis, Department of Civil, Construction, and Environmental Engineering, North Carolina State University, Raleigh, North Carolina, Jun 2005, 116p.

Mattock, A.H.; Kriz, L.B.; and Hognestad, E., "Rectangular Concrete Stress Distribution in Ultimate Strength Design" American Concrete Institute -- Journal, v 32, n 8, Feb, 1961, p 875-928

Mansur, M. A.,Chin, M. S. and Wee, T.H., "Flexural Behavior of High-Strength Concrete Beams", ACI Structural Journal, Vol. 94, No. 6, 1997, pp. 663-674.

Maghsoudi, A.A. and Akbarzadeh B. H., "Effect of ρ ′on Ductility of High-Strength Concrete Members Under Bending", ACI Symposium Publication 228, "Seventh International Symposium on the Utilization of High-Strength/High-Performance Concrete", pp. 363-380

Mertol, H.C., "Behavior of High-strength Concrete Members Subjected to Combined Flexure and Axial Compression Loadings", Ph.D, Dissertation, Department of Civil, Construction, and Environmental Engineering, North Carolina State University, Raleigh, North Carolina, Dec 2006, 238p.

Naaman, A. E., "Rectangular Stress Block and T-section Behavior", PCI Journal, Vol. 47, No.5, 2002, pp. 106-112.

Ozcebe, G., Ersoy, U.and Tankut, T., "Minimum Flexural Reinforcement for T-beams Made of Higher Strength Concrete", Canadian Journal of Civil Engineering, Vol. 26, No. 5, 1999, pp. 525-534.

Pam, H. J., Kwan, A. K. H. and Islam, M. S.,"Flexural Strength and Ductility of Reinforced Normal- and High-Strength Concrete Beams", Proceedings of the Institution of Civil Engineers: Structures and Buildings, Vol. 146, n 4, 2001, pp. 381-389.

Park, R. and Paulay, T., “Reinforced Concrete Structures”, John Wiley and Sons, New York, N.Y. 1975

Pastor, J.A., Nilson, A. H. and Slate,F.O., “Behavior of High-strength Concrete Beams ”, Research Report No. 84-3, Department of Structural Engineering, Cornell University, Ithaca, N.Y., 1984, 331pp

Paulson, K.A., Nilson, A. H., and Hover, K. C. “Long-term Deflection of High-strength Concrete Beams”, ACI Materials Journal (American Concrete Institute), v 88, n 2, Mar-Apr, 1991, p 197-206

Polak, M.A., Blackwell, K.G. and Killen, D.T. “Influence of Reinforcement Size and Distribution on Deflection of RC Members”, ACI Symposium Publication 210 “Deflection Control of the Future”, pp. 19-35

Popovics, S., “A Numerical Approach to the Complete Stress-Strain Curve of Concrete”, Cement and Concrete Research, v 3, n 5, Sep, 1973, pp 583-599

Rashid, M.A., and Mansur, M.A., “Reinforced High-strength Concrete Beams in Flexure”, ACI Structural Journal, v 102, n 3, May/June, 2005, pp. 462-471

Response-2000, Reinforced Concrete Sectional Analysis, Response Version 1.0.5, Bentz and Michael P. Collins.

Sarkar, S., Adwan, O. and Munday, J.G. L., “High Strength Concrete: an Investigation of the Flexural Behavior of High Strength RC Beams” Structural Engineer, Vol. 75, No.7, 1997, pp. 115-121.

Shin, S., Ghosh, S. K. and Moreno, J., “Flexural Ductility of Ultra-High-Strength Concrete Members”, ACI Structural Journal, Vol. 86, No. 4, 1989, pp. 394-400.

Suzuki, M., Suzuki. K., Abe. K. and Ozaka. Y., “Mechanical Properties of Ultra High Strength Concrete Beams Subjected to Pure Bending Moment”, Fourth International Symposium on the Utilization of High Strength/High Performance Concrete 29-31 May 1996, Paris, France, pp. 835-844.

Swamy, R. N. and Anand, K. L., “Structural Behavior Of High Strength Concrete Beams”, Building Science, Vol. 9, No.2, 1974, pp. 131-141.

Van Mier, J.G.M., “Multiaxial Strain-Softening of Concrete, Part 1:Fracture”, Materials and Structures, No. 111, 1986, pp. 179-190.

Vecchio, F.J., and Collins, M.P., "The Modified Compression Field Theory for Reinforced Concrete Elements Subjected to Shear," ACI Journal, Vol. 83, No. 2, Mar.-Apr. 1986, pp.219-231

Wolanski, A. J., “Flexural Behavior of Reinforce and Prestressed Concrete Beams Using Finite Element Analysis”, Marquette University, Milwaukee, Wisconsin, May, 2004

Weiss, W. J., Guler, K. and Shah, S. P. “Localization and Size-Dependent Response of Reinforced Concrete Beams”, ACI Structural Journal, Vol. 98, No.5, 2001, pp. 686-695.

Wiegrink, K; Marikunte, S. and Shah, S. P., "Shrinkage Cracking of High-Strength Concrete" ACI Materials Journal, Vol. 93, No.5, 1996, pp. 409-415.

Yi, S-T., "Effect of Specimen Sizes on ACI Rectangular Stress Block for Concrete Flexural Members", ACI Structural Journal, v 99, n 5, September/October, 2002, pp 701-708